IN-VENTO2022

XVII Conference of the Italian Association for Wind Engineering

POLITECNICO DI MILANO
September 4th-7th, 2022

In collaboration with
Fondazione Politecnico di Milano

Sponsor
pininfarina

Scientific Committee

Gianni Bartoli, Università degli Studi di Firenze
Luca Bruno, Politecnico di Torino
Massimiliano Burlando, Università degli Studi di Genova
Luca Caracoglia, Northeastern University, USA
Giampiero Manara, Permasteelisa
Claudio Mannini, Università degli Studi di Firenze
Sara Muggiasca, Politecnico di Milano
Francesco Petrini, Università degli Studi di Roma "La Sapienza"
Maria Pia Repetto, Università degli Studi di Genova
Francesco Ricciardelli, Università degli Studi della Campania "Luigi Vanvitelli"
Daniele Rocchi, Politecnico di Milano
Ilaria Venanzi, Università degli Studi di Perugia
Alberto Zasso, Politecnico di Milano

Organizing Committee

Alberto Zasso (Conference Chairman)
Marco Belloli
Daniele Rocchi
Gisella Tomasini
Tommaso Argentini
Sara Muggiasca
Paolo Schito
Filippo Calamelli
Giulia Pomaranzi
Giorgio Frontini

Contacts

https://www.in-vento2022.org
invento@polimi.it

INDEX

Wind load assessment of unitized double skin facades

F. Ricciardelli [1], G. Manara [2], G. Lori [3]

[1]University of Campania "Luigi Vanvitelli", Aversa, IT, friccia@unicampania.it
[2]Permasteelisa SpA, Vittorio Veneto, IT, g.manara@permasteelisagroup.com
[3]Permasteelisa SpA, Vittorio Veneto, IT, g.lori@permasteelisagroup.com

1. ABSTRACT

Weather tightness of building curtain wall envelopes can be reached either by sealing or by pressure control. The former strategy is more intuitive and cheaper in principle, but it has a number of disadvantages, among which is durability. The latter strategy, on the other hand, is nowadays considered as the State-of-the-Art technology for high performance building envelopes and it governs also the multiple skin related behaviour, designed in a way that cavity pressure prevents water from penetrating the building.

Global wind loads are not affected by the details of the envelope, and in particular by whether this is made of a single or by multiple skins. However, when designing multiple skin envelopes, the additional question arises of how the wind loads are shared among the skins, which influences the design of the skins themselves and of the fixing elements. To this purpose, double skin facades can be classified according to the following criteria: a) the absolute and relative permeability of the skins, b) the absolute and relative stiffness of the skins, c) the depth of the cavity and air circulation mechanism. In particular, cavity depths in the wide range of 100 to 2000 mm are used, and the term large cavity is used for values of the depth in the range of 600 to 2000 mm, whereas the term small cavity is used for smaller values of the depth. More recently, the concept of unitized compact double skin facades has been developed, with cavity depths in the range of 100 to 300 mm. Ventilation can be either natural of artificial, and in both cases it is governed by the size and location of openings, and by unintentional leakage. A relatively novel type of double skin is represented by the Closed Cavity Façade (CCF), which has no openings and a very limited unintentional leakage; in that case, only a minimal ventilation is exerted through the artificial injection of a small flow of dry air, which is mainly designed to prevent condensation.

In 1995, ENV1991-2-4 (CEN, 1995) appeared, containing a method for calculating pressures on external walls or roofs with more than a skin; the method was calibrated with measurements on facades with a cavity depth smaller than 150 mm, and it was argued that for larger values it would have underestimated the load on the external skin. In 2005, EN1991-1-4 (CEN, 2005) superseded ENV 1991-2-4, containing a modified version of the load sharing criterion for double skin facades.

Based on full scale pressure measurements (Permasteelisa, 2018) on a unitized compact ventilated double skin facade unit (Fig. 1), in this paper an attempt is made to assess the accuracy of current Code specifications. The tested specimen has a nominal width of 1500 mm and a total height of 4000 mm, and is divided into a vision area and a spandrel area. The vision area inner skin is provided with an operable inward glazing. Cavity depth is 160 mm in the vision area and 137 mm in the spandrel area.

Figure 1. Experimental setup

Three types of tests were carried out: cavity air leakage tests, static tests and dynamic tests. The first are aimed at assessing the effect of pressure difference on total leakage and at the quantification of the unintended leakage. The second are aimed at assessing the propagation into the cavity of static external pressures. The third are aimed at quantifying the effects on such propagation of the fluctuation of external pressures.

Cavity air leakage tests revealed that for large values of the external porosity, the discharge equation well describes the total leakage, whereas for smaller values of porosity or in the case of sealed units, measured and calculated values tend to diverge, especially for lower values of the cavity pressure. Static tests revealed a pronounced non-linear behaviour of pressure propagation, mainly the effect of the unintended leakage through the operable glazing when subjected to a positive pressure. Dynamic tests were carried out applying a sinusoidal pressure fluctuation at 0.067, 0.25, 0.4 and 1.0 Hz, and allowed quantifying the filtering effect of the unit.

In this paper, the experimental outcomes are adopted to characterize the wind load sharing behaviour of the tested facade and a comparison with the current Code approach is carried out.

REFERENCES

European Committee for Standardization (CEN), 1995, ENV1991-2-4, Eurocode 1: Basis of design and actions on structures, Part 2-4: Actions on structures – Wind actions.Metalliche, 4, pp. 209-243

European Committee for Standardization (CEN), 2005, EN1991-1-4, Eurocode 1: Actions on structures, Part 1-4: General actions - Wind actions.

European Committee for Standardization (CEN), 2020, prEN1991-1-4, Eurocode 1: Actions on structures, Part 1-4: General actions - Wind actions.

Permasteelisa Group, 2018, Multiple skin load sharing, Parts 1 and 2, Internal Research Report.

17th Conference on Wind Engineering – IN-VENTO 2022
Politecnico di Milano, IT 4 – 7 September 2022

Urban air mobility: a wind engineering perspective

S. Cammelli [1], J. Millar [2], R. Wayland [3], K. Gouder [4]

[1]*WSP, London, United Kingdom, stefano.cammelli@wsp.com*
[2]*WSP, London, United Kingdom, joshua.millar@wsp.com*
[3]*WSP, London, United Kingdom, rhys.wayland@wsp.com*
[4]*Imperial College London, London, United Kingdom, kevin.gouder04@imperial.ac.uk*

SUMMARY
Urban air mobility (UAM) is an emerging concept in air transportation featuring highly automated aircraft that are expected to include a mix of piloted, remotely piloted, and fully autonomous vehicles. The aim of UAM is to provide a wide range of services at an intra-city level, including on-demand air taxis, air shuttles, cargo air vehicles and medical emergency vehicles. Despite the significant technological advancements made in the UAM industry in recent years, wind remains the most challenging natural physical phenomena electric-powered vertical take-off and landing capable aircraft - known as eVTOLs - will need to contend with. This technical paper will discuss both the weather-related and the urban-environment-related challenges that will need to be considered during the planning stage of flightpaths and vertiports.

Keywords: urban air mobility, boundary layer wind tunnel testing, computational fluid dynamics

1. INTRODUCTION
With an ever-growing urban population around the world, cities and mega-cities will inevitably look at UAM as an alternative transportation mode to help reduce pollution levels, improve connectivity, and reduce strain on existing transport networks. In the context of UAM, the ‘agility’ of eVTOLs makes them the perfect mobility solution for densely built-up urban environments. eVTOLs are expected to cruise within a certain UAM corridor at an altitude below the airway of conventional aircraft. These small aircraft will then be relying on a network of vertiports which will provide the necessary infrastructure for landing, recharging, and taking-off - a network that will need to be integrated within the urban canopy of existing and future cities and mega-cities. Urban environments present a range of challenges to eVTOLs. Wind conditions near high-rise buildings can in fact be particularly complex: wakes behind buildings, downdrafts, updrafts, funneling between neighboring buildings, shear layers close to the building corners and horseshoe vortices can all produce rapid changes of speed and turbulence along certain flightpaths which can result in a sudden drop in lift. Site-specific predictive tools will be required to ensure these building-induced hazards are taken into consideration during the planning stage of flightpaths and vertiport siting. The tools will also need to be updated to account for the evolution of cityscapes with time and will need to predict the effect of future developments.

2. BACKGROUND
The risk associated with atmospheric turbulence and structure-induced turbulence in relation to flight operations; the risk associated with proximity to tall and bulky structures such as adjacent buildings; the importance of an adequate separation between the heliport and any upstream structures; as well as the need of an air gap between the landing area and the supporting building, are all important concepts and principles that are well described in CAP 437 (2021) and CAP 1264 (2019). Both standards also specify two thresholds of the standard deviation of the vertical airflow velocity that are to be followed to ensure safe operating conditions over the helideck and to avoid and minimise operating restrictions. The risks

associated with low-level flying in a confined and mixed-use airspace are also presented in CAP 2272 (2021).

3. STRATEGY AND INITIAL FINDINGS

Weather events as well as their complex interaction with cities and mega-cities can influence many components of UAM: safety, operations, and passenger comfort. Vertiports will be equipped with automated weather stations, LIDARs and wind profilers to provide automatic weather alerts and to inform vital 'no-go' decisions. However, within the modelling and simulation design space, city-level as well as vertiport site-specific extensive wind studies will be required to quantify complex airflow patterns within the urban canopy. An initial assessment of city-level historical weather conditions, with a focus on viability and operations, will be crucial. Design tools such as boundary layer wind tunnel testing and computer-based simulations will then need to be employed to resolve the complex city- and site-specific three-dimensional turbulent flow features described above. The result of a detached eddy simulation (DES) performed with time- and space-dependent turbulent inlet conditions modelled using a synthetic eddy method (SEM) is shown in Figure 1: in this plot, the standard deviation of the vertical airflow velocity of the complex 3D wind field across a site in west London is normalised by the corresponding 10 m height mean wind speed at Heathrow Airport. A similar simulation could be used to optimise the siting of a vertiport, or with a database of such simulations from all wind directions, it would be possible to obtain real-time turbulence and wind speed along arbitrary flightpaths.

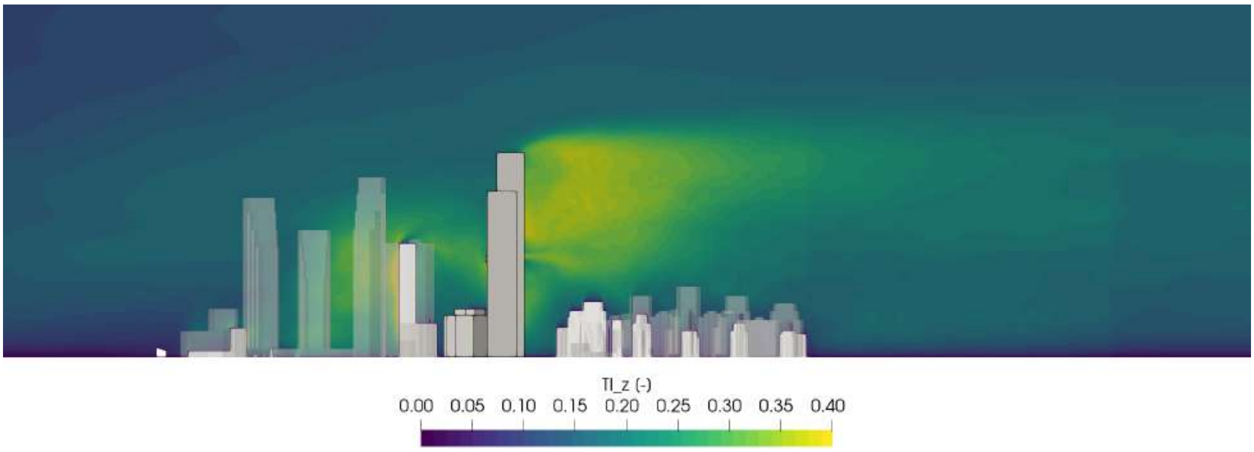

Figure 1. Normalised standard deviation of the airflow vertical velocity component

REFERENCES

CAP 437, 2021. Standards for Offshore Helicopter Landing Areas. Civil Aviation Authority, London, UK.

CAP 1264, 2019. Standards for Helicopter Landing Areas at Hospitals. Civil Aviation Authority, London, UK.

CAP 2272, 2021. Key Considerations for Airspace Integration within an Urban Air Mobility Landscape. Civil Aviation Authority, London, UK.

The effect of central gap and wind screens on the aeroelastic stability of long-span bridge decks: comparison of numerical analyses and experimental results

A. Camera [1], A. Bagnara [2], A. Larsen [3], S. Cammelli [4], G. Piccardo [5]

[1] *WSP, London, United Kingdom,* andrea.camera@wsp.com
[2] *NOVA Fluid Mechanics, Teddington, United Kingdom,* anna@novafluidmechanics.com
[3] *COWI, Kongens Lyngby, Denmark,* aln@cowi.com
[4] *WSP, London, United Kingdom,* stefano.cammelli@wsp.com
[5] *Università degli Studi di Genova, Genoa, Italy,* giuseppe.piccardo@unige.it

SUMMARY
As long-span bridges are usually built at exposed locations and high winds can cause disruptions to the traffic flow, relatively tall wind screens are often used to protect vehicles which are prone to suffer from wind induced accidents. This paper presents the results of a series of two-dimensional discrete vortex method simulations of laminar incompressible flow past standard aerofoil mono-boxes and twin-boxes, conducted to investigate the aerodynamic impact of wind screens on bridge decks in relation to steady-state and divergent instability (classical flutter) behavior. A comparison with the outcome of a series of parametric wind tunnel tests is also presented, finding that numerical simulations can reflect the observed experimental behavior. This means that designers, under certain conditions, could rely on computational bridge aerodynamics at feasibility or early design stages to identify potential instabilities and introduce mitigation measures aimed at optimizing the aerodynamic performance of the deck.

Keywords: long-span bridges, computational bridge aerodynamics, wind tunnel testing

1. INTRODUCTION

Modern suspension bridges normally employ a trapezoidal steel box girder deck which typically lacks aerodynamic performance regarding flutter when spans grow longer. To increase the critical wind speed for flutter the deck can be divided into two sections: the introduction of an air gap may lead to a more aerodynamically efficient cross-section capable to remain stable in high winds.

In recent years, the need to guarantee a continuous flow of traffic on long-span bridges has forced designers to introduce relatively tall wind screens to ensure that these bridges can be operational also in extreme weather conditions. On the other hand, wind screens can be rather intrusive and significantly change the aerodynamic behavior of the cross-section. Somehow, these high barriers represent a sort of step backwards in the quest of building ultra-long aerodynamic bridges and the experience gained in the past 60 years by wind engineers seems again challenged.

The main purpose of this research project is to investigate the aerodynamic impact of wind screens on standard aerofoil mono-boxes and twin-boxes in relation to classical flutter both numerically and experimentally. To achieve this, a specific cross-section was chosen as a good representation of a standard box girder design (Figure 1) and 3m tall, 50% porous slatted wind screens located along the edges of the deck were considered (Figure 2). To make findings more generally applicable, the gap width has not been described by its absolute value, but as its ratio to the depth of the deck. The numerical simulations have been carried out using DVMFLOW, COWI's property software (Larsen and Walther, 1997; Larsen and Walther, 1998), which provides two methods for determining the critical wind speed for flutter.

With the first method, the software generates the eight aerodynamic derivatives for the two-degrees-of-freedom system by simulating and extracting the motion-induced aerodynamic forces on the bridge deck when undergoing forced vertical translation and rotation. The aerodynamic derivatives were then used to calculate the critical wind speed for flutter. To achieve this, both the Theodorsen method (Thedorsen, 1935) and the AMC (Air Material Command) method (Smilg and Wassermann, 1942; Scanlan and Rosenbaum, 1962) were followed. However, as the two methods led to very similar results, only the outcome of the Theodorsen routine is presented within this technical paper.

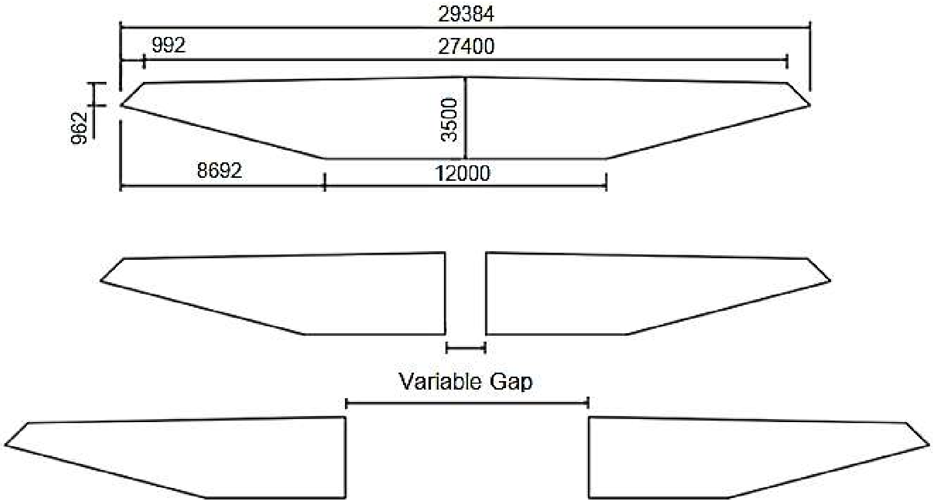

Figure 1. Geometrical properties of the bridge deck in mm (top); minimum (middle) and maximum (bottom) gap widths considered (0.5 and 3 times the maximum depth of the cross-section respectively)

Figure 2. Wind screens layout and arrangement for the mono-box configuration

The second method involves simulations of the two-degrees-of-freedom motion of the bridge deck when elastically suspended in the flow. Various runs were carried out for a wide range of increasing wind speeds. The critical velocity was determined by monitoring the development of the oscillations between consecutive wind speeds until flutter occurs as the system absorbs more energy from the flow than it is being dissipated through structural damping. The results of the numerical simulations have subsequently been compared to the findings of a wind tunnel testing campaign conducted within the aeronautical wind tunnel facility (Tunnel 5) of what once was the 'Wind Engineering' business unit of BMT Group (now NOVA Fluid Mechanics) in Teddington (London, UK). The laminar flow wind tunnel tests made use of a 1:40 scale section model with the same geometrical characteristics as the ones used for the computer simulations. To ensure consistent boundary conditions between the numerical and the experimental works, the measured properties of the wind tunnel setup were provided as input data for the numerical simulations. As geometry and structural parameters are kept constant, the aerodynamic derivatives obtained in DVMFLOW can be used to evaluate the theoretical flutter wind speed whilst the results of the elastic suspended simulations can be directly compared to the experimental critical velocities.

2. RESULTS

The main results are presented in Figure 3 in terms of (model scale) critical wind speed for different gap-to-width ratios. For the bare deck, the wind tunnel tests showed an increase in the flutter wind speed only for gap-to-width ratios up to one. The critical flutter speed then decreases before plateauing above a gap-to-width ratio of two. When wind screens are introduced, the critical wind speed achieves higher values than the ones of the bare deck configuration for gap-to-width ratios greater than 1.5. This is a very remarkable result: for gaps larger than the height of the cross-section, wind screens both improve the aeroelastic behavior of the bridge deck and protect vehicles from wind-induced accidents.

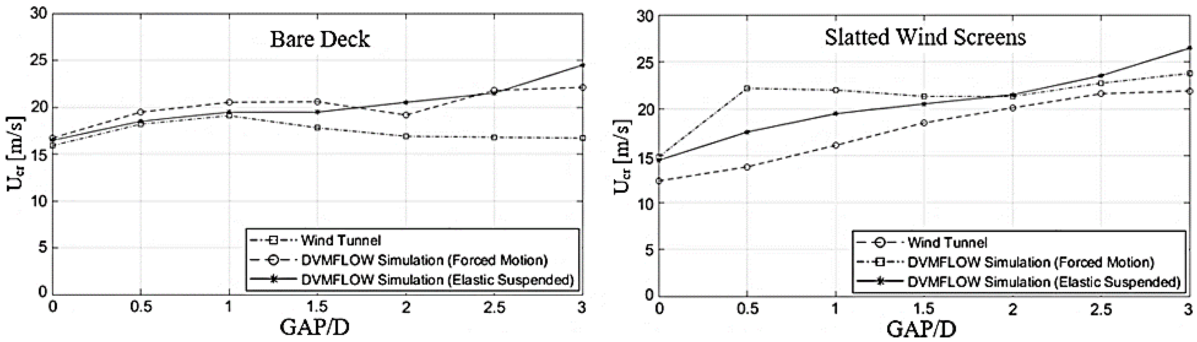

Figure 3. Comparison between numerical and experimental results without (left) and with (right) wind screens.

The reliability of the elastic suspended (free motion) simulations is excellent for smaller gap widths for the bare deck configuration; if wind screens are present, the free motion simulations are capable to accurately replicate the increasing behavior of the critical wind speed across the full range of gap-to-width ratios. In terms of the forced motion simulations, a strong dependence on the critical angle for flutter was observed. However, for the bare deck configuration, this type of simulations can follow the decreasing behavior of the measured critical velocity up to a gap-to-width ratio of 2. When wind screens are introduced, the accuracy of the results improves as the gap width increases.

In general, the numerical results are found to be in good to great agreement with the experiments. This means that simulations could be used at feasibility or early design stages with a certain confidence, with a dependance on the type of wind screens yet to be determined.

REFERENCES

Larsen, A., Walther, J.H., 1997. Aeroelastic analysis of bridge girder sections based on discrete vortex simulations. Journal of Wind Engineering and Industrial Aerodynamics 67&68, 253 – 265.

Larsen, A., Walther, J.H., 1998. Discrete vortex simulation of flow around five generic bridge deck sections. Journal of Wind Engineering and Industrial Aerodynamics 77&78, 591 – 602.

Scanlan, R.H., Rosenbaum, R., 1962. Introduction to the Study of Aircraft Vibration and Flutter, The MacMillan Company, New York, New York, USA.

Smilg, B., Wassermann, L.S., 1942. Application of three-dimensional flutter theory to aircraft structures. AAF Technical Report 4798, July.

Theodorsen, T., 1935. General theory of aerodynamic instability and the mechanism of flutter. NACA TR 496.

A numerical characterization of the attractor for a fluid structure interaction problem

Clara Patriarca [1], Filippo Calamelli [2], Paolo Schito [3], Tommaso Argentini [4], Daniele Rocchi [5]

[1] *Politecnico di Milan, Milan, Italy, clara.patriarca@polimi.it*
[2] *Politecnico di Milan, Milan, Italy, filippo.calamelli@polimi.it*
[3] *Politecnico di Milan, Milan, Italy, paolo.schito@polimi.it*
[4] *Politecnico di Milan, Milan, Italy, tommaso.argentini@polimi.it*
[5] *Politecnico di Milan, Milan, Italy, daniele.rocchi@polimi.it*

SUMMARY
In this paper, starting from some known theoretical results, the long-term dynamics of a fluid-structure interaction problem for a Poiseuille flow through a 2D channel containing a rectangular obstacle are investigated from a numerical point of view. From a physical point of view, the wind-induced motions of the deck of a bridge are modeled similarly to a wind tunnel experiment at large times. In particular, we are concerned about the explicit characterization of the global attractor of the problem, that is the subset of the phase space to which eventually all the trajectories of the system approach.

Keywords: fluid structure problem, global attractor, numerical characterization

1. INTRODUCTION AND MAIN PURPOSE OF THE PAPER

Nowadays, the understanding of the dynamic response to turbulent wind is a crucial issue in the design of long-span bridges. Numerous phenomena affect suspension bridges, like vortex-induced oscillations, buffeting and flutter instabilities (see Simiu and Scanlan 1996, Dowell 2015 and Gazzola 2015). Specifically, flutter instability occurs at high wind velocities (>70 m/s for long-span bridges) at which the vertical and torsional motion of the deck synchronize, leading the deck to oscillate with growing amplitudes and eventually causing the bridge to collapse (Agar 1988, Agar 1989 and Frandsen 2004).

From an engineering point of view, the flutter instability onset can be predicted with different approaches, i.e. experimental, numerical or hybrid methods (Diana et al. 2015). Experimental methods rely on wind tunnel testing of full-bridge aeroelastic models (Argentini et al. 2020) while numerical approaches typically involve Computational Fluid Dynamics (CFD) simulations. Hybrid methods are widely employed due to the implementation complexity of aeroelastic models, and they usually combine numerical models of the structure with experimentally identified aerodynamic coefficients (Argentini et al. 2016, Diana et al. 2020, 1-2). On the other hand, Scanlan's linearized theory constitutes the most widely used approach to estimate the flutter limit (see Simiu and Scanlan 1966, Scanlan and Tomko 1971, and Scanlan 1978). In the 2D case, a major contribution is also due to Theodersen's inviscid flat-plate theory (Theodorsen 1935) and the approximate formula by Selberg (Selberg 1961). These studies are used as a modeling framework to select which experimental coefficients are to be evaluated during wind tunnel tests, namely the so-called *flutter derivatives*.

From a mathematical point of view, aerodynamic instabilities can be studied by considering the asymptotic behavior of the body-fluid (bridge-wind) system as time goes to infinity. In general, any dynamical system, like the one at consideration, can be seen as described by the solution y(t) of the differential equation:

$$\frac{dy}{dt} = F_\lambda\big(y(t)\big)$$

where F is a mapping depending on some physical parameter λ. The phenomena that are observed depend on λ, which governs the transition of the system among different states. From an analytical point of view, it is not easy to predict to which state a given dynamical system will evolve as time goes to infinity. However, to provide a proper description of the long-term dynamics, one usually searches small subsets of the phase space able to describe the typical behavior of the system, namely to attract all the orbits and reduce the degrees of freedom of the system. To this purpose, the most natural object to use in the theory of infinite-dimensional dynamical systems is the global *attractor* (see Chepyzhov and Vishik 2002, and Temam 1997). For instance, in the context of fluid dynamics systems, the global attractor is the set confining all possible flows corresponding to all possible initial data. Once the existence of the global attractor is known, the spontaneous following question concerns the characteristics of such a set, which might be more or less complicated, even exhibiting a fractal nature.

Accordingly, the main purpose of this paper is to provide an explicit characterization of the global attractor associated with a fluid-structure interaction problem, by numerically modeling the deck of a suspension bridge interacting with wind, similarly to what is done in a wind tunnel experiment. Indeed, this could be considered comparable to the practical problem of determining which permanent state will be observed after a short transient period in a wind tunnel. To provide a description of the global attractor and, thus, create an explicit link between the analytical and experimental framework, we intervene through numerical simulations, by which we are able to capture some orbit of the dynamical system at consideration. In particular, we simulate the static and dynamic behavior of the cross-section of the deck immersed in a fluid flow at different conditions. Specifically, the deck is allowed to oscillate just in the vertical direction. The reason for this constraint is that the decoupling of the vertical and torsional degrees of freedom is a first step towards the assessment of the behavior of the deck of a bridge interacting with the wind.

REFERENCES

T. Agar, The analysis of aerodynamic flutter of suspension bridges. Computers & Structures 30, 593–600 (1988)

T. Agar, Aerodynamic flutter analysis of suspension bridges by a modal technique. Engineering Structures 11, 75–82 (1989)

T. Argentini, G. Diana, D. Rocchi and C. Somaschini, A case-study of double multi-modal bridge flutter: Experimental result and numerical analysis. Journal of Wind Engineering and Industrial Aerodynamics 151, 25–36 (2016)

G. Diana, D. Rocchi and M. Belloli, Wind tunnel: a fundamental tool for long-span bridge design. Structure and Infrastructure Engineering 11, 533–555 (2015)

V. Chepyzhov and M.I.. Vishik, Attractors for equations of mathematical physics. American Mathematical Society Colloquium Publications, 49. American Mathematical Society, Providence, RI, 2002. (2002)

G. Diana, S. Stoyanoff, K. Aas-Jakobsen, A. Allsop, M. Andersen, T. Argentini, M. C. Montoya, S. Hernández, J. Ángel Jurado, H. Katsuchi, I. Kavrakov, H.-K. Kim, G. Larose, A. Larsen, G. Morgenthal, O. Øiseth, S. Omarini, D. Rocchi, M. Svendsen and T. Wu, Iabse task group 3.1 benchmark results. part 2: Numerical analysis of a three-degree-offreedom bridge deck section based on experimental aerodynamics. Structural Engineering International 30, 411–420 (2020)

G. Diana, S. Stoyanoff, K. A.-J. Dr, A. Allsop, M. Andersen, T. Argentini, M. C. Montoya, S. Hernández, J. Ángel Jurado, H. Katsuchi, I. Kavrakov, H.-K. Kim, G. Larose, A. Larsen, G. Morgenthal, O. Øiseth, S. Omarini, D. Rocchi, M. Svendsen and T. Wu, Iabse task group 3.1 benchmark results. part 1: Numerical analysis of a two-degree-of-freedom bridge deck section based on analytical aerodynamics. Structural Engineering International 30, 401–410 (2020)

E. Dowell, A Modern Course in Aeroelasticity, 5th ed. Springer (2015)

J. Frandsen, Numerical bridge deck studies using finite elements. part i: flutter. Journal of Fluids and Structures 19, 171–191 (2004)

F. Gazzola, Mathematical Models for Suspension Bridges - Nonlinear Structural Instability. Springer-Verlag (2015)

R. Scanlan, The action of flexible bridges under wind, I: flutter theory. Journal of Sound and Vibration 60 (1978)

R. Scanlan and J. Tomko, Airfoil and bridge deck flutter derivatives. ASCE Journal of Engineering Mechanics Division 1717–1737 (1971)

A. Selberg, Oscillation and aerodynamic stability of suspension bridges. Technical Report Acta Polytechnica, Scandinavica Cil3 (1961)

Simiu, E. and Scanlan, R.H., 1996. Wind effects on structures. John Wiley and Sons, New York, NY, USA.

R. Temam, Infinite-Dimensional Systems in Mechanics and Physics. Springer (1997)

T. Theodorsen, General theory of aerodynamic instability and the mechanism of flutter. Technical Report 496, NACA (1935)

Determination of Design Wind Loads in Tornadoes on Low-Rise Buildings

Osmany Hernandez [1], Gregory A. Kopp [2]

[1] *University of Western Ontario, London, Canada, ohernan3@uwo.ca*
[2] *University of Western Ontario, London, Canada, gakopp@uwo.ca*

SUMMARY
Modern wind testing methods like Atmospheric Boundary Layer (ABL) Wind Tunnels and Tornado Vortex Generators cannot be used to determine design wind loads in tornadoes given the complexity of the wind field and the present limitations in such facilities. To accomplish this task, it is proposed the use of a methodology based on a storm passage approach with an aerodynamic model to account for wind loads, as well as including the effects of the static and internal pressures. Validation will be made using data and results from previous tests on tornado vortex generators. Preliminary results show good agreement between the numerical simulations and the experimental data. It is also shown that results depend on the tornado wind field model used, sources of uncertainty in the results are examined and discussed.

Keywords: Tornadoes, Numerical model, Low-Rise Buildings

1. EXTENDED ABSTRACT

It is well known that given the low probability of a tornado hitting a particular location and the high intensity of the winds the availability of full-scale measurements is scarce. The interaction of the wind inside the tornado vortex structure with the building differ from the aerodynamics present on ABL winds as suggested by Kopp and Wu (2020), i.e., the strong vertical wind velocity component, the static pressure gradient, translational and rotational wind speed, among others, rule out the use of ABL Wind Tunnels for determination of design wind loads in tornadoes. Tornado vortex simulators, like the WINDEE Dome at University of Western Ontario (Refan and Hangan, 2016), have been built as a tool to study these wind fields. However, despite the insight on vortex structure and aerodynamics that these facilities offer, there are some caveats. According to Baker and Sterling (2019), the characteristics of the wind fields depends greatly on the facility in which were generated. Some facilities are bigger than others, limiting the variety of wind fields that can simulate; some can move the wind field with a limited velocity, experiments take time to complete and the way of measuring without interfering with the air flow possess a challenge using available instruments.

In order to calculate design wind loads in tornadoes, a different approach is needed. So, it is proposed to use a simulation approach that can generate a wide range of tornadic wind fields with enough accuracy and without the time constraint. The numerical model proposed is integrated by a wind field model (Dunn and Twisdale, 1979), a Quasi-Steady vector model (Wu and Kopp, 2016, 2018) to account for the building aerodynamics, the internal pressure is estimated through the Multiple Discharge Equation method (Oh 2004) and the static pressure effects were also considered.

The wind field model used is of a deterministic type based on the work of Kuo (1971) combined with field observations. The consideration of the three wind components (Radial, Tangential, and Vertical), and the treatment of various tornado characteristics as random variables makes this wind field model suitable for the task as it can generate a wide variety of tornado events. To include the effects of the building aerodynamics in a tornadic flow regime, the contribution of both the wind azimuth, θ, and elevation angle, β, to the instantaneous pressure coefficient,

Cp_{inst}, are of crucial importance to estimate the surface pressures, given the rapid movement of the wind field and the presence of considerable vertical and rotational wind components.

Wu and Kopp (2016, 2018, 2020) developed a vector model based on the Quasi-Steady assumption that includes the effects of both angles. The model assumes a decomposition of the wind load into an aerodynamic part and a static part and uses local wind velocities as reference. Fig. 1 shows the main stages of the numerical simulation with the results obtained on each one of the steps.

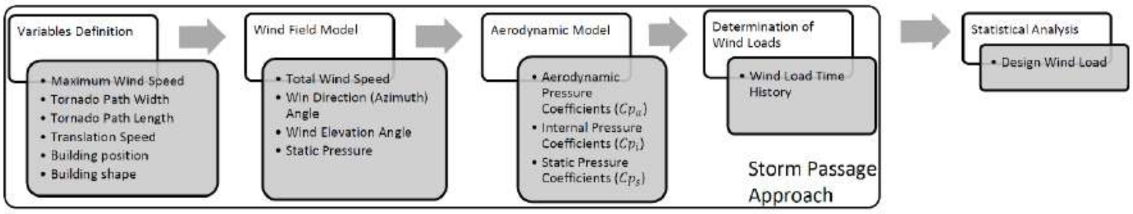

Figure 1. Flowchart of the methodology to determine wind loads in tornadoes.

Some adjustments are made trying to match results from experimental data, i.e., tornado vortex generator experiments. A discussion on sources on uncertainty is also made, as these limit the reach and applicability of the methods used on the research, as both, experimental and numerical are based on assumptions. Preliminary results on Fig. 2 A, B, C and D, show good agreement compared to results from Roueche et al., (2020).

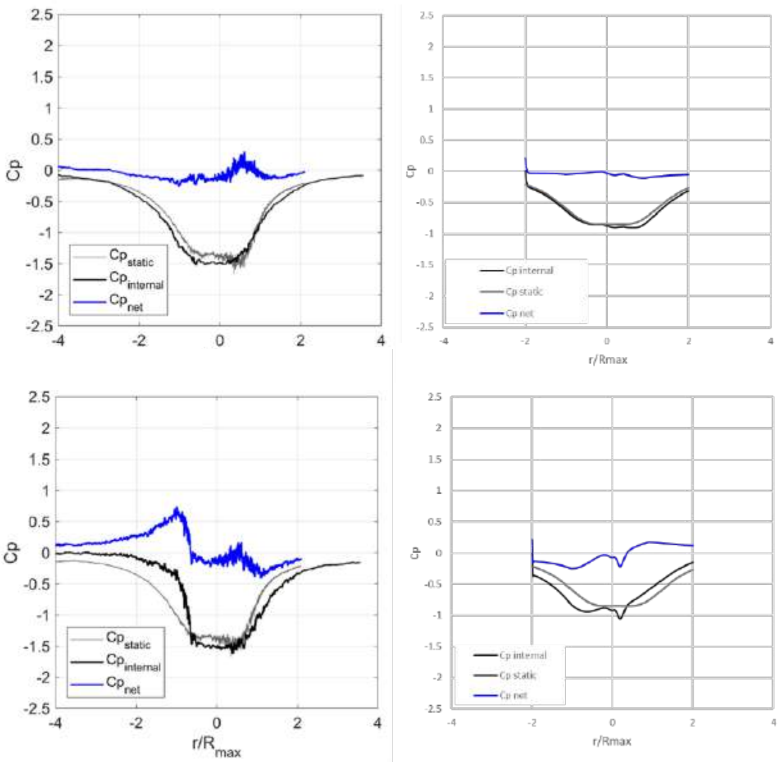

Figure 2. Estimated internal pressures under tornado flow; Enclosed building **(A)**: experimental, **(B)**: numerical. Opening on one wall with added leakage **(C)**: experimental, **(D)**: numerical.

REFERENCES

Baker, C., & Sterling, M. (2019). Are Tornado Vortex Generators fit for purpose? Journal of Wind Engineering and Industrial Aerodynamics, 190, 287–292. https://doi.org/10.1016/j.jweia.2019.05.011

Dunn, W. L., & Twisdale, L. A. (1979). A synthesized windfield model for tornado missile transport. Nuclear Engineering and Design, 52(1). https://doi.org/10.1016/0029-5493(79)90015-3

Kopp, G. A., & Wu, C. H. (2020). A framework to compare wind loads on low-rise buildings in tornadoes and atmospheric boundary layers. Journal of Wind Engineering and Industrial Aerodynamics, 204, 104269. https://doi.org/10.1016/j.jweia.2020.104269

Kuo, H. L. (1971). Axisymmetric Flows in the Boundary Layer of a Maintained Vortex. Journal of the Atmospheric Sciences, 28(1). https://doi.org/10.1175/1520-0469(1971)028<0020:afitbl>2.0.co;2

Refan, M., Hangan, H., and Wurman, J. (2016). Characterization of tornado-like flow field in a new model scale wind testing chamber. J. Wind Eng. Indus. Aerodyn. 151, 107-121. https://doi.org/10.1016/j.jweia.2016.02.002

Roueche, D. B., Prevatt, D. O., & Haan, F. L. (2020). Tornado-Induced and Straight-Line Wind Loads on a Low-Rise Building With Consideration of Internal Pressure. Frontiers in Built Environment, 6, 18. https://doi.org/10.3389/fbuil.2020.00018

Wu, C. H., & Kopp, G. A. (2016). Estimation of wind-induced pressures on a low-rise building using quasi-steady theory. Frontiers in Built Environment, 2. https://doi.org/10.3389/fbuil.2016.00005

Wu, C. H., & Kopp, G. A. (2018). A quasi-steady model to account for the effects of upstream turbulence characteristics on pressure fluctuations on a low-rise building.

Oh, J. H. (2004). Wind-induced internal pressures in low-rise buildings. Faculty of Graduate Studies, University of Western Ontario, London, Ont.

Global pressure coefficients for building roofs revisited

A. Malasomma [1], V. Picozzi [2], A.M. Avossa [3], F. Ricciardelli [4]

[1]*University of Campania "Luigi Vanvitelli", Aversa, IT,* antonio.malasomma@unicampania.it
[2]*University of Campania "Luigi Vanvitelli", Aversa, IT,* vincenzo.picozzi@unicampania.it
[3]*University of Campania "Luigi Vanvitelli", Aversa, IT,* albertomaria.avossa@unicampania.it
[4]*University of Campania "Luigi Vanvitelli", Aversa, IT,* friccia@unicampania.it

1. INTRODUCTION

Italian National Research Council Guidelines for the assessment of wind actions and effects on structures (CNR, 2018) consider three set of pressure coefficients. The first set is denoted as $c_{p,1}$ and allows the design of cladding elements which surface is equal to or less than 1 m^2. The second set of pressure coefficients is denoted as $c_{p,10}$ and allows the design of structural members for which the influence area is equal to or larger than 10 m^2. Finally, the third set, denoted global coefficients, allows the design of main structural elements and foundation loads; this is derived as a simplification of the $c_{p,10}$ coefficients. Global pressure coefficients are under consideration also for inclusion also in Eurocode 1, prEN1991-1-4:2020 (CEN, 2020).

The purpose of this paper is the calibration of a revised set of global pressure coefficients for roofs, based on wind tunnel measurements available from aerodynamic databases. Extreme Value (EV) analysis is applied to define the design values of the global pressure coefficients. Then, a comparison is made between current and proposed coefficients by evaluating the global effects of the wind action on the roof of a rectangular building.

2. METHODOLOGY

The Tokyo Polytechnic University (TPU) provides a data collection of pressure coefficients measured on model low-rise buildings (Quan et al., 2007). In order to evaluate the global pressure coefficients, the database of isolated buildings is used.

For the evaluation of global pressure coefficients, when the wind is orthogonal to one of the building faces the pressure distribution on the roof can be considered as constant along the cross-wind direction. Within this assumption, area-averaging is applied to the pressure coefficients:

$$c_{p,i}(t) = \sum_{j=1}^{N} c_{p,ij}(t)\, A_{ij} \tag{1}$$

Where the subscripts i and j are representative of the location of the considered tap along the depth d and bredth b, respectively, and A_{ij} is the corresponding tributary area. The time series of Eq. (1) allow evaluation of the mean wind loading of the roof as a function of the alongwind position, $\bar{c}_{p,i}$ (see Figure 1a). On the other hand, in the case of skew winds the pressure distribution can be highly variable in the two plan direction, and can possibly give rise to larger resulting loads.

In order to define a simplied load pattern for Code implementation, equivalent pressure coefficients must be defined. Their design values are representative of the maximum (positive) and minimum (negative) values within a reference period $T = 10$ min, such that combined with the return velocity pressure they provide the return wind load. EV analysis is needed to assess their value, and according to the work of Cook and Mayne (1979) based un the UK wind climate, these turn out to be the 78-fractile of the Fisher-Tippet Type 1 (FT1) distribution.

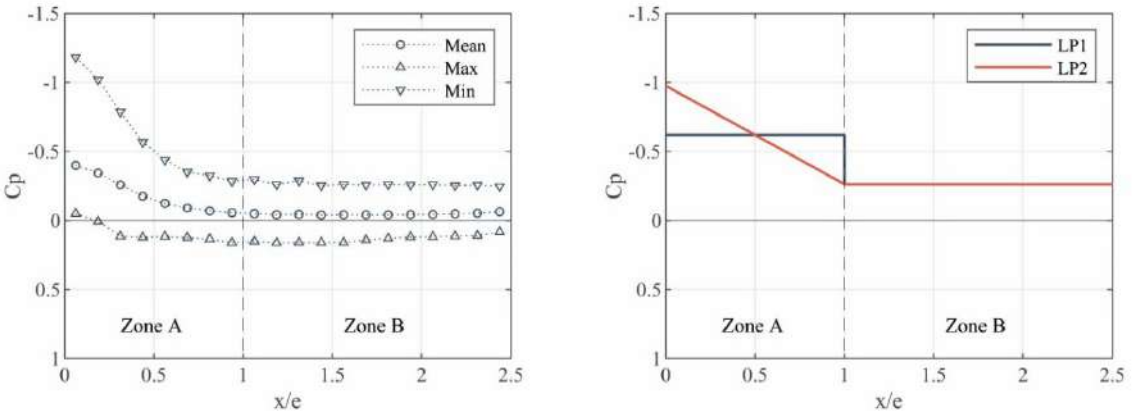

(a) (b)

Figure 1. Effective (a) and simplified (b) patterns for pressure coefficients for a building with a plan ratio *d*:*b* = 5:2, and an aspect ratio *h*:*b* = 1:2.

For example, in the case of flat roofs, two load patterns (LP) are proposed, based on the current wind loading zones of the CNR Guidelines: LP1, in which the coefficient of pressure is assumed as a constant within the two loading zones; LP2, in which the coefficient of pressure is assumed as linearly distributed in zone A, and constant in zone B (see Figure 2b). The coefficients $c_{p,A}$ and $c_{p,B}$ for both load patterns LP1 and LP2 are thus calibrated.

3. EXPECTED RESULTS

In the full paper, a comparison among the different proposed load patterns will be carried out, as well as a comparison with the current values. Current global pressure coefficients are the result of an envelope of the $c_{p,10}$ coefficients with varying building dimensions; the latter, in turn, are an envelope done in the occasion of the writing of the BS6399-2 (BSI, 1995) of the directional coefficients proposed by Cook (Cook, 1990). Therefore, it is expected that current values may lead an overestimation of the global wind load.

REFERENCES

British Standards Institution (BSI), 1995. BS6399-2 Loading for buildings – Part2: Code of practice for wind loads, London, UK.

European Committee for Standardization (CEN), 2020, Eurocode1: Actions on structures – Part 1-4: General actions – Wind actions (prEN1991-1-4:2020).

Consiglio Nazionale delle Ricerche (CNR), 2018. Istruzioni per la valutazione delle azioni e degli effetti del vento sulle costruzioni (CNR-DT 207 R1/2018) (in Italian)

Cook, N.J., Mayne, J.R., 1979. A Novel Working Approach to the Assessment of Wind Loads for Equivalent Static Design. Journal of Wind Engineering and Industrial Aerodynamics, 4, 149–164.

Cook, N.J., 1990. The designer's guide to wind loading of building structures, Part 2. Building Research Establishment, Butterworths, London, UK.

Quan, Y., Tamura, Y., Matsui, M. Cao, S.Y., Yoshida, A., 2007. TPU aerodynamic database for low-rise buildings. Proceedings of 12th International Conference on Wind Engineering (ICWE), Cairns, Australia

State augmentation method for buffeting analysis of structures subjected to non-stationary wind

Simian Lei [1,2], Wei Cui [3], Luca Patruno [4], Stefano de Miranda [5], Lin Zhao [6], Yaojun Ge [7]

[1]Tongji University, Shanghai, China, 1810723@tongji.edu.cn
[2]University of Bologna, Bologna, Italy, simian.lei@unibo.it
[3]Tongji University, Shanghai, China, cuiwei@tongji.edu.cn
[4]University of Bologna, Bologna, Italy, luca.patruno@unibo.it
[5]University of Bologna, Bologna, Italy, stefano.demiranda@unibo.it
[6]Tongji University, Shanghai, China, zhaolin@tongji.edu.cn
[7]Tongji University, Shanghai, China, yaojunge@tongji.edu.cn

SUMMARY
Extreme winds such as hurricanes and thunderstorms often present non-stationary characteristics, having time-varying mean wind speeds and non-stationary wind fluctuations. When concerning the wind-induced vibrations under non-stationary winds, the excitation will be a non-stationary process, and the wind-structure coupled system can be represented by a linear time-varying system. The aim of this study is to present a state augmentation method to investigate the non-stationary buffeting of a model bridge tower subjected to a non-stationary wind with consideration of the aeroelastic damping. Based on the theories of stochastic differential equations and Itô's lemma, the statistical moments of the non-stationary buffeting response are derived through solving a first-order ordinary differential equation system. The proposed method is validated by comparisons with Monte Carlo simulations. The result shows that the state augmentation method has higher accuracy and efficiency than the well-known Monte Carlo method.

Keywords: Non-stationary winds, Buffeting response, Itô's lemma

1. INTRODUCTION

Extreme wind events such as hurricanes and thunderstorms always exhibit considerable non-stationary characteristics, having time-varying mean wind speeds and non-stationary wind fluctuations. The rapid changes in these flows can potentially amplify aerodynamic loads on structures and result in higher non-stationary buffeting responses. When considering aeroelastic effects, the aerodynamic damping will be time-dependent due to the time-varying mean wind speed, and the wind-structure coupled system can be thus represented as a linear time-varying (LTV) system (Hu et al., 2013).

In view of these non-stationary effects, many attempts have been made to develop random vibration theory for non-stationary buffeting, including the Monte Carlo method, generalized frequency-domain method, and pseudo excitation method. However, some methods may need intensive calculations due to time-integration process, and some may be difficult to consider time-dependent system properties.

Based on the theory of Itô's stochastic differential equation, Grigoriu (Grigoriu and Ariaratnam, 1988) proposed the state augmentation method to calculate the stochastic response of linear systems subjected to stationary excitations. With this method, the moments of any order of the response can be directly obtained by solving a system of linear differential equations with high efficiency. Although this method has been applied in several wind engineering problems, such as non-Gaussian turbulence (Cui et al. 2022), it has not been reported for non-stationary buffeting analysis. The aim of this paper is to extend the state augmentation method to investigate the non-stationary buffeting of a bridge tower under non-stationary winds.

2. METHODS

As an example of application of the present method, the bridge tower during construction stage is considered, as shown in Fig. 1. Only the vibration in the along-wind direction is considered for the sake of simplicity.

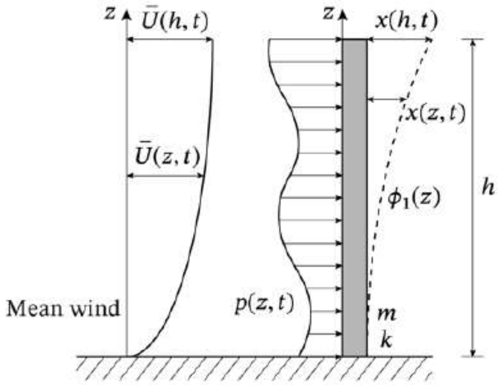

Figure 1. Schematic of the bridge tower.

The non-stationary wind speed is characterized as a time-varying mean and uniformly modulated wind fluctuations. To formulate the non-stationary buffeting forces, the strip and quasi-steady theories are invoked. The aeroelastic term is included by considering the relative velocity of the structural velocity and the total wind speed. By using the Ornstein–Uhlenbeck process to approximate wind fluctuations, the augmented states of the system and the excitation are written as an Itô-type stochastic differential equation. Based on Itô's lemma, the moments equation of the non-stationary response is derived as a system of first-order ordinary differential equations

$$\dot{\mathbf{m}} = \mathbf{P}\mathbf{m} + \mathbf{Q} \tag{1}$$

in which $\mathbf{m}$ is the vector of the response variances; $\mathbf{P}$ and $\mathbf{Q}$ are the deterministic time-depending coefficients matrixes corresponding to the structure and wind field properties.

3. RESULTS

To illustrate the reliability of the state augmentation method, the proposed method is applied to calculate the buffeting response of a bridge tower subject to a non-stationary wind field consisting of a time-varying mean and a stationary wind fluctuation. Fig. 2 shows the time-varying mean wind speed and the Simiu's spectrum for the stationary wind fluctuations.

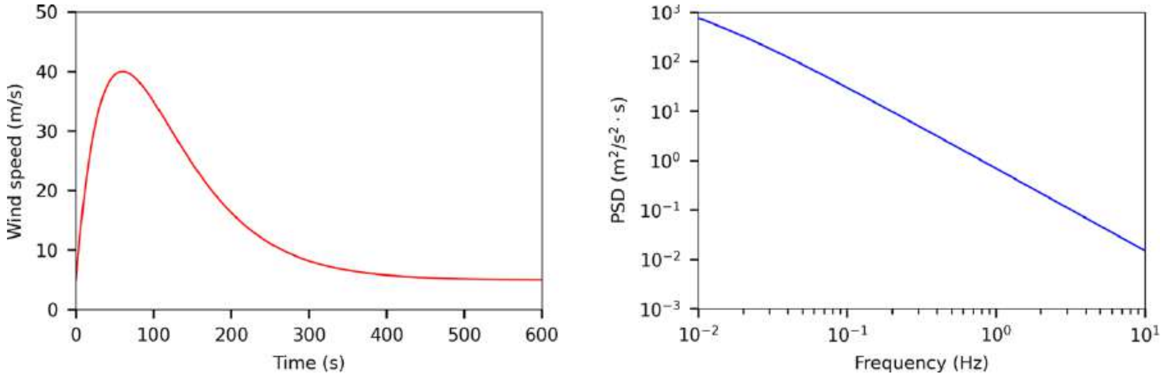

(a) (b)

Figure 2. Adopted non-stationary wind speed model: (a) time-varying mean wind speed; (b) PSD of the stationary fluctuating wind component based on Simiu's spectrum.

The obtained results are validated by comparing them with those obtained using Monte Carlo simulations. The stationary wind fluctuation samples for the Monte Carlo simulation are generated from the Simiu's spectrum given by Fig. 2 (b). A fourth-order Runge-Kutta method with an error estimator of fifth order is used to calculate the time history responses, with integration step $\Delta t = 0.01$ s, and the statistical characteristics of the responses at each instant of time are estimated over 1000 random samples. Fig. 3 shows the RMS at each instant of time for the along-wind displacement at the top of the bridge tower, given by the proposed state augmentation (SA) method and by the Monte Carlo (MC) simulation. These results are calculated from 0 s to 600 s.

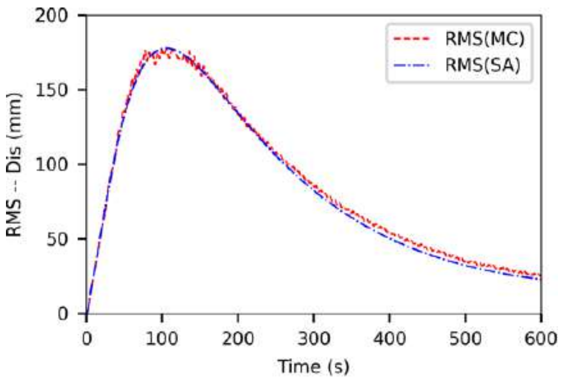

Figure 3. Displacement RMS of the tower top.

As shown in Fig. 3, the results obtained from the two methods are in very good agreement, which shows the reliability of the proposed method for determining the non-stationary buffeting response. Moreover, the computational efficiency of the proposed method (0.87 s) is much higher than that of the Monte Carlo simulations (2.6 h).

4. CONCLUSIONS

This study investigated the non-stationary buffeting of a bridge tower subjected to non-stationary wind loads. The strip and quasi-steady assumptions are adopted to formulate the buffeting forces and taking the motion-induced force into account. Based on the stochastic differential equation theory and Itô's lemma, a state augmentation method has been presented to calculate the statistical moments of the non-stationary buffeting response. The proposed state augmentation method is validated by comparisons with Monte Carlo simulations. In the Monte Carlo method, intensive simulations are needed due to the non-stationary characteristics of the response, whereas the proposed method is far more efficient.

ACKNOWLEDGEMENTS

The study was supported by the National Natural Science Foundation of China (grant No. 52008314 and 51978527) and the China Scholarship Council (No.202106260170).

REFERENCES

L. Hu, Y.-L. Xu, W.-F. Huang, 2013. Typhoon-induced non-stationary buffeting response of long-span bridges in complex terrain. Engineering Structures, 57, 406-415.

M. Grigoriu, S. Ariaratnam, 1988. Response of linear systems to polynomials of gaussian processes.

W. Cui, L. Zhao, Y. Ge, 2022. Non-gaussian turbulence induced buffeting responses of long-span bridges based on state augmentation method, Engineering Structures, 254, 113774.

Gust factor of the alongwind response of structures subjected to thunderstorm outflows

Luca Roncallo [1], Federica Tubino [1]

[1]*University of Genoa, Genoa, Italy, luca.roncallo@edu.unige.it*
[1]*University of Genoa, Genoa, Italy, federica.tubino@unige.it*

SUMMARY
This study investigates the possibility of generalizing the well-established Davenport gust factor technique to thunderstorm outflows. In particular, the sensitivity of the gust factor of the dynamic response of structures subjected to thunderstorm outflows on the parameters defining the slowly-varying mean wind velocity (the intensity of the background wind and the duration of the intense phase) is analyzed. At first, the intervals of variation of the parameters shaping the wind velocity are obtained from the analysis of 129 full-scale thunderstorm records. The gust factor is then analytically evaluated on varying said parameters. Results show that the dependence of the gust factor on these parameters is not negligible, especially for flexible and lowly-damped systems.

Keywords: Alongwind Response; Gust Factor; Non-stationarity; Thunderstorm outflows.

Over the last decades, a significant amount of research in the wind engineering field has been dedicated to the study of thunderstorm outflows and their impact on structures, aiming to develop models and tools to pursue a safer and cost-efficient structural design. However, the complexity of the phenomenon and the lack of data over which to validate the proposed models have prevented the development of an efficient and handy approach for the estimate of the maximum dynamic response as the one developed by Davenport for synoptic winds. Starting from a large number of wind velocity records collected in the Hight Tyrrenian Sea, Roncallo and Solari (2020) developed an Evolutionary Power Spectral Density (EPSD) model for thunderstorm wind speed, introducing a novel analytical representation for the slowly-varying mean wind velocity characterized by two parameters which possess a physical interpretation: the duration of the intense phase of the thunderstorm wind velocity and a measure of its intensity with respect to the background wind. Successively, the model has been adopted to estimate the maximum alongwind response of Single Degree of Freedom (SDOF) systems through a generalized formulation of the Davenport's gust factor using suitable equivalent parameters (Michaelov et al. 2001, Kwon and Kareem 2019), showing a satisfying agreement with the one obtained from full-scale thunderstorm records (Roncallo et al. 2022a, 2022b).

On the basis of these previous studies, the present paper investigates the sensitivity of the generalized gust response factor to the parameters characterizing the slowly-varying mean wind velocity. The problem is formulated in non-dimensional form, introducing suitable non-dimensional parameters. A new model for the modulating function for the slowly-varying mean wind velocity is proposed which allows to derive a closed-form solution of the Evolutionary Frequency Response Function (EFRF), required for the calculation of the EPSD of the dynamic response. The gust factor is thus evaluated for a set of SDOF systems characterized by fundamental frequency in the range [0.05 - 3] Hz and damping ratio in the range $\xi = [0.2 - 5]\%$, employing both the new modulating function and one of the models proposed by Roncallo and Solari (2020), fixing their parameters to best represent the ensemble of the 129 functions extracted from the thunderstorm records available (Roncallo and Solari 2020). Results show that, although the models for the slowly-varying mean wind velocity modulating function are mathematically different, they provide very similar results. This allows to employ the closed-form solution of the EFRF to carry out the analyses without affecting the quality of the results while drastically reducing the computational burden. Successively, the model is employed to fit individually the 129 records of the modulating functions and, per each of them, the two parameters are extracted. The range of variability of said parameters is thus estimated and adopted to carry out the sensitivity analysis on the gust factor. Results show that for highly-damped systems the sensitivity of the gust factor is very limited, whilst for lowly-damped ones it is significantly affected by their variability (Fig. 1). Fig. 1a shows that neglecting the role of the background wind (provided by the non-dimensional parameter γ^*), as assumed by other models in the literature (Kwon and Kareem 2019), may not be conservative. Moreover, Fig. 1b shows that the gust factor increases on increasing the non-dimensional duration of the intense phase of the thunderstorm, provided by the parameter $\mathcal{T}$.

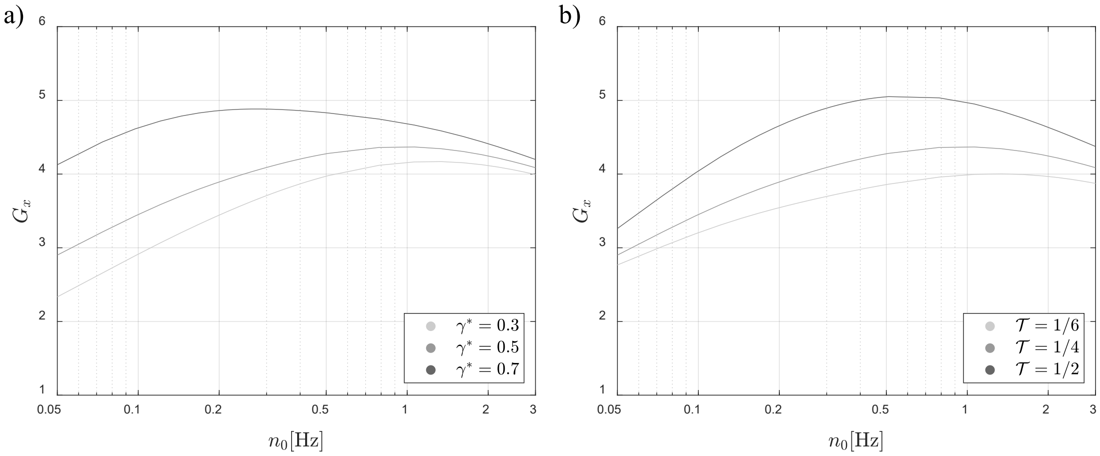

Figure 1. Gust factor variation on varying the non-dimensional background wind speed intensity γ^* ($\mathcal{T}$=1/4) (a) and the non-dimensional duration of the intense phase $\mathcal{T}$ (γ^*= 0.5) (b), for systems with damping ratio ξ = 0.2%.

ACKNOWLEDGEMENTS
This research is funded by the European Research Council (ERC) under the European Union's Horizon 2020 research and innovation program (grant agreement No. 741273) for the project THUNDERR - Detection, simulation, modelling and loading of thunderstorm outflows to design wind-safer and cost-efficient structures - supported by an Advanced Grant 2016. The authors are deeply grateful to Prof. Giovanni Solari for his essential contributions to the conceptualization and supervision of this research.

REFERENCES

Kwon, D.-K., Kareem, A., 2019. Towards Codification of Thunderstorm/downburst Using Gust Front Factor: Model-Based and Data-Driven Perspectives. Engineering Structures 199: 109608.

Michaelov, G., Lutes L. D., Sarkani, S., 2001. Extreme Value of Response to Nonstationary Excitation. Journal of Engineering Mechanics 127(4), 352–363.

Roncallo, L., Solari, G., 2020. An Evolutionary Power Spectral Density Model of Thunderstorm Outflows Consistent with Real-Scale Time-History Records. Journal of Wind Engineering and Industrial Aerodynamics 203: 104204.

Roncallo, L., Solari, G., Tubino, F., Muscolino, G., 2022a. Maximum dynamic response of linear elastic SDOF systems based on an evolutionary spectral model for thunderstorm outflows. Journal of Wind Engineering and Industrial Aerodynamics (under review).

Roncallo, L., Tubino, F., Muscolino, G., 2022b. Alongwind dynamic response of SDOF systems to thunderstorm outflows based on an evolutionary spectral loading model. Proceedings of the 14th American Conference on Wind Engineering.

An analysis of truck-driver system response to crosswind in tunnel exit conditions

R. Prakash [1], A. Cioffi [2], E. Sabbioni [3], M. Vignati [4], P. Schito [5]

[1]*Politecnico di Milano, Milano, Italy, anirudh.raghu@mail.polimi.it*
[2]*Politecnico di Milano, Milano, Italy, antonio.cioffi@polimi.it*
[3]*Politecnico di Milano, Milano, Italy, edoardo.sabbioni@polimi.it*
[4]*Politecnico di Milano, Milano, Italy, michele.vignati@polimi.it*
[5]*Politecnico di Milano, Milano, Italy, paolo.schito@polimi.it*

SUMMARY
Adverse weather conditions lead to accidents on extra-urban roads. Cross-wind is one of the major causes in the case of heavy vehicles. When considering high-sided vehicles characterized by big lateral surface area, the aerodynamic forces due to cross-wind are not negligible. When these forces are high, risks as adjacent lane invasion, wheel lift-off and, in the worst cases, roll-over may happen. To mitigate them, the interaction between cross-wind and vehicle-driver system has been studied. Given that this phenomenon is aggravated by structure interaction, the tunnel-exit condition has been investigated in this work. Vehicle and aerodynamic models have been developed to model the phenomenon. An ad-hoc scenario has been created and tested with the help of the dynamic driving simulator of Politecnico di Milano and 28 test drivers. They tested a combination of different vehicle and wind speeds. This numerical-experimental methodology can be adopted and modified accordingly to investigate similar phenomena.

Keywords: Vehicle-Driver Interaction, Driver Simulator, Vehicle-Wind Interaction

1. INTRODUCTION

According to the survey ISTAT, 2018 on road accidents in Italy, it is estimated that about 10% of the total crashes on extra urban roads can be attributed to adverse weather conditions. When considering high sided vehicles, characterized by a big lateral surface, crosswind can be considered dangerous for the driver and road users. The risk is mainly connected to the turbulent nature of the flow, and the dynamic excitation that it can induce on the vehicle and on the driver response.

Studies on this topic have been conducted by Rocchi et al., 2012. The authors proposed a numerical-experimental methodology to study the response of a truck when subject to the wake of a bridge tower under crosswind. After characterizing the aerodynamic coefficients of the vehicle through wind tunnel tests, the respective loads are introduced in the dynamic model following a procedure proposed by Charuvisit et al., 2004.

In this study, the vehicle-driver system response to crosswind when exiting a tunnel is investigated. The entire work has been performed on the DiM-400 dynamic driving simulator of Politecnico di Milano. The aim is to fully understand the phenomenon to avoid the rise of critical situations like lane invasion or vehicle rollover.

The article is organized as follows. At first, the methodology is presented. Then, the numerical models used are described. Finally, the results and the major conclusions drawn have been reported.

2. METHODOLOGY

For this study, a vehicle and aerodynamic model have been coupled to study the vehicle-driver system response when subject to crosswind at tunnel exit condition.

Everything has then been tested on the DiM-400 dynamic driving simulator facility available at the Politecnico di Milano. After calibrating the model on the driving simulator, an experimental campaign with 28 different drivers was carried out.

The results have been analyzed to assess the relation between vehicle behavior like yaw, roll and driver control inputs (primarily in terms of steer angles and steer torque application). Other global parameters such as vehicle lane deviation and normalized load transfers have also been evaluated.

3. NUMERICAL MODELS

In this section the vehicle model, aerodynamic model and the simulation scenario will be described.

3.1. Vehicle model

The vehicle dynamics model has been developed using the multibody software VI-CarRealTime, from VI-Grade. The relevant vehicle data for the models have been obtained from previous studies carried out by Cheli et al., 2011. A simplified suspension system has been used. The steering system was modelled carefully to reproduce appropriate values of steering torque. The tires have been modeled using the Magic Formula MF-05 of Pacejka, 2012.

3.2. Aerodynamic model

To reproduce the crosswind excitation on the vehicle, a Simulink model was developed. The loads are calculated using a quasi-static approach. Thus, the relative wind speed is computed at first. Then, the angle of attack is evaluated. This angle is used to evaluate the aerodynamic coefficients through lookup tables. The coefficients have been obtained from the work performed by Cheli et al., 2011. Finally, the loads are obtained. To reproduce the tunnel exit condition, the loads are applied proportionally to the exposed area.

3.3. Scenario

The simulation scenario has been created using Roadrunner. It consists of a straight road with a length of 2 km. On the road, 5 tunnels of length 75m have been placed. The tunnels are equally spaced. In each section and for each driver, different wind speeds have been selected to conduct the experiment. The wind speed and orientation (wind blowing from left or right) were chosen in a random manner for each section. The driver was assigned the task to remain at the center of the lane.

The test matrix is reported in Table 1. Both turbulent and non-turbulent wind has been tested.

Table 1. Test Matrix.

Vehicle Configuration	Vehicle Speed	Wind Speed
Empty	65 km/h	± 15/20/25 m/s
	80 km/h	± 15/20/25 m/s
Laden	65 km/h	± 20/25/30 m/s
	80 km/h	± 20/25/30 m/s

4. RESULTS

In this section the results obtained from the experimental campaign will be reported.

4.1. Lateral deviation

The mean and standard deviation of the maximum lateral displacement with respect to the center of the lane is reported in Fig. 1. It refers only to the empty vehicle configuration.

On increasing both vehicle and wind speed, there is an increase in the lateral displacement from the lane center.

4.2. Normalized load transfer (NLT)

The NLT is computed, and the mean and standard deviation of its maximum are plotted in Fig. 1. Again, the data plotted is referred to the empty vehicle configuration. Also in this case, increasing vehicle and wind speed, there is an increase in NLT.

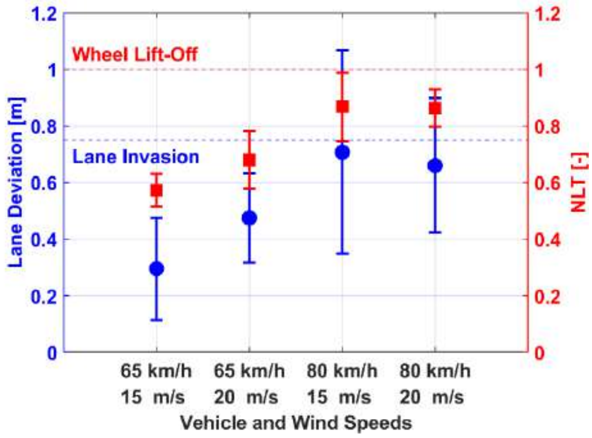

Figure 1. Mean and std. deviation of lane deviation and NLT for different vehicle and wind speed conditions

4.3. Driver-Control response

The primary control input for the driver is the steering torque. From preliminary investigation, there is no marked correlation between vehicle and wind speed and the time delay for reaching the maximum steering torque. However, there is an increase in the absolute value of both the mean and standard deviation of the maximum steering torque, as shown in Fig. 2.

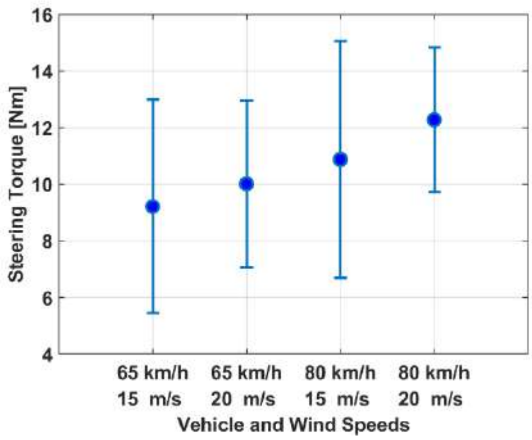

Figure 2. Mean and std. deviation of steer torque

5. CONCLUSIONS

A numerical-experimental procedure has been defined to study crosswind at tunnel exit. This method can be further developed to understand the effect of wind fences, bridge towers, etc. on the vehicle-driver response.

Thanks to these tests, a driver model can be realized or tuned to guarantee the same response shown from the real driver. Developing such a model is necessary to correctly test the effect of wind fences for mitigating the crosswind phenomenon.

Moreover, the use of a driving simulator allows to further develop and create scenarios (adding other vehicles, low visibility, rain/snow, and crosswind combination, etc.) that can be used to better understand the human driver reaction in such challenging conditions.

REFERENCES

Charuvisit, S., Kimura K. and Fujino Y., "Effects of wind barrier on a vehicle passing in the wake of a bridge tower in cross wind and its response", Journal of Wind Engineering and Industrial Aerodynamics, Vol. 92, 2004, pp. 609–639.

Charuvisit, S., Kimura K. and Fujino Y., "Experimental and semi-analytical studies on the aerodynamic forces acting on a vehicle passing through the wake of a bridge tower in cross wind", Journal of Wind Engineering and Industrial Aerodynamics, Vol. 92, 2004, pp. 749–780.

Cheli, F., Corradi R., Sabbioni E., Tomasini G., "Wind tunnel tests on heavy road vehicles: Cross wind induced loads-Part 1", Journal of Wind Engineering and Industrial Aerodynamics, Vol. 99, 2011, pp. 1000-1010.

Cheli, F., Ripamonti F., Sabbioni E., Tomasini G., "Wind tunnel tests on heavy road vehicles: Cross wind induced loads-Part 2", Journal of Wind Engineering and Industrial Aerodynamics, Vol. 99, 2011, pp. 1011-1024.

ISTAT, "Incidenti Stradali", 2018

Pacejka, H., "Tire and Vehicle Dynamics", Butterworth-Heinemann ,2012.

Rocchi, D., Rosa L., Sabbioni E., Sbrosi M., Belloli M., "A numerical–experimental methodology for simulating the aerodynamic forces acting on a moving vehicle passing through the wake of a bridge tower under cross wind", Journal of Wind Engineering and Industrial Aerodynamics, Vol. 104–106, 2012, pp. 256-265.

Effects of downsampling on the prediction of the Italian extreme winds

A. Akbaba [1], V. Picozzi [2], A.M. Avossa [3], F. Ricciardelli [4]

[1]*University of Campania "Luigi Vanvitelli", Aversa, IT,* andac.akbaba@unicampania.it
[2]*University of Campania "Luigi Vanvitelli", Aversa, IT,* vincenzo.picozzi@unicampania.it
[3]*University of Campania "Luigi Vanvitelli", Aversa, IT,* albertomaria.avossa@unicampania.it
[4]*University of Campania "Luigi Vanvitelli", Aversa, IT,* friccia@unicampania.it

1. INTRODUCTION

The primary step to assess wind actions on structures is the evaluation of design wind speeds and velocity pressures, which require statistical treatment of historical wind records. Extreme value analysis or spectral methods are commonly used, some of which have been reviewed by Palutikof et al. (1999). The available procedures are highly affected by the bias and randomness in the data, as well as by model and fitting uncertainties. Bias or systematic error can be corrected, whereas uncertainty can only be accounted for in reliability analyses. Design wind speeds can be either 10-min or 1-hour averages, or gust values. For an accurate analysis, averaged wind speeds must be measured continuously; therefore, if 10-min averages are selected, in compliance with the Eurocode format, the sampling period shall also be 10 minutes, which gives rise to 144 readings a day. Yet, the availability of such records is limited, and mostly 10-min averages are sampled three hourly (SYNOP) or one hourly/ half-hourly (METAR). While correction of the available datasets for roughness, orography, anemometer height and averaging time is commonly carried out, correction for downsampling is very seldom made. Unfortunately, the effect of downsampling has not been investigated extensively, and just a few researchers contributed to this topic, e.g., Larsen and Mann (2006), Chiodi and Ricciardelli (2011), and Li (2018).

In this paper, the effect of downsampling on the prediction of design wind speed for the Italian territory is studied, using a correction method for synoptic events recently proposed by the authors. Possible mixed wind climates are not in the scope of the study. The datasets consist of SYNOP records from 26 Italian stations, which have a sampling period of three hours. The mean wind velocities were transformed into standard conditions considering the effects of anemometer height. The observation period varies from station to station, and years lacking 10% of the data or more are removed from the datasets.

2. METHODOLOGY

To quantify the effect of downsampling with available wind data, datasets are artificially downsampled, and from 3 hourly sampled data, sub-datasets with different sampling periods are created up to 24 hours of a sampling period. For each subsampling period, expected values of the yearly maximum wind speeds are calculated, and the expected yearly maxima coming from the different subsampled records are averaged, producing one single expected value for each sampling period. All the mean wind speed values from different sampling periods are then divided by the expected value of the averaged wind speed. The inverse of this value is plotted against the sampling period and fitted to the Equation:

$$\rho_{\Delta T}(T_s) = \frac{V_{Ts}}{V_{\Delta T}} = \left[1 - a^* \cdot log\left(\frac{\Delta T}{T_s}\right)\right]^{-1/b^*} \tag{1}$$

using nonlinear Least Square Method, so to obtain the parameters a^* and b^*. In Eq. (1) ΔT and T_S are the original and target sampling periods, respectively.

The correction factor to be applied to each epoch maximum of a heterogeneous datasets turns out to be:

$$\rho_{\Delta T} = \frac{V_{10'}}{V_{\Delta T}} = \frac{V_{10'}}{V_{Ts}} \cdot \frac{V_{Ts}}{V_{\Delta T}} = \frac{\rho_{\Delta T}(T_s)}{\rho_{10'}(T_s)} = \rho_{Ts} \cdot \rho_{\Delta T}(T_s) \tag{2}$$

The correction coefficient for heterogeneously sampled datasets is evaluated year by year through Eq. (2) and used to correct the maximum yearly wind speed; the latter are then used for EV analyses.

3. EXPECTED RESULTS

The maximum downsampling correction coefficient was calculated as 1.27 for the Lamezia Terme (LICA) station, and the minimum value is 1.11 for the Grazzanise (LIRM) station. The average downsampling correction coefficient was calculated as 1.16 for three hourly downsampled SYNOP stations. Table 1 shows the results of 4 out of 26 stations; EV analysis was carried out by fitting the yearly maxima to the EV Type I distribution using the Ordinary Least Square Method with Gringorten plotting positions.

Table 1. Uncorrected and corrected Gumbel parameters and 50-year return wind speeds for the stations of Napoli Capodichino (LIRN), Roma Ciampino (LIRA), Milano Malpensa (LIMC) and Pisa San Giusto (LIRP).

ICAO Code	Anemometer Height	Height Correction Factor	α	α*	β	β*	V_{50}	V^*_{50}
	[m]	[–]	[–]	[–]	[m/s]	[m/s]	[m/s]	[m/s]
LIRN	6.5	1.0885	2.68	3.21	16.58	19.82	26.93	36.50
LIRA	10.5	0.9909	2.37	2.51	16.32	16.98	24.64	28.57
LIMC	10	1.0000	1.80	1.96	15.97	17.44	22.29	26.16
LIRP	6.5	1.0885	1.91	2.29	15.14	17.80	21.58	26.92

REFERENCES

Palutikof, J. P., Brabson, B. B., Lister, D. H., Adcock, S. T., 1999. A review of methods to calculate extreme wind speeds, Meteorological Applications n. 6, pp. 119–132.

Larsén, X. G., Mann, J., 2006. The effects of disjunct sampling and averaging time on maximum mean wind speeds,
Journal of Wind Engineering and Industrial Aerodynamics n. 94, pp. 581–602.

Chiodi, R., Ricciardelli, F., 2014. Three issues concerning the statistics of mean and extreme wind speeds, Journal of Wind Engineering and Industrial Aerodynamics n. 125, pp.156–167.

Li, S.H., 2018. Effect of disjunct sampling on calibration of design wind speed, Journal of Wind Engineering and Industrial Aerodynamics n. 183, 283–294.

Picozzi, V., Akbaba, A., Avossa, A.M., Ricciardelli, F., 2022. Correction of historical records to improve the reliability of design wind speeds, Engineering Structures (under revision).

Insights into the transcritical Reynolds number range based on field measurements of a wind turbine tower

Ika Kurniawati [1], Francesca Lupi [1,2], Marc Seidel [3], Hans-Jürgen Niemann [1,2], Rüdiger Höffer [1,2]

[1]*Ruhr-Universität Bochum, Bochum, Germany, ika.kurniawati@ruhr-uni-bochum.de*
[2]*Niemann Ingenieure GbR, Bochum, Germany*
[3]*Siemens Gamesa Renewable Energy GmbH & Co. KG, Hamburg, Germany*

SUMMARY
The estimation of vortex shedding load is essential for the prediction of Vortex-Induced Vibration (VIV) on slender bodies. The application of the VIV model to a full-scale slender tower, such as wind turbine towers and chimneys, depends on the estimation of actual vortex shedding load under field conditions. This paper aims to provide insight on the vortex shedding load and its spectrum for a full-scale wind turbine tower through a field measurement campaign. The transcritical flow regime, which requires high effort to observe in the wind tunnel scale, is addressed by pressure and response measurements at full scale. The effects of surface roughness on the tower prototype as well as the influence of ambient condition such as wind profile, wind direction and turbulence intensity are discussed. Global Strouhal number in high Reynolds numbers, spectrum of tower response in lift direction, and the estimation of critical velocity are calculated.

Keywords: Field measurement, Transcritical Reynolds number range, Vortex shedding

1. INTRODUCTION

The development of VIV models began in the 1960s to this day encompasses a wide range of approaches, mainly distinguished between 1-DOF or 2-DOFs models. In between, the models are also distinguished by their approach, such as wake-oscillator models, aerodynamic damping models, and effective correlation length models. Currently, the Vickery&Basu approach (Vickery and Basu, 1983) for VIV model is used as a basis in the European building code Eurocode 1 2010 and in the CICIND guidelines 2010 and 2011. In this approach, 1-DOF equation of motion is used and the aeroelastic interaction is represented by the "*aerodynamic damping*", K_a (See Eq. (1) and (2))

$$\sigma_{y,n}^2=S_{L,n}(f_n)\cdot\frac{1}{(\omega_n^2\cdot M_n)^2}\cdot\frac{\omega_n}{8\cdot\frac{\rho\cdot d^2}{m_{eq,n}}\cdot\left(\frac{Sc}{4\pi}-K_a\right)} \tag{1}$$

$$K_a=K_{a0}\cdot\left[1-\left(\frac{\sigma_y}{a_L\cdot d}\right)^2\right] \tag{2}$$

This model introduces that the response of a structure when VIV occurs is influenced by the interaction of structural damping and aerodynamic damping. The model describes the structural response σ_y and the vortex shedding load $S_{L,n}$.

However, this model often overestimates the structural response, as shown in recent studies on full-scale structures (Lupi et al., 2017). Through a series of wind tunnel experiments, Lupi et al. (Lupi et al., 2018) developed a model called "Damping Modified Spectral Method" (DMSM) based on the Vickery&Basu (V&B) approach. This model has a new aerodynamic damping function (See Eq. (3), where a, b, and c are constants) that differs in terms of the shape of K_a curve, however it improves the prediction of structural response closer to the measured full-scale data. Several other studies had supported the proposed model (Guo et al., 2021; Arunachalam et al., 2020). Full-scale measurement series are needed to further evaluate the model, especially for flow conditions that are rarely achieved in wind tunnel experiments. For example, high Reynolds numbers above Re=10^6 occurred easily and frequently in the flow around the full-scale wind turbine tower. The applicability of the model to predict VIV in full-scale can then be investigated by comparison to the field measurements.

$$K_a = a \cdot e^{-b \cdot \left(\frac{\sigma_y}{D}\right)} \cdot \left(\frac{\sigma_y}{D}\right)^{-c} \tag{3}$$

The first step in this currently ongoing investigation is to model the vortex shedding load as a narrow band spectral process centered around the Strouhal frequency, e.g. following the Vickery's approach using a Gaussian spectrum (Vickery and Clark, 1972). Then, to estimate the modal vortex shedding load (i.e. $S_{L,n}$, see equation 4) along the height of the structure. This paper focuses on addressing the vortex shedding spectrum directly from the full-scale pressure measurement data complemented by response measurements and estimating the global Strouhal frequency. In addition, the sectional Strouhal numbers and its integration along the height will be discussed. Field conditions such as wind direction and turbulence intensity, as well as tower surface roughness, are also considered to provide a realistic interpretation of the Reynolds number effects. For this purpose, two wind turbine towers are measured at the Østerild test site, and a MET tower nearby is also available.

$$S_{L,n}(f_n,z) \cong 2\lambda \cdot \int_0^H \left(\frac{1}{2}\rho V_m(z)^2\right)^2 \cdot D(z)^3 \cdot \frac{\sigma_{cL}^2}{\sqrt{\pi} \cdot St(z) \cdot \frac{V_m(z)}{d(z)} \cdot B} \cdot \exp\left(-\left(\frac{1-\frac{f_1}{St(z)\cdot\frac{V_m(z)}{d(z)}}}{B}\right)^2\right) \cdot \Phi_n(z)^2 \cdot dz \tag{4}$$

2. FIELD MEASUREMENT AND PREVIEW OF THE RESULTS

Two wind turbine towers located in Østerild test field in Denmark are subjected to the field measurement. Tower 1 (D8) is a single wind turbine tower without nacelle and Tower 2 (SG 1-222 DD, shorten to SG14) is erected with nacelle and blades. Bending moment at the bottom and acceleration at top of the tower were measured on D8, while for SG14, includes pressure measurements along the tower circumference. Period of data of D8 lasts from July until February 2022, while SG14 measurement campaign starts from December 2021 onwards. A MET Mast available for this analysis is located 1.23 km 210º southwest from D8 (Fig. 1), with available wind speed data for z/H=1.202, 1.168, 1.048, 0.747, and 0.447. Surrounding area of the test fields includes flat land with grass and small partitions of 10-20m height forest with dominating wind coming from the west.

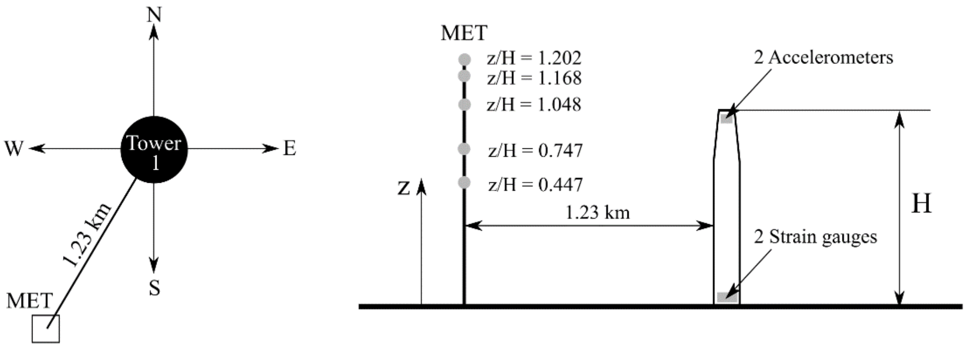

Figure 1. Sketch of Tower 1 and MET Mast tower

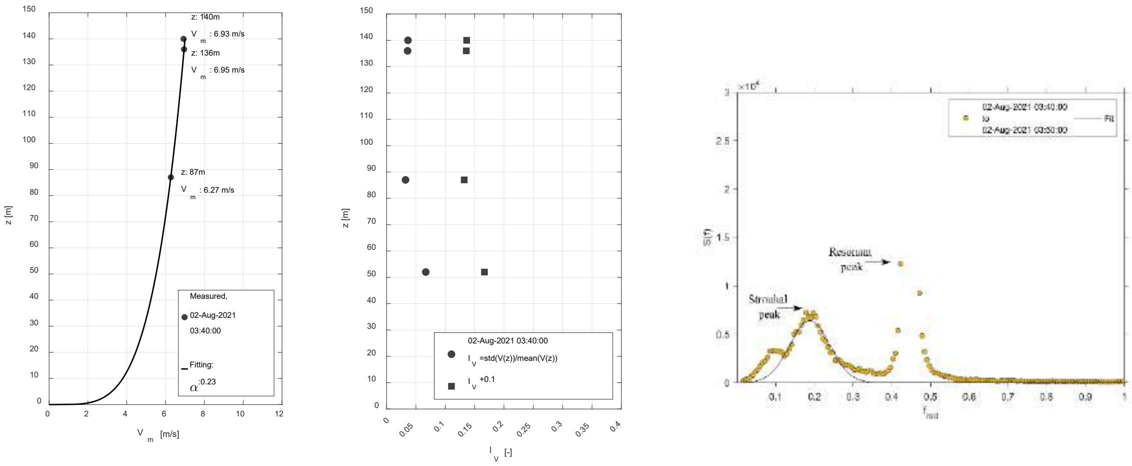

Figure 2. Samples of 10-minute wind profile and spectrum of the response in lift direction (Tower 1)

The wind turbine tower without nacelle D8 has the shape of a tapered circular cylinder with effective diameter D_{eff}=5.03 m and normalized height H/D_{eff}=23.15. Based on the measured data, the critical velocity is estimated around 15 m/s. To observe the vortex shedding spectrum, the signal from bending moment at the bottom of D8 Tower is evaluated. The data are processed and classified as a 10-minute time history, for both tower response and wind conditions. Fig. 2 shows the sample of 10-minute wind profile along the normalized height z/H and spectrum of the response S(f). Numerous wind speed with high transcritical Reynolds number ranges up to $Re \approx 9.4 \cdot 10^6$ are found throughout the data period.

The selection of appropriate dataset to observe the vortex shedding spectrum is important, where a clear and visible Strouhal peak usually occurs at wind speeds that are far from resonance. The Strouhal frequency, which corresponds to the vortex shedding spectrum, is calculated in the frequency domain by fitting a Gaussian function (Vickery and Clark, 1972). Several factors are also considered in this investigation, such as wind direction, turbulence intensity, and the quality of the data. Some exemplary results to examine the global vortex shedding peak are shown in Fig 3. (a) and (b). The wind direction and turbulence intensity I_V are discussed in relation the parameters bandwidth B. Evaluation on St and B values are further done to four datasets from four different dates that have different wind direction.

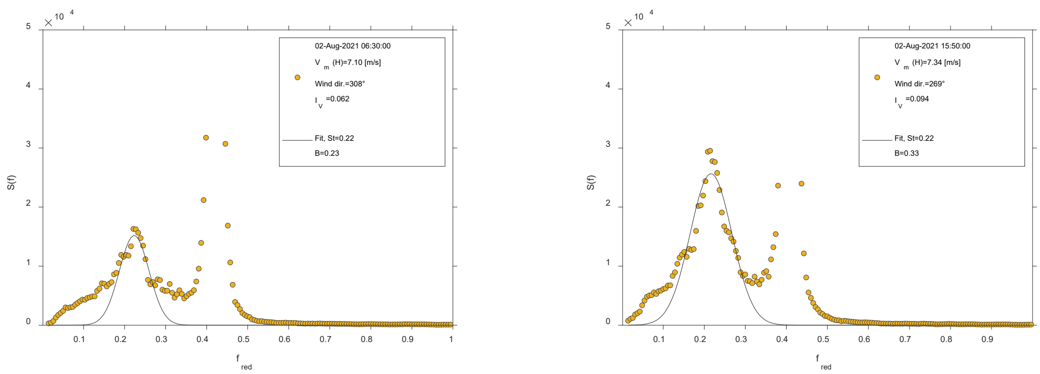

(a) (b)

Figure 3. Spectrum of response (Bending Moment, Tower 1) (a) Turbulence intensity, I_V = 0.062, (b) I_V = 0.094

ACKNOWLEDGEMENTS

This project is funded by the Deutsche Forschungsgemeinschaft (DFG, German Research Foundation) – Project number 493357786 and 426322127. The authors would like to also acknowledge CICIND (International Committee for Industrial Construction) for the support through the CICIND research project "Reynolds number disparity and its effect on vortex excitation – Insight from full-scale tests at wind turbine towers. Last but not least, we are very thankful to Siemens Gamesa Renewable Energy for providing the measurement data and excellent measurement system. The supports are gratefully acknowledged.

REFERENCES

Arunachalam, S., Lakshmanan, N., 2020. Non-linear modelling of vortex induced lock-in effects on circular chimneys. Journal of Wind Engineering and Industrial Aerodynamics 202.

Guo, K., Yang, Q., Liu, M., Li, B., 2021. Aerodynamic damping model for Vortex-induced Vibration of suspended circular cylinder in uniform flow. Journal of Wind Engineering and Industrial Aerodynamics 209.

Lupi, F., Niemann, H.-J., Höffer, R., 2017. A novel spectral method for cross-wind vibrations: Application to 27 full-scale chimneys. Journal of Wind Engineering & Industrial Aerodynamics 171, 353-365.

Lupi, F., Niemann, H.-J., Höffer, R., 2018. Aerodynamic damping model in vortex-induced vibrations for wind engineering applications. Journal of Wind Engineering & Industrial Aerodynamics 174, 281-295.

Vickery, B. J., Clark, A. W., 1972. Lift or Across-Wind Response to Tapered Stacks. Journal of the Structural Division 98(1).

Vickery, B.J., Basu, R.I., 1983. Across-wind vibrations of structures of circular cross-section. Part I. Development of a mathematical model for two-dimensional conditions. Journal of Wind Engineering and Industrial Aerodynamics 12(1), 49-73.

Stabilizer optimization for coupled flutter of long-span bridges with single wide box girders

Shengyi Xu [1], Genshen Fang [2], Yaojun Ge [3]

[1]*Tongji University, Shanghai, China, xushengyi@tongji.edu.cn*
[2]*Tongji University, Shanghai, China, fgs_root@163.com*
[3]*Tongji University, Shanghai, China, yaojunge@tongji.edu.cn*

SUMMARY
The installation of an appropriate stabilizer has a beneficial contribution on flutter. Plenty of research on the control effects of stabilizers has been done and it is gradually realized that the influence on flutter stability depends on the type of stabilizers. However, the mechanism of stabilizer optimization still needs further analysis. In this study, the flutter characteristics of two single wide steel box girders is investigated by setting up various types of UCVS (upper central vertical stabilizer), BCVS (lower central vertical stabilizer) and HS (horizontal stabilizer) and their combinations. Flutter derivatives are identified before the influence of stabilizers on damping characteristics is analyzed. A new indicator called NTC (nominal torsional center) is proposed to intuitively demonstrate the flutter modality accounting for both the influence of phase difference and amplitude ratio. The correlation between nominal torsional center and flutter derivatives and other indicators of flutter modality are compared to explain the influence of flutter derivatives on flutter modality and flutter critical wind speed.

Keywords: Stabilizer, Aerodynamic optimization, Coupled flutter analysis

1. FLUTTER PERFORMANCE AND AERODYNAMIC DAMPING RATIO

In this study, the Lingdingyang Suspension Bridge (1666 m) is utilized as the engineering background. The main girder with the heights of 4 m (Model A) and 5 m (Model B) are proposed during the design stage. The detailed geometric dimensions of two models are illustrated in Fig.1. The following parameters need to be defined: Relative height of UCVS $\kappa_1 = \mathrm{H}_1/\mathrm{H}$, relative height of BCVS $\kappa_2 = \mathrm{H}_2/\mathrm{H}$, relative length of HS $\gamma_1 = \mathrm{D}/\mathrm{H}$ to determine the length of HS.

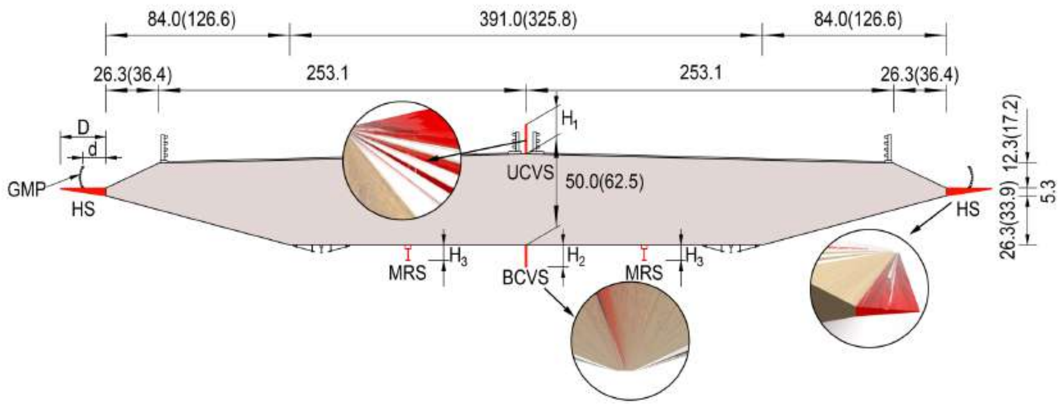

Figure 1. Cross-section of the sectional model (Unit: mm)

The SBS method (Ge et al., 2009) is used to solve the aerodynamic damping ratio ξ_a under difference wind speed. The aerodynamic damping ratio can be divided into the direct part and the indirect part, which can explain the reason of the variation of critical wind speed (U_{cr}), as shown in Fig.2-3. The installation of UCVS will increase the U_{cr} significantly at AOA (attack of angle) of 3° due to increase of aerodynamic damping ratio of the direct part. Contrary, BCVS shows positive influence at the AOA of -3°. The reason is that the decline of the indirect part is more significant than the direct part compared the original girder. The simultaneous installation of UCVS and BCVS allows the U_{cr} at AOA of 0° to increase dramatically, which is because of the continuous decline of the indirect part with the increase of the total height of CVS and the direct part almost remains unchanged. AOA of +2°is the most sensitive AOA to the control effects of HS and U_{cr} can be increased up to 50%.

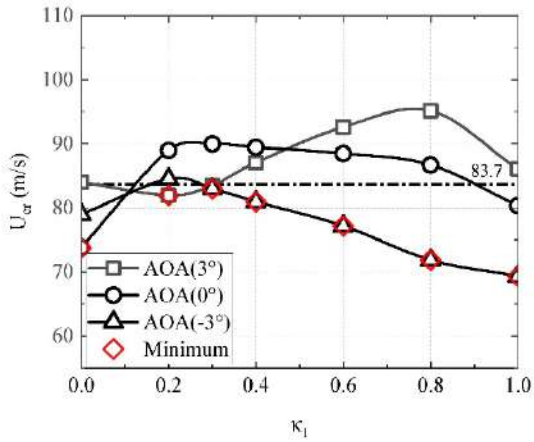

Figure 2. U_{cr} with UCVS

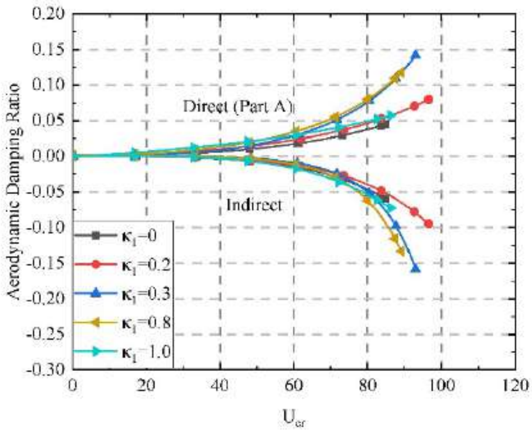

Figure 3. ξ_a with UCVS

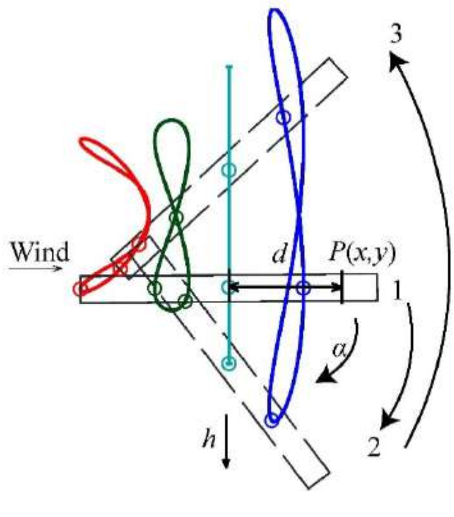

Figure 4. Motion curves

2. FLUTTER PERFORMANCE AND AERODYNAMIC DAMPING RATIO

The NTC (nominal torsional center) is proposed accounting for the combined effects of Ψ (amplitude ratio) and ψ (phase difference), which is defined as the point in the horizontal axis of the bridge deck with the shortest trajectory during flutter vibration, as shown in Fig.4. The mathematical expression of the nominal torsional center can be defined as:

$$\begin{aligned}\mathrm{NTC} &= \underset{2d/B}{\arg\min}\, [\oint_L ds \\ &= \underset{2d/B}{\arg\min}\, d \cdot \omega_f \int_0^{2\pi/\omega_f} \sqrt{\{\sin[\cos(\omega_f t)]\cdot\sin(\omega_f t)\}^2 + \{\frac{\sin[\cos(\omega_f t)]\cdot\sin(\omega_f t)}{\cos[\cos(\omega_f t)]\cdot\sin(\omega_f t)+\Psi\cdot B/_{2d}\cdot\sin(\omega_f t+\psi)}\}^2 dt}\end{aligned} \tag{1}$$

where $\oint_L ds$ is the curvilinear integral to calculate the length of trajectory, d is the distance related to the cross-section center, B is the width of the girder, ω_f is the flutter circular frequency.

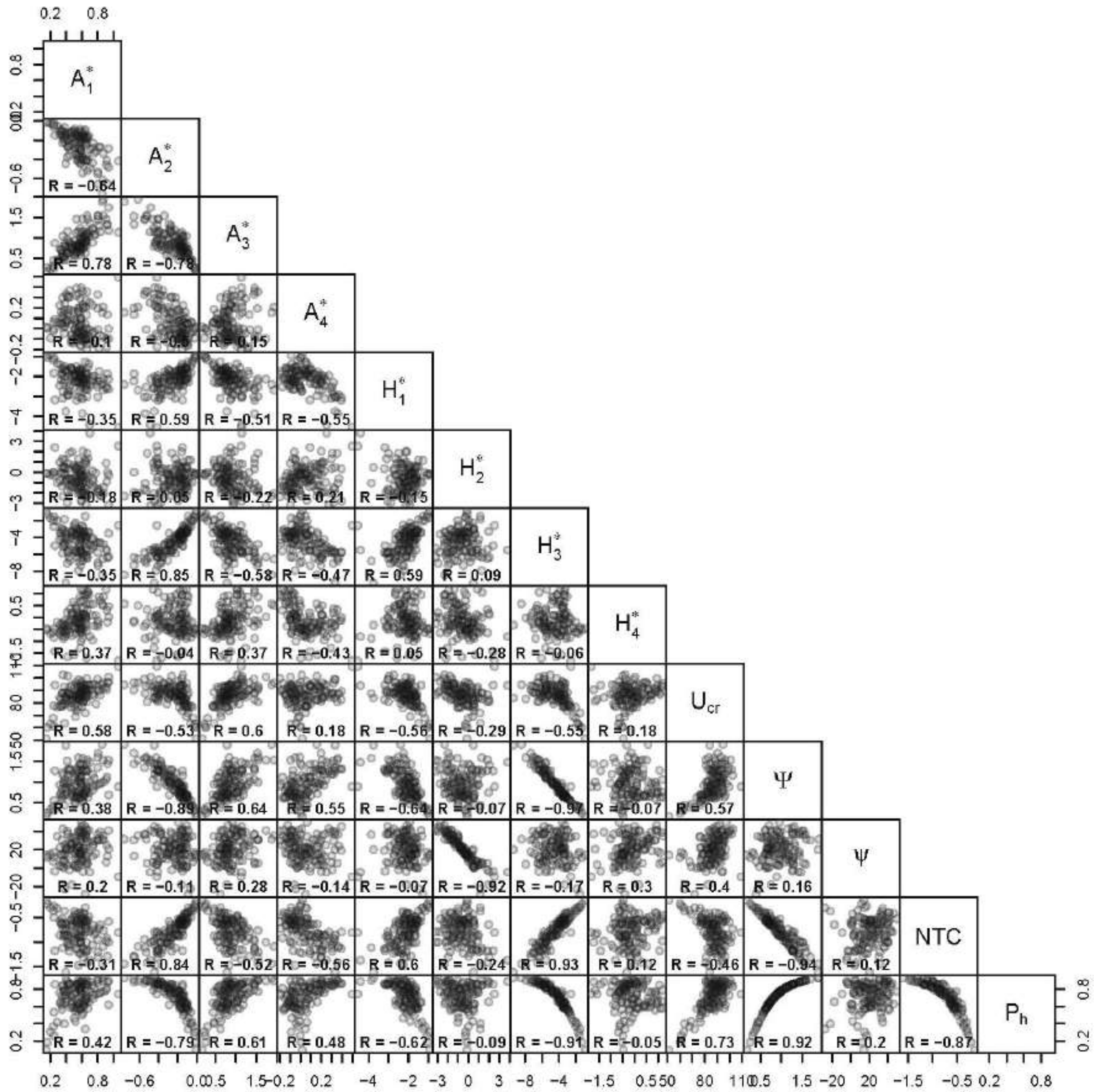

Figure 5. Correlation matrix

The intercorrelations between flutter derivatives, U_{cr} and indexes of flutter modality at the flutter onset of all cases are studied, as shown in Fig.5. Four indexes including Ψ, ψ, NTC and energy participation level (Mei et al., 2020) of the vertical bending motion are selected to describe the flutter modality. The correlation between Ψ and H3, ψ and H_2^* is observed, which means Ψ and ψ are mainly influenced by the self-excited lift force generated by torsional displacement or torsional velocity, respectively. Strong correlation between H_3^* and NTC or energy participation level also observed because of the transfer correlation between the indexes, as shown in Fig.6. Besides, moderate correlations are observed between flutter derivatives such as A_1^*, A_2^* and A_3^*, A_2^* and H_1^*, A_2^* and H_3^*, A_3^* and H_3^*, A_4^* and H_1^*, H_1^* and H_3^*.

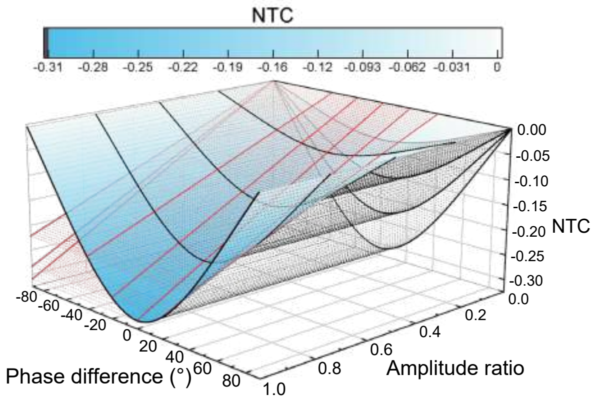

Figure 6. Parametric analysis

3. CONCLUSION

The appropriate installation of UCVS and BCVS can vary the direct or indirect aerodynamic ratios independently which allows targeted adjustment of the total aerodynamic damping ratio.

NTC shows the flutter modality intuitively and the correlation analysis shows that NTC has strong dependency on the derivatives of H_3^*. But the flutter modality has little dependency on the U_{cr} mainly because of the derivatives of A_1^* has no clear correlation with flutter modality and cannot be neglected in the calculation of aerodynamic damping ratio.

ACKNOWLEDGEMENTS

The authors gratefully acknowledge the support of the National Natural Science Foundation of China (51778495, 51978527, 52108469), the Shanghai Pujiang Program (20PJ1413600), the independent subject of Key Laboratory of Wind-Resistant Technology for Bridges, Ministry of Communication (KLWRTBMC-07).

REFERENCES

Ge, Y., Zou, X. and Yang, Y., 2009. Aerodynamic stabilization of central stabilizers for box girder suspension bridges. Wind & structures, 12(4), pp.285-298.

Mei, H., Wang, Q., Liao, H. and Fu, H., 2020. Improvement of flutter performance of a streamlined box girder by using an upper central stabilizer. Journal of Bridge Engineering, 25(8), p.04020053.

Analytical model of the interaction between downburst outflows and atmospheric boundary layer winds

Masoud Moeini [1], Djordje Romanic [1]

[1] *Department of Atmospheric and Oceanic Sciences, Faculty of Science, McGill University, Montreal,Quebec, Canada, masoud.moeini@mail.mcgill.ca ; djordje.romanic@mcgill.ca*

SUMMARY
Downbursts are negatively buoyant downdrafts from thunderstorms that hit the earth's surface and create an outflow that spreads radially from the touchdown. The downburst outflow, however, is not spreading through a calm environment, but rather through an atmosphere characterized by larger-scale atmospheric boundary layer (ABL) winds. This interaction between ABL winds and downbursts forms an outflow that is more complex than the outflow created by an isolated downdraft. The focus here is to propose a new analytical model of nonlinear interaction between isolated downburst outflows and ABL winds when the ratio of downdraft velocity to the ABL velocity at the cloud base is large. The proposed analytical model is compared against field measurements of downbursts and wind tunnel simulations of downburst-like outflows.

Keywords: downbursts, atmospheric boundary layer winds, analytical model

1. INTRODUCTION

A realistic parametrization of downburst wind loading on structures and aircraft is hinged on the proper understanding of the dynamics of these wind systems. While the onset of a downburst is negative buoyancy of air subjected to evaporation and melting inside and beneath the cloud, the research has demonstrated that the near-surface outflow caused by downbursts can properly be modelled using the statically neutral impinging jets in a laboratory setting (Canepa et al, 2022; Romanic et al. 2020). Although this modelling approach has been successful in describing downburst-like outflows in some cases (Hjelmfelt, 1988), these experiments describe an idealized downdraft released into calm ambient only. This assumption is not necessarily consistent with observational evidence that downbursts are often generated in thunderstorms that move in the horizontal direction and, moreover, the descending downdraft is propagating through an atmosphere characterized by large-scale atmospheric boundary layer (ABL) winds (Xhelaj et al., 2020; Burlando et al., 2020; 2017). While the research suggests that the storm motion can be added to the isolated downburst (DB) as a vector addition of the two flows (e.g., Xhelaj et al., 2020; Holmes and Oliver, 2000), this method is not reliable in the description of the interaction between DB and ABL winds (Romanic and Hangan, 2020). Herein, we propose a new analytical model of DB-ABL wind interaction (i.e., a model of DBABL winds).

In the proposed model, the base state of the outflow is considered to be an isolated downburst-like impinging jet that is assumed to be known and properly represented using empirical data. The model is based on the quasi-universality of a renormalization group whose degrees of freedom and domain of validity are determined from physical experiments. The correspondence of the variables employed in these renormalization groups to an actual downburst exposed to ABL winds is discussed in the next section. While the proposed model is not a closed-form solution of Navier-Stokes equations in turbulent flows, its analytical formulation is consistent with the mass continuity equation. The present model is applicable to the part of the outflow in which the ABL winds and DB outflow have the same sense. In the absence of ABL winds our model degenerates into equations of Poreh et al. (1967) for an isolated downburst, which is supported by field measurements of Hjelmfelt (1988).

2. MODEL DEVELOPMENT

The model is developed based on the use of the renormalization group:

$$\frac{u - u_{\mathrm{ABL}}}{u_m - u_{\mathrm{ABL}}} = 2.269\mathrm{e}^{-\frac{1.505z}{\delta}}\left(\frac{z}{\delta}\right)^{0.305} \tag{1}$$

that describes numerous laboratory measurements of velocity profiles of turbulent jets issuing into both quiescent and crossflowing backgrounds. Here, $u = u(r, z)$ is the radial velocity parallel to the ground and caused by the DBABL interaction, u_m is the maximum value of u at a given radial distance r, δ is the half-height, defined as the value of z at which $u - u_{\mathrm{ABL}} = 0.5(u_m - u_{\mathrm{ABL}})$, u_{ABL} is the ABL wind velocity in the same direction as u. Here, r and z represent the two cylindrical coordinates measured from the downdraft's centerline of impingement and ground, respectively. The present model assumes a "known" base state—corresponding to an isolated downburst—and determines the interaction between the two flows by way of perturbation analysis.

It can be demonstrated that, under certain assumptions, the vertical profile of ABL winds in the atmosphere can be modelled as:

$$u_{\mathrm{ABL}} = \begin{cases} 0.97u_{\mathrm{H}}\left(\frac{z}{z_m}\right)^{\frac{1}{7}}, & z \leq z_m \\ u_H, & z > z_m \end{cases} \tag{2}$$

where u_{H} is the ABL wind speed at the height of the cloud base (H) and z_m is the height of the maximum horizontal velocity in the DBABL outflow.

We further assume that any given state of DBABL at large ratios of DB to ABL velocities ($\lambda_J \equiv U_J/u_H$, where U_J is the centerline velocity in the descending downdraft at the cloud base) can be described by a 'base state', which corresponds to DB ($\lambda_J \to \infty$), perturbed by weak ABL winds. The base state in the proposed model is represented using the DB equations of Poreh et al. (1967). Namely, we postulate that the DBABL variables can be represented as:

$$u = \bar{u} + u' \tag{3}$$

$$u_m = \bar{u}_m + u'_m \tag{4}$$

$$\delta = \bar{\delta} + \delta' \tag{5}$$

where the overbar denotes the base state (DB), and the primed variables represent small perturbations caused by ABL winds.

Carrying out the perturbation analysis by substituting Eqs. (3–5) into Eq. (1), using Eq. (2) and further using the mass continuity equation in the integral form to determine δ' (note: many derivation steps and few additional assumptions are now omitted in this extended abstract), we arrive at a closed-form solution for the horizontal velocity in a DBABL outflow:

$$u = \bar{u} + u_{ABL} - \frac{6.25\bar{u}\left(\frac{r}{H}\right)^{0.2}(-0.1129 + \gamma_0 - \xi_0)\frac{z - \bar{z}_m}{H}}{\sqrt{c_w}\lambda_J\frac{D}{H}} \tag{6}$$

Here, $\gamma_0 - \xi_0 = 2.6$ and c_w (usually ≈1, but not >1) are constants that are derived from physical experiments of downburst-like impinging jets in wind tunnels and D is diameter of the downdraft.

3. RESULTS

Fig. 3 shows the modelled outflow velocity, u, by Eq. (6) as a function of height, z, corresponding to three different ABL winds. The parameters H, D and U_J in are selected to be consistent with the corresponding parameters measured for numerous downbursts during the Joint Airport Weather Studies (JAWS) Project field campaign measurements (Table 1 in Hjelmfelt, 1988). The profiles exhibit the well-known nose-shaped dependency with the height regardless of the intensity of ABL winds. The ABL winds result in the horizontal velocity, but the augmentation of the DB outflow nonlinearly depends on the height (and r but not shown in Fig. 1).

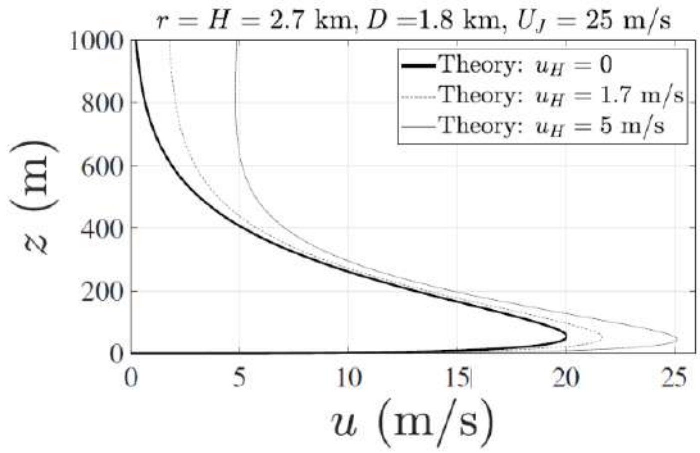

Figure 1. Vertical profile in the DBABL outflow using downburst parameters in Hjelmfelt (1988).

Model predictions are compared against wind tunnel measurements and a well-known DB model of Oseguera and Bowles (1998) in Fig. 2. The parameter c_w depends on the velocity profile at the nozzle and it was unknown in Romanic and Hangan (2020); hence, we tested two different values. The model matched the experiments better in the region above the height of the maximum velocity. Figure 2 further shows that our model gives similar predictions to Oseguera and Bowles' (1998) model when $\lambda_J \to \infty$. The matching between the two models is not perfect because our base state is represented by Poreh et al. (1967) rather than Oseguera and Bowles (1998). In contrast to Oseguera and Bowles (1998), our model accounts for the radial dependency of δ that is observed in laboratory tests of impinging jets.

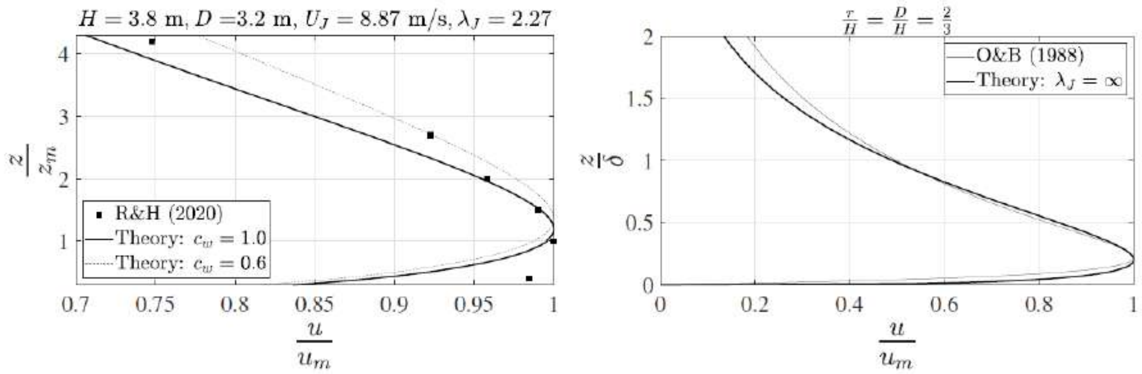

Figure 2. Comparison of the analytical model against (left) experimental measurements of downburst-like impinging jets released in ABL-like winds in Romanic and Hangan (2020); and (right) analytical model of Oseguera and Bowles (1998).

4. CONCLUSIONS

This research proposed a model of nonlinear interaction between an isolated downburst (DB) and atmospheric boundary layer (ABL) winds—the DBABL outflow. The way downbursts interact with ABL winds was taken to be analogous with the way impinging jets interact with ABL-like crossflows. Adapting this assumption, the perturbation analysis for large DB velocities compared to weak ABL winds provided a closed-form solution to the perturbation quantities. Using a DB-like impinging jet by Poreh et al. (1967)—constituting a base state that was assumed to be known—and the classic ABL wind profile, the DBABL velocity was analytically determined (see Eq. 6). The model is applicable to the part of the outflow where DB and ABL winds have the same sense.

ACKNOWLEDGEMENTS

This research was funded by the Wares Science Innovation Prospectors Fund grant (McGill University).

REFERENCES

Burlando, M., Romanic, D., Boni, G., Lagasio, M., Parodi, A., 2020. Investigation of the weather conditions during the collapse of the Morandi bridge in Genoa on 14 August 2018 using field observations and WRF model. Atmosphere 11.

Burlando, M., Romanic, D., Solari, G., Hangan, H., Zhang, S., 2017. Field data analysis and weather scenario of a downburst event in Livorno, Italy, on 1 October 2012. Monthly Weather Review 145, 3507–3527.

Canepa, F., Burlando, M., Romanic, D., Solari, G., Hangan, H., 2022. Experimental investigation of the near-surface flow dynamics in downburst-like impinging jets. Environmental Fluid Mechanics.

Hjelmfelt, M.R., 1988. Structure and life cycle of microburst outflows observed in Colorado. Journal of Applied meteorology and Climatology 27, 900–927.

Holmes, J. D., Oliver, S.E., 2000. An empirical model of a downburst. Engineering Structures 9.

Oseguera, R. M., Bowles, R. L., 1988. A simple, analytic 3-dimensional downburst model based on boundary layer stagnation flow. Tech. Rep. 100632, NASA Langley Research Center, Hampton, VA, USA.

Poreh, M., Tsuei, Y. G., Cermak, J. E., 1967. Investigation of a turbulent radial wall jet. Journal of Applied Mechanics 34, 457–463.

Romanic, D., Nicolini, E., Hangan, H., Burlando, M., Giovanni, S., 2020. A novel approach to scaling experimentally produced downburst-like impinging jet outflows. Journal of Wind Engineering and Industrial Aerodynamics 196.

Xhelaj, A., Burlando, M., Solari, G., 2020. A general-purpose analytical model for reconstructing the thunderstorm outflows of travelling downbursts immersed in ABL flows. Journal of Wind Engineering and Industrial Aerodynamics 207.

17th Conference on Wind Engineering – IN-VENTO 2022
Politecnico di Milano, IT 4 – 7 September 2022

Generation and application of synthetic inflow turbulence

Luca Patruno [1], Stefano de Miranda [2]

[1]*University of Bologna, Bologna, Italy, luca.patruno@unibo.it*
[2]*University of Bologna, Bologna, Italy, stefano.demiranda@unibo.it*

SUMMARY
The generation of synthetic inflow turbulence represents a crucial step in the setup of scale resolving simulations for wind loading assessment. In the last decade, the number of techniques proposed in the literature to this purpose has rapidly increased, often starting from widely different perspectives. While many of these prove satisfactory after appropriate tuning, some aspects are well-known to be problematic. In particular, after being "released" in the computational domain, turbulence often undergoes modifications and unphysical pressure fluctuations arise at the inlet. In this contribution, we discuss the main problems which need to be solved when generating synthetic turbulence. Then, we describe a new technique, the Variationally Based Inflow Correction, VBIC, which allows to apply unsteady velocity fields at the inflow patch, greatly moderating the insurgence of pressure fluctuations. The method is conceived in order to be extremely general and allows to be used in conjunction with any existing turbulence generation method.

Keywords: Synthetic turbulence, Inflow turbulence, Unsteady inflow conditions

1. INSTRUCTION

The generation of synthetic turbulence presents remarkable advantages with respect to other available methods such as the full wind tunnel simulation and recycling methods (Tabor and Baba-Ahmedi, 2010). In principle, it allows to have a much deeper control over the incoming turbulence, allowing to selectively change its characteristics and avoiding cumbersome calibrations in the case setup. In practice, many difficulties arise in the generation and application of synthetic turbulence, so that results often do not meet expectations fully. The problem lies in the fact that studies assessing turbulence generators performance consider different criteria: for instance, if the goal is to evaluate the velocity field only, spurious pressure fluctuations at the inlet might be a minor problem.

As it is well known, synthetic turbulence generation methods fall mainly into two categories; those based on the superposition of compact structures, usually denoted as Vortex Methods, VM, and those based on the superposition of planar waves, denoted as Spectral Methods, SM.

There are many aspects of the physics of turbulence which might be considered in devising a successful turbulence generation method. Without a doubt, complying with Navier-Stokes, NS, equations and appropriate boundary condition is a prerequisite to allow a smooth transmission of the synthetic field inside the computational domain. Unfortunately, many of the available turbulence generation methods do not meet such requirement: VM often privileges momentum conservation (linearized in the proximity of the time-averaged velocity field) while SM privileges mass conservation. In the following, we present two techniques useful for the generation and application of unsteady synthetic inflows.

2. PRFG[3]

To generate an inflow, the first step is to produce an appropriate random velocity field. Spectral methods usually move from time spectra and, by means of randomly generated numbers and imposing the divergence-free condition, obtain a three-dimensional random field (Huang et al. 2010). The Prescribed-wavelength Random Flow Generator[3] (Patruno and Ricci, 2018), PRFG[3], instead moves from a complete three-dimensional spectrum of the velocity field (each velocity component decomposed in three spatial directions) and imposes *a priori* both mass and momentum conservation. The imposition of the divergence-free constraint requires the fulfillment of existence conditions which must be accommodated modifying the selected three-dimensional target spectrum as little as possible. The target spectrum can be approximated starting from the knowledge of the integral scales.

3. VBIC

Once a synthetic field is generated, in the best-case scenario, it respects an approximation of NS. This is usually possible for homogeneous turbulence but, for inhomogeneous turbulence, such property is partially lost (the approximation gets poorer with increasing inhomogeneity). This is the typical condition found in atmospheric boundary layers. Additionally, the synthetic field does not respect boundary conditions on the edges of the inflow patch. For instance, see Fig. 1 (a), the fluxes on the sides of the inflow patch shall be prevented if symmetry conditions are adopted on the sides of the computational domain. The Variationally Based Inflow Correction Method (Patruno and de Miranda, 2020), VBIC, requires in input a random velocity field (generated with any of the available methods) and applies minimal corrections in order to impose the divergence-free condition and the appropriate boundary conditions on the sides of the inflow patch. The adopted corrections allow for a smooth transmission of the synthetic inflow inside the computational domain, reducing of approximately one order of magnitude the strength of spurious pressure fluctuations. For instance, Fig. 1 (b) reports the application of a simple synthetic inflow which is not divergence-free, so that strong spurious pressure fluctuations arise. A divergence-free inflow is shown in Fig. 1 (c), showing that undesired pressure fluctuations are still present at the inflow patch boundary. The application of VBIC helps in moderating all pressure fluctuations, as shown in Fig. 1 (d).

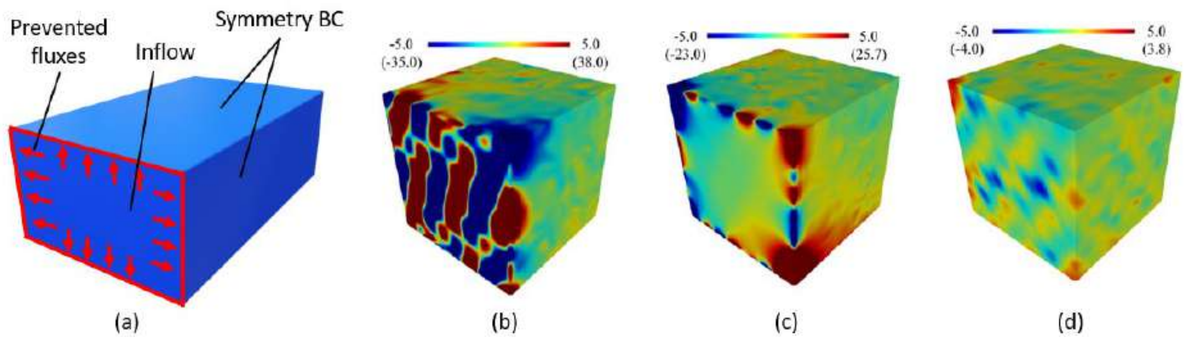

Figure 1. The VBIC method: (a) the prevented fluxes at the inflow patch, (b), (c) and (d) pressure fluctuations corresponding to non div-free inflow, div-free inflow and non div-free inflow with VBIC, respectively.

REFERENCES

Tabor, G., Baba-Ahmedi, M., 2010. Inlet conditions for large eddy simulation: a review, Comput. Fluids, 39, 553–567.

Huang, S., Li, Q., Wu, J., 2010. A general inflow turbulence generator for large eddy simulation, J. Wind Eng. Ind. Aerodyn. 98, 600–617.

Patruno, L., Ricci, 2018. M. A systematic approach to the generation of synthetic turbulence using spectral methods. Comp Meth App Mech Eng, 340, 881-904.

Patruno, L., de Miranda, S., 2020. Unsteady inflow conditions: A variationally based solution to the insurgence of pressure fluctuations. Comp Meth App Mech Eng, 363, 112894.

A numerical assessment to estimate the dynamic factor for wind excited façade elements having a natural frequency smaller than 5 Hz

Lori Guido [1], Manara Giampiero [1,2]

[1]*Permasteelisa Group, Vittorio Veneto, Country, g.lori@permasteelisagroup.com*
[2]*Permasteelisa SpA, City, Vittorio Veneto, g.manara@permasteelisagroup.com*

1. ABSTRACT

It is well known that, generally, wind is the major action affecting a façade and local effects are the leading ones.

The European standard about wind loads on buildings, Eurocode EN 1991-1-4 (CEN, 2005), follows an equivalent static approach, which allows to determine the wind acting forces:

$$F_w = c_c c_d \cdot \sum_{surfaces} w \cdot A_{ref}$$

To take into consideration possible resonance phenomena, it introduces the $c_s c_d$ structural factor, which should account for the effect on along-wind actions deriving from the non-simultaneous occurrence of peak wind pressures on the surface (c_s), together with the effect of the vibrations of the structure due to turbulence (c_d).

On such respect, at clause 6.2 (b) this standard reads: "For facade and roof elements having a natural frequency greater than 5 Hz, the value of $c_s c_d$ may be taken as 1". If this condition is not fulfilled, the standard proposes a formula for calculating the $c_s c_d$ value, which will result greater than 1. This remains a static approach and it doesn't ask for any investigation of what is the actual dynamic response of the façade element.

Moreover, no consensus exists in the scientific community about the 5 Hz limit adequacy, which may involve façade glass panes having sizes quite frequent nowadays and no justification is provided about the choice of this value.

Furthermore, not only glass infill panels may be affected by this rule: most of recent façades frequently show sun-shadings and other elements (fins etc.), protruding from the façade surface and having a slender shape.

Hence, it is worth to understand how far, or how close, the actual dynamic response of a façade element is to its static behaviour when excited by wind turbulence and then check for which natural frequency the non-static response might prevail.

In this paper we will calculate the dynamic response effects for along wind-actions, which might affect some façade elements and we will compare this value with the $c_s c_d$ value proposed by the standard.

Figure 1. An example of a façade with large glass panes and external glass fins

The analysis will be carried out considering a single degree of freedom (SDOF) approach, varying mass, stiffness, damping factor and wind pressure of the examined element, so to identify a correlation between natural frequency and dynamic effects which might results in a more reasonable frequency limit definition, consistent with the current design practice. Validation of the approach by means of an example of finite element calculation will be conducted, using experimental wind pressure measurements as loading inputs. The results of the assessment will show how the damping factor is of primary importance for the dynamic amplification and why it should be taken as governing parameter in a classification of those façade elements which may be prone to dynamic effects, together with their corresponding critical natural frequencies. Further future studies will be focused on assessment by multi degrees of freedom (MDOF) systems in order to validate the proposed analysis approach in a more extensive way.

REFERENCES

European Committee for Standardization (CEN), 2005, EN1991-1-4, Eurocode 1: Actions on structures, Part 1-4: General actions - Wind actions.

Uncertainty quantification in the aeroelastic response of a twin-box deck depending on the inlet conditions by CFD studies

Antonio J. Álvarez [1], Giuseppe G. Lobriglio [2], Félix Nieto [3], José Á. Jurado [4], Santiago Hernández [5]

[1] *University of A Coruña, A Coruña, Spain, antonio.jose.alvarez@udc.es*
[2] *University of Pavia, Pavia, Italy, giuseppegrazia.lobriglio01@universitadipavia.it*
[3] *University of A Coruña, A Coruña, Spain, felix.nieto@udc.es*
[4] *University of A Coruña, A Coruña, Spain, jose.angel.jurado@udc.es*
[5] *University of A Coruña, A Coruña, Spain, santiago.hernandez@udc.ess*

SUMMARY

The stochastic collocation method is applied to assess the impact of uncertainties in the angle of attack and the turbulence intensity in the force coefficients and flutter derivatives of a twin-box deck. A level-3 sparse grid has been adopted, and the deterministic realizations have been obtained by means of 2D URANS simulations. It has been found that the uncertainty in the aerodynamic and aeroelastic outputs is low to moderate, and in general, is higher for the flutter derivatives at larger reduced velocities. The adoption of nested quadrature points has enable an efficient use of the computational resources, by requiring a reasonable number of CFD simulations for the deterministic realizations.

Keywords: Uncertainty quantification, stochastic collocation, twin-box deck

1. INTRODUCTION

The identification of aerodynamic and aeroelastic characteristics of interest in bridge engineering, such as force coefficients and flutter derivatives, is sensitive to uncertainties in a number of parameters such as inaccuracies in the geometric details in sectional models, measurement errors or insufficient characterization of the incoming flow in wind tunnel testing. Several authors have addressed this topic in bridge engineering applications, such as Bruno and Fransos (2011); Mannini and Bartoli (2015) or Fang et al. (2020), among others.

Twin-box decks have proved to be a feasible alternative for long-span bridges as the central slot has proved to have a positive impact in flutter performance. Nevertheless, it is important to assess how uncertainties in the incoming flow may affect the aerodynamic and aeroelastic parameters. This work addresses this issue by conducting CFD simulations and applying probabilistic propagation of the uncertainty in the chosen random variables with assumed probability density functions.

2. PROBLEM DESCRIPTION AND METHODOLOGY

The uncertainty parameters chosen have been the turbulence intensity and the angle of attack, as the main goal has been studying the impact of uncertainties in the inflow conditions upon force coefficients and flutter derivatives. Previous research by others has shown the limited impact of the inflow turbulence length scale (Mariotti et al., 2016). The ranges of variation considered are $[-1º, +1º]$ for the flow angle of incidence and $[0.001, 0.03]$ for the turbulence intensity, assuming a uniform probability density function for both.

The stochastic collocation method (the interested reader may refer to Xiu (2010) for a general overview) has been applied adopting the Smolyak sparse grid extension of level-3 Clenshaw-Curtis quadrature points, following the procedure in Mariotti et al. (2016). The Clenshaw-Curtis nodes assure the "nestedness" of the one-dimensional nodes for increasing levels of the sparse grid. The procedure is applied increasing the level of the Clenshaw-Curtis nodes by one, at each stage, seeking to avoid the risk of oversampling. For the level-3 adopted herein, this defines 13 pairs of values for the angle of attack and turbulence intensity within the considered ranges in the random variables requiring a deterministic realization. The suitability of the chosen approach relies on the low dimensionality of the problem being considered. Alternative approaches based on uniformly distributed interpolation points, or non-nested quadrature points, may result in high computational demands, as each collocation point requires a CFD simulation. The use of non-uniformly distributed points decreased the interpolation error of the polynomial approximation in the vicinity of the boundaries. Due to the number of points used in the level 3 approximation, the maximum order of the Lagrange polynomials is four. The deterministic realizations for the quantities of interest (force coefficients and flutter derivatives) have been obtained by means of 2D URANS simulations of the so-called g22 twin-box cross-section in Nieto et al. (2020), whose verification and validation studies were reported in that last reference.

3. RESULTS: FORCE COEFFICIENTS AND FLUTTER DERIVATIVES

Based on the deterministic results for the integral parameters of the 13 cases considered, the stochastic mean and standard deviation values have been obtained for level-3 Clenshaw-Curtis quadrature points, and they are reported in table 1 below.

Table 1. Stochastic mean and standard deviation for integral parameters.

	C_D	C_L	C_m	$std(C_D)$	$std(C_L)$	$std(C_m)$
Stochastic mean	0.03143	-0.14146	0.01389	0.00279	0.07733	0.00546
Stochastic Std. dev.	0.00778	0.03334	0.01202	0.00316	0.08474	0.00590

In figure 1, the stochastic mean ± the stochastic standard deviation obtained for the force coefficients is reported along with the experimental data obtained by wind tunnel testing.

Similarly, the stochastic values for the flutter derivatives of the g22 short-gap twin-box deck have been obtained, based also on the level-3 sparse grid CFD forced oscillation simulations in heave and pitch degrees of freedom. In figure 2, for selected flutter derivatives, the stochastic mean ± stochastic standard deviation are provided along with the wind tunnel values for comparison. The agreement between the numerical flutter derivatives and the wind tunnel test is reasonable. Furthermore, the uncertainty propagation in the flutter derivatives is low to moderate, depending on the particular flutter derivative considered, although in general the stochastic standard deviation increases with the reduced velocity.

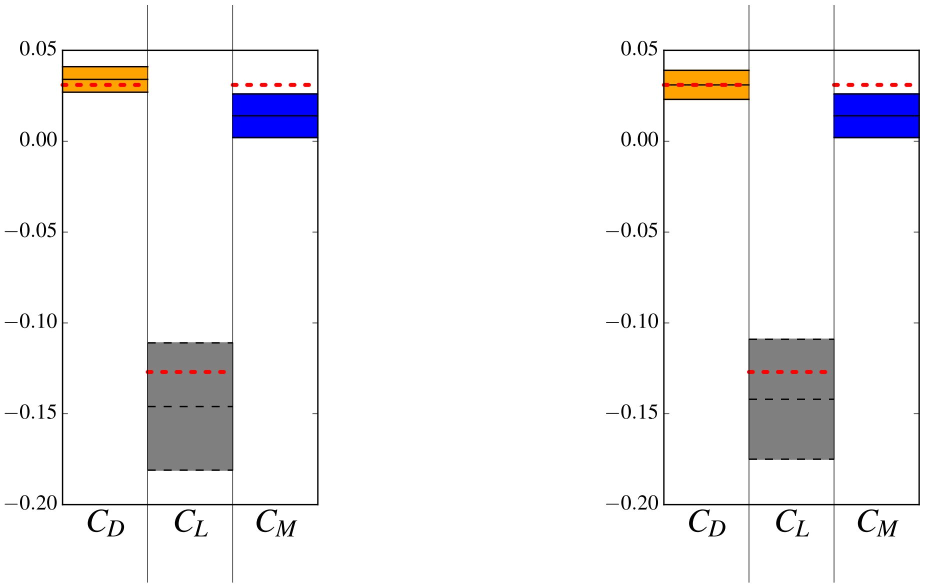

(a) (b)

Figure 1. Stochastic mean ± stochastic standard deviation for the force coefficients including experimental values as dotted red lines. (a) Level 2 quadrature points; (b) level 3 quadrature points.

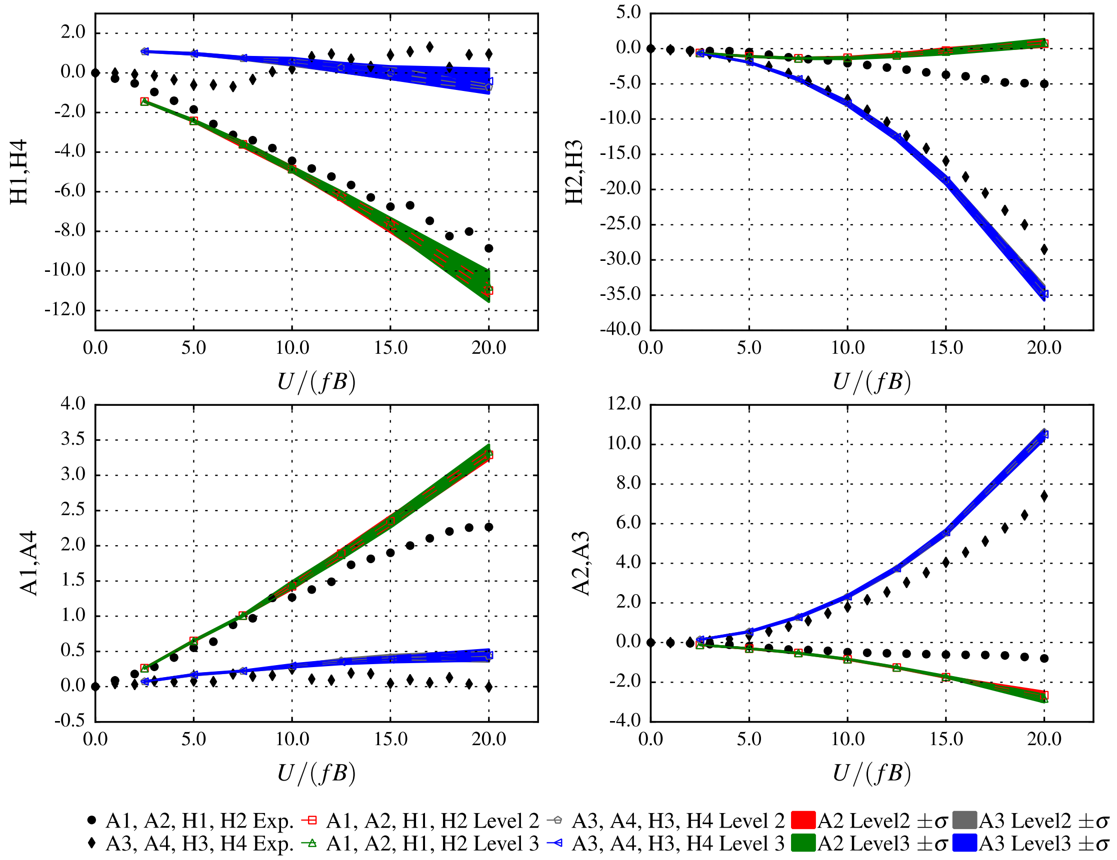

Figure 2. Stochastic and experimental values for the flutter derivatives.

4. CONCLUSIONS

This work reports the uncertainty propagation of the flow angle of attack and turbulence intensity in the integral parameters and flutter derivatives of a twin-box deck. The stochastic collocation method has enabled the assessment of the sensitivity of the quantities of interest to the uncertainty of certain flow parameters. It has been found that for the flutter derivatives, this sensitivity is not negligible, depending on the reduced velocity and the particular derivative considered. Furthermore, the adoption of nested quadrature points has enable an efficient use of the computational resources by limiting the number of required 2D URANS simulations.

ACKNOWLEDGEMENTS

This research has been funded by the Spanish Ministry for Science and Innovation (project PID2019-110786GB-I00), and the Xunta de Galicia (Galician Regional Government), including FEDER funding, (ED431C 2021/33). The Erasmus+ Higher Education Traineeship program has funded Giuseppe G. Lobriglio.

REFERENCES

Bruno, L., Fransos, D., 2011. Probabilistic evaluation of the aerodynamic properties of a bridge deck. Journal of Wind Engineering and Industrial Aerodynamics, 99, 718-728.

Fang, G., Cao, J., Yang, Y., Zhao, L., Cao, S., Ge, Y., 2020. Experimental uncertainty quantification of flutter derivatives for a PK section girder and its application on probabilistic flutter analysis. Journal of Brige Engineering, ASCE 25(7): 04020034.

Mannini, C., Bartoli, G., 2015. Aerodynamic uncertainty propagation in bridge flutter analysis. Structural Safety 52, 29-39.

Mariotti, A., Salvetti, M.V., Shoeibi Omrani, P., Witteveen, J.A.S., 2016. Stochastic analysis of the impact of free stream conditions on the aerodynamics of a rectangular 5:1 cylinder. Computers and Fluids, 136, 170-192.

Nieto, F., Cid Montoya, M., Hernández, S., Kusano, I., Casteleiro, A., Álvarez, A.J., Jurado J.Á., Fontán, A., (2020) Aerodynamic and aeroelastic responses of short gap twin-box decks: box geometry and gap distance dependent surrogate based design. Journal of Wind Engineering and Industrial Aerodynamics, 201: 104147.

Xiu, D., 2010. Numerical methods for stochastic computations: a spectral method approach. Princeton University Press, New Jersey, USA

Calibration of wind action combination factors from experimental data

V. Picozzi [1], F. Ricciardelli [2], J. D. Sørensen [3]

[1]University of Campania "Luigi Vanvitelli", Aversa, IT, vincenzo.picozzi@unicampania.it
[2]University of Campania "Luigi Vanvitelli", Aversa, IT, friccia@unicampania.it
[3]Aalborg University, Aalborg, DK, jdas@build.aau.dk

1. INTRODUCTION

In modelling wind action, the Davenport Wind Loading Chain is commonly used describing the physical phenomenon, i.e. how the wind speed interact with the structure and the surrounding. Accordingly, once the wind action (effect) is evaluated, then design criteria are required to design a structure with respect to the wind action. Following the Eurocode format (CEN, 2002), the Italian building Code (MIT, 2018) is based on the semi-probabilistic method. Accordingly, the evaluation of combined load and effects on structures is based on a set of load partial factors γ and of combination factors ψ. The first account for the uncertainty associated with the evaluation of the characteristic value of the actions and of their effects, the latter account for the non-simultaneous occurrence of extreme events represented by the characteristic value of the action.

In Italy, Limit State analyses have become mandatory in 2008, and most of the load and combination factors have been adapted from the Eurocodes. On the other hand, it is known that their calibration requires the use of reliability methods involving appropriate stochastic models for both loads and resistance. In particular, in the case of climatic actions, e.g. wind, a regional climate analysis would be required for the calibration.

When two or more variable loads have to be combined, the stochastic models are not enough to calibrate load factors. In fact, the sum of individual maxima can lead to extremely conservative estimates. A complete description of variable loads in terms of stochastic processes should be adopted, providing information on the variation in time of the load. However, for design purposes it is complicated to model and then combine the stochastic load processes, thus evaluating their maximum effects. For this reason, through the years simplifications have been introduced in modelling stochastic processes leading to the combinations rules to be used within Codes (Ferry-Borges and Castanheta, 1972; Turkstra and Madsen, 1980).

In this paper, combination factors for wind actions are calibrated based on available Italian climatic data, with the purpose of assessing the values currently in use. First, an overview on the methods for the calibration of load combination factors is presented. Then, historical wind speed measurements are used to calibrate the probabilistic models for the Italian wind climate. Finally, calibrations are presented for the combination factor for wind action to be combined with imposed loads, and the results are discussed.

2. METHODOLOGY

In current work, two methods are applied for the calibration of combination factors. The first method (Method 1) is the classical simplified method involving the Ferry-Borges and Castanheta's approach and the Turkstra's rule. Instead, the second method (Method 2) is based on the simulations of the combined load effects. Within Method 1, the following equation is used for a first quick calibration of the combination factors, consistent with the recommendations in EN1990:

$$\psi_{01} = \frac{F^{-1}_{Q_1,T}(P_c)}{F^{-1}_{Q_1,T}(P_d)} \; ; \qquad \psi_{02} = \frac{F^{-1}_{Q_2,T}(P_c^{n_1})}{F^{-1}_{Q_2,T}(P_d)} \tag{1}$$

where P_c and P_d are the probabilities associated to the combination value and the design value of the considered load, $F_{Q,T}(q)$ is the distribution function of the maximum values Q of the load $Q(t)$ in the reference period T, and n_1 is the number of independent repetitions of Q_1 in the reference period T. According to the Design Value Format method, $P_d = \Phi(0.7\beta_T)$ and $P_c = 0.28\beta_\tau$, where $\beta_T = 3.8$ is the target reliability index for $T = 50$ yrs, and β_τ is equal to $0.7\beta_T$ in the case of load Q_1 and equal to $\Phi^{-1}\left[\Phi(0.7\beta_T)^{n_1/n_2}\right]$ in the case of load Q_2.

Within Method 2, to model the distribution function $F_S(s)$ of the T-yrs maximum values of the combined load effect $S(t)$, simulation of time histories of the loads is made. The following steps are required for the Monte Carlo method:

1. Simulations of T years of the imposed load $Q_1(t)$ and of its effect $S_1(t)$ (see Figure 1a).
2. Simulations of T years of the wind action $Q_2(t)$ and of its effect $S_2(t)$ (see Figure 1b).
3. Evaluation of T years of the combined load effect $S(t) = S_1(t) + S_2(t)$.
4. Evaluation of the maximum value of $S(t)$ in the simulated T years.
5. Repetitions of Steps 1 to 4 for N simulations.

The number of simulations N shall be chosen based on the minimum probability value to reach, i.e. on the expected maximum reliability index β. Based on the Design Value Format and on the Turkstra's rule, the design value S_d of the combined load effect is given by:

$$S_d(\psi_{01}, \psi_{02}) = \max\begin{Bmatrix} S_{1d} + \psi_{02} S_{2d} \\ \psi_{01} S_{1d} + S_{2d} \end{Bmatrix} \tag{2}$$

where S_{1d} and S_{2d} are the design values associated with the load effects S_1 and S_2. For given values of S_{1d} and S_{2d}, a solution exists for the pair of values (ψ_{01}, ψ_{02}) such that the probability $P(S_d)$ of the combined load design value S_d is equal to $P_d = \Phi(0.7\beta_T)$, according to the Design Value Format method. However, when a linear relationship between loads and their effects is considered, then a relative weighting factor α_s could be considered between the two load effects. This allows the definition of $S_{1d} = \alpha_s Q_{1d}$ and $S_{2d} = (1 - \alpha_s) Q_{2d}$. In this case, Eq. (2) could be valid for each value of α_s leading to the definition of an optimization problem where the pair of values (ψ_{01}, ψ_{02}) could be evaluated as:

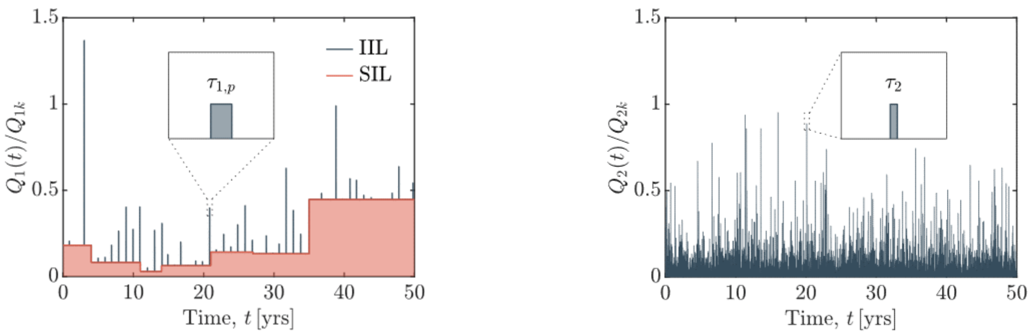

(a) (b)

Figure 1. Example of 50-yrs simulation of process for (a) imposed load and (b) wind action.

$$(\psi_{01}, \psi_{02}) = \arg\min\{[\beta(\psi_{01}, \psi_{02}) - 0.7\beta_T]^2\} \tag{3}$$

For calibration of the combination factors for wind action to be combined with imposed loads, probabilistic models for both loads are required. The models used in current work are mainly based on the Probabilistic Model Code (JCSS, 2001). Variable loads are represented as the product of a time-variant load $Q(t)$ and a time-invariant component X_Q.

The time-variant uncertainty of imposed load is given by the sum of a sustained component and an intermittent component. The sustained load accounts for the weight of furniture and normal people occupancy; its changes usually corresponds either to changes in use or of users in building. Instead, the intermittent load accounts for exceptional events like crowding or stacking of furniture during refurbishment. Four categories of use are considered in current study: residence, office, school classroom, and industrial. The time-invariant part is related to the uncertainty in model the imposed load.

In the case of wind action, the time-variant component is representative of extreme wind climate, i.e. of maximum values of the wind speed or velocity pressure in the reference period T. It is site-related and regional climatic data are needed for its modelling. For Italy, the probabilistic model is derived from the work of Ballio et al. (1991). Instead, the time-invariant part is related to the exposure coefficient, pressure coefficient, and dynamic coefficient.

3. EXPECTED RESULTS

The methodology outlined above is applied to each of the forty stations for which the characteristics of the extreme wind climate are given in Ballio et al. (1991). Moreover, for each station, the calibration is made for the effects of the wind action combined with the effects of the imposed load considering each of the four categories of buildings use. It is expected that:

- Different values of the combination factor are estimated for each station and for each category of use. As an example, the results of the application of Method 1 are shown in Figure 2.
- Larger values are derived from Method 1 with respect to Method 2.
- Current values of combination factors suggested by Eurocode lead to an overestimation of the design value of the combined load effects.

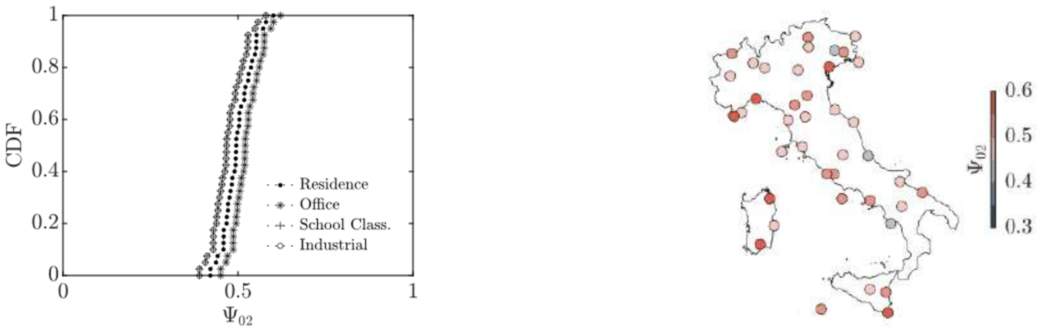

(a) (b)

Figure 2. Combination factors ψ_{02} for wind action resulting from the application of Method 1 to Italy: (a) CDF of ψ_{02} and (b) calibration at local scale for office use.

REFERENCES

Ballio, G., Lagomarsino, S., Piccardo, G., Solari, G., 1991, A first step towards a map of Italian extreme winds. Part 2: results, repercussion on standards, design implications. Costruzioni Metalliche, 4, 209-243.

European Committee for Standardization (CEN), 2002, EN1990:2002, Eurocode 1 – Basis of structural design.

Ferry-Borges, J., Castanheta, M., 1972, Structural Safety (2nd edition). Laboratiorio Nacional de Engenharia Civil, Lisbon.

Joint Committee on Structural Safety (2001). Probabilistic Model Code, JCSS.

Ministero delle Infrastrutture e dei Trasporti (MIT), 2008, Norme Tecniche per le Costruzioni (NTC 2018), D.M. 17/01/2018 (*in Italian*).

Turkstra, C.J., Madsen, H.O., 1980, Load combinations in codified structural designi. Journal of the Structural Division ASCE, 106 (12), 2527-2543.

Wind-borne debris resistance of façades: code and standard requirements versus experimental data

Angela Mejorin [1], Gregory A. Kopp [2]

[1]University of Western Ontario, London ON, Canada, amejorin@uwo.ca
[2]University of Western Ontario, London ON, Canada, gakoppp@uwo.ca

SUMMARY
In extreme winds, wind-borne debris can impact building envelopes at high speeds, causing failure. In many areas prone to these events, codes and standards requirements are set and façade designers must go through building envelope testing procedures that have been settled in the last few decades. These tests have been developed through an empirical approach that considers typical debris elements such as roof gravel. This project purposes alternative wind-borne debris testing procedures that consider local building components that could fail due to wind pressure. The alternative tests are based on the current understanding of wind-borne debris aerodynamics, wind-induced failures, wind loading, and impact dynamics. A specific case study, examining roof tile failure and flight, demonstrates the impact energy that the façade should withstand to guarantee its endurance in extreme wind events. The innovative design approach is generic and could be adopted by designers in various specific context.

Keywords: wind-borne debris, impact test, building design

1. INTRODUCTION

Wind-borne debris impact is one of the most common causes of building damage in extreme wind events. Debris sources are represented by objects of the urban environment and by surrounding building components that fail due to sustained winds (ASCE 2014; Butler & Kareem 2012; Nishimura et al. 2009). This work presents a methodology for designing specific debris-resistant building envelopes. It is based on current knowledge of wind-borne debris aerodynamics, wind-induced failures, wind loading, and impact dynamics. The impact energy that the façade must withstand to ensure its durability in extreme wind occurrences is shown through a specific case study in which roof tile failure and flight are examined. For the impact resistance of building envelopes, the methodology will be generalized so that designers can address case-specific building conditions. This approach is compared to the existing code and standard requirements in (ASCE 2016; ASTM 2019 & 2020).

2. METHODS

This study provides a solution for façade designers to address the current gap in façade test criteria for wind-borne debris' impact in extreme winds. The ASTM standard techniques are the current best practices in terms of impact testing to replicate wind-borne debris in windstorm situations (ASCE 2018). Standard projectors and impact velocities are used to certify building envelope components in specific wind zones, based on the level of protection of the building. There is no database on wind-borne debris speeds in hurricane and tropical cyclone winds, and therefore the ASTM impact energies are not based on the aerodynamics of wind-borne debris in local contexts (Kordi 2009).

The ASTM standard criteria already allow façade designers to use engineering assumptions to create ad-hoc wind-borne debris impact tests for their designs, using "different missiles" and speeds for the impact test (ASTM 2019 & 2020). Since their competence is advanced in areas other than wind engineering, this alternative is rarely investigated by designers and/or window and façade suppliers. The impact energy a building envelope should withstand is calculated considering the trajectory and the velocity of specific debris typologies founded in the urban environment.

The methodology used in this study employs a fragility analysis to estimate building component failure from a source building while also considering various types of wind-borne debris. Fragility analyses have been utilized in the past to construct impact risk assessments and vulnerability models (Zhang et al. 2014); however, the goal of this study is to emphasize and focus on a design tool.

This research adopts an analytical approach to analyze two experimental databases that have been created at the University of Western Ontario. They present experimental setups that are comparable both in their geometric features and in their testing settings. Data about wind-borne debris failure wind velocity and related building envelope pressure coefficients can therefore be discussed. Through the unique experimental database on roof tiles' failure and flight (Kordi 2009), and the one that assessed wind loads on roof sheathing of houses (Gavanski et al. 2013), an innovative scheme for building envelope design is developed.

Ultimately, the ASCE 7 (2016) requirements for building components and cladding design are analyzed and discussed in their adequacy for specific building components design, with reference to a particular case study: the roof tile.

3. RESULTS

The research provides a design framework (Figure 1) for wind-borne debris impact design of target façades. Its aim is to be site-specific instead of adopting standardized impact projectors and velocities. The building envelope performances are therefore related to building aerodynamics and wind-borne debris flight analysis. This approach is particularly addressed to critical infrastructure facilities in metropolitan areas, such as hospitals, which are mandated to provide protection for people in disaster events (IBC 2021).

The process for setting wind-borne debris-resistance test criteria is discussed through a specific example which is the roof tile in a case-study section, although the proposed design tool could be used for any device that potentially fails in a windstorm.

This method enables a conversation regarding other materials such as gravel, roof tiles, shingles, sheathing, and structural components, the most prevalent sources of wind-borne debris, by analyzing a specific building component in its failure mechanism (Kordi 2009).

4. CONCLUSION

This research considers the most recent wind engineering research on building aerodynamics and wind-borne debris failure in wind events. The analysis takes to the development of a design tool for façade impact performance design when it comes to wind-borne debris. Following various steps presented in the design framework, the impact test requirements would therefore be, for the first, based on wind engineering analysis. The validation of the design model for wind-borne debris resistance of façades is represented by the database that has been developed by Kordi (2009). The design technique is based on the aerodynamics of wind-borne debris, and it is intended to assist designers in analyzing site-specific circumstances to order to provide building envelopes' resistance to local wind-borne debris.

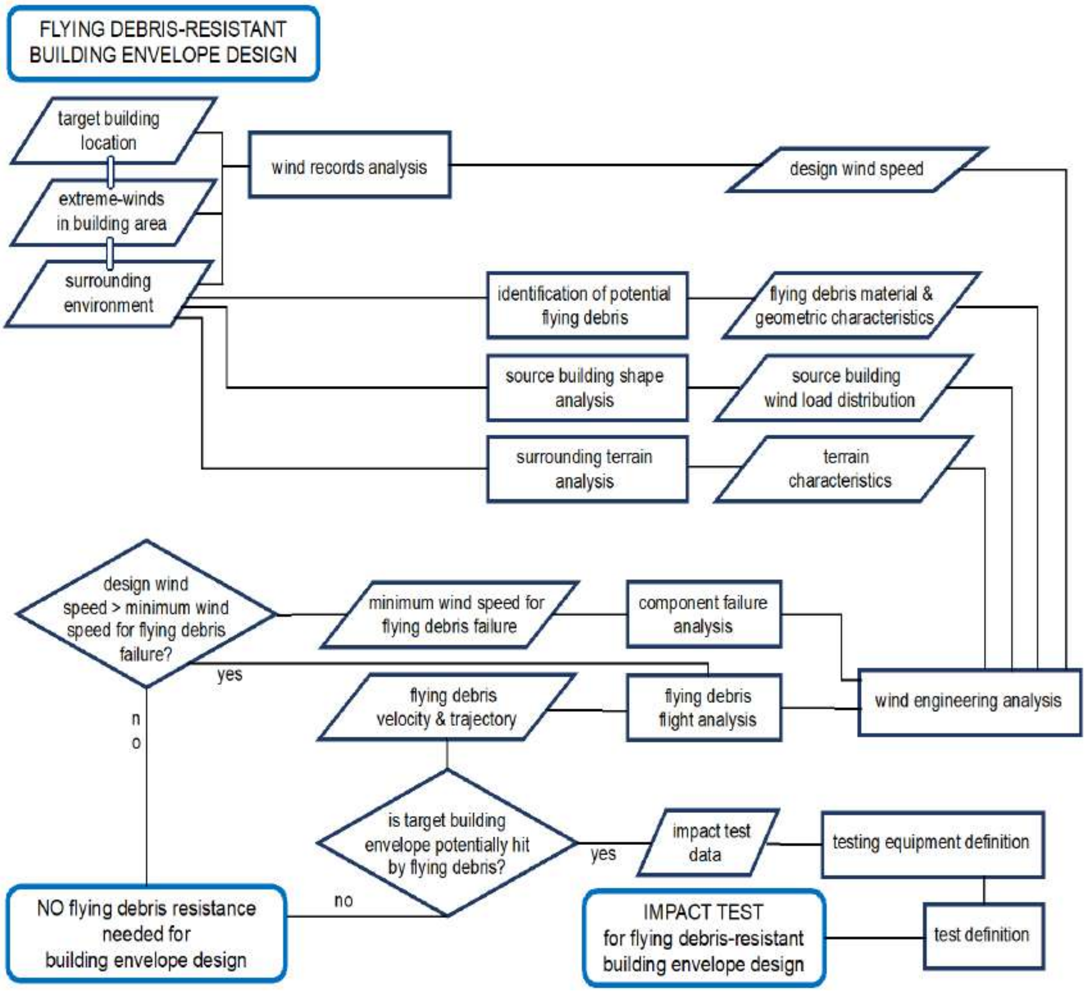

Figure 1. Alternative wind-borne debris impact test of façades

REFERENCES

ASCE, 2014. Engineering Damage Assessments Following Hurricanes
ASCE, 2018. Wind-Borne Debris Hazards
ASTM E1996-20. Standard Specification for Performance of Exterior Windows, Curtain Walls, Doors and Storm Shutters Impacted by Windborne Debris in Hurricanes
ASTM E1886-19. Standard Test Method for Performance of Exterior Windows, etc. impacted by Missile(s) and Exposed to Cyclic Pressure Differentials
Butler, K., Kareem, A., 2012. Anatomy of Glass Damage in Urban Areas during Hurricanes. In: Advances in Hurricane Engineering: Learning from Our Past. ASCE
Kordi, B., 2009. Aerodynamic of wind borne plate debris. University of Western Ontario Ph.D. Thesis
International Building Code (IBC) 2021. International Code Council (ICC)
Nishimura, T., Taniguchi, T., Maruyama, T., 2009. Analysis on Trajectories of Wind-borne Debris and Impact Test of Building Components. GBRC Technical report, vol. 34
Zhang, X., Hao, H., 2013. Laboratory test and numerical simulation of laminated glass window vulnerability to debris impact. In: International Journal of Impact Engineering 55

Mitigation of interference-induced vibrations for towers in group arrangements

Francesca Lupi [1,2], Marc Seidel [3], Rüdiger Höffer [1,2], Norbert Hölscher [2], Hans-Jürgen Niemann [1,2]

[1]Ruhr-Universität Bochum, Bochum, Germany, francesca.lupi@ruhr-uni-bochum.de,
[2]Niemann Ingenieure GbR, Bochum, Germany,
[3]Siemens Gamesa Renewable Energy GmbH & Co. KG, Hamburg, Germany

SUMMARY
The paper studies tower vibrations in closely spaced group arrangements due to vortex excitation and interference galloping. The ever-growing development of the wind energy industry has recently led to an in-depth examination of the subject, particularly with regard to the transport of towers for offshore wind turbines. Due to the small natural frequencies typical of steel towers and the need of transporting and installing towers in all possible weather scenarios, the range of verification for aeroelastic instabilities is extended until very high reduced wind velocities. In addition, many configurations of towers in group arrangements need to be considered. The paper presents a synthesis of aeroelastic wind tunnel tests in multiple configurations for spacings a/D ≤ 2,5, being "a" the axis-to-axis distance.

Keywords: offshore wind turbines, vortex induced vibrations, interference galloping

1. INTRODUCTION

Interference effects in tower groups involve various aeroelastic phenomena, ranging from predominant vortex induced vibrations for larger spacings to interference galloping for smaller spacings. Interaction between vortex induced vibrations and galloping-like vibrations may occur for intermediate distances. Reviews on the topic are presented for example in Alam (2013), Sumner (2010) and Zdravkovich (1988).

The amplification of the response due to interference effects in vortex induced vibrations is taken into account by the Eurocode EN 1991-1-4 through the reduction of the Strouhal number and the increase of the lift coefficient. With regard to interference galloping, the Eurocode contains an equation to calculate the onset velocity based on the distance between towers, the Scruton number and an instability parameter (see EN 1991-1-4, E.3). This approach goes back to Ruscheweyh (1981, 1983). However, vortex induced vibrations and interference galloping are treated by the Eurocode as two separate and independent phenomena. Instead, for tower spacings (axis-to-axis) smaller than 2,5D (being D the diameter), the two phenomena strongly interact for small until moderately high Scruton numbers. The interaction further amplifies the response. Additionally, the interaction is made more complex by multiple vortex shedding frequencies that may occur from each tower in the group arrangement.

Whereas a practical solution to avoid interference galloping for chimneys in groups is to couple them at the top, this option is not practicable for towers of offshore wind turbines, due to difficulties to disconnect the towers at the sea. These challenges require development of advanced application methods in the near future.

2. WIND TUNNEL EXPERIMENTS

Aeroelastic wind tunnel experiments on vibrating models are carried out at the WISt Boundary Layer Wind Tunnel of the Ruhr University Bochum (Figure 1). The models are elastic cantilevered circular cylinders anchored to the foot at a forced balance. The forces and bending moments at the base of each model are measured. The oscillations at the top of the models are calculated by considering the distribution of inertial forces in resonance. This procedure has proved to be more accurate than simply applying the static stiffness to relate dynamic reactions to oscillations.

Figure 1. Wind tunnel tests on towers in group arrangement at the Ruhr University Bochum

An important aspect for the interpretation of the aeroelastic test results is the accurate knowledge of the structural damping. This is measured through snap-back tests in still air. The contribution of still air damping in the free-decay tests is expected to be small and is therefore not separated from pure structural damping in the analysis. Depending on the model properties, the structural damping may deviate from the assumption of linear viscous damping. This results in an amplitude dependent structural damping. Therefore, considerations are made regarding the choice of proper amplitude ranges to determine representative values for the structural damping.

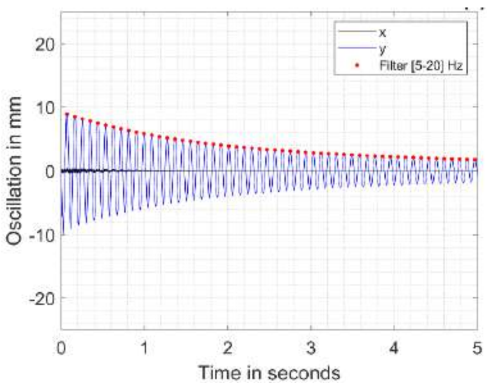

Figure 2. Free decay tests to estimate structural damping (D = 50 mm)

The wind tunnel tests include a wide range of parameter variations: (1) the spacing between cylinders varies from a/D = 1,5 (small spacing), a/D = 1,9 (medium spacing) to a/D = 2,5 (large spacing). The Scruton number varies until Sc ca. 40. The group configurations include 2 cylinders, 4 cylinders in line, 4 cylinders placed in two adjacent rows of 2 cylinders each (2x2) with the associated subset 2+1 (one cylinder at the side). The wind direction varies between 0° and 90° (in line and perpendicular to the main axes of the group, respectively), including inclined wind directions in the range 0°÷15° and diagonal winds.

3. DISCUSSION OF RESULTS

The wind tunnel results are discussed in relation to the Eurocode design approach. The Eurocode approach for interference galloping is originally developed in Ruscheweyh (1983), Dielen& Ruscheweyh (1995). It introduces a combined instability parameter that includes both the linearization of force coefficient through its derivative at small oscillation angles around zero (stationary approach) and the phase shift between across-wind force and oscillation of the cylinder placed in staggered arrangement. The instability parameter is derived by Ruscheweyh from wind tunnel tests at sufficiently high Scruton numbers, which allow clear separation between vortex induced vibrations and galloping. In principle, extension of the concept to other group configurations is permitted by Eurocode.

However, for very small spacings and/or for different group configurations full separation between vortex induced vibrations and interference galloping can be difficult, even for moderately high Scruton numbers. For example, Figure 3 shows the complexity of the phenomenon in 2x2 group configuration (Sc ca. 20). Here, due to the small Strouhal number (St < 0,1), the critical velocity is shifted to high reduced velocities ($V_{cr,red}$ ca. 16), but still in the range of verification for towers of offshore wind turbines.

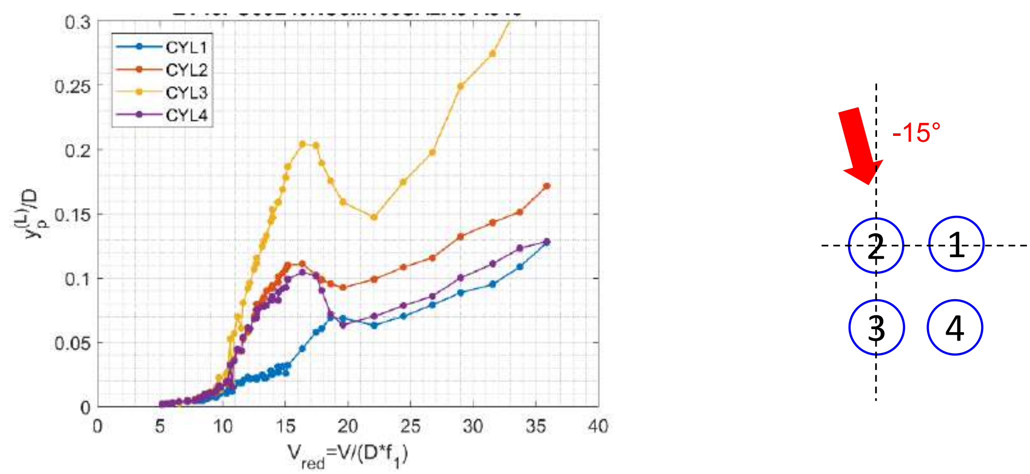

Figure 3. Aeroelastic wind tunnel tests for 2x2 group configuration, a/D = 1,5, Sc ca. 20

4. CONCLUSIONS

The paper studies tower oscillations in group arrangements by means of wind tunnel tests on aeroelastic models. The interaction of vortex induced vibration and interference galloping occurs for small distances between cylinders and/or complex group configurations. Multiple vortex shedding frequencies with small Strouhal numbers shift the lock-in range towards high wind speeds. This enhances the interaction with interference galloping. The results of the tests are discussed in the paper in relation to the current Eurocode design approach.

ACKNOWLEDGEMENTS

The authors acknowledge the German Research Foundation (DFG – Deutsche Forschungsgemeinschaft) for supporting the author FL in that part of this work regarding vortex induced vibrations through the Project number 426322127.

REFERENCES

Alam M.M., Meyer J.P., 2013. Global aerodynamic instability of twin cylinders in cross flow, Journal of Fluids and Structures, Volume 41, 135-145.

DIN EN 1991-1-4:2010-12 Eurocode 1: Einwirkungen auf Tragwerke – Teil 1-4: Allgemeine Einwirkungen, Windlasten, Deutsche Fassung EN 1991-1-4:2010, Deutsches Institut für Normung e.V., Dez. 2010.

Ruscheweyh H., 1983. Aeroelastic interference effects between slender structures, Journal of Wind Engineering and Industrial Aerodynamics, Volume 14, Issues 1–3, Pages 129-140.

Dielen B., Ruscheweyh H., Mechanism of interference galloping of two identical circular cylinders in cross flow, Journal of Wind Engineering and Industrial Aerodynamics, Volumes 54–55, Pages 289-300, 1995.

Sumner D., 2010. Two circular cylinders in cross-flow: A review. Journal of Fluids and Structures, Volume 26, Issue 6, Pages 849-899.

Zdravkovich M.M., 1988. Review of interference-induced oscillations in flow past two parallel circular cylinders in various arrangements, Journal of Wind Engineering and Industrial Aerodynamics, Volume 28, Issues 1–3, Pages 183-199.

The aerodynamic behavior of porous surfaces in external flows: modeling approaches in CFD

Mao Xu [1], Luca Patruno [2], Stefano de Miranda [3]

[1]*University of Bologna, Bologna, Italy, mao.xu2@unibo.it*
[2]*University of Bologna, Bologna, Italy, luca.patruno@unibo.it*
[3]*University of Bologna, Bologna, Italy, stefano.demiranda@unibo.it*

SUMMARY
The aerodynamic behavior of porous surfaces currently represents a problem of growing interest for the wind engineering community. However, as the size of the pores is generally one to three orders of magnitude smaller than the overall structure dimensions, it is extremely difficult to study the aerodynamics of porous surfaces in wind tunnel experiments. Computational Fluid Dynamics, CFD, simulations in which the pore geometry is explicitly modeled are in no way easier than wind tunnel tests, as their computational costs are substantially unaffordable due to the large number of cells required to represent the tiny pores. In such context, an alternative approach is to use appositely defined homogenized models in order to account for the presence of the porous surfaces, usually represented by the so-called pressure-jump approach. In this study, the performance of the pressure-jump-based approach is evaluated by investigating the flow through structures composed of porous surfaces simulated using both explicit models and pressure jumps.

Keywords: Porous surface, Porosity, Computational Fluid Dynamic, Pressure-jump

1. INTRODUCTION

Because of their aesthetic value, sun-shielding effect, and the ability to maintain ventilation while providing space separation, porous surfaces are becoming popular in modern architecture (Pomaranzi et al., 2021). However, due to the remarkable length scale separation existing between the overall structure and the pores, the presence of small-scale pores poses serious difficulties: in wind tunnel experiments, representative reduced scale models are not easily built; in CFD, a large number of cells are needed to accurately simulate the flow through pores, which consequently require unaffordable computational costs.

In order to solve the problem, homogenization techniques can be adopted, which account for the presence of the porous elements by considering the forces they exchange with the fluid. When such forces are exchanged along the surface normal direction, this leads to the so-called Pressure-Jump, PJ, approach. This approach has been widely assessed for confined flows but external aerodynamic problems are rarely discussed. In this contribution, firstly, a new model relating the surface porosity (ε) to the consequent PJ is formulated. The model, in comparison with previous ones, provides a more detailed explanation of the mechanisms involved in the PJ generation, thus highlighting details that might have remarkable importance in the interpretation of experimental measurements.

Then, the flow through structures composed of porous surfaces is investigated by using both Explicit Models, EM, in which the geometry of the porous surface is completely modeled, and PJ-based simulations. This has the twofold objective of assessing the effectiveness of PJ-based simulations and providing insights into the aerodynamics of porous bluff bodies.

2. A NEW PRESSURE-JUMP MODEL

We started by considering the simplest possible case, in which a perforated plate of vanishing thickness is traversed by a normal flow at a high Reynold number. The model derivation is based on momentum and mass conservation of the volume of fluid upstream of the barrier, the barrier itself, and the volume of fluid downstream of the barrier. The model agrees well with previously available relations, with detailed numerical simulations (see Fig. 1 (a)) and with experimental results, as can be seen in Fig. 1 (b) (Allori et al., 2013). The model has been extended also to the case of non-null attack angles (θ) using well-known approaches, showing good results, see Fig. 1 (c).

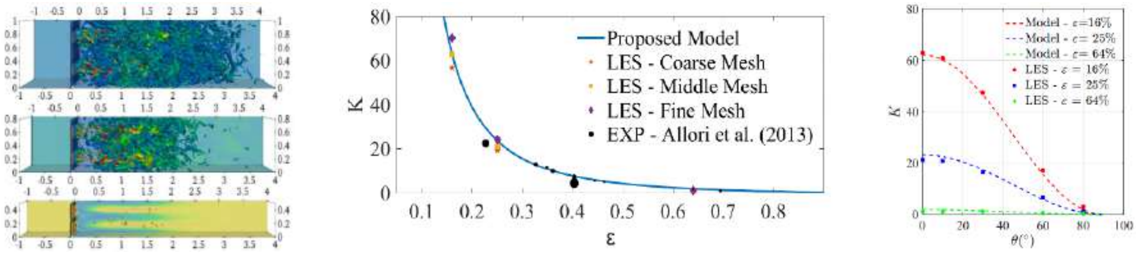

(a) (b) (c)

Figure 1: Results of the present investigation: (a) Q iso-surfaces of the *EM*-based simulations, (b) comparison of the proposed model with simulations and experimental results, (c) variation of the *PJ* with the angle of attack.

3. PRESSURE-JUMP ACCURACY ASSESSMENT

Once the *PJ* can be evaluated according to the previous model, it is possible to study the aerodynamic behavior of porous bluff bodies and bodies which present porous screens. The authors thus proceed to study the bridge decks equipped with porous screens experimentally analyzed in (Buljac et al. 2020), comparing wind tunnel results, *EM* and *PJ*-based simulations using 2D-URANS, see Fig. 2 (a). Finally, a hollow 5:1 rectangular cylinder composed of porous surfaces has been analyzed considering *EM* and *PJ* using LES at different porosities, see Fig. 2 (b). Overall, reasonable results are obtained but limitations in the use of *PJ* approach can be envisaged and the convergence toward *EM* results appears to be difficult to be achieved.

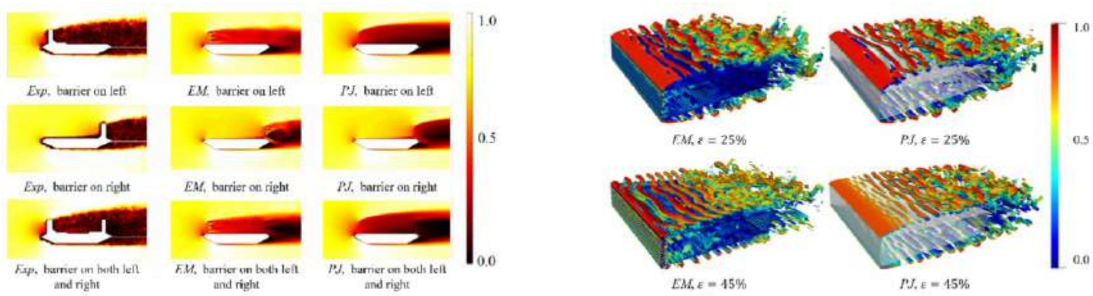

(a) (b)

Figure 2: Results of the present investigation: (a) bridge decks with porous screens, (b) the porous 5:1 rectangular cylinder.

REFERENCES

Pomaranzi, G., Bistoni, O., Schito, P., Rosa, L. and Zasso, A., 2021. Wind Effects on a Permeable Double Skin Façade, the ENI Head Office Case Study. Fluids, 6(11), p.415.

Allori, D., Bartoli, G. and Mannini, C., 2013. Wind tunnel tests on macro-porous structural elements: A scaling procedure. Journal of Wind Engineering and Industrial Aerodynamics, 123, pp.291-299.

Buljac, A., Kozmar, H., Pospíšil, S., Macháček, M. and Kuznetsov, S., 2020. Effects of wind-barrier layout and wind turbulence on aerodynamic stability of cable-supported bridges. Journal of Bridge Engineering, 25(12), p.04020102.

On the azimuthal resolution for determining the aerodynamic effect in pedestrian-level wind studies

A. McLoughlin [1], J. Millar [2], E. Hii [3], S. Cammelli [4]

[1] *WSP, Manchester, United Kingdom, aidan.mcloughlin@wsp.com*
[2] *WSP, London, United Kingdom, joshua.millar@wsp.com*
[3] *WSP, London, United Kingdom, elvin.hii@wsp.com*
[4] *WSP, London, United Kingdom, stefano.cammelli@wsp.com*

SUMMARY
The determination of an urban environment's aerodynamic effect is an important step in the assessment of pedestrian-level wind conditions in the vicinity of a proposed development. A method is proposed whereby the explicitly evaluated wind directions in a wind microclimate study are chosen based on each direction's frequency of occurrence. The maximum azimuthal resolution of 10° is maintained for more frequent wind directions, while those that are less frequent are grouped together. The method is tested on a case study in Birmingham, UK. Results indicate that evaluating the aerodynamic effect at the highest azimuthal resolution is unnecessary and that a method of computing fewer directions based on their frequency meets the level of robustness required by wind microclimate guidelines produced by city councils in the UK.

Keywords: CFD, wind microclimate, computational wind engineering

1. INTRODUCTION

A pedestrian-level wind study, the aim of which is to assess the local wind microclimate around a proposed development, usually consists of four key steps:

1. Collection and processing of appropriate historical wind data.
2. Determination of the built environment's aerodynamic effect.
3. Combination of the above steps to assess pedestrian wind comfort.
4. Comparison against a set of criteria.

This technical paper introduces a bespoke program written in Python, which gathers and treats weather data from the NOAA integrated surface dataset (National Centers for Environmental Information (NCEI), 2021), to address the first step. The second step, the determination of the aerodynamic effect, should consider all wind directions. As measured wind data have an azimuthal resolution of 10°, considering 36 directions will provide the best possible accuracy. The City of London guidelines (Wind microclimate guidelines for developments in the City of London, 2019) stipulate that wind microclimate studies should be carried out for 36 equally spaced wind directions. However, this can be computationally expensive when either computing the aerodynamic effect through CFD simulations or physical wind tunnel testing. In this technical paper it is postulated that wind directions which occur infrequently will not contribute significantly to the overall pedestrian comfort ratings and that fewer than 36 directions are sufficient.

A case study is presented to test this hypothesis. Multiple groupings of wind directions are tested using CFD to evaluate the aerodynamic effect. An evaluation is also carried out based on 36 equally spaced directions. Both methods (i.e., a reduced set of wind directions and a full set of 36 wind directions) are then used to assess pedestrian comfort and compared against the Lawson criteria (Lawson, 2001), which addresses the remaining steps of a typical pedestrian-level wind study listed above.

2. METHODOLOGY

A method is proposed which uses the maximum azimuthal resolution for more frequent wind directions while a lower azimuthal resolution is used for those that are less frequent. The directions are weighted according to their frequency of occurrence, the 'p' term in a set of Weibull coefficients. The method can be expressed mathematically with the following expression:

$$s_k = \{p_{\theta[i]}, p_{\theta[i+1]}, \dots, p_{\theta[i+n]}\} : \sum_{i=1}^{|s_k|} p_{\theta[i]} \leq p_{max}$$

Where s_k is the k^{th} partition of the full set of 36 wind directions, $p_{\theta[i]}$ is the probability of occurrence for the $\theta[i]^{\text{th}}$ wind direction and p_{max} is the maximum probability of occurrence of any one wind direction in the full set. In practical terms, the method creates a set of new partitions such that the sum of each element in each partition does not exceed the highest probability of a single wind direction in the full set. The resultant wind directions are calculated annually and seasonally while capturing the prevailing sectors with the highest azimuthal resolution of 10°, meaning some less-frequent wind directions are grouped together. Typically, this will result in approximately 19-26 wind directions, offering a significant computational cost saving.

3. ILLUSTRATIONS AND DIAGRAMS

A proof-of-concept case study is introduced, which considers a 500m radius of existing buildings in Birmingham, UK. In order to cover all the resolved wind directions, the aerodynamic effect is calculated for 36 equally spaced wind directions, as well as for some 5° increments. The CFD simulations were performed using HELYX Core v3.0.0, the Engys fork of OpenFOAM.

Results show that fewer than 36 wind directions, when grouped according to frequency of occurrence, can be sufficient to accurately describe the wind microclimate in terms of pedestrian wind comfort, compared to the highest azimuthal resolution. Using a reduced set of wind directions results in a time and cost saving. While the results presented are case-specific, the authors have used the same methodology for several other pedestrian-level wind studies and have drawn the same conclusion. This suggests that evaluating the aerodynamic effect at the highest azimuthal resolution is unnecessary and could therefore potentially be removed as a strict prescribed requirement in wind microclimate guidelines produced by city councils in the UK.

REFERENCES

National Centers for Environmental Information (NCEI). (2021). *Global Hourly - Integrated Surface Database (ISD)*. [online] Available at: www.ncei.noaa.gov/products/land-based-station/integrated-surface-database.

Wind microclimate guidelines for developments in the City of London. (2019). Available at: www.cityoflondon.gov.uk/assets/Services-Environment/wind-microclimate-guidelines.pdf.

Lawson, T., 2001. Building aerodynamics, Imperial College Press [ISBN 1-86094-187-7].

Aeolian coastal protection: Experimental-computational performance assessment of a sinusoidal berm

Lorenzo Raffaele [1,2,4], Nicolas Coste [3,4], Jeroen van Beeck [2]

[1] *Department of Architecture and Design, Politecnico di Torino, IT*
[2] *Environmental and Applied Fluid Dynamics Department, von Karman Institute for Fluid Dynamics, Waterloosesteenweg 72, B-1640,Sint-Genesius-Rode, BE*
[3] *Optiflow Company, 160, Chemin de la Madrague-Ville, F-13015, Marseille, FR*
[4] *Windblown Sand Modelling and Mitigation joint research group, IT-FR*

Keywords: coastal protection, sand mitigation measure, wind tunnel tests, computational wind engineering

1. ABSTRACT

Aeolian sand hazard affects built environment, human activities, and ecological systems in sandy coastal zones, such as buildings, urban areas, transport infrastructures, and coastal dunes. Ongoing climatic changes have increased the frequency and magnitude of wind storms along coastal regions in extra tropical regions, Europe included. This results in an increment of sand transport events from sandy beaches to built environment. Windblown sand interacts with ground-mounted obstacles of any kind inducing sand erosion and sedimentation around them and detrimental effects, such as transport infrastructure loss of capacity and destructive failures (Bruno et al. 2018).

Several Sand Mitigation Measures (SMMs) design solutions to mitigate windblown sand effects have been proposed so far (Bruno et al. 2018). They aim to prevent sand from reaching the protected system. Most of them are located between the sand source and the protected system, and they are intended to trap incoming sand by promoting wind speed lowering and sand sedimentation (Path SMMs). SMMs usually translates into nature-based solutions, such as berms, ditches, porous vegetation belts, or artificial obstacles, such as man-made porous and solid barriers.

With some remarkable exceptions, the rigorous design and performance assessment of SMMs remain at their early stage in the engineering literature, while they are mostly based on trial-and-error approaches in the technical practice. According to the authors, this is due to the multidisciplinary and multiphysics/multiscale nature of the phenomenon coupling fluid dynamics and aeolian processes. On one hand, research should benefit from disciplines adjacent and partially overlapping, e.g. fluid dynamics, wind engineering and aeolian geomorphology. On the other hand, experimental and numerical approaches should be mutually supporting to model multiphase windblown sand processes.

Wind-Sand Tunnel (WST) testing is almost entirely carried out by scaling the characteristic length L of the surface-mounted obstacle for both economic and practicality reasons. Conversely, sand grain diameter d can hardly be scaled to avoid switching from sand to dust particles and underlying physics. This opens the door to physical similitude theory based on dimensionless numbers (e.g. Re or Fr numbers) referred to the whole multiphase/multiscale flow (Raffaele et al. 2021). The numerical simulation of windblown sand flow, herein called Erosion-Transport-Deposition (ETD) simulation, is mainly carried out through the resolution of fully Eulerian models coupling wind flow aerodynamics and aeolian processes resulting in in-air sand concentration and the morphodynamic evolution of the sand bed. Among them, Eulerian ETD simulations adapt well to the engineering needs of modelling large-scale

processes and cutting costs with respect to WST and full-scale tests (Lo Giudice and Preziosi, 2020). However, ETD simulations have to be always calibrated and validated on physical measurements (Raffaele et al. 2022).

In this study, the authors take advantage of both WST tests and ETD simulations to assess the performance of a sinusoidal berm SMM. WST tests are carried out in the Wind Tunnel L-1B of von Karman Institute to characterize the sand flux in open-field conditions and around the SMM (Fig. 1a-c). The SMM performance is assessed by taking into account the progressive loss of performance of the SMM caused by the gradual accumulation of sand around it. WST measurements are adopted to properly tune and validate ETD simulations carried out with the same scaling of the WST tests. Finally, a full-scale ETD simulation is performed in order to quantify the performance under real-world conditions and quantify the experimental distortion resulting from non-compliance of physical similitude (Fig. 1d).

The complementary combination of WST and ETD provides deep insight into the scaling effects to SMM performance, lowering the costs with respect to in-situ full scale testing.

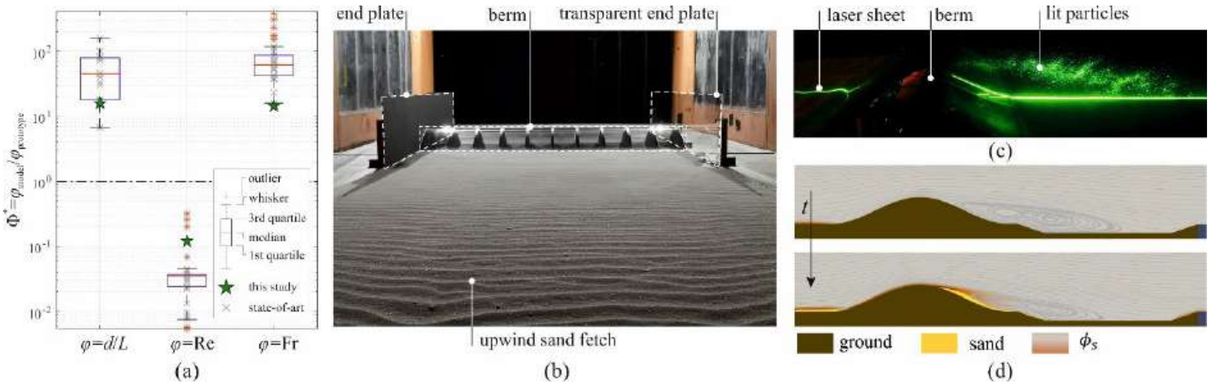

Figure 1. WST setup dimensionless numbers (a), front view of the tested sinusoidal berm SMM (b), laser sheet for PTV grain counting and morphodynamic evolution (c), full-scale ETD simulation for varying time t (d)

ACKNOWLEDGEMENTS
The study has been developed in the framework of the MSCA-IF-2019 research project Hybrid Performance Assessment of Sand Mitigation Measures (HyPer SMM, hypersmm.vki.ac.be). This project has received funding from the European Union's Horizon 2020 research and innovation programme under the Marie Sklodowska-Curie grant agreement No. 885985. The study has been jointly developed in the framework of the research project PROtection Technologies from Eolian Events for Coastal Territories (PROTEECT, www.proteect.polito.it). This project has received founding from Italian Ministry for University and Research (PON-FESR) and Politecnico di Torino.

REFERENCES

Bruno, L., Horvat, M. and Raffaele, L. (2018). Windblown Sand along Railway Infrastructures: A review of Challenges and Mitigation Measures. Journal of Wind Engineering and Industrial Aerodynamics 177, 340-365.

Raffaele, L. and Bruno, L. (2019). Windblown sand action on civil structures: Definition and probabilistic modelling. Engineering Structures 178, 88-101.

Lo Giudice, A. and Preziosi, L. (2020). A fully Eulerian multiphase model of windblown sand coupled with morphodynamic evolution: Erosion, transport, deposition, and avalanching. Applied Mathematical Modelling 79, 68–84.

Raffaele, L., van Beeck, J., and Bruno, L. (2021).Wind-sand tunnel testing of surface-mounted obstacles: Similarity requirements and a case study on a Sand Mitigation Measure. Journal of Wind Engineering and Industrial Aerodynamics 214.

Raffaele, L., Coste, N. and Glabeke, G. (2022) Life-Cycle Performance and Cost Analysis of Sand Mitigation Measures: Toward a Hybrid Experimental-Computational Approach. Journal of Structural Engineering 148.7: 04022082.

An efficient algorithm for the Bispectral Analysis of Large Structures subjected to Turbulent Wind

Michele Esposito Marzino [1], Vincent Denoël [2]

[1]*Structural & Stochastic Dynamics, University of Liège, Belgium, michele.espositomarzino@uliege.be*
[2]*Structural & Stochastic Dynamics, University of Liège, Belgium, v.denoel@uliege.be*

SUMMARY
Stochastic dynamic analysis of structures to turbulent wind loading has been widely recognised for its effectiveness and computational power with respect to classical time domain Monte Carlo simulations. In recent years evidence along many studies have shown the importance to consider the non-Gaussian nature of the loading processes. In such context, higher-order stochastic dynamic analysis is required. This work aims at providing an optimised numerical algorithm for the computation of the skewness coefficients of the structural response, which overcomes the known burdens of the computation of higher-order spectra in a non-Gaussian context.

Keywords: non-Gaussian, bispectral stochastic analysis, numerical optimisation.

1. INTRODUCTION

Wind induced vibrations may play a crucial role for flexible structures, such as long-span bridges, tall buildings, large-span roofs (Cui et al., 2022). For these types of structures, common analyses as suggested in Code Standards are no more applicable because of the fall of some crucial hypotheses. In these cases, structural engineers opt for a measured and/or computed aerodynamic pressure field to perform the buffeting analysis. The subsequent structural analysis might be carried either in time or frequency domain, as well as in a nodal, modal or hybrid basis. Usually, in a Gaussian context, analysis is typically handled by a spectral analysis following the Davenport Chain. In this analysis, the Power Spectral Density (PSD) of the structural response can be obtained through a sequential multiplication of the turbulence components PSDs', an aerodynamic and a mechanical admittance (Cui et al., 2022). This approach has undoubted analytical advantages since, in case of linear mechanical structural behaviour, the structural response happens to be Gaussian too, so it can be fully characterised by the first two statistical moments only, mean and variance.

However, even though wind turbulence is assumed to be a random Gaussian process, wind pressure is known to be a priori non-Gaussian, because of the nonlinear transformation of wind velocities to wind pressure (Gioffrè 2001, Denoël, 2009). Indeed, for common structures subjected to wind, due to the low turbulence intensity of common winds, the effects of the quadratic terms on most of the civil structures might be neglected (Benfratello et al., 1996). In (Holmes, 1981) it is shown how for increasing wind turbulence intensities, the actual Probability Density Function (PDF) of the wind pressure obtained from wind velocities, rapidly diverges from a Gaussian-like distribution if the quadratic term is considered. Also, (Kareem, 1984) points out that even though the quadratic term of the wind turbulence does lead to actual small relative error in the estimation of the wind force, what is important actually is the frequency energy distribution of the non-linear process, which might be close to the dynamics of the system. Hence, there might be cases in which neglecting the quadratic term can lead to significant overestimations/underestimations of the structural response. Therefore, if the statistical description of input and/or output in a given system differs from Gaussian, conventional methodologies may no longer be valid in order to ensure safety and reliability of structures (Kwon and Kareem, 2009).

2. CONTEXT

In the context of non-linear buffeting analysis, where the wind loading follows a-priori a non-Gaussian probability distribution, the stochastic approach would require the evaluation of higher-order statistical moments –higher than the second– to properly characterise and quantify the diversion of the PDF of the structural response from a Gaussian-like distribution, when a closed form expression of such a PDF cannot be determined (Benfratello and Muscolino, 2000). In the theory of probability, higher order statistical descriptors that quantify non-Gaussian variables are the skewness, 3rd order descriptor, which quantifies the asymmetry, and the kurtosis or excess, at 4th order, which quantify the flattening of the tails of the PDF distribution. As of today, even though the wind engineering community is starting to increasingly admit the non-Gaussianity of the wind loading, almost never it is actually considered for many reasons (Gurley et al., 1997).

Nonetheless, as to the non-Gaussian nature of the wind loading, there exist analytical solutions for the computation of power spectrum and bispectrum of aerodynamic wind forces as a combination of the PSDs of the wind turbulent components u(t),v(t),w(t), by means of Volterra Series expansions and Fourier analysis, see e.g. Denoël (2006). These expressions are not much more complicated than the usual 2nd order spectral analysis.

Following the same concepts of a spectral analysis, the bispectrum of the loading can be expressed as a function of the PSDs of the three Gaussian components of the wind velocity vector $S_u,\ S_v,\ S_w$:

$$B_f = g(S_u, S_v, S_w) \tag{1}$$

Also, the bispectrum of the response is the result of the multiplication of the bispectrum of the loading B_f – non-Gaussian wind forces – and a kernel:

$$B_q(\omega_1, \omega_2) = K_B(\omega_1, \omega_2)\, B_f(\omega_1, \omega_2) \tag{2}$$

Where

$$K_B(\omega_1, \omega_2) = H(\omega_1) H(\omega_2) \overline{H}(\omega_1 + \omega_2) \tag{3}$$

$H(\omega)$ being the Fourier Transform of the transfer function of the system, the overbar $\overline{H}$ indicating the complex conjugate operator. If x(t) is a zero-mean non-Gaussian random process, then the third statistical moment is given by

$$m_{3,x} = \int_{-\infty}^{\infty} \int_{-\infty}^{\infty} B_x(\omega_1, \omega_2)\, d\omega_1 d\omega_2 \tag{4}$$

The skewness coefficient is given by

$$\gamma_{3,x} = \frac{m_{3,x}}{\left(m_{2,x}\right)^{\frac{3}{2}}} \tag{5}$$

being m_2 the second order statistical moment, the variance, obtained from well-known 2nd order spectral analysis.

3. ALGORITHMIC ARRANGEMENT

As of today, no proof of application of bispectral analysis to real MDOFs structures is found. Some authors have successfully applied it to very small structures (<10 DOFs, Gusella and Materazzi, 1998) but the effort in modelling larger structures has apparently never matured. The reasons are found in the very high computational costs required in:

- Projecting the $ndofs \times ndofs \times ndofs$ 3D-matrix of wind forces $B_f(\omega_1, \omega_2)$ in the modal basis for each pair of frequencies (ω_1, ω_2) of the discretised frequency space. This is the most expensive operation.
- Performing the double integration in Eq. (4) in the frequency space of B_q bispectrum of the structural modal responses for each $nmodes \times nmodes \times nmodes$ combination of mode triplets (m, n, l).

With the goal of making the bispectral analysis appealing for its application to relatively large structures of some hundreds of DOFs or more, an optimised numerical algorithm has been developed to tackle the most demanding aspects. This algorithm is based on some basic concepts, which have been fitted ad-hoc to the considered problem, still leaving space for some sort of generalisation:

- Subdivision of the frequency space into an ensemble of points grouped into basic, independent geometrical shapes (rectangles, triangles), at which, in a first stage, the loading information (bispectrum, $B_f(\omega_1, \omega_2)$) is computed.
- Secondly, a data interpolation approach specifically designed for the case, for an efficient and smart computation of $B_x(\omega_1, \omega_2)$, bispectrum of the structural response.

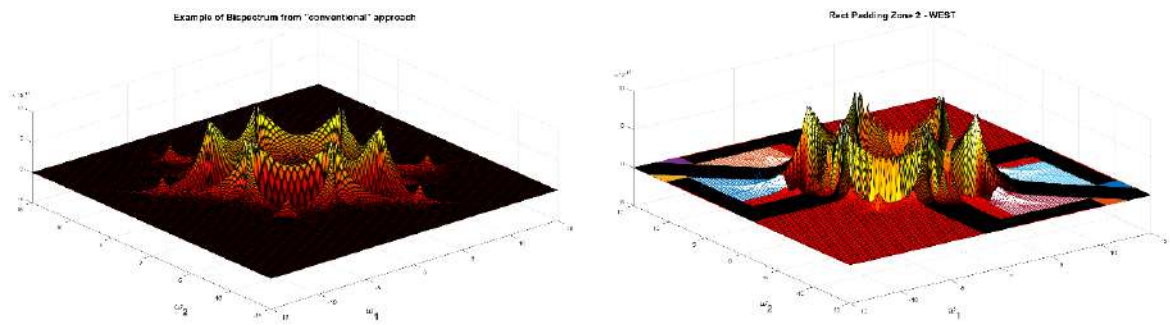

(a) (b)

Figure 1: (a) example of auto-bispectrum. (b) illustration of the same spectrum with the proposed representation in which each color represents a patched area.

4. CONCLUSIONS

First developments of this optimised algorithm have shown an important step toward making bispectral analysis more appealing to a wider range of day-to-day applications. Though its application to very small structures has shown no significant improvement in CPU time – mostly because of the non-negligible overhead in the patching of the frequency space– its effectiveness has proven as soon as the dimensions – i.e., complexity – of the problem increase. Its application to a 300-dofs bridge model, with 7 modes of vibration, considering auto-bispectrum only, has carried a speedup factor between 2-8 with respect to the conventional approach with a systematic, regular, meshing of the frequency space. This speedup depends on the refinement level and type of the patched areas, with discrepancy in the skewness coefficient < 1%. Yet, much higher speedup is expected when considering the complete 3D bispectrum matrices.

ACKNOWLEDGEMENTS
Part of this research project has been supported thanks to a research project funded by the Walloon Region (Convention Nb. 8096, FINELG2020)

REFERENCES

Benfratello S, Caddemi S, Muscolino G, 2000. Gaussian and Non-Gaussian stochastic sensitivity analysis of discrete structural system. Journal of Computers and Structures, 78:425-434.

Benfratello S, Falsone G, Muscolino G, 1996. Influence of the quadratic term in the along-wind stochastic response of SDOF structures. Journal of Engineering Structures, 18:685-695.

Cui W, Zhao L, Ge Y, 2022. Non-Gaussian turbulence induced buffeting responses of long-span bridges based on state augmentation method. Journal of Engineering Structures, 254:432-439.

Denoël V., Degée H., 2006. Influence of the non-linearity of the aerodynamic coefficients on the skewness of the buffeting drag force, International Journal of Wind and Structures, Vol. 9 (6), 457-471.

Denoël V., 2009. Polynomial approximation of aerodynamic coefficients based on the statistical description of the wind incidence, Probabilistic Engineering Mechanics, Vol. 24 (2), 179-189.

Denoël V, 2011. On the background and biresonant components of the random response of single degree-of-freedom systems under non-gaussian random loading. Journal of Engineering Structures, 33(8):2271-83.

Gioffrè M, Gusella V, 2002. Numerical analysis of structural systems subjected to non-gaussian random fields. Journal of Meccanica, 37:115-128.

Gioffrè M, Gusella V, Grigoriu M, 2001. Non-Gaussian Wind Pressure on Prismatic Buildings. Journal of Structural Engineering, 127:981-989.

Gurley K. R, Tognarelli M. A, Kareem A, 1997. Analysis and simulation tools for wind engineering. Journal of Probabilistic Engineering, 12(1):9-31.

Gusella V, Materazzi A. L, 1998. Non-Gaussian Response of MDOF Wind-Exposed Structures: Analysis by Bicorrelation Function and Bispectrum. Journal of Meccanica, 33:299-307.

Holmes J. D, 1981. Non-Gaussian Characteristics Of Wind Pressure Fluctuations. Journal of Wind Engineering and Industrial Aerodynamics, 7:103-108.

Kareem A, 1984. Nonlinear wind velocity term and response of compliant offshore structures. Journal Engineering Mechanics, 110:1573-1578.

Evaluation of wind comfort over the balconies of an irregular tall building by using Computational Wind Engineering

E. Amaya-Gallardo [1], M.A. Velázquez-Santiago [1], A. Pozos-Estrada [1]

[1] *Institute of Engineering, Mexico City, Mexico,* eamayag@iingen.unam.mx, marco.vs@comunidad.unam.mx, apozose@iingen.unam.mx

SUMMARY
In the last decade, the construction of tall buildings in Mexico has greatly increased, which has raised the need for open spaces to provide comfort to the inhabitants. The comfort of people in balconies can be impaired due to adverse wind effects. Although current Mexican standards contemplate service condition assessments from the structural approach, there are still no guidelines to establish criteria due to wind direct perception. In this work, numerical simulations are performed by means of Computational Wind Engineering to numerically evaluate wind velocities in the balconies of a tall building. These wind velocities were used to evaluate wind comfort with the Beaufort modified scale, which associates wind speeds with physical sensations in people. Based on this, the less comfortable building balconies were identified.

Keywords: wind comfort, wind direct perception, computational wind engineering

1. INTRODUCTION

In the last decade, the construction of tall buildings in Mexico has greatly increased, which has raised the need for open spaces, e.g., building balconies, to provide comfort in people. The comfort of people in balconies can be impaired due to adverse wind effects. The structural design approach usually focuses only on structural safety; however, numerous research has shown the need not only to guarantee structural performance but also to improve service and comfort conditions (Pozos-Estrada, 2010; Montazeri *et al*., 2013; Omrani *et al*., 2017; Zheng *et al*., 2020).

Since wind effects on structures depend to a great extent on their geometry, national building codes sometimes do not have enough information to design some structures as well as measures to mitigate the discomfort of the users. In order to compensate this lack of information, different methodologies are often used, such as full-scale experimental tests, experimental boundary layer wind tunnel tests (BLWT), aerodynamic databases, or computational fluid dynamics (CFD).

The main objective of this study is to numerically evaluate wind comfort in the balconies of a tall building with irregular shape by using Computational Wind Engineering (CWE).

2. GEOMETRY OF THE BUILDING AND WIND DIRECTIONALITY

The building under study is 158 m height with plan dimensions shown in Figure 1a. The use of the building is residential and offices. The building presents an irregular façade with balconies. The balconies present an irregular shape in plan with dimensions shown in Figure 1b. To characterize the wind direction, meteorological information from 48 years (1973–2021) was provided by the National Oceanic and Atmospheric Administration (NOAA) to identify the most critical incident directions for the tall building. As can be seen in the compass rose (Figure 1c), the prevailing wind direction is East. In this study, the easterly wind direction is considered for the numerical analysis.

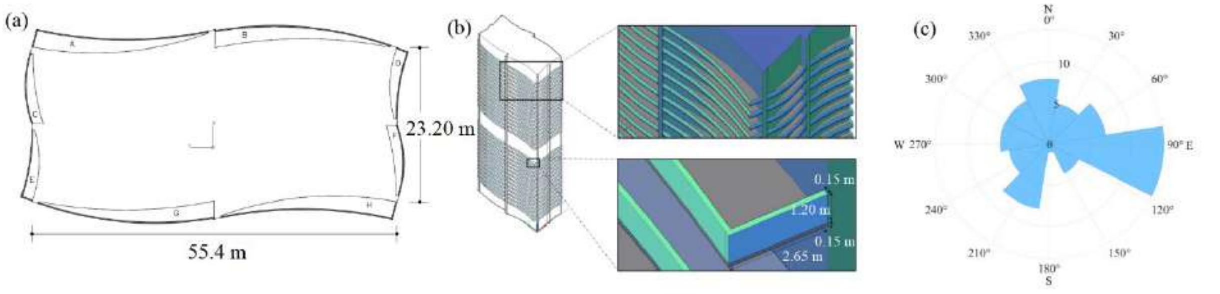

Figure 1. Views of the building: (a) plan view; (b) isometric and details of the balconies; (c) Site compass rose with predominant incident velocities

3. NUMERICAL ANALYSES AND RESULTS

The wind velocities in the balconies of the building under studied are estimated by means of numerical wind simulations with OpenFOAM using the steady RANS formulation for three different incident mean wind speeds (5, 10, and 15 m/s) and for a single wind incidence angle (easterly wind direction) employing the k–ω SST turbulence model. The numerical simulations were performed following the best CFD practice guidelines (Franke, 2004; Franke *et al*., 2007; Blocken *et al*., 2007; Tominaga *et al*., 2008; Franke *et al*., 2011). The ABLWT wind profiles (wind speed (U), turbulence intensity (I_U), turbulence kinetic energy (k) and turbulence dissipation rate (ε)) were simulated by using the following equations:

$$U(y) = \frac{u^*_{ABL}}{\kappa} \ln\left(\frac{y - y_g + y_0}{y_0}\right) \tag{1}$$

$$k(y) = \frac{u^{*2}_{ABL}}{\sqrt{C_\mu}} \tag{2}$$

$$\varepsilon(y) = \frac{u^{*3}_{ABL}}{\kappa(y - y_g + y_0)} \tag{3}$$

$$\omega(y) = \frac{\varepsilon(y)}{C_\mu k(y)} \tag{4}$$

where $U(y)$ is the velocity profile (m/s), $k(y)$ is the turbulence kinetic energy profile (m^2/s^2), $\varepsilon(y)$ is the turbulence dissipation rate (m^2/s^3), and $\omega(y)$ is the specific dissipation rate (s^{-1}); u^*_{ABL} is the atmospheric boundary layer (ABL) friction velocity (m/s), y_g is the minimum height from the ground (m) which for practical purposes is considered equal to zero, y_0 is the aerodynamic roughness length (m) and c_μ is a turbulence model empirical constant (≈0.09). Further, the empty domain test was carried out to validate the conditions of the flow simulation (i.e., U, I_U, k and ε), the results of this test are presented in Figure 2. Good agreement is observed in the input and output profiles considered.

It is noted that at a qualitative level, bluff-body aerodynamics indicates that the results are certainly influenced by the specific building and balcony shapes and that the worst conditions are expected at the balconies E, G, and H, especially close to the building corners (wind flow separation). The latter is to be validated numerically with CWE. The computed wind velocities were used to evaluate wind comfort according to the Beaufort modified scale (Lawson and Penwarden, 1975) threshold values, which associates wind speeds with physical sensations in people. On this basis, the less comfortable building balconies were identified depending on the wind velocities and a person's posture.

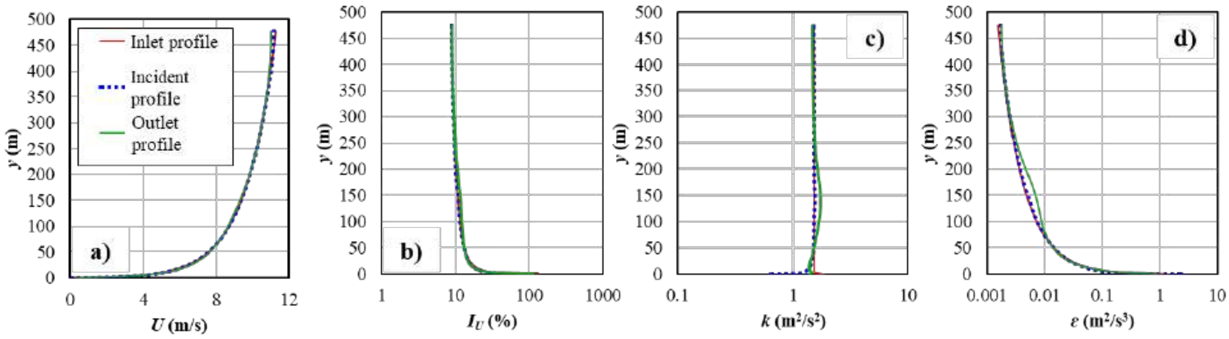

Figure 2. ABL wind profiles: (a) mean velocity; (b) turbulence intensity; (c) turbulence kinetic energy and (d) turbulence dissipation rate

Table 1. Evaluation of comfort on balconies for U_5 for people standing condition

Zone	Balcony	U_{BZ} (m/s)	U_L (m/s)	A_F	Effect	Comfort level
1	A	7.15	3.00	0.42	Gentle breeze: difficulty reading the newspaper	Good
	B		2.00	0.28	Light breeze: wind perceived in the face	Good
	C		2.00	0.28	Light breeze: wind perceived in the face	Good
	D		1.00	0.14	Light air: no noticeable wind	Good
	E		8.94	1.25	Strong breeze: difficulty walking, unpleasant noise in the ears	Moderate
	F		1.00	0.14	Light air: no noticeable wind	Good
	G		6.94	0.97	Cool breeze: tripping hazard when entering a windy area	Moderate
	H		8.94	1.25	Strong breeze: difficulty walking, unpleasant noise in the ears	Moderate

U_5= Simulation for mean velocity of 5 m/s; U_{BZ}= Undisturbed velocity at corresponding building zone; U_L= Balcony local velocity; A_F= Amplification factor (U_L / U_{BZ})

It is observed in Table 1 that for an amplification factor, AF, less than 1, the comfort condition is good, while for values close to 1, the condition is moderate. This exhibits the most uncomfortable balconies (E, G, and H), being mainly those located on the windward surface (G and H). Figure 3 presents the study areas along the height of the building and local wind velocity contours at balcony levels. It is observed in Figure 3 that balconies E and H, close to the corner, present the worst condition, as expected, with amplification factors equal to 1.25 for both cases. The effects that the inhabitants of the building with access to balconies E and H would experience difficulty in walking and unpleasant noise in the ears. Similar results are observed for Zones 2 to 4, except that the contour plots of local speed magnitude present variation in their distribution.

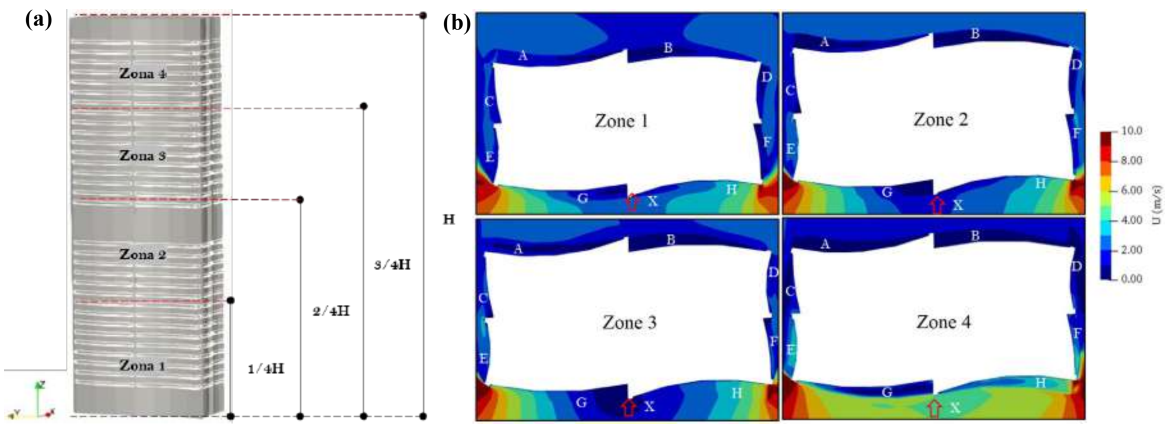

Figure 3. Study areas: (a) areas along the height of the building; (b) Plan view of local wind velocity contours at balcony level + 1.70 m (height of a standing person) in the *x*-direction for the different building zones

4. CONCLUSIONS

Numerical simulations were performed by means of CWE to numerically evaluate local wind velocities in the balconies of a tall building with irregular geometry. These local wind velocities were used to evaluate wind comfort with the Beaufort modified scale, which associates wind speeds with physical sensations in people. More specifically, the following conclusions are drawn:

- The amplification factor is a simple and useful measure to evaluate comfort levels.
- The balconies close to the corners in the windward face present the worst conditions, as expected. The effects that the inhabitants of the building with access to such balconies would experience difficulty in walking and unpleasant noise in the ears.
- Good comfort levels are experienced in the balconies of the leeward face.

ACKNOWLEDGEMENTS
The financial support received from the Institute of Engineering of the National Autonomous University of Mexico (UNAM) and the National Council on Science and Technology of Mexico (CONACYT) are gratefully acknowledged.

REFERENCES

Blocken B, Stathopoulos T, Carmeliet J (2007b) CFD simulation of the atmospheric boundary layer: Wall function problems. Atmospheric Environment 41(2):238-252, https://doi.org/10.1016/j.atmosenv.2006.08.019

Franke J (2004) Introduction to the prediction of wind loads on buildings by computational wind engineering (CWE). In: Stathopoulos T, Baniotopoulos CC (eds) Wind effects on buildings and design of wind-sensitive structures. Springer, Vienna, Austria, 67-103

Franke J, Hellsten A, Schlünzen H, Carissimo B (2007) Best practice guideline for the CFD simulation of flows in the urban environment. COST Action 732, Quality Assurance and Improvement of MicroscaleMeteorological Models, The European Cooperation in Science and Technology, Brussels, Belgium

Franke J, Hellsten A, Schlunzen KH, Carissimo B (2011) The COST 732 best practice guideline for CFD simulation of flows in the urban environment: A summary. International Journal of Environment and Pollution 44:419, https://doi.org/10.1504/IJEP.2011.038443

Lawson, T.V., Penwarden, A.D., (1975). The effects of wind on people in the vicinity of buildings. 4th International Conference on Wind Effects on Buildings and Structures. Cambridge University Press. Heathrow, pp. 605-622.

Montazeri, H., Blocken, B., Jassen, W.D., van Hooff, T. (2013). CFD evaluation of new second-skin facade concept for wind comfort on building balconies: Case study for the Park Tower in Antwerp. Building and Environment, 68, pp. 179-192. https://doi.org/10.1016/j.buildenv.2013.07.004

Omrani, S., Garcia-hansen, V., Capra, B., Drogemuller, R., (2017). On the effect of provision of balconies on natural ventilation and thermal comfort in high-rise residential buildings. Building and Environment, Volume 123, 2017, Pages 504-516, ISSN 0360-1323. https://doi.org/10.1016/j.buildenv.2017.07.016

Pozos-Estrada, A., Hong, H. and Galsworthy, J. (2010). Serviceability design factors for wind-sensitive structures. Department of Civil and Engineering, University of Western Ontario, London, ON N6A 5B9, Canada. https://doi.org/10.1139/L10-013

Tominaga Y, Mochida A, Yoshie R, Kataoka H, Nozu T, Yoshikawa M, Shirasawa T (2008) AIJ guidelines for practical applications of CFD to pedestrian wind environment around buildings. Journal of Wind Engineering and Industrial Aerodynamics 96(10-11):1749-1761, https://doi.org/10.1016/j.jweia.2008.02.058

Zheng, X., Montazeri, H., Blocken, B. (2020). CFD simulations of wind flow and mean surface pressure for buildings with balconies: Comparison of RANS and LES. Building and Environment. Volume 182, September 2020, Pages 107017. https://doi.org/10.1016/j.buildenv.2020.106747

Effect of upstream-corner sharpness in experiments and simulations of the flow around rectangular cylinders of different aspect ratios

M.V. Salvetti [1], G. Lunghi [1], A. Mariotti [1]

[1]*Dipartimento di Ingegneria Civile e Industriale, Università di Pisa, Largo Lucio Lazzarino 2, Pisa, Italy,* mv.salvetti@ing.unipi.it

SUMMARY
We analyze the importance of upstream-corner sharpness in experiments and LES of rectangular cylinders of different aspect ratios, viz. 1:1, 3:1, and 5:1. The first is characterized by a separated mean flow, for the second the mean flow is about to reattach along the lateral side of the cylinder and for the latter the mean flow reattaches. In numerical simulations, a negligible effect of the upstream-corner sharpness is found for the square cross-section, whereas a significant difference is present between sharp edges and rounded edges for the 3:1 and 5:1 rectangular cylinders even for a very small value of the curvature radius. Sharp edges lead to a premature onset of Kelvin-Helmholtz instability in the shear layers detaching from the upstream corners and this moves upstream the reattachment of the mean flow on the cylinder side for the 3:1 and 5:1 cases. In the experiments, a lower sensitivity is found also when pushing the rounding value to very small values. By further increasing the corner rounding up to r/D=0.0360, D being the cylinder width, differences are not significant both in experiments and simulations, while starting from r/D=0.0781 the size of mean recirculation region on the cylinder side decreases noticeably by increasing r/D.

Keywords: rectangular cylinders, upstream-corner sharpness, experiments and LES

1. INTRODUCTION

The flow around square/rectangular cylinders is of interest in civil engineering because it can be considered a model problem for tall buildings or bridges. The square cylinder is characterized by a separated mean flow, the 3:1 rectangular cylinder by the mean flow that is about to reattach along the lateral side of the cylinder, and for the 5:1 cylinder the mean flow reattaches. Rocchio et al. (2020) recently studied the effects of small rounding of the upstream edges of the 5:1 rectangular cylinder showing that even small values of the curvature radius, which are difficult to detect in experimental models, significantly increase the length of the mean recirculation region and, hence, the agreement with the experimental data is considerably improved. This is because sharp edges introduce significant velocity fluctuations in the shear-layer at separation that, when not artificially damped by numerical or SGS dissipation, cause an upstream roll-up of the shear layers and a short mean recirculation region. This effect seems to be a numerical one related to the flow resolution typical of LES simulations since the impact of upstream edge rounding was found to be much smaller in DNS simulations in Chiarini and Quadrio (2022) at lower Reynolds numbers. Now we want to investigate whether a similar behavior is found in LES and experiments of rectangular cylinders of different aspect ratios. To this aim, we also considered a square cross-section and a rectangular one having an aspect ratio of 3:1, which are characterized by different flow topologies. Sharp upstream edges and different values of the upstream corner rounding are investigated. Both experiments and LES are carried for 3:1 and 5:1 aspect ratios, while the square cylinder case is investigated only through LES.

2. PROBLEM DEFINITION AND INVESTIGATION METTHODOLOGY

We consider the incompressible flow around rectangular cylinders, whose chord-to-depth ratios are 1:1, 3:1, and 5:1 at zero angles of attack. The upstream edges are sharp or rounded with curvature radii r/D=0.0037, 0.0360, 0.0781, 0.1104, being D the depth of the cylinder. The Reynolds number, based on the cylinder depth and the freestream velocity, is set to 40000. The numerical simulations are performed by employing Nek5000, an open-source code based on a high-order spectral element method. Details on numerical methodology and simulations set-up can be found in Mariotti et al. (2017) and Rocchio et al (2020). Experiments are carried out in the subsonic wind-tunnel of the University of Pisa for the 3:1 and 5:1 cases for the same values or r/D as in the simulations.

3. RESULTS AND DISCUSSION

Mean flow streamlines and isocontours of the instantaneous vortex-indicator λ_2 for r/D=0 and r/D=0.0037 are shown in Fig. 1. For the square cross-section, which is characterized by a separated mean flow (Figs. 1a, d), a negligible effect of the upstream-corner sharpness is found. Upstream-corner sharpness is important for the 3:1 and 5:1 cylinders, even for this very small value of the curvature radius, with a more upstream Kelvin-Helmholtz instability and a shorter mean recirculation region on the cylinder side for perfectly sharp edges. In the experiments, a lower sensitivity is found also when pushing the rounding value to very small values. By further increasing the corner rounding up to r/D=0.0360, differences are not significant both in simulations and experiments, while starting from r/D=0.0781 the size of mean recirculation region on the cylinder side decreases noticeably by increasing r/D, because of a modification of the inclination of the detaching shear layers.

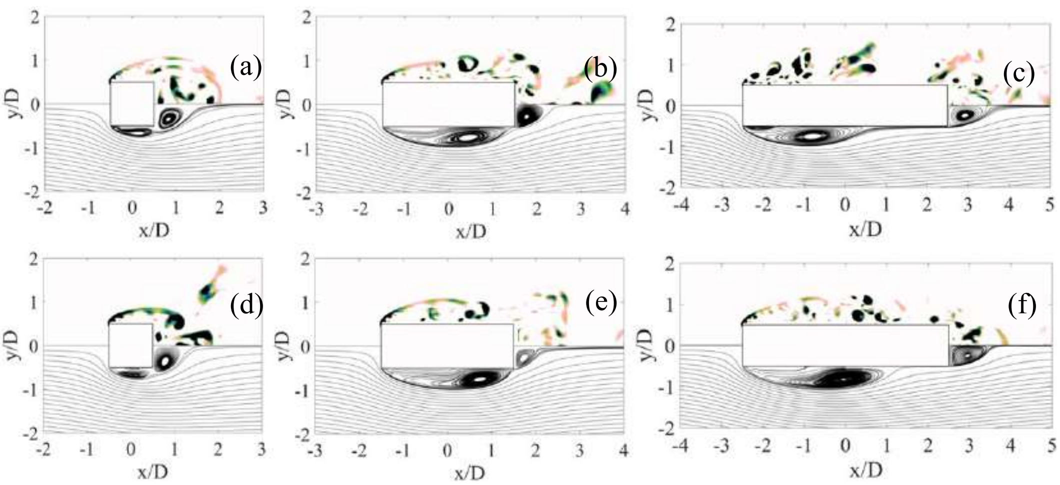

Figure 1. Mean flow streamlines (top) and instantaneous vortex-indicator λ_2 (bottom) for the cases: (a) 1:1 and r/D=0, (b) 3:1 and r/D=0, (c) 5:1 and r/D=0, (d) 1:1 and r/D=0.0037, (e) 3:1 and r/D=0.0037, and (f) 5:1 and r/D=0.0037.

REFERENCES

Chiarini, A., Quadrio, M. 2022 The importance of corner sharpness in the BARC test case: A numerical study. Wind and Structures, An International Journal. 34(1), 43-58.

Mariotti, A., Siconolfi, L. and Salvetti, M.V., 2017. Stochastic sensitivity analysis of large-eddy simulation predictions of the flow around a 5:1 rectangular cylinder. European Journal of Mechanics B/Fluids 62, 149-165.

Rocchio, B., Mariotti, A. and Salvetti, M.V., 2020. Flow around a 5:1 rectangular cylinder: Effects of upstream-edge rounding. Journal of Wind Engineering and Industrial Aerodynamic 204, 104237.

Aspects of the dynamic wind loading of solar PV structures

Zachary J. Taylor [1], Matthew T.L. Browne [2], Francesco Dorigatti [3], Chiara Pozzuoli [4]

[1]*RWDI, Guelph (ON), Canada, zachary.taylor@rwdi.com*
[2]*RWDI, Guelph (ON), Canada, matthew.browne@rwdi.com*
[3]*RWDI, Milan, Italy, francesco.dorigatti@rwdi.com*
[4]*RWDI, Milan, Italy, chiara.pozzuloi@rwdi.com*

SUMMARY
Wind design is an important aspect for structural efficiency to help minimize cost and maximize the long-term reliability of any solar installation. Over the last several years, prescriptive load methodologies have arisen for the static wind loads of rooftop solar systems and ground-mounted solar systems. However, these prescriptive load methodologies assume that the solar structure does not move in the wind. Movement of flexible structures in the wind can lead to additional loads or in some cases can lead to wind-induced divergent motion causing structural failures. These failures have led to substantial economic losses due to downtime of the solar installations affected and to significant costs for retrofits and improvements to existing sites.

Keywords: Solar PV structures, wind-tunnel testing, aerodynamic instabilities, wind loading

1. INTRODUCTION

One of the challenges facing building code committees is the definition of what makes a solar structure flexible or not. The ASCE 7 standard (ASCE/SEI, 2021) defines a flexible structure based on the natural frequency threshold of 1 Hz. This criterion was developed primarily with buildings in mind and has been shown to be inadequate for smaller structures such as solar PV installations. Experience from full-scale installations and evidence from wind tunnel testing on scale models clearly show that ground mounted single-axis trackers are flexible enough to move due to wind even though most have frequencies beyond 1 Hz, to a point where these structures have had well documented structural failures due to wind. Despite the related economic losses, it is from the analysis and retrospective investigations of these failures, as well as from the increasing amount of wind tunnel testing on scale models carried out to support the solar system design, that an improved understanding of the interaction between solar structures and wind has been gained. This knowledge can now be leveraged to strive towards more robust and reliable structural designs.

2. SCIENTIFIC INNOVATION AND RELEVANCE

There are two main concerns related to the interaction between solar structures and wind: (i) aerodynamic instability, and (ii) dynamic wind loading. The approach to assess the aeroelastic susceptibility of solar structures is to first assess the likelihood for aerodynamic instability, which has the potential to cause divergent motion of the structure and, in turn, structural failure, and then investigate the dynamic wind loading, which provides the information needed for structural design, once the risk of instability has been ruled out.

2.1. Aerodynamic instability

Divergent aerodynamic instabilities causing large amplitude rotational motions have been observed primarily in ground-mounted single-axis solar trackers, which tend to present a relatively low torsional stiffness by design. For these single-axis trackers there are two broad categories of aerodynamic instability: (i) stiffness-driven, and (ii) damping-driven.

Although the large amplitude oscillations of stiffness-driven and damping-driven instability appear similar, measurements of aerodynamic stiffness and damping undertaken through wind tunnel testing have clarified the differences of the underlying phenomena that cause each type of instability. Wind tunnel tests on full aeroelastic models (e.g., Figure 1) are currently undertaken to establish the critical wind speeds for the onset of aerodynamic instabilities.

2.1.1. Stiffness-driven torsional divergence/galloping

The stiffness-driven instability consists of a loss of structural stiffness in the tracker system caused by 'negative' aerodynamic stiffness being introduced by the wind action. As the negative stiffness contribution introduced by the wind increases with the wind speed, at elevated wind speed its magnitude becomes large enough to eventually overcome the inherent structural stiffness of the system, which causes significant motions. Stiffness-driven instability has been observed and well documented through wind tunnel testing on aeroelastic scale models. It often occurs at low tilt angles (e.g., < 20°) and, due to non-linearities in the combined fluid-structure system, the divergent motions that it causes are often observed to lead to limit cycle oscillations.

2.1.2. Damping-driven torsional flutter

For greater tilt angles (e.g., > 20°) the aerodynamic instability is observed to be driven by changes in damping. At elevated wind speeds the aerodynamics of the flow around photovoltaic modules is observed to create negative aerodynamic damping. Once the negative aerodynamic damping exceeds the inherent structural damping of the system, then the system becomes negatively damped. When this condition is reached, the tracker system absorbs more energy from the wind flow than what it can dissipate internally, which leads to excessive dynamic rotations.

2.2. Dynamic wind loading

Wind loading is generally composed of three parts: the mean wind load, the fluctuating background load, and the inertial wind loads. In the solar industry the mean and background wind loads are referred to as the "static" wind loads since they do not depend on the motion of the structure. However, the fluctuating background wind loads can cause a structure to move which induces additional inertial wind loads that must be resisted by the structure. These inertial wind loads are referred to as the "dynamic" wind loads.

There is currently an open question about what threshold or criterion should define when dynamic loads may be important. As previously discussed, the 1 Hz threshold used for buildings (ASCE/SEI, 2021) has been proven to be not appropriate for solar structures. The commentary to the National Building Code of Canada (NRC, 2017) suggests that 10 Hz may be a suitable threshold above which dynamic loads are not likely to be important.

Dynamic wind loads are complex and therefore difficult to account for through prescriptive methods. Wind tunnel testing on rigid models instrumented for pressure measurements is the most accurate method to determine dynamic wind loads. Alternatively, an analytical approach assessed in this study to derive the inertial wind loads, (i.e., dynamic wind loads) is based on first principles of wind loading and atmospheric turbulence and relies on a relatively straightforward equation that can be computed with readily available structural properties and design criteria. It can be shown that the ratio of peak inertial forces, $\hat{F}_i$, to the total force, $\hat{F}_t = \hat{F}_s + \hat{F}_i$, (where $\hat{F}_s$ is the static force) can be approximated through

$$\frac{\hat{F}_i}{\hat{F}_t} = 0.3 \cdot \left(\frac{3\, m}{L_c}\right)^{\frac{1}{2}} \zeta^{-\frac{1}{2}} \overline{U}^{\frac{5}{3}} xL_u^{-\frac{1}{3}} f_n^{-\frac{1}{3}} \left(\frac{1}{\overline{U}^{\frac{4}{3}} + (2 f_n L_c)^{\frac{4}{3}}}\right) \tag{1}$$

In Eq. (1), ζ is the structural damping ratio to critical, $\overline{U}$ is the mean wind speed at structure height, xL_u is the longitudinal integral length scale, f_n is the natural frequency for the mode of interest, and L_c is the chord length of the photovoltaic module. It should be noted that a dependance of the peak inertial forces on the aerodynamic admittance function is implicit in this formulation, which assumes that the dynamic loads collapse reasonably well when scaled by the reduced frequency $f_n L_c/\overline{U}$.

3. RESULTS AND DISCUSSION

3.1. Aerodynamic instability

Results from several different aeroelastic model tests carried out at RWDI have been anonymized and the critical reduced gust speeds are shown in Figure 2. The critical reduced gust speed is defined as the peak structurally averaged gust speed U divided by the natural frequency f_n (typically taken for the first torsional mode of vibration) and chord length L_c. The envelope of the data is shown in the gray shaded region in Figure 2 while the blue shaded region shows one standard deviation either side of the mean. To explain the relatively large scatter of this dataset, it should be noted that there are significant differences in terms of chord, tracker elevation, structural damping, and overall architecture of the ground-mounted single-axis systems from which the data were derived.

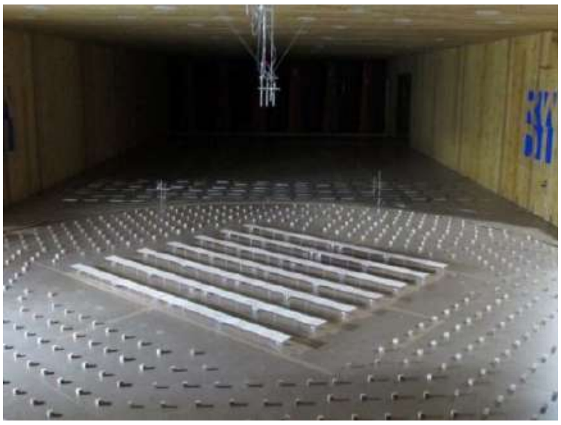

Figure 1. Full aeroelastic model in the wind tunnel

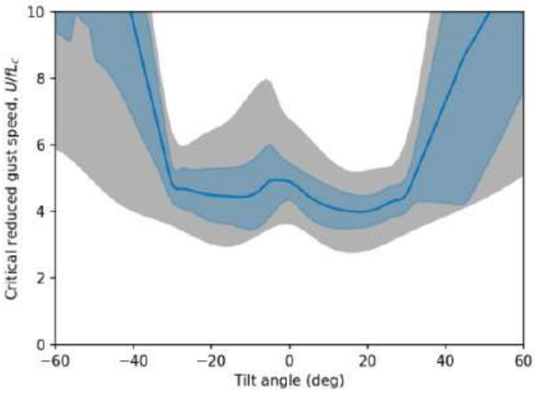

Figure 2. Critical wind speeds from several aeroelastic model wind tunnel studies

Based on these results, a conservative lower bound can be provided such that aerodynamic instability could occur when

$$U > 2.5 L_c f_n \tag{2}$$

The peak structurally averaged gust speed (U) is not straightforward to calculate; however, it can be approximately related to the mean wind speed ($\overline{U}$) by $U = 1.4\overline{U}$ such that the criterion becomes

$$\overline{U} > 1.8 L_c f_n \tag{3}$$

3.2. Dynamic wind loading

Several dynamic wind load measurements obtained through wind tunnel testing of rigid models instrumented for pressure (Browne et al., 2020) of a wide range of different ground-mounted solar structures are compared to predictions obtained from Eq. (1) in Figure 3. The agreement between the upper bound of the experimental data and the analytical results from Eq (1) confirms that this equation can be used conservatively to predict the dynamic wind load contribution on a solar system depending on its structural and geometrical parameters and on the characteristics of the atmospheric wind. Based on that prediction, a criterion is suggested that considers not significant for design any dynamic wind loading less than approximately 10% of the total loading, i.e., $\hat{F}_i/\hat{F}_t < 0.1$. However, it is recommended that wind engineering guidance be sought if the suggested criteria are not met.

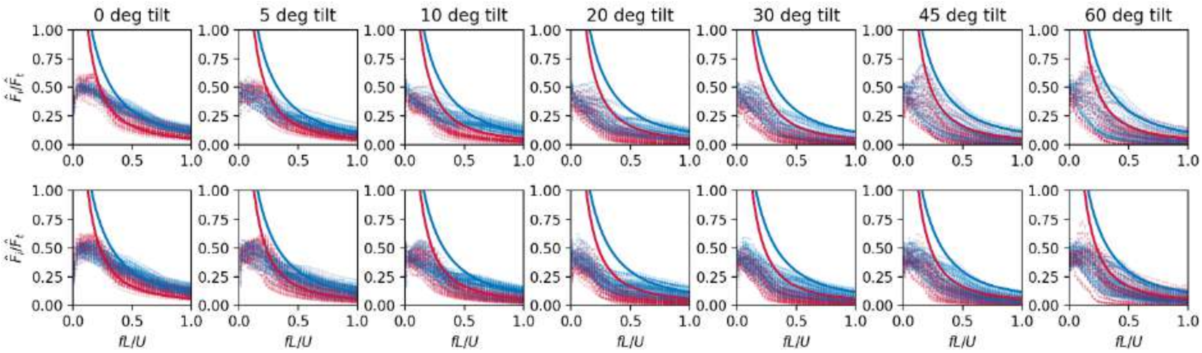

Figure 3. Evaluation of Eq. (1) compared to data points as measured from wind tunnel tests. Structural damping is taken as 1% of critical in each case. Top and bottom rows represent perimeter and central zones, respectively; solid lines show Eq. (1) while dots represent wind tunnel data points; blue is for $L_C \sim 4$ m, red for $L_C \sim 2$ m

REFERENCES

ASCE/SEI, 2021. ASCE 7-22: Minimum Design Loads and Associated Criteria for Buildings and Other Structures.

NRC, 2017. Structural Commentaries: (User's Guide - NBC 2015: Part 4 of Division B).

Browne, Z. J. Taylor, S. Li, and S. Gamble, 2020. A wind load design method for ground-mounted multi-row solar arrays based on a compilation of wind tunnel experiments, J. Wind Eng. Ind. Aerodyn., vol. 205, no. July, p. 104294

Tintagel footbridge: wind-tunnel assisted design and pedestrian induced vibration assessment via monitoring

Emanuele Mattiello [1], Pierre-Olivier Dallaire [2], Guy Larose [3], Francesco Dorigatti [4]

[1]*RWDI, Milan, Italy, emanuele.mattiello@rwdi.com*
[2]*RWDI, Bromont (QC), Canada, pierre.dallaire@rwdi.com*
[3]*RWDI, Ottawa (ON), Canada, guy.larose@rwdi.com*
[4]*RWDI, Milan, Italy, francesco.dorigatti@rwdi.com*

SUMMARY
This paper presents the engineering approach taken to overcome the climate, local complex topography and comfort considerations influencing the design of the Tintagel footbridge, a remarkable pedestrian bridge on the south-west coast of England. RWDI conducted wind-tunnel tests to support the design, including a topographic model assessment of the local wind conditions and sectional model testing of the bridge deck. After completion in 2019 and prior to the official opening of the bridge, RWDI conducted field tests of the bridge dynamic behaviour under prescribed live load to verify the tuned-mass damper system. The field tests enabled correlation analyses between the measured response and numerical simulations.

Keywords: footbridge, wind-tunnel testing, pedestrian-induced vibrations

1. INTRODUCTION

The Tintagel Footbridge is a pedestrian bridge close to Tintagel, Cornwall, UK, with a total span of 66 m and a width of 3 m connecting the mainland with the island where the castle ruins are located. The bridge floats 55 m above the sea level and consists of two independently built cantilevers nearly touching at mid-span. Each cantilever is composed by a thin deck and a truss-type arch supporting system. Figure 1 shows a side view of the bridge.

Figure 1. Photo of the Tintagel bridge connecting mainland and the ancient castle ruins on the island.

RWDI conducted the following studies in 2016: i) wind climate, site analysis and topographical wind-tunnel study, ii) sectional model wind-tunnel study of the complete bridge, and iii) wind induced buffeting analysis and derivation of wind loads. After the bridge completion in 2019 and prior to the public opening, RWDI carried out full-scale site measurements to document and assess the performance on the bridge under pedestrian excitation.

2. WIND-TUNNEL TESTING – TOPOGRAPHIC STUDY

The interaction between the atmospheric boundary layer and complex terrain in mountainous regions can lead to changes in the mean wind speed, flow direction and turbulence properties when compared to the flow on a site of similar exposure but surrounded by flatter terrain.

For the proposed Tintagel footbridge, a topographic model study was conducted to address the influence of the complex terrain surrounding the site (Figure 2-left). The objective of the study was to provide, in a short period of time, an evidence-based description of the variation of the mean wind speeds with height and wind direction at the location of the bridge across the escarpment and a prediction of the expected characteristics of the turbulence at deck level. These are the input necessary to consider storm winds in the design.

The wind-tunnel study was conducted using a 1:500 scale model centered on the bridge crossing. The model was tested in RWDI's 2.7 m × 2.0 m open jet boundary layer wind tunnel in Milton Keynes, UK, such that the topography surrounding the site was modelled within a radius of approximately 750 m. The topographic model was based on high resolution Lidar measurements of the topography of the site and the terrace approach was used to machine high density foam to model the topography at 1:500 scale in steps of 2 mm.

Figure 2. Tintagel bridge wind-tunnel topographic testing (left) and sectional testing (right).

Detailed flow data were obtained using a multi-hole pressure probe measuring over the full range of wind directions in 10° steps and at the bridge axis directions which are 35° and 215°.

2.1. Results

The experiments revealed that the complexity of the terrain, in particular the proximity of the escarpments and the uneven surface of the lower ridge below the location of the bridge had a strong effect on the flow at deck level. The local topography's major effect was to cause the mean wind to reach the bridge deck with a significant positive angle of attack (between +16° and +24°) - i.e. blowing up towards the bridge deck. The cliffs located near the proposed bridge site also had the effect of steering the Southwest winds to become nearly perpendicular to the bridge axis. No significant local increase of the wind speed at deck level was observed however during the experiments. The mean angle of wind incidence was established to be +21° for the design winds normal to the bridge as shown in Figure 5, both from south-west and north-east.

3. WIND-TUNNEL TESTING – DECK SECTIONAL TESTING

The objectives of the sectional model tests were to examine the aerodynamic stability for vortex-shedding induced oscillations, flutter and galloping of the proposed bridge deck and to measure the static aerodynamic force and moment coefficients. A sectional model of the bridge was constructed at a scale of 1:14, see Figure 2-right. The combined analysis of the topographical wind-tunnel study, the site exposure and the directional factors from the Eurocode, UK National Annex (based on climatology analyses) identify that the most critical winds are Southwest winds coming from the sea, at 220°. The wind speed criteria for divergent aerodynamic instability of the complete bridge was 58.3 m/s at deck level (55 m), perpendicular to the bridge axis and approaching the deck from the bottom-up with an angle of +21°.

3.1. Results

The wind-tunnel tests revealed that proposed deck cross-section was not prone to vortex-shedding induced vibrations, even in smooth flow conditions, with low structural damping and high angles of attack. During the wind-tunnel tests, no galloping or flutter instability was observed at wind speeds lower than the wind speed criteria for divergent instabilities of 58.3 m/s. It is believed that the presence of the truss below the deck is beneficial with regards to the aerodynamic stability of the bridge, since its depth varies gradually along the span reducing the possibility of having coherent vortices shed in the wake.

4. PEDESTRIAN-INUCED VIBRATION FULL-SCALE TESTING

RWDI performed site monitoring activities in Summer 2019. The objective was to carry out pedestrian-induced vibration measurements to evaluate the sensitivity of the bridge to pedestrian live loads, for different scenarios of pedestrian circulation. The field campaign also included the identification of the as-built frequencies and mode shapes of the structure through a series of ambient and forced vibration measurements. The measurements were carried out before the vertical and lateral tuned-mass dampers (TMDs) planned for the bridge to enhance user comfort were tuned to the as-built frequencies of the structure. This was a great opportunity to correlate field data for selected crowd activities with numerical modelling techniques to evaluate the peak accelerations under such loading scenarios.

The instrumentation used consisted of six triaxial accelerometers which allowed for the sampling of longitudinal, vertical and lateral accelerations of the deck at various locations.


Figure 3. Pedestrian loading activities: crossing as a group (left) and with random distribution (right).

Ambient vibration measurements were carried out to identify the principal modes of vibrations of the structure with TMDs installed and compare them with the dynamic properties estimated by the structural engineer. Forced vibration measurements were carried out to assess the performance of the TMDs installed for the identified principal modes of vibrations, i.e., 1st and 2nd vertical and 1st lateral mode. Output of ambient vibration measurements showed good agreement between the full-scale frequencies and the analytical predictions.

Different pedestrian activities were simulated on the bridge with up to 15 people participating during testing. The size of the group corresponded to a traffic class of TC1 (Heinemeyer et al., 2009). The simulated scenarios were as follow: uncorrelated (random) and correlated (tuned to the principal modes of the structure) walking as a group (Figure 3-left) and with random distribution (Figure 3-right), uncorrelated and correlated jogging as a group and with random distribution, uncorrelated and correlated jumping as a group.

4.1. Results

For the uncorrelated walking scenario, the pedestrian frequencies were similar to the 1st vertical frequency of the bridge. Therefore, this scenario was considered as appropriate baseline for extrapolation of the measurements to higher traffic densities, i.e., up to TC4-5. A simple principle from random vibration theory was used to scale the measured accelerations to a different desired density following Eq. (1):

$$a_{p2} = a_{p1} \cdot \sqrt{n_{b2}/n_{b1}} \tag{1}$$

where n_{b1} is the number of pedestrians for scenario 1, a_{p1} is the peak acceleration observed for scenario 1 (9% of gravity for TC1 in this case), n_{b2} is the number of pedestrians for the desired scenario and a_{p2} is the extrapolated peak acceleration for the desired scenario. The obtained results in terms of accelerations and comfort level are given in Table 1 shown below.

Table 1. Estimations of vertical accelerations for various traffic classes, walking activities.

Traffic class	Density of people	Corresp. no. of people	Longitudinal accelerations (% of g.)	Lateral accelerations (% of g.)	Vertical accelerations (% of g.)	Corresponding SETRA comfort (SETRA, 2006)
TC1	0.09	13	1	1	9	Mean
TC2	0.2	29	2	2	14	Minimum
TC3	0.5	74	2	2	21	Minimum
TC4	1	174	3	3	30	Unacceptable
TC5	1.5	221	4	4	37	Unacceptable

Notes: the above extrapolations do not account for non-linear behaviour of TMDs; a volume of traffic corresponding to TC4 and higher is well expected for bridge opening day or large events.

These measured peak accelerations were found to be in agreement with the time domain simulations that emulated the different scenarios. After the monitoring activities performed by RWDI, the tuned-mass damper units were optimally tuned in-situ and the bridge has been opened to the public and has been in operation for its intended use ever since.

5. CONCLUSIONS

RWDI conducted a series of wind-tunnel tests to inform the design of the Tintagel footbridge, set to be a unique landmark in the harsh and complex environment of Tintagel, Cornwall, UK. Prior to the bridge opening to public, RWDI performed full-scale vibration measurements to document the performance on the as-built structure under different pedestrian loading scenarios and successful comparisons were made with predictions based on numerical simulations.

ACKNOWLEDGEMENTS

The authors acknowledge English Heritage for the cooperation and free access to the site during the monitoring activities and full-scale vibration testing.

REFERENCES

Heinemeyer, C. et al., 2009. Design of Lightweight Footbridges for Human Induced Vibrations. Prepared under the JRC - ECCS cooperation agreement for the evolution of Eurocode 3

SETRA, 2006. Footbridges. Assessment of vibrational behaviour of footbridges under pedestrian loading

Effect of the lateral mean recirculation characteristics on near-wake and bulk quantities of a 5:1 rectangular cylinder

G. Lunghi [1], E. Pasqualetto [1], A. Mariotti [1], M.V. Salvetti [1]

[1]*Dipartimento di Ingegneria Civile e Industriale, Università di Pisa, Largo Lucio Lazzarino 2, Pisa, Italy, gianmarco.lunghi@phd.unipi.it*

SUMMARY
A database of many Large-Eddy Simulations carried out on the high-Reynolds number flow around a 5:1 rectangular cylinder is analyzed to highlight the effect of the lateral mean recirculation characteristics on the near-wake flow features and on some bulk quantities. Different simulation set-ups are considered by varying the grid refinement in the spanwise direction and the amount of SubGrid-Scale (SGS) dissipation for rectangular cylinders with sharp edges and, moreover, considering different values of the upstream-edge roundings. Among the selected characteristic lengths defining the mean recirculation, the streamwise length of the recirculation is the most important parameter. The increase of the lateral mean recirculation length causes a linear increase of the wake width, and a linear decrease of the vortex-shedding non-dimensional frequency and of the drag coefficient, the latter due to a reduction of the suctions on the base. Finally, a significant increase of the fluctuations of the lift coefficient is found.

Keywords: rectangular cylinders, Large-Eddy Simulations, lateral and near-wake flow features

1. INTRODUCTION

The high-Reynolds number flow around a 5:1 rectangular cylinder is paradigmatic of many wind-engineering applications, such as tall buildings or bridge decks. The flow presents a shear-layer separation from the upstream edges. Vortical structures of different size form from the roll up of these shear layers, move downstream and interact with the classical vortex shedding further downstream in the wake. The mean flow shows a recirculation region ending with a reattachment close to the trailing edge. The LES simulations in Mariotti et al. (2017) and Rocchio et al. (2020) showed that the length of the mean recirculation region is highly sensitive to grid refinement, SGS modeling, and upstream edge treatment. Now we want to investigate possible quantitative links between the features of the mean recirculation region and some quantities of practical interest, such as force coefficients and pressure distribution. To this aim, the results of many LES are analyzed; these simulations give significantly different mean flow features on the cylinder side and, thus, represent a useful database for our analysis (Lunghi et al., 2022). The different mean recirculation regions are due to a different location of the instability onset in the shear layers detaching from the upstream corners, which may be, in turn, related to edge sharpness, grid resolution and SGS viscosity. Therefore, we think that these results may be considered as possible instances of this kind of flow, with different introduction at the upstream edge and different evolution along the shear layer of the fluctuating kinetic energy. Some characteristic lengths of the mean recirculation region are identified and the relevant effects on the wake width, the vortex-shedding Strouhal number, the base pressure and the lift-coefficient fluctuations are addressed.

2. PROBLEM DEFINITION AND INVESTIGATION METHODOLOGY

All the revisited LES are carried out through the open-source code Nek5000, based on a high-order spectral-element method. The details on the numerical methodology and on the simulation set-up are described in Mariotti et al. (2017) and Rocchio et al. (2020). In the simulations, the adopted filter is a sharp cut-off with a quadratic transfer function for the modes in the range $k_c \leq k \leq N$, being $k_c = N - 3$ in this case. Thus, the transfer function of the filter can be written as:

$$\begin{cases} \sigma_k = 1 & k < k_c \\ \sigma_k = 1 - \mathrm{w}\left(\dfrac{k - k_c}{N - k_c}\right)^2 & k_c \leq k \leq N \end{cases} \tag{1}$$

where w is the filter weight. This filter introduces dissipation on the highest resolved modes only and it can be considered as a SGS dissipation. For w and for the spanwise grid resolution the following values are used w = (0.018, 0.05, 0.0912, 0.1218) and Δz = (0.649D, 0.558D, 0.437D, 0.346D), respectively. Sharp upstream edges are considered in the simulations in Mariotti et al. (2017), whereas different upstream-edge roundings in the ones in Rocchio et al. (2020), viz. r/D = (0.0037, 0.0177, 0.0360, 0.0500). An additional simulation is carried out to match the value of the roundness of the experiments in Pasqualetto et al. (2022), i.e. r/D=0.0005.

3. RESULTS AND DISCUSSION

The wake width, tw, evaluated at 2D downstream of the rectangular cylinder, and the Strouhal number related to the vortex-shedding frequency are linearly correlated with the characteristic length of the recirculation region, lp, as can be seen in Fig. 1a and Fig. 1b, respectively. A clear trend is found: a shorter recirculation leads to a narrower wake and to a higher vortex-shedding Strouhal number. The increase of the inward curvature of the mean flow streamlines bounding the recirculation region seems to be the main cause of the narrowing of the wake. In Figure 1c, we single out the effect of the streamwise length on the averaged value of the pressure coefficient acting on the rear face of the cylinder, ⟨Cp⟩base. A linear decrease of the suctions acting on the rear base of the body by increasing the characteristic lengths of the mean recirculation is found. The trends observed in the present analysis are qualitatively consistent with those of previous works on the BARC configuration. Physical discussion on these effects and the analysis of others bulk parameters and flow features will be given in the final presentation.

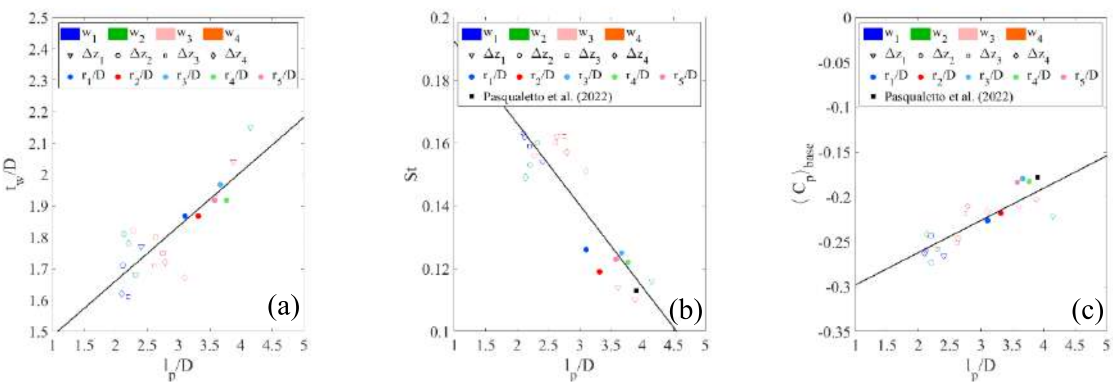

Figure 1. Effect of the streamwise length of the mean recirculation, l_p, (a) on the wake width, t_w, (b) on the Strouhal number, St, and (c) on the time- and base-averaged pressure coefficient, $\langle Cp \rangle_{base}$.

REFERENCES

Lunghi, G., Pasqualetto, E., Rocchio, B., Mariotti, A. and Salvetti, M.V., 2022. Impact of the lateral mean recirculation characteristics on the near-wake and bulk quantities of the BARC configuration. Wind and Structures, an International Journal 34(1), 115-125.

Mariotti, A., Siconolfi, L. and Salvetti, M.V., 2017. Stochastic sensitivity analysis of large-eddy simulation predictions of the flow around a 5:1 rectangular cylinder. European Journal of Mechanics B/Fluids 62, 149-165.

Pasqualetto, E., Lunghi, G., Rocchio, B., Mariotti, A. and Salvetti, M.V., 2022. Experimental characterization of the lateral and near-wake flow for the BARC configuration. Wind and Structures, an International Journal 34(1), 101-113.

Rocchio, B., Mariotti, A. and Salvetti, M.V., 2020. Flow around a 5:1 rectangular cylinder: Effects of upstream-edge rounding. Journal of Wind Engineering and Industrial Aerodynamic 204, 104237.

Flow around twin rough cylinders at low wind incidence: bi-stability and gap flow

Raphaël Dubois [1], Elena Di Silvestro [2], Sigrid Jacobs [3], Thomas Andrianne [1]

[1] *Wind Tunnel Lab, University of Liège, Belgium, raphael.dubois@uliege.be*
[2] *CRM Group, Liège, Belgium*
[3] *ArcelorMittal, Zwijnaarde, Belgium*

SUMMARY
Wind tunnel experiments are performed on twin rough cylinders with a centre-to-centre spacing ratio L/D = 1.2 at two different Reynolds numbers, Re = 45k and 275k, corresponding to the sub- and post-critical flow regimes, respectively. The wind incidence is varied from 0° to 10°. A strong gap flow is observed for the largest incidences in both flow regimes and appears at the same wind incidence in the sub- or post-critical flow regimes. The frequency analysis of the lift forces reveals the existence of bi-stabilities before the appearance of the gap flow.

Keywords: Two cylinders, bi-stability, gap flow.

1. INTRODUCTION

Cylinder-like structures can be found in many engineering applications. Therefore, fluid flows around circular cylinder have been extensively studied in the past. Such flows occur in the case of heat exchangers, chimneys, power lines, buildings, offshore structures, struts, landing gears, cables, etc. A part of those applications corresponds to multiple-cylinder configurations. The particular case of two cylinders lying in a flow field was subjected to many studies throughout the years but most of them have been limited to the sub-critical flow regime, as pointed out by Sumner (2010). Because of the continuous increase of the dimensions of engineering structures, it is also necessary to extend the understanding of the flow around two cylinders to the post-critical flow regime. In this regime, the boundary layers, separated shear layers and eddies are all turbulent. The twin-tube tracks of the Hyperloop concept (Fig. 1) represent a particular illustration of a two-cylinder configuration in the post-critical flow regime. The present study investigates the unsteady flow around two closely spaced rough cylinders at small wind incidence in the sub- and post-critical flow regimes.

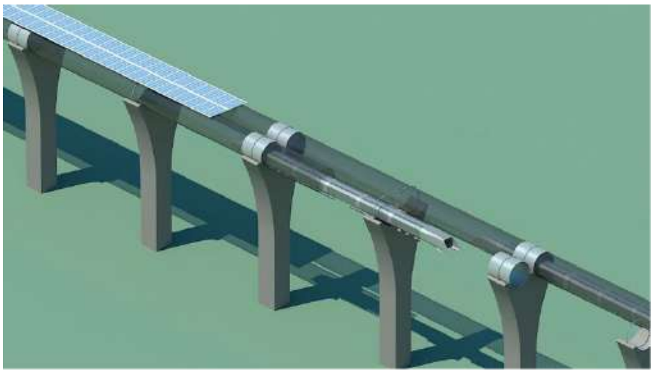

Figure 1. Twin-tube structure of the Hyperloop project (Hyperloop Alpha (2013)).

2. METHODOLOGY

The approach consists in an experimental test campaign on two static rough cylinders in the low-subsonic wind tunnel of the University of Liège. The experimental set-up is shown in Fig. 2 and is extensively described by Dubois and Andrianne (2022). Surface roughness are added to the cylinders in order to reach the post-critical flow regime at lower Reynolds numbers. The experiments are performed at two different Reynolds numbers, Re = 45k and 275k, which respectively correspond to the sub- and post-critical flow regimes. The wind incidence is accurately varied from 0° to 10° by using the turn-table of the wind tunnel. In this study, the cylinders are closely spaced: $L/D = 1.2$. L is the centre-to-centre distance between the cylinders and D is the external diameter. Pressure measurements are performed on each cylinder at 48 taps linearly distributed at mid-span with a sampling frequency of 600 Hz. The flow is characterised by a low level of turbulence (<0.2%).

Figure 2. Experimental set-up installed in the wind tunnel of the University of Liège.

3. LIFT FORCE COEFFICIENTS

Fig. 3(a-b) shows the variation of the time-averaged lift coefficient of each cylinder with the wind incidence in the sub- and post-critical flow regimes. Sub-figures (c-f) also show the *Power Spectral* Density (*PSD*) of the fluctuating lift signal of each cylinder as a function of the wind incidence in both flow regimes. The fluctuating lift signals are initially normalised by their respective standard deviation to allow the comparison of the frequency content at different wind incidences. The dimensionless Strouhal number $St=f\ D/U$ is used as the frequency variable. It takes values in the range $0 < St < 1$ in the present analysis. The superimposed black lines with different markers correspond to the different non-harmonic peaks observed in the spectra. Within the tested range of wind incidences, three different flow behaviours can be identified in the sub- or post-critical flow regime.

The first behaviour is observed at low wind incidences (α = 0° - 2°). In both flow regimes, the time-averaged lift coefficient of each cylinder remains close to zero, as shown in Fig. 3(a-b). It reveals that the flow around the twin-cylinder configuration is rather symmetric. Nevertheless, it can be observed that the lift coefficient of the front cylinder becomes slightly negative while the one of the rear cylinder becomes positive when increasing the wind incidence. The two flow regimes differ in the frequency contents of the lift signals. In the sub-critical flow regime, a strong peak is observed at $St \approx 0.14$. A second and weaker peak is also identified as an harmonic frequency of the fundamental one, $St \approx 0.28$ (see Fig. 3(c-d)). This observation was done by Dubois and Andrianne (2022) in the tandem configuration of cylinders (α = 0°). The presence of harmonic components was inferred to the alternate reattachment of the separated shear layers from the front cylinder onto the rear cylinder, as shown by Alam et al. (2003). In the post-critical flow regime, the frequency contents also reveal two peaks. However, those peaks are not identified at harmonic frequencies. This observation was done for the tandem configuration. Dubois and Andrianne (2022) concluded that it corresponds to a bi-stability due to the intermittent re-attachment of the separated shear layers from the front cylinder onto the rear cylinder.

A second behaviour is observed at intermediate wind incidences (α = 4° - 6°). Similarly to the low wind incidences, the lift coefficient of each cylinder remains small in both flow regimes. When increasing the wind incidence angle, the lift coefficient of the front cylinder slightly decreases and the one of the rear cylinder slightly increases. In the sub-critical flow regime, two peaks are still observed in the spectra of the lift signals (see Fig. 3(c-d)). Unlike the previous range of wind incidences, the peaks are identified at non-harmonic frequencies ($St \approx 0.14$ and 0.25). It is therefore assumed that they do emanate from two distinct processes. A bi-stability between two flow patterns takes place, leading to two different Strouhal numbers. The lowest identified Strouhal number increases when the wind incidence angle is increased from 4° to 6° while the other Strouhal number decreases. In the post-critical flow regime, a single peak is observed in the spectra at St ≈ 0.24 (Fig. 3(e-f)). This peak corresponds to the highest Strouhal number identified in the previous sub-range of wind incidence angles. Thus, it is stated that only the eddy shedding process related to this Strouhal number is present in this configuration.

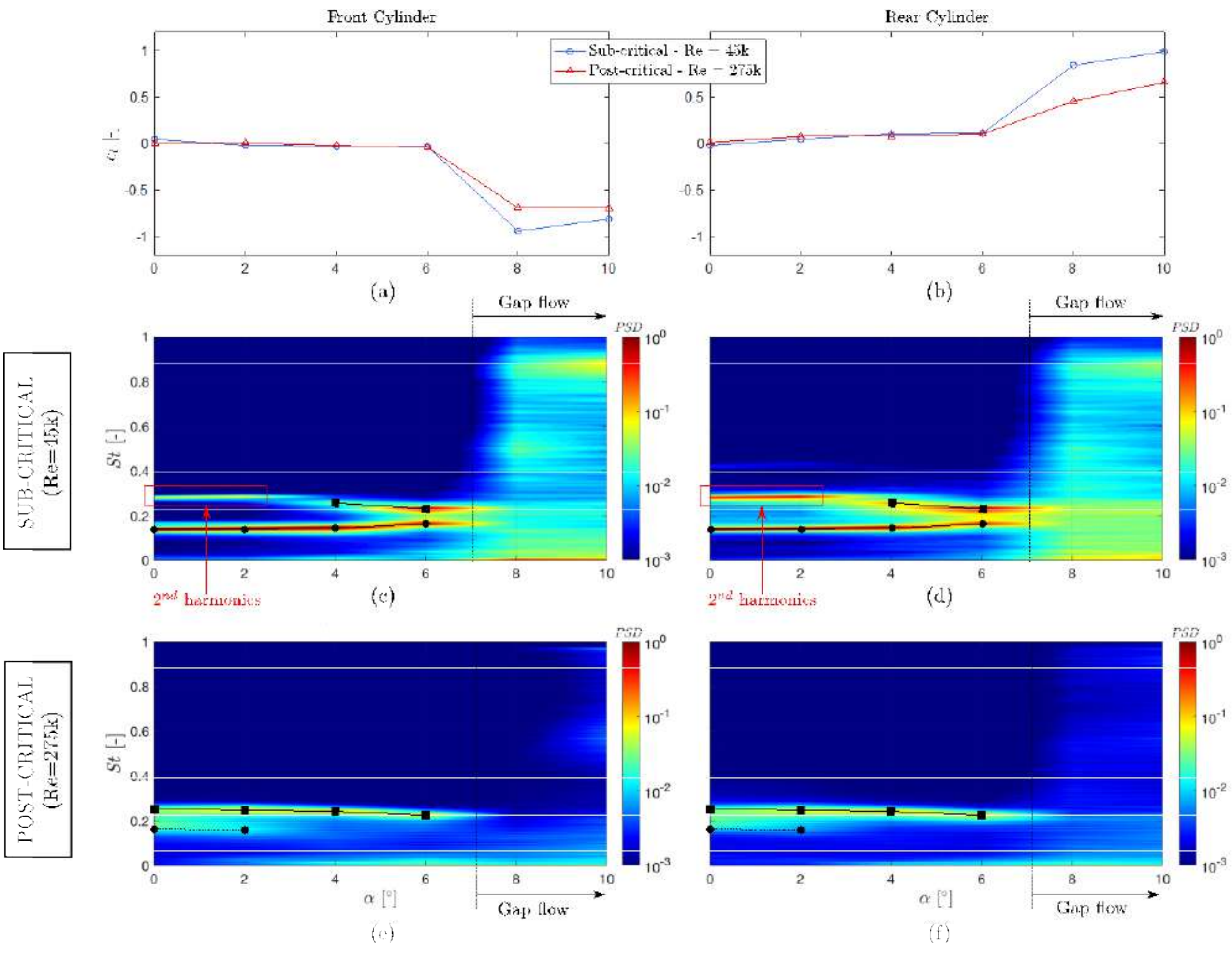

Figure 3. Variation of the time-averaged value and frequency content of the lift coefficient of each cylinder with the wind incidence in the sub- and post-critical flow regimes.

A third behaviour is observed at higher wind incidences (α = 8° - 10°). The time-averaged lift coefficients of the front and rear cylinders take large negative and positive values, respectively. The appearance of these large lift forces has already been observed in previous studies in the sub-critical flow regime (Zdravkovich (1987), among others) and is referred to the "inner" lift force. Those large lift forces are induced by a strong gap flow between the two cylinders. The gap flow occurs in the sub- and post-critical flow regime, as observed in Fig. 3(a-b). Based on the absolute values of the lift coefficients, it can be stated that the gap flow is stronger in the sub- than in the post-critical flow regime. The exact wind incidence angle at which the gap flow appears cannot be identified but it is expected between α = 6° and 8° for both flow regimes. Concerning the frequency content of the lift signals, it is observed that it is broadband within this range of wind incidences (see Fig. 3(c-f)). In both flow regimes, the occurrence of the broadband spectra coincides with the presence of a strong gap flow. Based on this observation, it can be stated that the gap flow strongly impacts the eddy shedding process behind the twin-cylinder configuration.

4. CONCLUSIONS & FURTHER WORK

Pressure measurements are performed on static twin rough cylinders in the sub- and post-critical flow regimes. The analysis of the variation of the time-averaged force coefficients highlights the appearance of a strong gap flow at a particular wind incidence. The latter is the same in the post-critical flow regime than in the sub-critical flow regime. Then, the analysis of the frequency contents of the lift force shows the presence of bi-stabilities at particular wind incidences: two peaks at non-harmonic frequencies appear in the spectra. It is assumed that two flow patterns co-exist in these particular cases. When the strong gap flow occurs, the frequency content becomes broadband.

The analysis of the present results will be completed by a thorough investigation of the pressure distributions in order to extract the different flow patterns around the cylinders.

This work is performed in the scope of the analysis of the wind effects on large twin cylinders with a focus on post-critical flow regime.

ACKNOWLEDGEMENTS

The authors would like to thank ArcelorMittal and the CRM Group which are the industrial partners of this project.

REFERENCES

Alam, M. M., Moriya, M., Takai, K., & Sakamoto, H. (2003). Fluctuating fluid forces acting on two circular cylinders in a tandem arrangement at a subcritical Reynolds number. Journal of Wind Engineering and Industrial Aerodynamics, 91(1-2), 139-154.

Dubois, R., & Andrianne, T. (2022). Flow around tandem rough cylinders: Effects of spacing and flow regimes. Journal of Fluids and Structures, 109, 103465.

Sumner, D. (2010). Two circular cylinders in cross-flow: a review. Journal of Fluids and Structures, 26(6), 849-899.

Zdravkovich, M. M. (1987). The effects of interference between circular cylinders in cross flow. Journal of fluids and structures, 1(2), 239-261.

Investigation on the aerodynamics force of a square cylinder in accelerating flows

Hao-Yu Bin [1], Stefano Brusco [2], Yuan-Lung Lo [3], Giuseppe Piccardo [4]

[1]*University of Genova, Genova, Italy, hao-yu.bin@edu.unige.it*
[2]*University of Genova, Genova, Italy, stefano.brusco@edu.unige.it*
[3]*National Taipei University of Technology, Taipei, Taiwan, yllo@mail.ntut.edu.tw*
[4]*University of Genova, Genova, Italy, giuseppe.piccardo@unige.it*

SUMMARY
Through the use of the multiple fan wind tunnel of the Tamkang University (MFWT-TKU), experimental simulations of the transients typical of thunderstorm outflows are carried out in order to investigate the effects exerted on the aerodynamics forces of a two-dimensional sharp-edged square cylinder. The results obtained have shown strong non-stationary and non-Gaussian characteristics, therefore requiring ensemble statistics analysis. Wavelet-based techniques are employed to study the data in the transients, with the aim of determining the most relevant differences compared to traditional wind-loading design.

Keywords: Accelerating flows, Thunderstorm outflows, Transient aerodynamics.

1. INTRODUCTION

Wind engineering has consolidated methods for the design on structures concerning steady flows (e.g., synoptic winds), while corresponding methods for the action of transient events (e.g., thunderstorm outflows) are still scarce (e.g., Letchford and Chay, 2002; Solari, 2020). In the past, there were not enough mature technologies to record and simulate extreme climate events in laboratories, such as thunderstorms and tornadoes. With the rapid development of science and technology in recent years, wind and structural monitoring systems and non-synoptic wind simulators were developed and built. In particular, the Giovanni Solari Wind Engineering and Structural Dynamics Research Group (GS-WinDyn, University of Genoa), thanks to the knowledge gained from an extensive monitoring network in the High Thyrrenian Sea, carried out a series of studies regarding thunderstorms, including detection, simulation, modeling and aerodynamic loading due to downbursts. Several lines of research were drawn from the pioneering work (see Solari, 2020), and the present study is amongst them, particularly focused on the transient aerodynamics of a sharp-edged square cylinder subjected to accelerating flows.

2. EXPERIMENTAL CAMPAIGN

Amongst the non-synoptic wind simulators in the new generation, multiple fan wind tunnels (MFWT, Fig. 1a) were conceived. While the original prototype was realized in Japan, other few facilities have been built in China (Tongji University) and Taiwan (Tamkang University). The present research is originated from a collaboration between Tamkang University and the University of Genoa. An extensive experimental campaign using the MFWT of Tamkang University has been carried out, aiming to investigate the changes of the aerodynamic coefficients of a two-dimensional square cylinder, equipped with pressure sensors, with respect the steady conditions analyzing different accelerating flows. Specific investigations are conducted on the effects of the flow parameters, namely the initial wind velocity, the target one, the acceleration, and the temporal spacing for which the target velocity is kept as constant (Fig. 1b). The flow positive and negative accelerations are consistent with those induced by full-scale thunderstorm outflows (Brusco et al., 2022). Since thunderstorm outflows are characterized by a strongly non-stationarity and non-Gaussianity (e.g., Solari, 2014), recourse to the concept of ensemble statistics was necessary to process the acquired data.

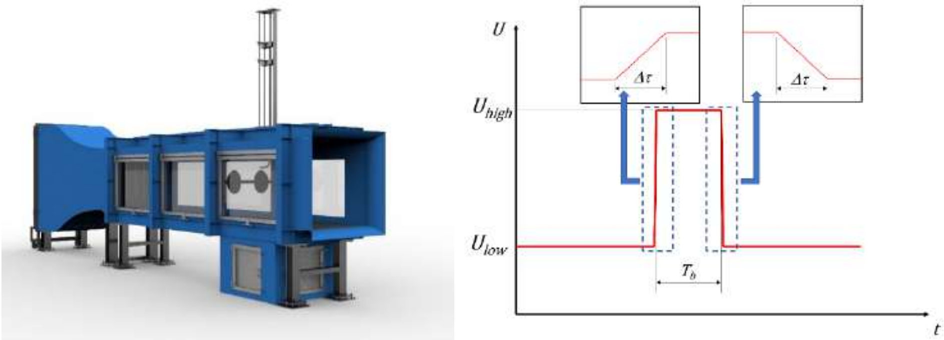

Figure 1. (a) Rendering of the MFWT-TKU, with the sectional model installed; (b) scheme of a wind velocity time history under unsteady flow conditions.

The 72 servo motors of the MFWT-TKU allow to control the parameters shown in Fig 1b. Two different experimental campaigns are thus designed. In the first one (Fig. 2a), the target velocities (U_{high}) and temporal spacing ($\Delta\tau$) are kept fixed, changing the initial velocities (U_{low}). In the second series of tests (Fig. 2b), U_{low} and U_{high} are constant whereas the duration of the target velocity (Tb) is changed. These two experimental campaigns allow it possible to investigate the effects of different accelerations and different plateau durations on the aerodynamic behavior of the square cylinder.

(a) (b)

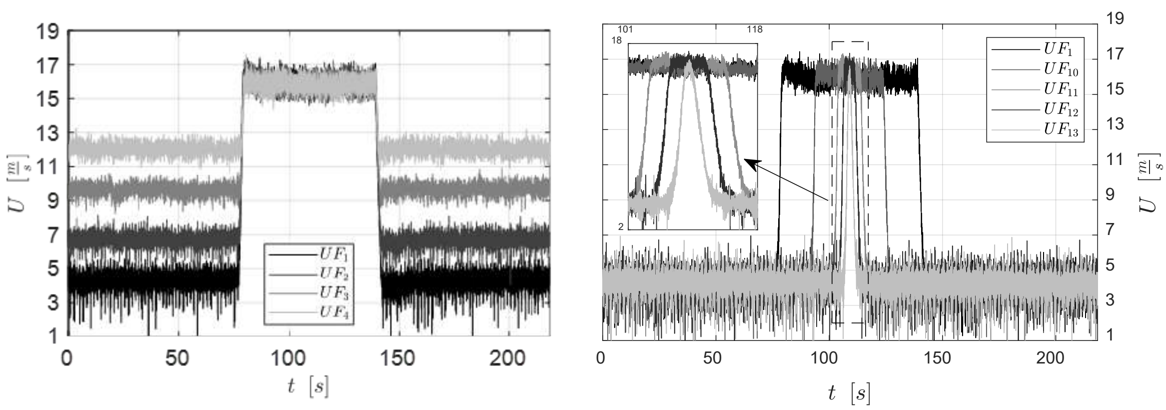

Figure 2. Comparison between time histories of the reference velocity selected from different tests: (a) UF_1, UF_2, UF_3, and UF_4; (b) UF_1, UF_{10}, UF_{11}, UF_{12}, and UF_{13}.

3. ANALYSIS METHODOLOGY

While the results in steady conditions are quite straightforward to be evaluated, for the analyses in the transient cases specific methodologies had to be conceived and developed. In particular, the relevant results are evaluated by collecting a number equal to or higher than 30 repeats (Fig 3), being the consequent ensemble averages and ensemble standard deviations satisfyingly stable. Tailored analyses are conducted by using wavelet-based techniques to define time-varying mean quantities through an energetic approach. Efforts are also dedicated to understanding whether the results could have been predicted by using theoretical approaches (see, e.g., Morison et al., 1950, 1953).

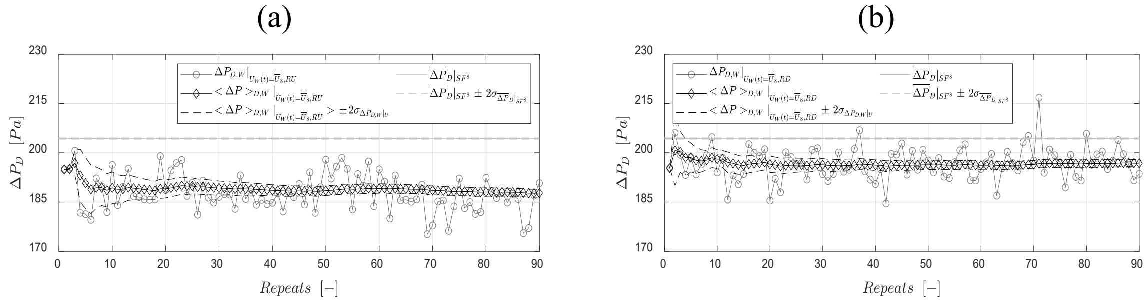

Figure 3. Ensemble mean of the aerodynamic drag, $\Delta P_{D,W}$, in accelerating conditions for UF_1: (a) ramp-up; (b) ramp-down.

4. PRELIMINARY CONCLUSIONS

According to the aforementioned results, the definition of the data collection is verified by the ensemble mean and the ensemble standard deviation in transient flow conditions. Concerning the influence on the aerodynamic parameters, the drag force coefficient shows reductions, compared to the corresponding values in steady conditions, as a function of the value of the acceleration of the flow, regardless of the duration of the target velocity.

ACKNOWLEDGEMENTS

Heartfelt thanks are due to the staff of the Wind Engineering Research Center of Tamkang University for kindly allowing the use of the MFWT-TKU and for the technical support. The scientific guidance of Prof. Guido Buresti is also greatly acknowledged. The authors thankfully acknowledge Professor Giovanni Solari, conceiver of the collaboration between the University of Genoa and Tamkang University.

REFERENCES

Brusco, S., Buresti, G. and Piccardo, G., 2022. Thunderstorm-induced means wind velocities and accelerations through the continuous wavelet transform. Journal of Wind Engineering and Industrial Aerodynamics, 221, 104886.

Letchford, C. W., Chay, M. T., 2002. Pressure distributions on a cube in a simulated thunderstorm downburst. Part B: moving downburst observations. Journal of Wind Engineering and Industrial Aerodynamics, 90, 733-753.

Morison, J. P., O'Brien, M. P., Johnson, J. W., and Schaaf, S. A., 1950. The force exerted by surface waves on piles. Petroleum Trans. AIME, 189, 149-154.

Morison, J.R., Johnson, J.W., and O'Brien, M.P., 1953. Experimental studies of forces on piles, Proceedings of the 4th Conference on Coastal Engineering, 340-370.

Solari, G., 2014. Emerging issues and new frameworks for wind loading on structures in mixed climates. Wind and Structures, 19, 295-320.

Solari, G., 2020. Thunderstorm Downbursts and Wind Loading of Structures: Progress and Prospect. Frontiers in Built Environment, 6, 63.

Wind loading assessment using LES: application to a high-rise building and a stadium roof

Jin Xing [1], Luca Patruno [1], Chiara Pozzuoli [2], Gonçalo Pedro [2], Stefano de Miranda [1]

[1]*University of Bologna, Bologna, Italy, jin.xing2@unibo.it*
[2]*RWDI, Via Thaon Di Revel, 21, 20159, Milano, Italy*

SUMMARY
Recently, the use of Computational Fluid Dynamics is rapidly expanding, allowing to complement traditional wind tunnel tests for wind loads assessment, even in the case of highly complex geometries. In this contribution, we present the wind loads prediction for two representative structures: (i) a high-rise building located in an urban environment and (ii) a newly designed large-span roof stadium located in a partially hilly terrain. The discussion includes the inflow generation, mesh sensitivity, global forces and peak pressures evaluation, as well as computational costs. An overview of the main factors which might contribute to the success of the analyses is presented. Good agreement between experimental and simulated results is obtained for the high-rise building. For the stadium roof, comparison with wind tunnel data is not available at the time of writing, but the results show the great advantages which can be obtained by performing preliminary simulations in the early stages of the design development.

Keywords: LES, high-rise building, large-span roof, wind loading

1. INTRODUCTION

This study aims at assessing the viability of the numerical simulations for wind loads assessments in cases characterized by real complexity (Thordal et al. 2020) and taking into consideration computational time/costs constrains. Several newly developed methods are adopted to obtain a smooth workflow and perform the analyses. The inflow is generated using the PRFG^3 method and applied to the computational domain using the VBIC method, recently developed by the authors (Patruno and de Miranda 2020), in order to avoid spurious pressure fluctuations.

In the first part of the work, we present the results for the estimation of wind loads for a newly designed tower denoted Porta Gioia 22 (see Fig. 1 (a)), located in Milan, Italy, for which wind tunnel tests have been performed by *RWDI*. In the second part, a preliminary structural response evaluation performed on the new roof of the Bologna Stadium (see Fig. 1 (b)), designed by *Studio Tecnico Majowiecki,* is reported.

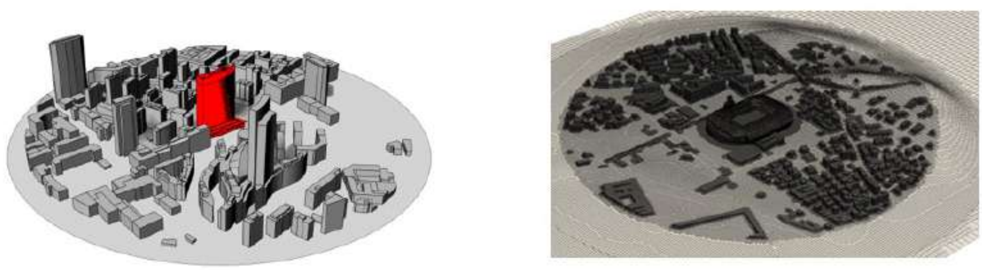

(a) (b)

Figure 1. Overview of the structures and the surroundings: Porta Gioia 22 (a) and Bologna Stadium (b).

2. TORRE GIOIA 22

Torre Gioia 22 is a newly designed high-rise building located in Milan. The tower is located in a densely urbanized area, so that the effect of the surroundings must be carefully considered in the simulations, consequently increasing the computational costs.

Firstly, the mesh sensitivity of the results is analyzed. This is particularly important in this case, due to the presence of decorative details on the facades which can be only coarsely meshed in the simulations and the presence of a crown, which required some defeaturing in order to allow the meshing operations.

Once an appropriate mesh has been selected for the purpose of the study, LES simulations show a good capability to reproduce the experimental data in terms of both global forces and peak pressures.

In addition, the computational cost and the economical viability of such kind of simulations are discussed. We notice that, in order to keep computational costs at a reasonable level, the addition of boundary layer cells is often unnecessary for the sharp-edged bluff bodies immersed in fully turbulent flows. Overall, considering the currently available computational power and computational resources prices, the cost of the analyses appears to be well-viable for preliminary computations, especially if only a single 10 min time series is simulated for each attack angle.

3. BOLOGNA STADIUM

The new roof over the Bologna Stadium is currently in its design stage. Although wind tunnel tests are not yet available at the time of writing, it has been chosen in order to show the advantages which might be obtained by an evaluation of the wind loads in the early stages of the design process.

Also, in this case the stadium surroundings, partially compose of a hilly terrain (see Fig. 1 (b)), have been reproduced. Then LES simulations have been performed for all attack angles and the consequent structural response was evaluated using Proper Skin Modes (PSMs) (Patruno et al. 2016). This also allowed to perform parametric studies in order to evaluate the effect of damping, so characterizing the structure sensitivity to such parameter. Finally, Equivalent Static Wind Loads, ESWLs, have been extracted, so allowing to provide design loads to the structural designer.

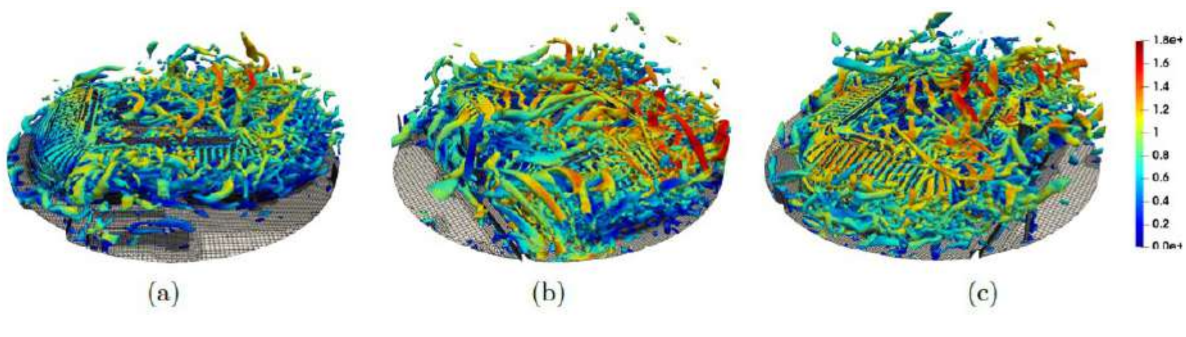

Figure 2. Overview of the simulated flow field around the Bologna stadium.

REFERENCES

Patruno, L., and S. de Miranda. 2020. Unsteady inflow conditions: A variationally based solution to the insurgence of pressure fluctuations, Computer Methods in Applied Mechanics and Engineering, 363: 112894.

Patruno, L., M. Ricci, S. de Miranda, and F. Ubertini. 2016. An efficient approach to the evaluation of wind effects on structures based on recorded pressure fields, Engineering Structures, 124: 207-20.

Thordal, Marie Skytte, Jens Chr Bennetsen, Stefano Capra, and H. Holger H. Koss. 2020. Towards a standard CFD setup for wind load assessment of high-rise buildings: Part 1 – Benchmark of the CAARC building, Journal of Wind Engineering and Industrial Aerodynamics, 205: 104283.

Experiments on the effect of the upstream-corner roundings and of the angle of attack on the flow around a 5:1 rectangular cylinder

A. Mariotti [1], G. Lunghi [1], E. Pasqualetto [1], M.V. Salvetti [1]

[1]*Dipartimento di Ingegneria Civile e Industriale, Università di Pisa, Largo Lucio Lazzarino 2, Pisa, Italy, alessandro.mariotti@unipi.it*

SUMMARY
We experimentally investigate the importance of upstream-corner sharpness and of the angle of attack on the high-Reynolds-number flow around a 5:1 rectangular cylinder, which is the focus of the international benchmark BARC. Experiments are carried out at Reynolds number $Re=DU_\infty/\nu=40000$, being D the crossflow dimension, U_∞ the freestream velocity and ν the kinematic viscosity of air. We consider almost-sharp upstream corners (r/D=0.0005), and different values of the upstream-corner rounding in the range r/D=[0.0037, 0.1104], together with different small angles of attack in the range [-2°, 2°]. Differently from numerical predictions, for a fixed α, a low sensitivity to the corner rounding is found also when pushing it to very small values. Differences are not significant up to r/D=0.0360, whereas starting from r/D=0.0781 the size of the mean recirculation region on the cylinder side decreases noticeably by increasing r/D. On the other hand, even small angles of attack have a significant impact on the length of the mean recirculation region. As in simulations, the growth of the velocity fluctuations along the shear layers detaching from the upstream corners is highly correlated with the location of the onset of Kelvin-Helmholtz instability and, in turn, with the length of the mean recirculation on the cylinder side. This, in turn, influences pressure distributions and the near-wake flow features.

Keywords: BARC benchmark, upstream-corner sharpness, angle of attack

1. INTRODUCTION

The high Reynolds number flow around a rectangular cylinder, having a streamwise to crossflow length ratio equal to 5, is experimentally analyzed. The flow is characterized by shear-layer separation from the upstream edges. Vortical structures of different sizes form from the roll-up of these shear layers, move downstream and interact with the classical vortex shedding in the wake. The corresponding mean flow is characterized by a recirculation region along the lateral surface of the cylinder, ending close to the trailing edge. The mean flow features on the cylinder side have been shown to be highly sensitive to the shear-layer dynamics, which is influenced by set-up parameters in both experiments and in simulations (see, e.g. Mannini et al. 2017, Mariotti et al. 2017). In numerical simulations, a significant difference is present between sharp edges and rounded edges, causing the former a premature onset of Kelvin-Helmholtz instability in the separated shear-layer, and even a small curvature radius significantly changes the flow features by moving downstream the mean flow reattachment point (Rocchio et al. 2020). Now we investigate experimentally the importance of upstream-corner sharpness and of the angle of attack on the BARC flow. We consider a variation of the upstream-corner rounding in a range such that they might be relevant for practical applications and of the angle of attack which takes into account the effect of a possible small misalignment with respect to the flow direction.

2. PROBLEM DEFINITION AND INVESTIGATION METHODOLOGY

Experiments are carried out following the set-up described in Pasqualetto et al. (2022) at Reynolds number $Re=DU_\infty/\nu=40000$, being D the crossflow dimension, U_∞ the freestream velocity, and ν the kinematic viscosity of air. Almost-sharp upstream corners (r/D=0.0005) and different values of the rounding are considered, i.e., r/D=0.0037, 0.0360, 0.0781, 0.1104. Different small angles of attack α= -2°, -0.79°, 0, 0.79°, 2° are investigated.

3. RESULTS AND DISCUSSION

The effect of the upstream-corner sharpness and of the angle of attack on the pressure distributions along the rectangular cylinder is shown in Fig. 1. For a fixed α, negligible differences are found among the cases r/D=0.0005, r/D=0.0037 and r/D=0.0360, whereas starting from r/D=0.0781 the size of the mean recirculation region on the cylinder side decreases by increasing r/D. On the other hand, the angle of attack has a significant impact on the mean recirculation length and, thus, on the pressure distribution. Physical discussion on these effects, in terms of the growth of the TKE along the shear layers borders and location of the Kelvin Helmholtz instability, will be given in the final presentation. Stochastic sensitivity techniques (generalized polynomial chaos) will be used to obtain continuous response surfaces of the quantities of interest in the parameter space and to quantify the impact of each parameter and of their coupling.

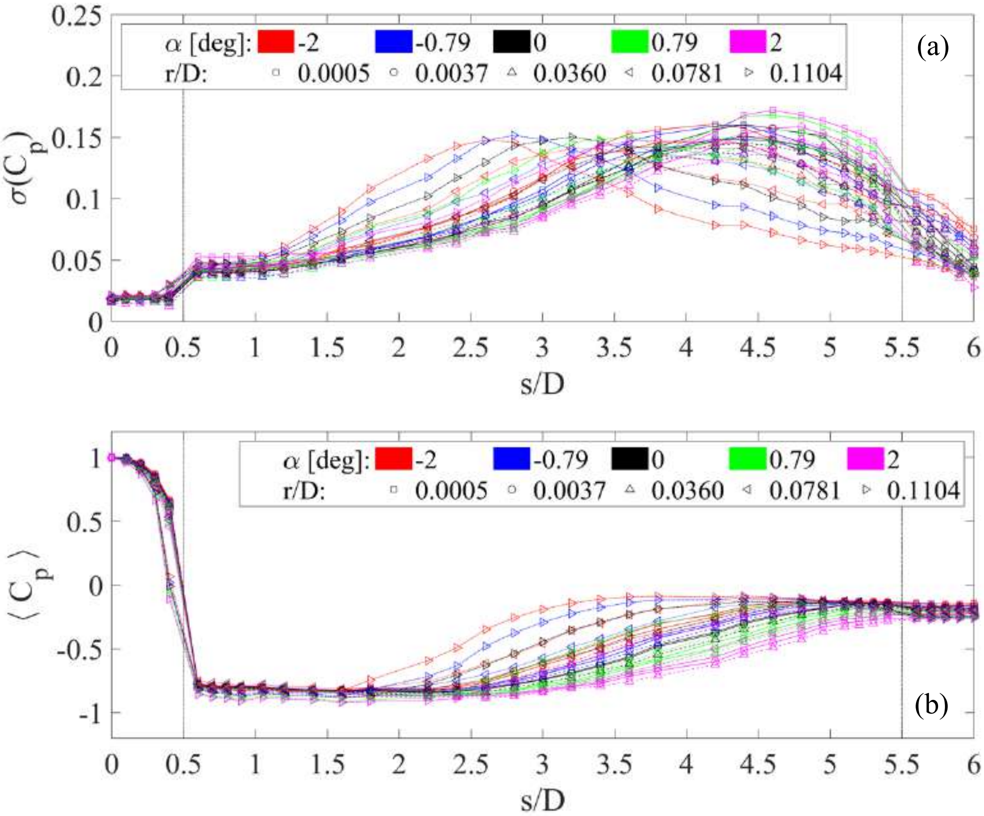

Figure 1. Experimental distributions (a) of the time-averaged pressure coefficient and of (b) standard deviation of the pressure coefficient. The symbols and the colors represents the different upstream roundings and the angles of attack, respectively.

REFERENCES

Mariotti, A., Siconolfi, L. and Salvetti, M.V., 2017. Stochastic sensitivity analysis of large-eddy simulation predictions of the flow around a 5:1 rectangular cylinder. European Journal of Mechanics B/Fluids 62, 149-165.

Pasqualetto, E., Lunghi, G., Rocchio, B., Mariotti, A. and Salvetti, M.V., 2022. Experimental characterization of the lateral and near-wake flow for the BARC configuration. Wind and Structures 34(1), 101-113.

Rocchio, B., Mariotti, A. and Salvetti, M.V., 2020. Flow around a 5:1 rectangular cylinder: Effects of upstream-edge rounding. Journal of Wind Engineering and Industrial Aerodynamic 204, 104237.

Wind tunnel tests for the validation of the CFD obtained flutter derivatives of twin-box bridge decks

José Ángel Jurado [1], Rameez Badhurshah [2], Santiago Hernández [3], Félix Nieto [4]

[1] *School of Civil Engineering, Universidade da Coruña UDC, Spain,* jose.angel.jurado@udc.es
[2] *School of Civil Engineering, Universidade da Coruña UDC, Spain,* rameezraja.badhurshah@udc.es
[3] *School of Civil Engineering, Universidade da Coruña UDC, Spain,,* hernandez@udc.es
[4] *School of Civil Engineering, Universidade da Coruña UDC, Spain,,* felix.nieto@udc.es

SUMMARY
A project funded by the Spanish Ministry for Science and Innovation has as the main objective to carry out the computational aerostructural shape optimization of bridge decks of long span cable supported bridges considering multiple aeroelastic phenomena, including flutter. Twin-box sections with big gap are being parametrized and a surrogate model is used later in the optimization. The flutter derivatives of the surrogate model designs are been assessment by CFD analysis, but some of them require experimental validation to guarantee an adequate results. This work shows the experiments with sectional models tested in an aerodynamic wind tunnel, the tests results and the CFD validation.

Keywords: twin-box bridge deck, flutter derivatives, wind tunnel, sectional model.

1. SECTIONAL MODEL

The aim of this study is to perform aerodynamic and aeroelastic tests of a sectional model of a twin-box bridge deck (Chowdhury and Sarkar (2003), Sarkar et al. (1992), Jurado et al. (2013)). We perform experimental as well as CFD simulations. CFD simulations are cost effective and mimic the actual dynamics of the fluid flow over the bridges. However, due to the truncation and numerical assumptions involved, the results may not match exactly with the actual flow over bridges (Jurado et al. (2013)). On the other hand, experiments require time as well as costs to understand the physics behind the flow over the bridges. However, experimental results are more accurate.

The gap between the two boxes, the depth and the width of the deck are taken as the design variables. Using Latin hypercube sampling, we obtain 15 different design sample points. We perform CFD simulations on all these 15 designs, however performing experiments on all the design points is not possible due to the cost and time involved. Thus, three samples are chosen to validate the results between the experiments and CFD. We employ a scale of 1:70 for performing the tests. Here, it is only showed results for one of the cases, for which the width of the deck (C) was 200.52 mm, the depth of the deck (D) was chosen as 35.54 mm and the gap between the decks was chosen as 121.20 mm. To provide stiffness to the deck, a central Aluminum rod passing through the entire span of each deck is placed. The deck length with the end plates is approximately 946 mm. Using 3D printer, we prepare the prototype and assemble it in the wind tunnel (see figures 1 and 2).

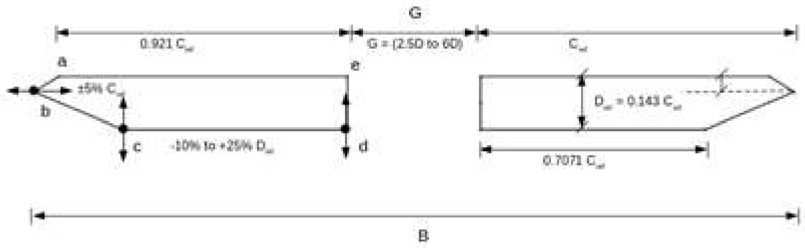

Figure 1. Twin-box sectional model. C refers to the width of a single deck, G is the gap between the two deck, D is the depth of the deck and B is the total width of the deck.

Figure 2. Twin-box sectional model. C refers to the width of a single deck, G is the gap between the two deck, D is the depth of the deck and B is the total width of the deck.

2. WIND TUNNEL TESTS

We place the assembly of the twin-deck in the one meter square test section of the wind tunnel (Jurado et al. (2014)). Aerodynamic coefficients are measured with the model fixed by bars, while the flutter derivatives are evaluated with the model supported by springs in free vibration. Initially, we perform the Reynolds dependency test by varying the wind speeds from 2 m/s to 15 m/s in steps of 1 m/s for three different angle of attacks (-20, 00, +20). It is observed from the wind speeds of 6 m/s onward, the force-coefficients largely remain constant. Thereby we choose wind speed of 12 m/s for performing the aerodynamic test.

Regarding the flutter derivatives and according to Simiu and Scanlan formulation (Jurado et al. 2011), the aeroelastic forces are linearized by functions of the displacements and velocities of the system for vertical w, lateral v and torsional rotation φ_x degrees of freedom (Figure 3). These expressions can be written as:

$$\mathbf{f}_a = \begin{Bmatrix} D_a \\ L_a \\ M_a \end{Bmatrix} = \frac{1}{2}\rho U^2 KB \cdot \begin{pmatrix} P_1^* & -P_5^* & -BP_2^* \\ -H_5^* & H_1^* & BH_2^* \\ -BA_5^* & BA_1^* & B^2A_2^* \end{pmatrix} \begin{Bmatrix} \dot{v} \\ \dot{w} \\ \dot{\varphi}_x \end{Bmatrix} + \frac{1}{2}\rho U^2 K^2 \cdot \begin{pmatrix} P_4^* & -P_6^* & -BP_3^* \\ -H_6^* & H_4^* & BH_3^* \\ -BA_6^* & BA_4^* & B^2A_3^* \end{pmatrix} \begin{Bmatrix} v \\ w \\ \varphi_x \end{Bmatrix} \quad (1)$$

$$\mathbf{f}_a = \mathbf{C}_a\dot{\mathbf{u}} + \mathbf{K}_a\mathbf{u}$$

where B is the deck width, ρ is the air density, U is the mean wind speed, $K = B\omega/U$ is the reduced frequency with ω the frequency of the response, and $P^*_i(K)$, $H^*i(K)$, $A^*_i(K)$ $i = 1...6$ are the flutter derivatives which are functions of K. $\mathbf{K}_a$ and $\mathbf{C}_a$ are called aeroelastic matrices.

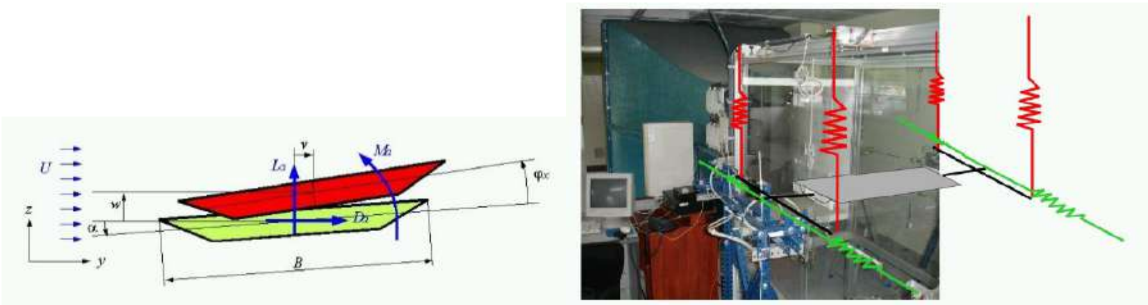

Figure 3. Aeroelastic wind forces and displacements of a sectional model and spring support system.

During the test the model is elastically sustained using springs. The stiffness of the springs determines the vibration frequencies of the system that together with the wind velocity in the tunnel determines the range of reduced frequency K. By changing the wind speed in the tunnel and the stiffness constants of the springs, a wide range of reduced velocities can be simulated. The dynamic balance equation for the sectional model is

$$\mathbf{M\ddot{u}} + \left(\mathbf{C} - \mathbf{C}_a\right)\mathbf{\dot{u}} + \left(\mathbf{K} - \mathbf{K}_a\right)\mathbf{u} = \mathbf{0} \tag{2}$$

Multiplying by $\mathbf{M}^{-1}$ and denoting $\mathbf{C}_m = \mathbf{M}^{-1}(\mathbf{C}\text{-}\mathbf{C}_a)$ and $\mathbf{K}_m = \mathbf{M}^{-1}(\mathbf{K}\text{-}\mathbf{K}_a)$ become

$$\mathbf{\ddot{u}} + \mathbf{C}_m\mathbf{\dot{u}} + \mathbf{K}_m\mathbf{u} = \mathbf{0} \tag{3}$$

To obtain the flutter derivatives, all terms of $\mathbf{C}_m$ and $\mathbf{K}_m$ matrices are evaluated from the time histories of the model displacements at free vibration. The flutter derivatives are calculated by subtraction to the terms matrices considering wind the same terms evaluated without wind.

3. RESULTS

The CFD simulations have been carried out with the open-source solver OpenFOAM and second order schemes where applied. After obtaining the experimental parameters in the wind tunnel the validation of the CFD simulations are carrying out. Figure 4 plots the results for the mean force coefficients of drag, lift and moment obtained from the experimental as well as numerical results.

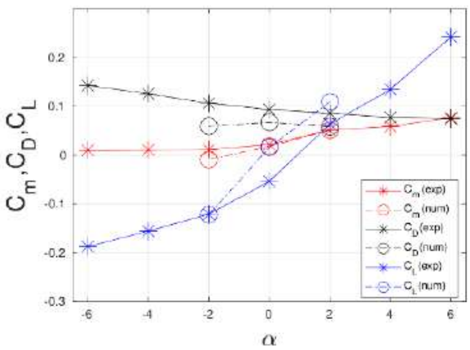

Figure 4. Comparison of the force coefficients from the experimental and numerical results.

For the experiments, we chose a wider range of angle of attack from -6º to +6º, whereas the CFD results are obtained at three angle of attacks, -2º, 0º and +2º. Similar trends between the experimental and the CFD results for all the three force coefficients are observed.

A comparison of the different values of the flutter derivatives in relation to the reduced speed U^* is shown in Figure 5, including values of the functions calculated with the quasi-static theory from the aerodynamic coefficients. Although there are some variation in the results, the tendency of the A_1^*, A_3^*, H_1^*, and H_3^* are relatively similar. The A_2^* function has a similar tendency, although the values are comparatively different. The H_2^* and the H_4^* functions show a different tendency in the case of the CFD method.

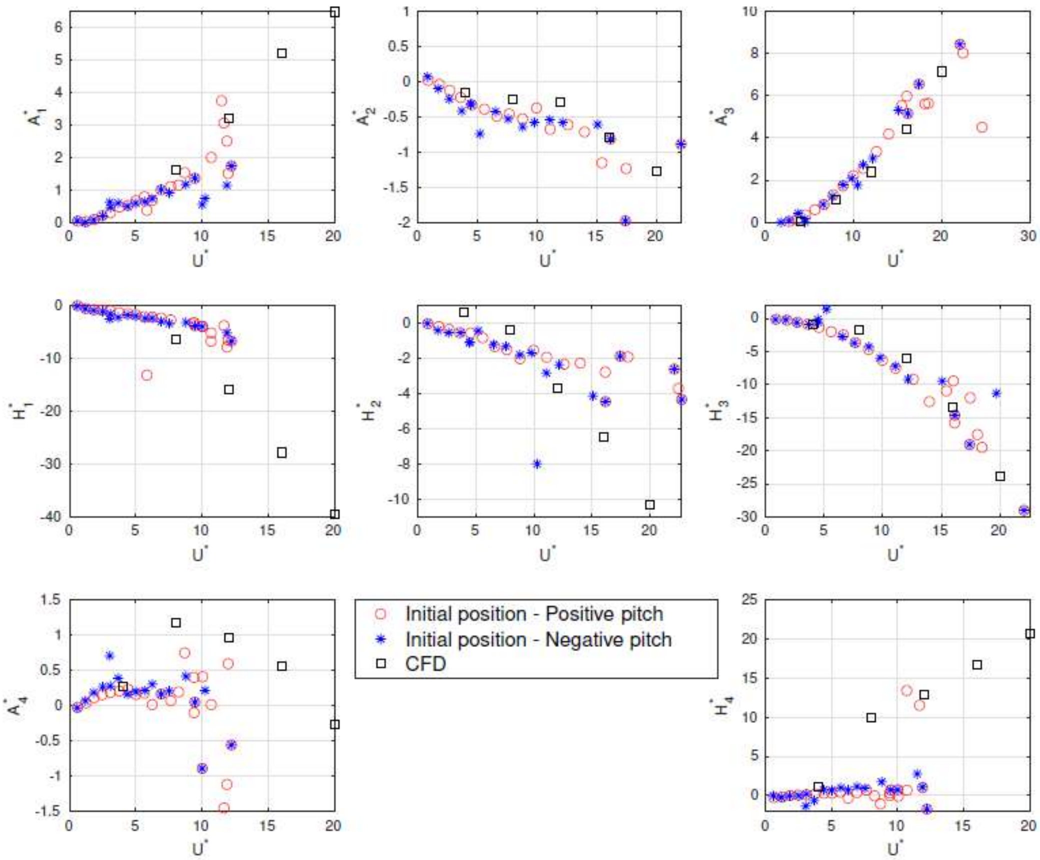

Figure 5. Validation of the values of the flutter derivatives obtained by experimental tests and CFD.

ACKNOWLEDGEMENTS
This research has been funded by the Spanish Ministry for Science and Innovation, in the frame of the research project PID2019-110786GB-I00.

REFERENCES

Jurado J.Á, Hernández S., Nieto F., Mosquera A. (2011). Bridge Aeroelasticity: Sensitivity Analysis and Optimal Design. WIT press. ISBN 978-1-84564-056-9.

Chowdhury A.G. and Sarkar P.P., (2003). A new technique for identification of eighteen flutter derivatives using a three-degree-of-freedom section model. Engineering Structures, 25 (14), p1763-1772

Sarkar P. P., Jones N. P. y Scanlan R. H. (1992) System identification for estimation of flutter derivatives, Journal of Wind Engineering and Industrial Aerodynamics 41-44 1243-1254.

Jurado J.Á., Kusano I., Hernández S., Nieto F. (2013) Improvement of multimodal flutter analysis code, FLAS. EACWE 2013. European and African Congress in Wind Engineering Cambridge, U.K.; July,7-11.

Jurado J.Á., Sánchez R., Hernández S., Nieto F. (2014). PCTUVI. Wind tunnel control software for aerodynamic and aeroelastic sectional model tests. CWE 2014, 6 International Symposium on Computational Wind Engineering, Hamburg Germany 8-12 June.

Prediction of wind flow in seaport areas and wind forces assessment on port infrastructures

Alessio Ricci [1,2], Bert Blocken [1,2]

[1]*KU Leuven, Department of Civil Engineering, Leuven, Belgium,* alessio.ricci@kuleuven.be , bert.blocken@kuleuven.be
[2]*Eindhoven University of Technology, Department of the Built Environment, Eindhoven, The Netherlands,* a.ricci@tue.nl , b.j.e.blocken@tue.nl

SUMMARY

Among the meteorological events, the wind is the most destructive natural phenomenon and most frequently the prime cause of accidents occurred in seaport areas. The characterization of winds is of primary importance towards the safety management of seaports and port infrastructures. In this paper, RANS and SAS simulations are used to predict the wind field and wind forces on a real case study, the Port of Rotterdam (the Netherlands). CFD wind velocity and wind direction time series near the quay area validated by means of on-site measurements carried out on the same area. The analysis shows that the choice of positions near the terminal for comparison of CFD and measured data might be crucial for an accurate prediction of wind field and wind forces around/on port infrastructures.

Keywords: on-site measurements, CFD simulations, port infrastructures.

1. INTRODUCTION

Coastal areas and seaport areas are the most densely settled in the world. Estimates indicate that approximately three billion people – about half of world's population – live within 200 km from a coastal line and by 2025 this number is likely to double (Population Reference Bureau, 2003). Since decades seaport areas have been increasing in order to host larger and larger cruise ships and container ships. Besides the positive impact on the global economy, the increasing ship size can also cause larger wind forces, which makes the navigation through these areas even more difficult especially on windy days (Janssen et al., 2017). Here, accidents caused by storm winds do not only imply considerable economic losses but also high risks for the workers (Solari et al., 2012). Therefore, the wind characterization is of primary importance towards the safety management of seaports and port infrastructures. Despite the great strides of Wind and Maritime Engineering communities, the prediction of wind conditions in such complex environments is still challenging. In this paper on-site measurements (OsM) and Computational Fluid Dynamics (CFD) are used to predict the wind field at the ECT terminal of the Port of Rotterdam (The Netherlands), in order to estimate the wind forces acting on port infrastructures.

2. METHODOLOGY

OsM were conducted with ultrasonic anemometer (P_A) and a 3D LiDAR scanner (P_{Li}) installed respectively at an undisturbed position in the middle of the ECT terminal. The LiDAR was set to measure with a radius of 1 km, with the aim of detecting the wind flow field over the whole area of the terminal, around the main port infrastructures (e.g. cranes, container stacks) and moored containerships. Wind statistics were calculated for the datasets of P_A (at 15 m above the sea level, ASL) and P_L at different heights ASL (i.e. 40, 70, 90 m). Next, a high-resolution computational grid was built to reproduce and simulate a neutral atmospheric boundary layer (ABL) wind on the seaport and its surrounding considering a large-scale area of 18 *x* 18 *x* 0.5 km^3. Two CFD approaches were used, (*i*) Reynolds-averaged Navier-Stokes (RANS) and (*ii*)

Scale-Adaptive Simulation (SAS). A complete set of transfer coefficients ($\gamma = U_{L,i}/U_A$) were calculated for the RANS case (and 12 wind directions, α), then used to (*i*) transfer the wind velocity time series measured at P_A to the *i-th* $P_{L,i}$ position (278 in total) and (*ii*) compare the transferred data with the wind velocities measured at *i-th* $P_{L,i}$ position. Finally, in order to better understand the flow dynamics and turbulence characteristics near the quay and port infrastructures the SAS results of the prevalent wind direction $\alpha = 210°$ were compared to OsM data.

3. CONCLUSIONS AND PERSPECTIVES

The analysis shows that the choice of positions near the terminal for comparison of CFD and OsM data might be crucial for an accurate prediction of wind field and wind forces on port infrastructures. Positions chosen too close to the quay are not recommended, since the geometrical simplifications and the assumption of port infrastructures in static configurations (dynamic in reality) make the flow field here potentially different with respect to reality (Fig. 1). In addition, SAS can provide a better prediction of the unsteady nature of the wind flow near the terminal than RANS, leading to a better estimation of wind forces acting on the port infrastructures.

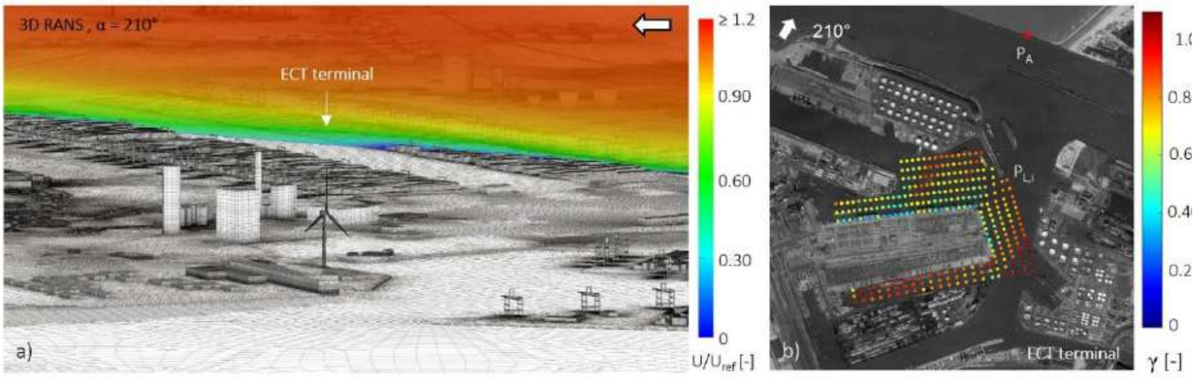

Figure 1. RANS results for $\alpha = 210°$: (a) contour of wind speed ratio and (b) transfer coefficient of wind speed (γ) at the ECT terminal ($P_{L,i}$) with an indication of the reference position (P_A).

ACKNOWLEDGEMENTS

The authors gratefully acknowledge the WINDLASS JIP consortium for the collaboration. Alessio Ricci is a senior postdoctoral fellow of the Belgian Research Foundation – Flanders (FWO) (no. 1256822N) and its financial support is gratefully acknowledged. The authors acknowledge the partnership with Ansys CFD.

REFERENCES

Population Reference Bureau, 2003. Ripple Effects: Population and Coastal Regions Measure Communication, 1875 Connecticut Ave., NW, Suite 520, Washington, DC 20009 USA.

Janssen, W.D., Blocken, B., van Wijhe, H.J., 2017. CFD simulations of wind loads on a container ship: validation and impact of geometrical simplifications. Journal of Wind Engineering and Industrial Aerodynamics 166, 106- 116.

Solari, G., Repetto, M.P., Burlando, M., De Gaetano, P., Pizzo, M., Tizzi, M., Parodi, M., 2012. The wind forecast for safety management of port areas. Journal of Wind Engineering and Industrial Aerodynamics 104-106, 266-277.

17th Conference on Wind Engineering – IN-VENTO 2022
Politecnico di Milano, IT 4 – 7 September 2022

Parameter identification of generalized vortex shedding model

Francois Rigo [1,2,3], Thomas Andrianne [1], Vincent Denoël [3]

[1] *Wind Tunnel Lab, University of Liège, Liège, Belgium, francois.rigo@uliege.be*
[2] *FRS-FNRS, National Fund for Scientific Research, Liège, Belgium*
[3] *Structural & Stochastic Dynamics, University of Liège, Liège, Belgium*

SUMMARY
This paper proposes a generalized model for vortex shedding around a static cylinder. This model is a first step to bridge the gap between two families of Vortex Induced Vibration (VIV) models, (1) stochastic spectral models (experimentally-based) and (2) wake-oscillator models with coupled structural and fluid equations. The present model generalizes the fluid equation by combining all third-degree terms and adjusting their coefficients on experimental trajectories in phase plane. A second specificity of the proposed model stems from the observation of a non-perfectly mono-harmonic lift force envelope measured for a static cylinder in low turbulence flow. In the proposed model, stochasticity is introduced to reproduce these fluctuations, as an additive exogenous noise with Von Karman spectrum. The methodology is applied to Wind Tunnel data of a static circular cylinder in subcritical and postcritical regimes. The lift fluctuation coefficient generated with the model matches results in the literature for the considered regimes and can be adapted to other cross-section shapes.

Keywords: Vortex shedding model, Circular cylinder, Wind tunnel experimental testing, Lift coefficient, Non-linear oscillator, Wake-oscillator

1. INTRODUCTION

Different models have been proposed to study VIV and can be classified into two groups according to the number of equations (one or two): (1) focus on the structural equation, with different ways to take into account the flow loading on the second member of the equation and (2) a coupled differential system with two variables: the structure and the wake. When the structure is static, models that take into account only the structure equation cannot simulate the fluid behaviour. Nevertheless, the model developed by (Vickery and Clark, 1972) is able to represent the fluid alone with a spectral formulation. Models (2) without structural motion simplify into one equation for the fluid. In this paper, focus is on the flow and resulting lift force on a static (fixed) cylinder. In this context, models describing the flow around static cylinders can be finally classified into two families: (1) data driven or empirical (spectrum) and (2) non-linear models such as the wake-oscillator (Hartlen and Currie, 1970; Tamura, 1981). The first family refers to experimentally-based models to obtain, directly, the spectrum of the lift force. In the second family, the dynamic of the lift coefficient is captured by a single non-linear equation: the second equation of a wake-oscillator model. The structural equation and corresponding coupling terms are discarded. In wake-oscillator models, non-linear terms are added to the fluid equation in the form of a Van der Pol or Rayleigh oscillator, to represent the lock-in features, with a certain range and self-limited amplitude.

A first objective of this paper is to use generalized nonlinear terms in the fluid equation and identify them from experimental data. In the case of a static cylinder, experimental evidences show fluctuations in the lift envelope and a randomization of the generalized model is necessary. Stochastic models where the fluid velocity is corrupted by noise are appropriate to model turbulence in the oncoming flow. Stochasticity in the envelope response is observable experimentally, though, even in case of uniform flow. In this context, another important feature of the proposed model is to randomize the deterministic generalized model with an additive noise which aims at capturing the turbulence in the near wake. This work can be seen as an effort to combine the advantages of two families of modelling: the stochasticity introduced by spectral methods and the self-limiting nature of wake-oscillator models. We show in this paper that the proposed model is able to accurately replicate experimental measurements. It is done by firstly adjusting a deterministic generalized model and secondly adding the turbulent content that allows to reproduce the fluctuations of experimental data.

2. METHODS

The parameters of the proposed generalized vortex shedding model are identified from experimental measurements. Pressure measurements are performed on a static cylinder in the Wind Tunnel Laboratory of University of Liège with 46 unsteady pressure taps equally spaced around the mid- span section of a circular cylinder (span $L/D = 10$, with $D = 0.1$m the diameter of the cylinder). The lift coefficient is obtained by integration of pressure coefficients. The data sets have been measured in uniform flow (turbulence intensity $I_u = \sigma_u/U < 0.2\%$). Reynolds numbers covered subcritical and postcritical regimes and two surface roughnesses were investigated (with k/D the relative roughness). The complete set-up description can be found in (Dubois and Andrianne, 2022). The proposed methodology was applied to three types of flow, two subcritical and one postcritical, see Table 1. The proposed model is new and generalizes usual non-linearities of Van der Pol, Rayleigh and energy-based equations (Hartlen and Currie, 1970; Krenk and Nielsen, 1999; Tamura, 1981), using four coefficients,

$$\ddot{q} + q = F(q,\dot{q}) = \dot{q}(\alpha q^2 + \beta q\dot{q} + \gamma \dot{q}^2 + \delta) \tag{1}$$

where $q = 2C_L/C_{L0}$ represents a scaled lift coefficient and the time is scaled with the Strouhal period $\tau = \omega t = 2\pi \mathrm{St}Ut/D$. The identification method is based on a phase portrait analysis of the observed lift. It consists in adjusting coefficients $\pi = (\alpha,\beta,\gamma,\delta)$ from experimental measurements of the fluid variable $q(t)$ (derived from the lift coefficient, $q = 2C_L/C_{L0}$), following these steps :

(1) Compute $\dot{q}$ and $\ddot{q}$ from q (using finite differences) to obtain and represent the experimental trajectories of $\ddot{q} + q$ as a function of q and $\dot{q}$.
(2) Adjust and fit the polynomial surface $F(q,\dot{q})$ on experimental trajectories, using a least-square fitting procedure, to identify model coefficients $\alpha,\beta,\gamma,\delta$, see Fig. 1.

A harmonic balance procedure showed that second (and all even) order terms do not participate to the dynamics. It also showed that β does not contribute to the amplitude of the limit cycle and therefore is chosen as $\beta = 0$. The known amplitude of the limit cycle gives a constraint on α,γ,δ. Also, the state space equation needs to be unstable at the origin, adding another constraint. To conclude, the optimization problem is solved for α,γ,δ and under the constraints: $\delta = -(\alpha + 3\gamma) > 0$. With the perspectives of deriving a model offering the advantages of the two (traditionally opposed) approaches, we suggest to introduce an additive forcing noise $\eta(t)$ to Eq. (1), to obtain the final form of the model:

$$\ddot{q} + q = F(q,\dot{q}) + \eta. \tag{2}$$

Indeed, fluctuations in the lift envelope and the residual on Fig. 2 suggested to force this nonlinear system by exogenous noise; the proposed modelling option differs from many of the existing solutions to include incoming turbulence but as an additive forcing noise in the equation because of the signature of a wake turbulence. Among several stochastic excitations, the Von Karman spectrum was found to best approach the experimental results. The Kolmogorov cascade (and the –5/3 slope in the PSD) is tentatively used to relate this choice to the wake turbulence.

$$\Phi_\eta(\omega) = \sigma_\eta^2 \frac{2L_\eta}{\pi U_\infty}\left(1+\left(1.339L_\eta\frac{\omega}{U_\infty}\right)^2\right)^{-\frac{5}{6}} \tag{3}$$

Parameters (σ_η,L_η) are selected to adjust the lift envelope of the model to the experimental one (based on the PDF and PSD). The procedure was applied to a circular cylinder at different Reynolds numbers and surface roughnesses.

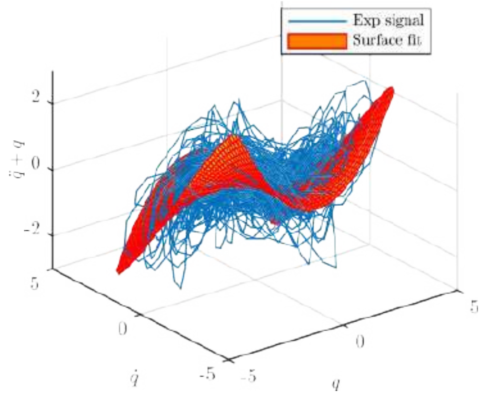

Figure 1. Experimental trajectories $\ddot{q}$ + q and deterministic polynomial surface fitting of $F(q,\dot{q})$ in phase spaces

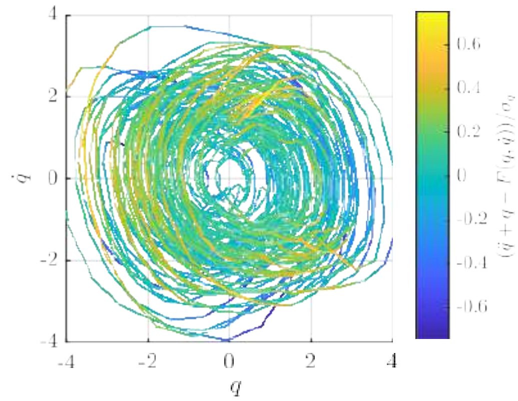

Figure 2. Residual between experimental trajectories of Figure 1 and deterministic fitted surface

3. RESULTS AND CONCLUSIONS

The evolution of model coefficients α,γ,δ and Von Karman parameters σ_η,L_η with Re and rough- ness were studied in sub- and postcritical regimes. In the subcritical regime, model parameters are almost Reynolds independent. In the postcritical regime, non-linearities decrease with Re and as well as the additive noise amplitude from wake turbulence. On Fig.3, the proposed model was com- pared to deterministic wake-oscillator and spectral models in terms of lift dynamics and statistics (PDF and PSD of lift and lift envelope). The exogenous noise is more suited to model wake turbulence than the white noise and results obtained with the present model match well experimental data. The fluctuating lift amplitude computed from generated signal of the model were compared to experimental data. The predictions of values of C'_L obtained with the proposed model are consistent with results from the literature in the subcritical regime, for smooth and rough cylinder surface, in low turbulence flow. Results on Fig. 4 show that the present model is able to correctly estimate C'_L of the circular static cylinder in different regimes and can be used in a prediction phase.

This work opens several perspectives. Among others, it offers a simple and robust way to identify nonlinear coefficients in the vortex shedding model for a static circular cylinder, together with the additive noise intensity and characteristic time. Static cylinders arranged in tandem configuration could benefit from this type of model. Moreover, this equation, combined with a structural one, can be used to model cylinders in free vibration with adapted coupling terms. Finally, by doubling the two-equation system, the extension to flexible cylinders in tandem arrangement is also possible.

Table 1. Wind Tunnel data, identified coefficients of the generalized model and exogenous noise for the three regimes

Regime	*Re*	*k/D*	α	γ	δ	σ_η	L_η
Sub1	$4.5 \cdot 10^4$	$4 \cdot 10^{-4}$	-0.085	0.009	0.057	0.55	1.15
Sub2	$4.3 \cdot 10^4$	$7 \cdot 10^{-3}$	-0.078	0.009	0.051	0.6	0.9
Post	$1.5 \cdot 10^5$	$7 \cdot 10^{-3}$	-0.016	0.002	0.011	0.2	1.2

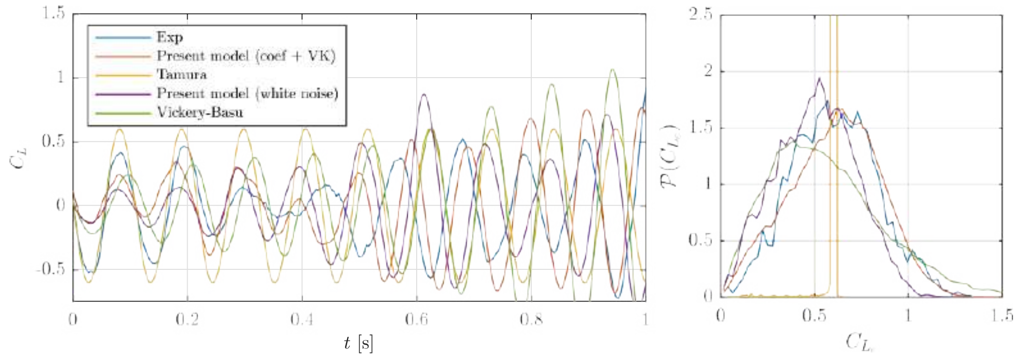

Figure 3. Comparison of experimental measurements (Sub1 case), present model prediction, Tamura's and Vickery-Basu's models: lift coefficient $C_L(t)$ and PDF of lift envelope used to adjust (σ_η,L_η)

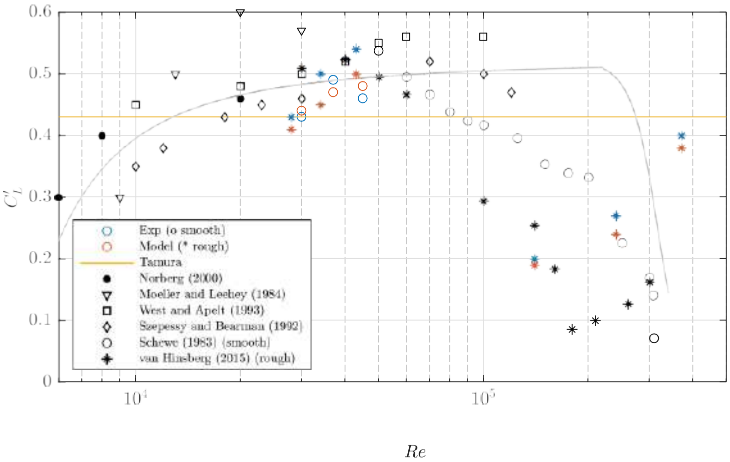

Figure 4. Lift fluctuation, experiments vs model prediction and literature, grey line is a trend from Norberg, 2003

ACKNOWLEDGEMENTS

This study was made possible thanks to the support of the National Fund for Scientific Research of Belgium (FNRS).

REFERENCES

Dubois, R. and Andrianne, T., 2022. Flow around tandem rough cylinders: Effects of spacing and flow regimes. Journal of Fluids and Structures 109, 103465.

Hartlen, R. T. and Currie, I., 1970. Lift-oscillator model of vortex-induced vibration. Journal of the Engineering Me- chanics Division 96, 577–591.

Krenk, S. and Nielsen, S. R., 1999. Energy balanced double oscillator model for vortex-induced vibrations. English.

Journal of Engineering Mechanics 125, 263–235.

Norberg, C., 2003. Fluctuating lift on a circular cylinder: review and new measurements. Journal of Fluids and Struc- tures 17, 57–96.

Tamura, Y., 1981. Wake-Oscillator Model of Vortex-Induced Oscillation of Circular Cylinder. Journal of Wind Engi- neering 1981, 13–24.

Vickery, B. J. and Clark, A. W., 1972. Lift or Across-Wind Response of Tapered Stacks. Journal of the Structural Division 98, 1–20.

LES simulations of an experimentally-produced inclined downburst: implications of a storm motion

Josip Žužul [1], Alessio Ricci [2,3], Massimiliano Burlando [1]

[1]*Department of Civil, Chemical and Environmental Engineering, University of Genoa, Genoa, Italy, josip.zuzul@edu.unige.it – massimiliano.burlando@unige.it*
[2]*Department of Civil Engineering, KU Leuven, Leuven, Belgium, alessio.ricci@kuleuven.be*
[3]*Department of the Built Environment, Eindhoven University of Technology, Eindhoven, the Netherlands, a.ricci@tue.nl*

SUMMARY
Downburst winds produced by an isolated stationary thunderstorm create their characteristic signatures in terms of a theoretically symmetric ring vortex and strong near-surface winds. However, there is a high likelihood for the storm to be moving rather than being stationary, which in turn changes the downburst flow features. The differences are mostly pronounced in the flow asymmetry based on the direction of storm propagation, which consequently subjects structures to different velocity profiles which affect the wind loading. To further investigate the implications of the storm motion, an experimentally-produced inclined downburst caused by the moving storm was replicated numerically. In this paper, the LES simulations of the inclined downburst were performed to focus on the full-field representation of the flow in the near-surface region. The flow field was visualized in terms of velocity contours and radial velocities were compared with measured data. Overall, the LES data show a good agreement with the measured data.

Keywords: Thunderstorm downburst, storm motion, LES simulations

1. INTRODUCTION

Thunderstorms can produce downburst winds which have the potential to endanger the integrity of low-rise structures. In the most simplified case, the downburst characteristics are defined solely by the vertical air impingement from the storm that produces the ring vortex and strong diverging winds above the surface (Fujita, 1981). However, a realistic downburst commonly includes additional contribution associated with the storm itself which is often translational instead of stationary. This contribution causes the downburst flow field to deflect from the theoretically symmetric one found in isolated stationary storms. The present work makes use of Large Eddy Simulations (LES) to support the experimental tests of an inclined downburst performed in the WindEEE Dome (Hangan et al., 2017) that aim to investigate its flow behavior due to the moving storm.

2. LES SIMULATIONS

LES simulations were performed on a computational domain replicating the WindEEE Dome with nozzle (D = 3.2 m) displaced from the chamber center (Fig. 1a). Hereby, the contribution of the storm motion was considered through the jet axis inclination angle of 30°. The average speed (Ujet) of 12 m/s imposed at the inlet of the domain was used to recreate the temporally and spatially correlated eddies through the synthetic turbulence generator by Poletto et al. (2013). The sub-grid scale turbulence was modeled by a dynamic method based on Lagrangian averaging (Meneveau et al., 1996). The no-slip conditions were imposed at the wall boundaries while the near-wall flow was modeled with the Spalding wall functions for smooth surfaces. Zero-static gauge pressure was prescribed at the outlet. Overall, the computational grid counted 18.2 million hexahedral cells, and the average y+ across the bottom surface reports values greater than 30 (Fig. 1b).

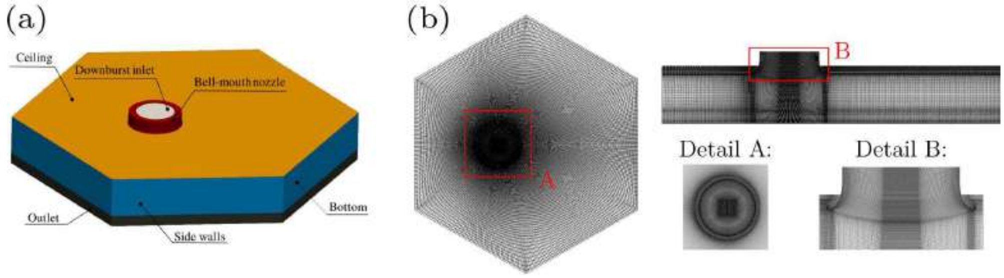

Figure 1. Computational domain with indications of boundary conditions (a), and computational grid (b).

3. RESULTS AND PERSPECTIVES

Contours of velocity magnitude plotted at the central vertical plane (Fig. 2a) show the asymmetric flow characteristics between the front and rear sides. Bigger vortex and strong winds are formed at the front side (right), compared to the rear side (left). Fig. 2b presents the time-history comparison of simulated and measured radial velocities at the selected probe location (R/D = 1.6 and z = 0.10 m) which indicates a considerable level of agreement. Further results will be presented in the full paper.

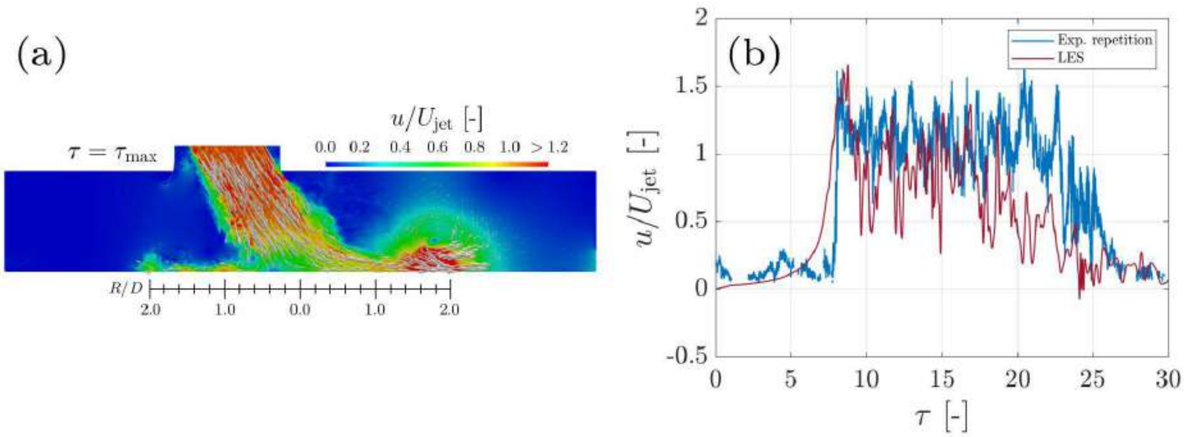

Figure 2. Results: (a) contour of velocity magnitude normalized by jet velocity U_{jet} in the time instance τ_{max} of maximum radial outflow, (b) comparison of measured and simulated instantaneous radial velocities at $R/D = 1.6$ and $z = 0.10$ m (*i.e.* right side of Fig a).

ACKNOWLEDGEMENTS

This work was carried out on the Dutch national e-infrastructure with the support of SURF Cooperative. J. Žužul and M. Burlando acknowledge the support of the European Research Council (ERC) under the European Union's Horizon 2020 research and innovation program (grant agreement no. 741273) for the project THUNDERR – Detection, simulation, modelling and loading of thunderstorm outflows to design wind-safer and cost-efficient structures – funded with an Advanced Grant 2016. The authors are deeply grateful to Prof. Giovanni Solari for his essential contributions to the conceptualization and supervision of this research.

REFERENCES

Fujita, T. T., 1981. Tornadoes and Downbursts in the Context of Generalized Planetary Scales. Journal of the Atmospheric Sciences 38, 1511–1534.

Hangan, H. et al., 2017. Novel techniques in wind engineering. Journal of Wind Engineering and Industrial Aerodynamics 171, 12–33.

Meneveau, C., Lund, T., and Cabot, W., 1996. A Lagrangian dynamic subgrid-scale model of turbulence. Journal of Fluid Mechanics 319, 353–385.

Poletto, R., Craft, T., and Revell, A., 2013. A new divergence free synthetic eddy method for the reproduction of inlet flow conditions for LES flow. Turbulence and combustion 91, 519–539.

Data-driven approaches to the gust wind speed for pedestrian-level wind simulations

J. Millar [1], A. Nicoli [2], A. McLoughlin [3], S. Cammelli [4]

[1] *WSP, London, United Kingdom,* joshua.millar@wsp.com
[2] *WSP, London, United Kingdom,* andrew.nicoli@wsp.com
[3] *WSP, Manchester, United Kingdom,* aidan.mcloughlin@wsp.com
[4] *WSP, London, United Kingdom,* stefano.cammelli@wsp.com

SUMMARY
The gust wind speed is commonly used in pedestrian-level wind analyses in order to quantify the effect of short-duration gusts on pedestrian comfort and safety. Simplified approaches based on summary statistics allow for the estimation of a gust wind speed from steady-state RANS simulations. However, analysis shows that these simplified approaches do not account for the complexity of urban flows, and their performance is therefore dependent on *a priori* selection of a peak factor. This work presents approaches which make use of large datasets and apply modern analysis techniques to construct more sophisticated data-driven models which provide more accurate estimations of the gust wind speed from RANS simulations.

Keywords: machine learning, wind microclimate, computational wind engineering

1. INTRODUCTION

In the analysis of the pedestrian-level wind environment, the gust wind speed is commonly used in addition to the mean wind speed to assess the comfort and safety of pedestrians. This gust wind speed is typically considered to be the peak 3-second gust, a concept which is commonplace in wind engineering, computed by taking the 1% exceedance of the 3-second moving average of the signal (Lawson, 1990). In practice, the gust wind speed, U_g, is divided by 1.85 (or 2.0 for locations immediately overlooking water) to obtain a gust equivalent mean, GEM. The comparison to criteria is then made with the maximum of the mean wind speed and the GEM for each measurement location. As the calculation of the 1% exceedance is not decomposable (i.e. requires the whole dataset to be stored in memory) and generally takes significantly more time than the mean and standard deviation to reach stationarity, a simplified estimate is commonly used:

$$U_g = \overline{U} + g\sigma$$

where $\overline{U}$ is the mean wind speed, σ is the standard deviation and g is a peak factor. As σ can be computed algebraically from the turbulent kinetic energy, k, a quantity which is commonly computed in RANS simulations, this approach appears to allow for the estimation of gusts from steady-state simulations.

However, with a constant g, this simplified approach embeds an assumption that all scales of turbulence contribute to the peak 3-second gust, which may not be the case. This has led to a wide range of proposed values for $g = 1.0 \rightarrow 3.5$ to attempt to achieve general agreement with experiments (Vita *et. al.,* 2020).

This paper presents ongoing work which uses modern data mining techniques to produce both a site-specific, and a generalised approach for estimating the gust wind speed from steady-state RANS simulations.

2. APPROACH AND INITIAL RESULTS

When CFD and wind tunnel are used in parallel, it is possible to create a regression model to estimate the gust wind speed using the measurements from the tunnel. This model needs to be created for each site and will typically be a polynomial model of the second- or third-order expansion of the non-dimensionalised velocity and turbulent kinetic energy fields from the CFD. This approach shows good agreement with experiment and is frequently used by the authors in practice.

For the creation of a generalised model, an unsteady detached eddy simulation was performed for a site in London (UK) where the gust wind speed was explicitly calculated from the time signal and for which experimental data was available. All dimensional and temporal parameters, as well as spatiotemporal inlet conditions were matched to the wind tunnel experiment, which allowed a validation of the simulation to be made, showing an excellent agreement. Figure 1 shows the peak factor, $g = (U_g - \overline{U})/\sigma$, computed from this simulation, which highlights the large amount of spatial variation due to the different flow mechanisms in such a complex urban environment.

With the validated CFD model, it is possible to investigate the relationship between mean quantities and U_g, and a number of regression models have been tested and their performance assessed and presented.

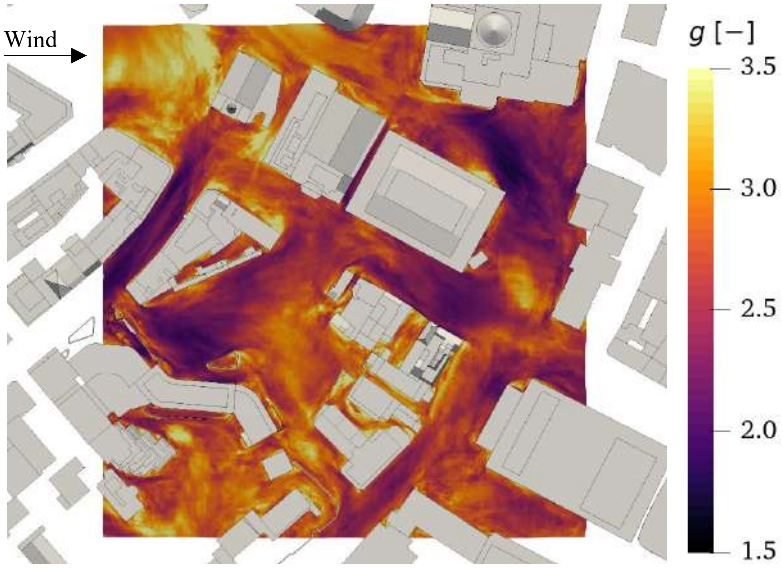

Figure 1. Contours of peak factor for a simulation around buildings in London (UK). Wind direction is left-to-right.

REFERENCES

Lawson, T.V., 1990. The determination of the wind environment of a building complex before construction. *Department of Aerospace Engineering, University of Bristol, Report Number TVL, 9025*.

Vita, G., *et al.*, 2020. On the assessment of pedestrian distress in urban winds. *Journal of Wind Engineering and Industrial Aerodynamics*, *203*, p.104200.

A multidisciplinary approach to optimize the gust loading on groups of wind turbine towers at the quayside

Alessandro Giusti [1], Alessio Torrielli [2,3]

[1]Siemens Gamesa Renewable Energy A/S, Brande, Denmark
alessandro.giusti@siemensgamesa.com
[2]R&D Engineering A/S, Hinnerup, Denmark, alt@rdas.dk
[3]Siemens Gamesa Renewable Energy A/S, Brande, Denmark
alessio.torrielli.ext@siemensgamesa.com

SUMMARY
Steel towers of offshore wind turbines are usually assembled at the quayside before being loaded onto the installation vessel and taken to the offshore wind farm. Towers are usually erected in groups at close distance on gravity-based foundations, which should be verified against the relevant environmental loads, including the wind load. The peculiarities of the system together with the necessity of optimization to limit the costs without compromising the safety inspired the development of an advanced multidisciplinary approach for the assessment of gust buffeting loads. The methodology aims at refining the calculation and introducing tailored input parameters. This is achieved through local wind measurements, wind tunnel tests and full-scale measurements. In this paper the methodology is presented and compared with the typical approach provided by EN 1991-1-4.

Keywords: gust buffeting, groups of towers, load optimization

1. INTRODUCTION
In the offshore wind energy industry, pre-assembly activities are usually carried out at the harbor quayside before components are loaded onto the installation vessel. Among them, towers are typically erected in groups at small distance on a gravity-based foundation. Pre-assembly activities usually last 6-12 months, and they have therefore a temporary character. In this framework, the foundation should be designed and verified against environmental loads.

2. METHODOLOGY
The assessment of gust buffeting loads on close groups of wind turbine towers is not fully covered by EN 1991-1-4. It is therefore necessary a multidisciplinary approach aimed at improving the aspects where the standard is incomplete or not sufficiently accurate. Table 1 presents a one-to-one comparison between a calculation based on the EN 1991-1-4 only and the methodology developed by Siemens Gamesa Renewable Energy to achieve a satisfying level of accuracy.

3. CONCLUSIONS
In this paper a multidisciplinary approach for the optimization of gust buffeting loads on groups of towers is presented together with a one-to-one comparison with the typical approach provided by EN 1991-1-4, in order to point out the main weakness of the standard when it is applied to this type of structures. Furthermore, the influence of the key parameters is studied through a sensitivity analysis.

Table 1. Flowchart for the assessment of gust buffeting loads on groups of towers.

Step	EN 1991-1-4 approach	Multidisciplinary approach
Geometry of the system	It is an input data of the problem.	It is an input data of the problem.
Reference wind velocity	National Annexes provide a description of the wind climate to be used for design purposes. They usually cover extended areas and therefore cannot capture local peculiarities of the construction site. The use of design standards is usually conservative.	Statistics of local wind data provide a detailed knowledge of the local wind climate through the assessment of the parent distribution and extreme event distribution (including directional and season factors). The latter permits to calculate the wind velocity corresponding to a given return period. It is needed a reliable dataset of at least 10 years of wind measurements (Cook, 1985).
Mean wind profile	The standard and National Annexes provide guidelines for the definition of the mean wind velocity profile for a given terrain category.	A site-specific assessment of the mean wind profile could help the optimization of gust buffeting loads, but it is not a common/cheap practice because it needs multi-level wind velocity readings.
Peak velocity pressure	The standard and National Annexes provide guidelines for the assessment of the peak velocity pressure for a given terrain category (e.g., intensity of turbulence).	A site-specific assessment of the intensity of turbulence and peak velocity pressures could help the optimization of gust buffeting loads, but it is not the common practice.
Aerodynamic coefficients	The standard provides guidelines for the assessment of force coefficients on parallel-sided cylinders, including corrections to consider the finite length of the cylinder (end-effect factor) and the proximity to other cylinders only in row arrangements. However, the extension of the standard to tapered cylinders and/or cylinders arranged in close groups is not straightforward and can lead to significant underestimations of the aerodynamic coefficients.	Wind tunnel tests address specific cases, like towers with variable geometry or interferences with neighboring structures, which are not covered by the design standards. Moreover, local wind conditions (e.g., wind profile and intensity of turbulence) can be modelled. Wind tunnel tests can provide a comprehensive understanding of the (mean) aerodynamic coefficients for all directions of the wind rose and are usually focused on the resultant actions at the base of the tower (Mannini et al., 2022), which drive the design of the foundation.
Structural damping	Table F.2 of the standard seems to underestimate the overall structural damping available on a wind turbine tower.	Full scale tests consider all possible sources of damping, given by the structure itself, internals and any added damper (e.g., tuned mass dampers and tuned liquid dampers inside the tower, or laminated elastomeric bearings at the tower-foundation interface).
Aerodynamic damping	The formulation in Annex F of the standard is approximated and in principle valid only for parallel-sided cylinders.	The knowledge of the mean force distribution along the height of the towers (through wind tunnel tests) combined with the theory permits a detailed calculation of the expected aerodynamic damping (Repetto and Solari, 2001). In absence of information about the force distribution, a simplified formulation can be developed starting from the aerodynamic coefficients of the force (or moment) at the tower base.
Structural factor	The formulation in Section 6, Annex B and Annex C of the standard considers only the correlation of the wind action but not the correlation induced by the structure itself.	The analysis of the maxima of the records of static wind tunnel tests (e.g., in accordance with Davenport-Rice approach) permits to embed the size factor in the (maximum) aerodynamic coefficient.
Gust buffeting loads	The standard provides guidelines for the calculation of forces but not moments.	Calculation of forces and moments.

REFERENCES

Cook, N.J., 1985. The designer's guide to wind loading of building structures. Part 1: Background, damage survey, wind data and structural classification. Building Research Establishment, Garston, Watford, UK.

EN 1991-1-4, 2007. Eurocode 1: Actions on structures - Part 1-4: General actions - Wind actions.

Mannini, C., Massai, T., Giachetti, A. and Giusti, A., 2022. Aerodynamic loads on wind turbine towers arranged in groups with and without helical strakes. Proceedings of the 17th International Conference of the Italian Association for Wind Engineering - IN-VENTO 2022, Milano, Italy, in press.

Repetto, M.P. and Solari, G., 2001. Dynamic alongwind fatigue of slender vertical structures. Engineering Structures 23, 1622-1633.

Verification of analytical wind load estimation methods of downburst through a full-scale wind and structural response monitoring

M.T. Mengistu [1], M.P. Repetto [2]

[1]*University of Genova, Genova, Italy, mekdestadesse.mengistu@edu.unige.it*
[2]*University of Genova, Genova, Italy, Repetto@dicca.unige.it*

SUMMARY
The effect of downburst winds on structures has been studied by many researchers and few analytical models for the calculation of wind loads during a downburst were also proposed. However, these analytical models have not been verified through full-scale structural monitoring. In this research, the response of a lighting pole during two downburst events is used to compare the response of the structure estimated from analytical methods with the registered response.

Keywords: Downburst, Structural monitoring

1. ABSTRACT

In the past 20 years, many researchers studied the effect of downburst winds on structures. Analytical models for the calculation of loads due to downburst outflow winds were also proposed. However, due to the small spatial and temporal scale of downbursts, validation of the proposed analytical models through registered structural response has not been sufficiently done. To fill this gap in research, full-scale monitoring of selected three slender structures has been initiated through the European Union funded project, THUNDERR (Solari et al., 2020). The aim of the full-scale monitoring is to study the response of simple slender structures under downburst winds and to conduct a validation study for the previously proposed analytical methods of downburst wind load response.

One of the structures that have been monitored through the THUNDERR project is a lighting pole located at the port of La Spezia, Italy (Figure 1a). The pole is 16.6 meters high with a cross-section of a 16-sided polygon. A steel ladder connects the bottom of the pole to the top. At about 10 meters above ground, the ladder is interrupted by an intermediate rectangular platform. At the top, a squared platform houses the lighting equipment and a security camera. The pole is equipped with strain gauges and accelerometers at two heights and an ultrasonic triaxial anemometer at the top. The sampling frequency is 10 Hz for the anemometer, 100 Hz for the strain gauges, and 200 Hz for the accelerometers.

Two case studies of downburst events whose wind and structural response data were registered by the monitoring system are selected for analysis. Figure 1 shows the 1hr time history of instantaneous as well as a running mean wind speed averaged over 10 minutes (b and d) and wind direction (c and d) for the two selected case studies of downbursts. In both cases, it is evident that there is a sudden increase in wind speed accompanied by a change in wind direction. Figure 2 shows the 10 minutes time history of instantaneous and slowly varying mean wind speed averaged over 30 seconds (a), wind direction (b), resultant strain obtained through two orthogonal strain gauges (c), and acceleration in the two orthogonal directions measured by the accelerometer at 10.5 m above the base (d) for the downburst event of October 02, 2019. It can be observed that the time history of mean strain follows a similar trend as the mean wind speed. In addition, the intensity of acceleration is correlated with the intensity of the wind speed increasing from zero to a higher intensity with an increase in wind speed. All records present transient properties that make them different from a typical synoptic wind response.

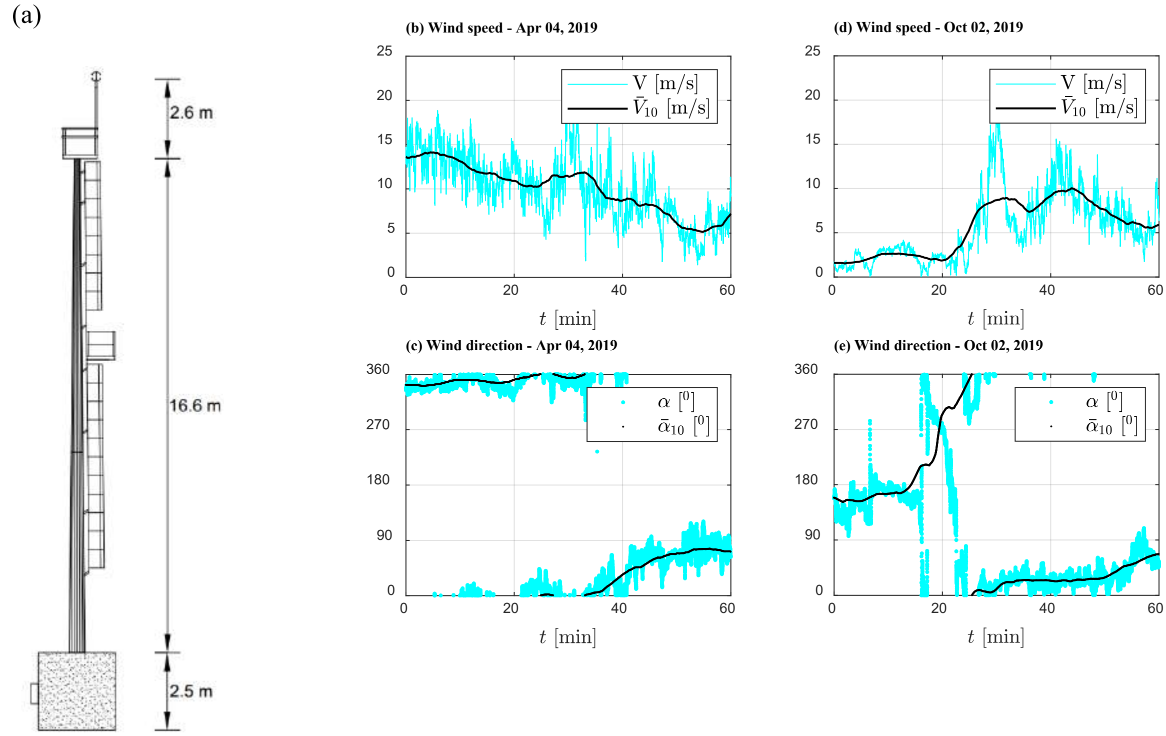

Figure 1. The monitoring station at La Spezia (a), 1-hour time history of wind speed (b & d), and wind direction (c & e) for the two case studies of downburst

Analytical methods for the calculation of wind load due to downbursts have been proposed in the literature. The thunderstorm response spectrum technique (TRST) is one of these methods and it intends to extend the response spectrum method, widely used for the calculation of earthquake loads on structures, to the calculation of wind loads due to thunderstorms (Solari et al., 2015; Solari and De Gaetano, 2018). The Generalized gust front factor (GGFF) method is another procedure proposed for the calculation of wind loads due to gust fronts and it generalizes the commonly used method of gust front factor, widely applied for atmospheric boundary layer (ABL) winds, to non-transient phenomena like downbursts (Kwon and Kareem, 2009). In this research TRST and GGFF methods were applied to calculate the maximum response of the structure during the two case studies of downbursts and the calculated displacement at the top of the structure. The results were compared with the top displacement obtained from strain gauge measurements. The uncertain parameters that are inputs for the calculation of the response using TRST and GGFF methods such as vertical wind profile, aerodynamic coefficient, damping ratio, and coherence of wind field are initially derived using time-domain analysis.

Comparison between the calculated response using the TRST and GGFF methods with the registered response showed that the along wind responses calculated using both methods are higher than the registered response for both selected downburst events. In the case of GGFF method, the estimated response is more than two times the maximum registered response. This research needs to be extended to different structures with a range of dynamic properties to serve as an input for the revision of analytical load calculation methods, optimizing safety and economy.

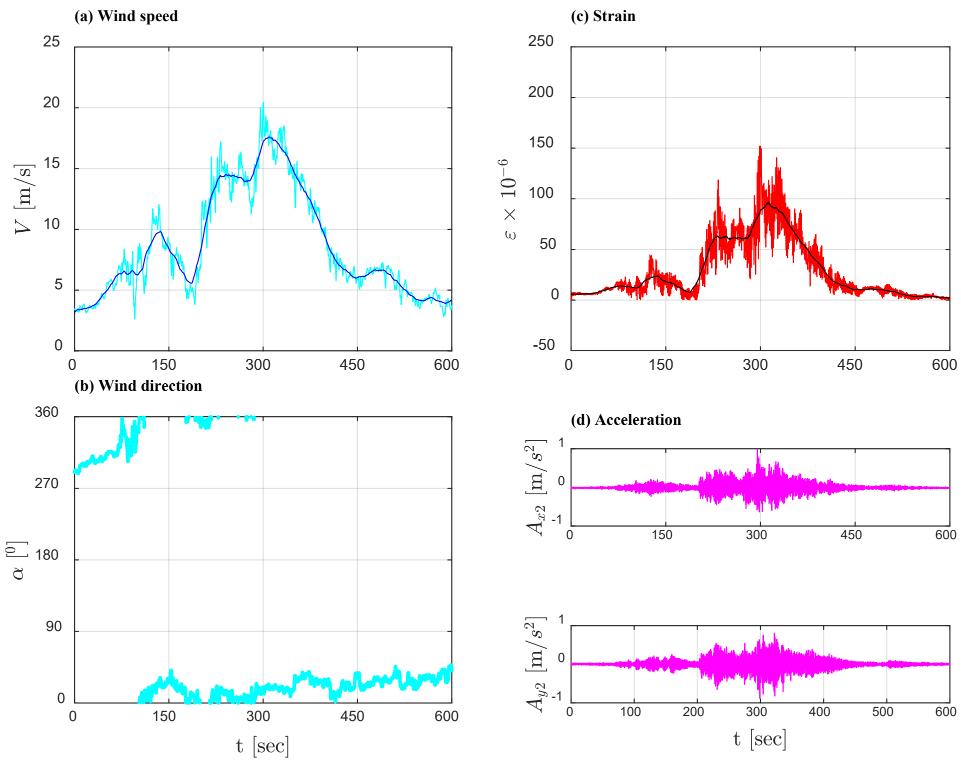

Figure 2. Wind and structural response for the downburst on October 02, 2019

ACKNOWLEDGEMENTS
The contribution of the second author is funded by the European Research Council (ERC) under the European Union's Horizon 2020 research and innovation program (grant agreement No. 741273) for the project "THUNDERR - Detection, simulation, modeling and loading of thunderstorm outflows to design wind-safer and cost-efficient structures" – through an Advanced Grant 2016. The monitoring system is co-funded by the Italian Ministry of Instruction and Scientific Research (MIUR), Prot. 2015TTJN95 in the framework of the Research Project of Relevant National Interest (PRIN 2015).

REFERENCES
D.K. Kwon & A. Kareem (2009). Gust-front factor: New framework for wind load effects on structures. Journal of Structural Engineering,135(6),717-732

G. Solari, M. Burlando, M.P. Repetto (2020). Detection, simulation, modeling, and loading of thunderstorm outflows to design wind-safer and cost-efficient structures. Journal of Wind Engineering and Industrial Aerodynamics, 200, 104142

G. Solari, P. De Gaetano & M.P. Repetto (2015). Thunderstorm response spectrum: Fundamentals and case study. Journal of wind Engineering and Industrial Aerodynamics, 143,62-77

G. Solari, & P. De Gaetano (2018). Dynamic response of structures to thunderstorm outflows: Response spectrum technique vs time-domain analysis. Engineering Structures, 176,188-207

On the modeling of self-damping in overhead electrical line conductors subject to vortex-induced vibrations

Francesco Foti [1], Luca Martinelli [2], Federico Perotti [3]

[1]*Dep. of Civil and Environmental Engng. Politecnico di Milano, Milano, Italy, francesco.foti@polimi.it*
[2]*Dep. of Civil and Environmental Engng. Politecnico di Milano, Milano, Italy, luca.martinelli@polimi.it*
[3]*Dep. of Civil and Environmental Engng. Politecnico di Milano, Milano, Italy, federico.perotti@polimi.it*

SUMMARY
The paper reviews some recent results of the authors' research group related to the modeling of the hysteretic behaviour of metallic stranded cables and applies them to the definition of a theoretical model for the self-damping of a widespread typology of overhead electrical line conductors, namely the ACSR conductors. Closed-form expressions of the dissipated power per unit of length of the conductor, previously derived by the authors, are cast in a new form that allows for a more expressive comparison with available experimental data of the literature.

Keywords: cable dynamics, self-damping, vortex induced vibrations

1. BACKGROUND AND MOTIVATION

Overhead electrical line conductors are prone to vortex-induced vibrations. The severity of vibration is typically evaluated through an application of the Energy Balance Principle (EBP): mono-modal vibrations are assumed and the balance between the input power provided by the wind and the power dissipated within the cable is imposed at each vibration frequency. As already argued in (EPRI, 2006), the accuracy and reliability of the outcomes of the EBP can be strongly affected by the criteria adopted to define the input data, namely: the wind input power and the cable self-damping (i.e. the power dissipated within the oscillating cable).

The current practice to characterize the self-damping of overhead electrical line conductors relies upon an empirical approach. Mono-modal vibration tests are performed on laboratory spans and the power dissipated per unit of length of the cable (P_d) is measured for different values of the antinode vibration amplitude Y, vibration frequency f and axial force T. The experimental data are then interpolated through the empirical power law: $P_d = k\, Y^l f^m\, T^{-n}$, where l, m and n are exponents with values that typically fall in the ranges: $l = 2\text{-}2.5$; $m = 4\text{-}6$; n=2-2.8 for the widespread class of Aluminium Conductors Steel Reinforced (ACSR) cables, while k is a proportionality coefficient. Whenever k is not defined from experimantal data, it can be computed on the base of both the internal geometry and material properties of the cable using empirical equations such as $k = D/\sqrt{\gamma RTS}$. Where D is cable diameter that has to be expressed in mm, γ is the mass per unit length of the cable, expressed in kg/m, and RTS is the rated tensile strength of the cable expressed in kN. This definition of k, however, leads to a dimensionally non-homogeneous equation.

Due to the power form of the empirical self-damping equation, even a small variation in the values of the exponents l, m and n can lead to large differences in the computed values of dissipated power. This, in turn, can significantly affect the reliability of the outcomes of the EBP method. This observation motivated the interest in developing a self-damping formulation based on a mechanical description of the hysteretic dissipation mechanism associated to the vortex-induced-vibration of overhead electrical conductors (Foti and Martinelli, 2018a; 2018b). That theoretical formulation is herein adopted as the base for a reparametrization of significant experimental results to provide a new insight into the physics behind the self-damping of cables.

2. THE PROPOSED SELF-DAMPING MODEL

Due to the peculiar internal structure of overhead electrical conductors, whenever they are bent, the wires tend to slide relative one to another. Sliding of the wires is the physical mechanism providing power dissipation in the conductors subject to vortex-induced-vibrations.

Starting from the theoretical description of the frictional interaction between the wires, two different dissipative phenomena have been identified by Foti and Martinelli (2018a, 2018b), i.e.: the Micro-Slip (MS) and the Gross-Sliding (GS) dissipation mechanisms. These two mechanisms are here assumed to control, respectively, the small-amplitude and large-amplitude vibration regimes. A quantitative threshold between the two different mechanisms is conventionally defined by comparing the modal curvature of the vibrating conductor to the "first-sliding" curvature χ_0 of the conductor cross section, that can be regarded as the curvature value related to the activation of gross-sliding phenomena between the wires of the cable. Using the model proposed in Foti and Martinelli (2018a, 2018b) and by assuming a mono-modal steady state vibration the conductor self damping can be calculated in closed form under both the assumption of MS and GS dissipation mechanism, yielding the two expressions:

$$P_d^{ms} = \alpha_{ms} Y^3 f^7 T^{-4} \tag{1}$$

$$P_d^{gs} = \alpha_{gs} Y^2 f^5 T^{-2} \tag{2}$$

where the superscripts refer to the assumed dissipation model while α_{ms} and α_{gs} are two dimensional coefficients that depend on the geometry and material properties of the conductor. Theoretical expression for α_{ms} and α_{gs} have been derived in Foti and Martinelli (2018a, 2018b) and read:

$$\alpha_{ms} = \frac{128\pi^5 \gamma^3 RTS EI_{max,ef}}{c_0 \mu} \tag{3}$$

$$\alpha_{gs} = 4\pi^4 \gamma^2 EI_{max,ef} \tag{4}$$

Where $EI_{max,ef}$ is the maximum bending stiffness of the cable cross-section, μ is the internal friction coefficient and c_0 is a geometric parameter with values in the 0.1-0.3 m^{-1} range for common ACSR conductors.

The theoretical predictions of Eq. (1) and Eq. (2) are compared in the present paper against a large and significant data-set of experimental data from the literature, obtained under different test conditions and for different conductor cross sections.

As an example of application, Fig. 1 shows, for a representative conductor, the non-dimensional dissipated power $\Pi = P_d/(C \cdot 4\chi_0^{\,2} l^2)$ as a function of the non-dimensional variable $J = \Phi^2/\rho^3$, where $C = 0.5 EI_{max,ef} \chi_0^{\,2} \sqrt{[T/(ml^2)]}$, l is the length of the cable span, m is the mass per unit of length of the cable, $EI_{max,ef}$ is the maximum bending stiffness of the cable cross section, Φ is the rotation angle (in absolute value) of a node in the mode shape and ρ is the ratio between the wave length of the mode and the length $2l$.

As it can be clearly appreciated from Fig. 1, all experimental data points tend to collapse on a single straight line, independent of the different testing conditions (i.e. different values of cable axial force, frequency and vibration amplitude).

For large values of J (i.e. greater to about 0.005), the slope of the line interpolating experimental data is approximately equal to one predicted by the GS damping model. For smaller values of J, instead, the experimental data are in closer agreement with the theoretical predictions of the MS damping model rather than to the ones of the GS damping model.

The comparison in Fig. 1 allows to appreciate as the conductor self damping predicted with the closed form equations reported in Eq.(1) and Eq.(2) give values close to those of the experimental data for a range of testing conditions typical of overhead conductors. Besides this first interesting result, the proposed reparametrization seems to confirm the occurrence of two different dissipation mechanisms, associated to different ranges of bending curvatures of the cable, which where only hypothetized in the previous studies of this research group. Further studies however are needed to precisely define the transition curvature between these dissipation regimes; this is the subject of an ongoing research.

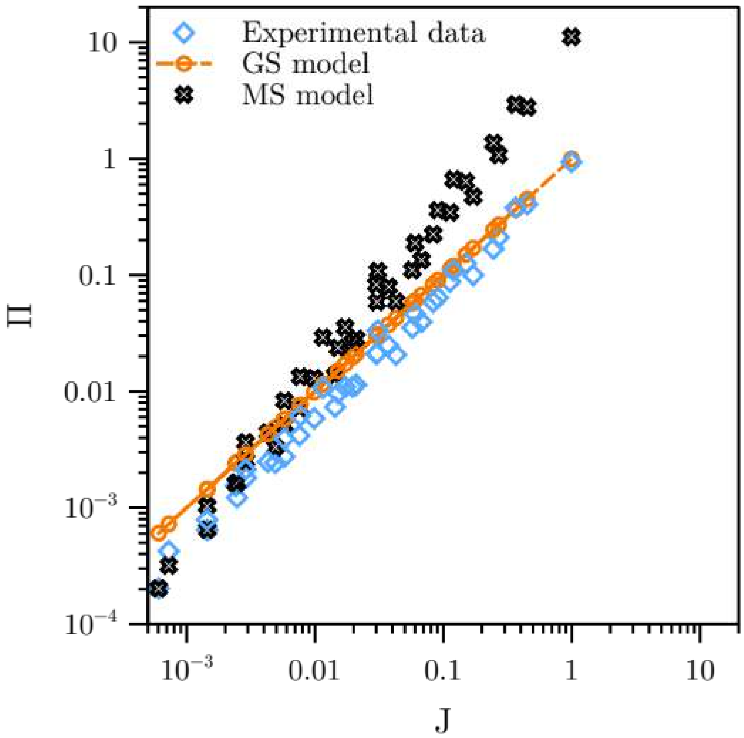

Figure 1. ACSR Bersfort conductor. Non-dimensional dissipated power per unit of length.

REFERENCES

EPRI - Electric Research Power Institute, 2006. Transmission Line Reference Book: Wind-induced Conductor Motion. U.S., Palo Alto.

F. Foti, L. Martinelli, 2018a, "A unified analytical model for the self-damping of stranded cables under aeolian vibrations", J. Wind Eng. Ind. Aerodyn., vol. 176, 225-238.

Foti, F., Martinelli, L., 2018b. An enhanced unified model for the self-damping of stranded cables under aeolian vibrations, Journal of Wind Engineering & Industrial Aerodynamics 182: 72-86.

Comparison of tornado-induced loads to ASCE/SEI 7-22 provisions for low-rise residential buildings.

Gabriel Narancio [1,2], Djordje Romanic [1,3], Jubayer Chowdhury [1,4], Han-Ping Hong [5], Horia Hangan [1,6]

[1]*WindEEE Research Institute, London, Canada, enaranci@uwo.ca*
[2]*IMFIA, Montevideo, Uruguay*
[3]*McGill University, Montreal, Canada*
[4]*CPP wind, Windsor, USA*
[5]*Western University, London, Canada*
[6]*Ontario Tech University, Toronto, Canada*

SUMMARY
This document presents a comparison of the provisions provided by ASCE-SEI 7-22 for tornadoes with the results of physical simulations of the interaction of tornado-like vortices with a residential community. The tests were performed at the WindEEE Dome, Western University, Canada. Assuming a velocity gust factor of 1.57 the ratio between the loads obtained from WindEEE and the ones based on ASCE 7-22 are less than 1.0 for EF2 and EF3-rated tornadoes. For EF1-rated tornadoes, the ratios are close to unity for the lateral forces with a maximum of 1.21, and for uplift forces, the values are higher than 1.0 with a maximum of 1.56. These results suggest the provisions are conservative for EF2 and EF3-rated tornadoes but insufficient for EF1-rated tornadoes. The choice of the value of the velocity gust factor can have a significant influence on the results and the value of 1.57 may not be conservative.

Keywords: Tornado-induced loads, low-rise buildings, ASCE/SEI 7-22.

1. INTRODUCTION

Even though tornadoes are a devastating force that generates extensive damage and loss across North America and other parts of the world, they have been historically considered an extreme event with a too low probability of occurrence to be considered for the design of light-frame structures. This consideration has changed during the last two decades. Today, it is known that most of the damage inflicted by tornadoes is caused by winds in the EF0-EF3 range. The intensity of winds in this range is comparable to hurricane winds for which design provisions have been available for decades (Prevatt et al., 2011). In addition, van de Lindt et al. (2013) observed from forensic analysis of the Tuscaloosa tornado in 2011 that for this range of winds it is possible to implement measures to mitigate damage. They proposed a dual-objective-based approach to design for tornadoes that considers reducing damage for tornadoes rated EF3 or lower and minimizing the loss of life for EF4-EF5 tornadoes.

The recent construction of several tornado-like vortex (TLV) generators big enough to conduct wind engineering experiments at relatively high Reynolds numbers (Hangan et al., 2017), coupled with the availability of Doppler radar measurements of actual events (Refan et al., 2017), has created the conditions to advance the characterization of the loads induced by tornadoes on low-rise buildings using properly scaled physical simulation (Refan et al., 2014).

Although much research has been done to determine tornado-induced loads, there is still a large discrepancy in the reported values, with ratios of tornado-induced to straight-line-induced pressure coefficients ranging from 5 to 1 (Jischke and Light, 1983; Bienkiewicz and Dudhia, 1993; Roueche et al., 2020).

ASCE/SEI 7-16 was the first standard to include guidelines for design under tornado-induced loads and the recent edition ASCE/SEI 7-22 is the first to have provisions. Although the provisions in ASCE 7-22 for tornadoes are for buildings in Risk Categories III and IV located in tornado-prone areas, they present a good opportunity to analyze their suitability for the design of residential buildings.

This article shows a comparison of the loads induced by several translating TLVs on 8 low-rise, residential building model houses measured at the WindEEE Dome with the provisions given in ASCE/SEI 7-22 for tornadoes. The simulations replicate a tornado event that occurred in the Ottawa-Gatineau region in 2018.

2. EXPERIMENTAL SETUP

The physical simulations that are presented in this research were performed at the Wind Engineering, Energy and Environment (WindEEE) Dome at Western University, Canada. This facility is capable of reproducing tornadoes, downbursts, gusts and currents, shear flows, and boundary layer flow at high Reynolds numbers. For details, the reader is referred to Hangan et al., (2017).

This research analyzes the interaction of three different translating TLVs and 8 model houses in a community. The flow characteristics of these TLVs were investigated by Refan and Hangan (2018). The reader is referred to the cited article for details on the flow characteristics. The swirl ratios for the three TLVs are S=0.48, 0.76, and 1.03 which corresponds to EF1, EF2, and EF3 tornadoes.

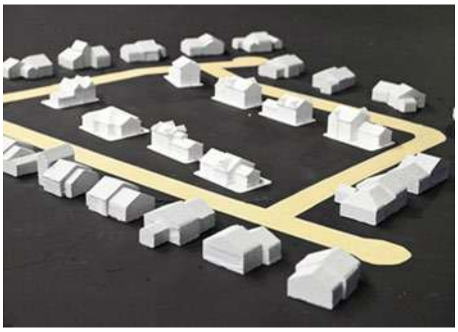

Figure 1. Model

The model houses are part of the community of Dunrobin, Ontario, that was hit by an EF3-rated tornado on September 21, 2018. The model consists of 8 instrumented residential low-rise buildings with 22 non-instrumented surrounding buildings at a 1:150 geometric scale (see Figure 1). The total number of pressure taps was 1152 distributed in the 8 instrumented houses and the ground.

The model was tested in 14 different configurations with translating TLVs. Two translating directions were selected: (1) 80º from North clockwise, which represents the actual path of the 2018 Dunrobin tornado, and (2) 45º which is the most probable orientation for strong tornadoes (Romanic et al., 2016), with 3 different offsets for each direction.

The translation speed was fixed at 1.3 m/s for all translating TLVs. The case with EF3-rated TLV and zero offsets was repeated 10 times. All other translating TLVs were repeated 5 times. 2018.

3. RESULTS

Here, the ratios of the overall force components on a house-fixed coordinate system on each house calculated using ASCE/SEI 7-22 to the ones obtained from the wind tunnel measurements are presented. Fx is the force along the ridge, Fy is transversal to the ridge and Fz is vertical.

Table 1. Ratios of ASCE-SEI 7-22 provisions to wind tunnel calculated force

	EF1			EF2			EF3		
House	Fx	Fy	Fz	Fx	Fy	Fz	Fx	Fy	Fz
1	0.80	0.85	1.13	0.55	0.67	0.70	0.47	0.48	0.51
2	0.98	0.90	1.56	0.61	0.55	0.99	0.52	0.41	0.69
3	0.76	0.70	1.03	0.60	0.54	0.83	0.44	0.34	0.50
4	0.89	0.96	1.13	0.81	0.63	0.99	0.63	0.44	0.60
5	1.21	1.03	1.13	0.80	0.70	0.82	0.72	0.56	0.53
6	0.89	0.91	1.30	0.68	0.62	0.83	0.53	0.42	0.60
7	1.01	1.15	1.12	0.73	0.66	0.86	0.57	0.53	0.61
8	0.87	0.94	1.10	0.56	0.57	0.75	0.47	0.43	0.54

In this article, we present only the ratios for the sealed building case without taking into consideration any modeling of the internal pressures.

The pressures on a building surface can be calculated from ASCE/SEI 7-22 using the following:

$$p_T = qG_T K_{dT} K_{vT} C_p - q_i (GC_{piT})\ (\mathrm{N/m^2}) \tag{1}$$

Where G_T=0.85 is the tornado gust-effect factor, K_{dT}=0.80 is the directionality factor, K_{vT}=1.1 is the tornado pressure coefficient adjustment factor for vertical winds, Cp is the external pressure coefficient, GC_{piT}=+1.0 is the internal pressure coefficient and

$$q_{hT} = 0.613 K_e V_T^2 (N/m^2); V_T \text{ in } m/s \tag{2}$$

With $q=q_i=q_{hT}$ in this case and K_e=1.0.

The maximum forces from the wind tunnel simulations are calculated by fitting a Gumbel distribution using Lieblein's BLUE method to the set of maximum forces in each repetition and finding the 78% percentile. Then, they are transformed to full scale using dimensional analysis.

Forces are calculated by a piecewise integration of the forces corresponding to each pressure tap with a tributary area assigned using Voronoi diagrams on each planar face.

The full-scale forces (F_{FS}) can be calculated, as mentioned before, from dimensional analysis, as:

$$F_{FS} = \frac{F_M}{{\lambda_v}^2 \lambda_L^2} \tag{3}$$

Where F_M is the model force and λ_v and λ_L are the velocity and length scales.

It can be shown that the ratios (r) of the forces calculated using ASCE/SEI 7-22 and the wind tunnel do not depend on the design velocity, but they are dependent on the velocity gust factor (G) as:

$$r \propto G^{-2} \tag{4}$$

The velocity gust factor G is the ratio of the 3-second gust wind speed to the mean wind speed and is dependent on the duration of the tornado. In the reported values in Table 2, a gust factor G=1.57 was used in line with the value used in Wang and Cao (2021) and similar to what was used by Haan et al. (2010), but note that lower values could be used which would result in higher ratios.

4. CONCLUSIONS

The ratios using a gust factor of 1.57 are less than 1.0 for EF2 and EF3-rated tornadoes. For EF1-rated tornadoes, the ratios are close to unity for the lateral forces with a maximum of 1.21 and for uplift forces the values are higher than 1.0 with a maximum of 1.56. These results suggest the provisions are conservative for EF2 and EF3-rated tornadoes but insufficient for EF-1 rated tornadoes. The choice of the value of the gust factor can have significant influence in the results. The results reported for a value 1.57 may not be conservative with significant increases in ratios if a lower gust factor is used. This subject needs to be analyzed in depth.

ACKNOWLEDGEMENTS
This work was supported by Mitacs through the Mitacs Accelerate program. The work by Gabriel Narancio was partially supported by ANII-CALDO.

REFERENCES

Bienkiewicz, B, Dudhia, P (1993). Physical modeling of tornado-like vortex and tornado effects on building loading. In Seventh US Conf. on Wind Engineering, UCLA, CA, June (pp. 27-30).

Haan Jr, FL, Balaramudu, VK, Sarkar, PP (2010). Tornado-induced wind loads on a low-rise building. Journal of structural engineering, 136(1), 106-116.

Hangan, H, Refan M, Jubayer, C, Romanic, D, Parvu D, LoTufo, J, Costache A, (2017) Novel Techniques in Wind Engineering, Journal of Wind Engineering and Industrial Aerodynamics, 171: 12-33.

Jischke, MC, Light, BD (1983). Laboratory simulation of tornadic wind loads on a rectangular model structure. Journal of Wind Engineering and Industrial Aerodynamics, 13(1-3), 371-382.

Prevatt DO, van de Lindt JW, Back EW, Graettinger AJ, Pei S, Coulbourne W, Gupta R, James D, and Agdas D (2012). Making the case for improved structural design: Tornado outbreaks of 2011. Leadership and Management in Engineering, 12(4):254-270.

Refan, M, Hangan H, Wurman, J, Kosiba, K, (2017) Doppler radar-derived wind field of several tornadoes with application to engineering simulations, Engineering Structures, 148: 509-521.

Refan, M, Hangan, H, Wurman, J, (2014) Reproducing Tornadoes in Laboratory Using Proper Scaling, Journal of Wind Engineering and Industrial Aerodynamics, 135: 136-148.

Refan, M, Hangan, H (2018). Near surface experimental exploration of tornado vortices. Journal of Wind Engineering and Industrial Aerodynamics, 175, 120-135.

Romanic, D, Refan, M, Wu, CH, Michel, G (2016). Oklahoma tornado risk and variability: A statistical model. International journal of disaster risk reduction, 16, 19-32.

Roueche, DB, Prevatt, DO, Haan, FL (2020). Tornado-induced and straight-line wind loads on a low-rise building with consideration of internal pressure. Frontiers in built environment, 6, 18.

Wang, J, & Cao, S (2021). Characteristics of tornado wind loads and examinations of tornado wind load provisions in ASCE 7–16. Engineering Structures, 241, 112451.

van de Lindt, JW, Pei, S, Dao, T, Graettinger, A, Prevatt, DO, Gupta, R, Coulbourne, W (2013). Dual-objective-based tornado design philosophy. Journal of Structural Engineering, 139(2), 251-263.

On the intrinsic approximation of the gust-effect technique applied to offshore wind turbine towers during installation

Alessio Torrielli [1,2], Alessandro Giusti [3]

[1] *Siemens Gamesa Renewable Energy A/S, Brande, Denmark,* *alessio.torrielli.ext@siemensgamesa.com*
[2] *R&D Engineering A/S, Hinnerup, Denmark,* *alt@rdas.dk*
[3] *Siemens Gamesa Renewable Energy A/S, Brande, Denmark,* *alessandro.giusti@siemensgamesa.com*

SUMMARY
Gust buffeting loads of tower-like structures are typically calculated through the gust-effect factor technique, which implicitly assumes that the probability density function of the maximum effect is sharp enough to be confused with its mean value. An underestimate of the probability of exceeding the resulting load may result if such a condition is not met. This paper assesses the probability to exceed the wind loads used for the design of a temporary foundation supporting offshore wind turbine towers during pre-assembly activities. The role played by different sources of statistical and epistemic uncertainty involved in the calculation of the gust-buffeting loads is investigated through a case study.

Keywords: gust-effect technique, statistical and epistemic uncertainty, reliability analysis

1. INTRODUCTION

ASCE 7-05 standard suggests a peculiar methodology for the determination of the design wind loads in the hurricane-prone region based on extreme values statistical analysis. The load amplification factor, traditionally applied to the characteristic actions in the framework of a semi-probabilistic design approach, is replaced by a basic design wind speed associated with a larger return period. Such an approach is appealing because it translates the safety level provided by load factor into a risk-equivalent wind speed, having a straighter probabilistic meaning given by the return period. However, this approach implicitly assumes that the full uncertainty of the wind loading, compensated by the load factor, stands in the stochastic uncertainty of the basic wind speed used for the design while no uncertainty is recognized neither to the calculation model nor to other key parameters.

The authors have recently faced the problem to assess the reliability of a temporary foundation supporting towers of wind turbine generators (WTG) subjected to the gust buffeting. The foundation was originally designed for 6-month usage period, which has been extended to 3 years because of a delayed installation process. This case study pushed the authors to reflect on the ASCE 7-05 approach, to clarify the role of the statistical uncertainty embedded in the calculation of the gust buffeting load as well as the role of the epistemic uncertainty of structural damping and aerodynamic force coefficients. As far as the authors know, all well-recognized standards for the design of tower-like structures against gust buffeting loads rely on the gust-effect factor (GEF). The GEF is defined as the ratio between the mean maximum value of a given structural effect (over 10-60 minutes) and the corresponding mean value (Piccardo and Solari, 2001). It is noteworthy that neglecting the true variability of the maximum effect around its mean value is correct only if the probability density function (PDF) is sufficiently sharp (Davenport, 1967). Otherwise, such an approximation may lead to an underestimate of the risk.

2. THE STRUCTURE

The WTG tower consists of a steel shell of about 6 m base-diameter and 90 m height, tapered at the top. The tower is supported by a gravity-based foundation. The 10-year return period basic wind speed of V_b=26.3 m/s is used for the calculation of the characteristic base bending moment (BBM) following the GEF technique; the design BBM of M_{dsg}= 49.1 MNm results by using a 1.6 load factor.

3. PROBABILITY OF FAILURE

The probability to exceed M_{dsg} over 3 years (P_{ex}) is assessed through two different approaches: simplified and probabilistic. The simplified approach considers the mean wind speed as the only probabilistic input for the calculation of M_{dsg}, whereas the dispersion of the 10-minute maximum BBM $M_{b.max}$ around its mean value (Pagnini, 2010) is neglected in line with the GEF technique. Under such a condition, P_{ex} coincides with the probability of the 3-year maximum wind speed to exceed the design value of $V_{dsg} = \sqrt{1.6} \cdot V_b$ = 33.3 m/s i.e., $P_{ex.1}$ = 2.74%. By contrast, the probabilistic approach considers as random variables the 3-year maximum wind speed, damping ratio associated with the first sway mode (Ξ) and aerodynamic moment coefficient (C_M), besides the dispersion of $M_{b.max}$ around its mean value.

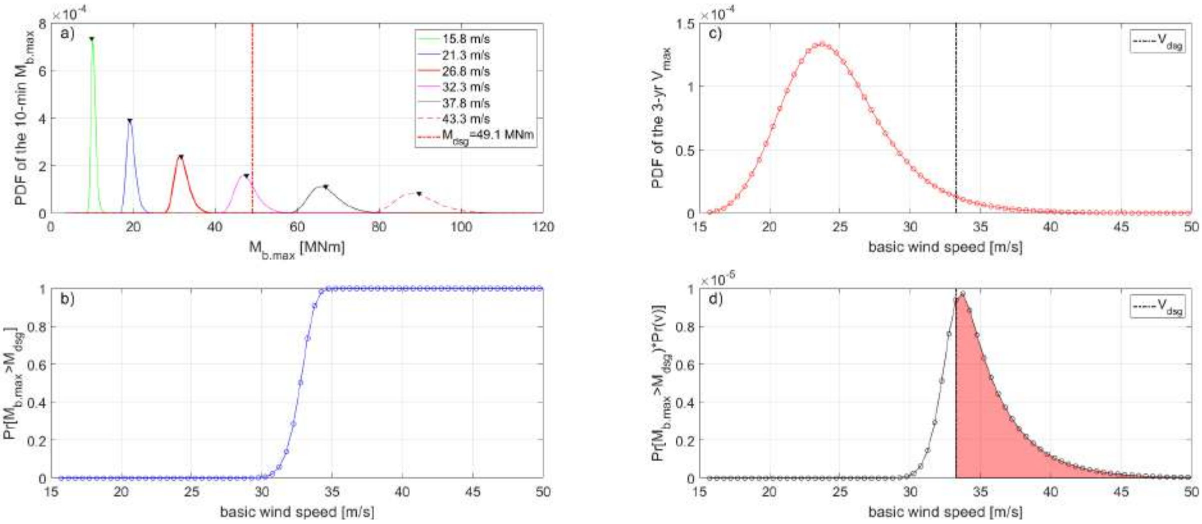

Figure 1. Breakdown of $P_{ex.2a}$ into velocity-bin contributions ($C_{M\text{-}2T}$ = 0.95, ξ_{str} = 1.0%)

The probabilistic approach is applied in two variations to clarify the role of the different sources of uncertainty: a) the statistical uncertainty of $M_{b.max}$ is considered, while Ξ and C_M are treated as deterministic; b) the epistemic uncertainty of Ξ and C_M is also included. Figure 1 shows the contributions related to given velocity-bins resulting in $P_{ex.2a}$ = 3.52%. The shape of PDF of $M_{b.max}$ changes with the velocity, and curves are flatter and wider as the wind speed increases, meaning that the approximation of the PDF with its mean value becomes less accurate for larger wind speeds. On the one hand, the probability that $M_{b.max}$ exceeds M_{dsg} increases with the velocity (Figure 1b); on the other hand the frequency of large wind speeds is small (Figure 1c). The trade-off of these two factors gives the contributions in Figure 1d. $P_{ex.2a}$ is larger than $P_{ex.1}$ because of the contributions of the velocity-bins whose mean $M_{b.max}$ is lower than M_{dsg} (see magenta line in Figure 1a). This is proved by cumulating only contributions in Figure 1d associated with velocity-bins whose mean $M_{b.max}$ is larger than M_{dsg}, resulting in a probability of failure equal to 2.82%. The probability of failure slightly reduces to $P_{ex.2b}$ = 3.15% when the epistemic uncertainty of Ξ and C_M is considered.

4. CONCLUSIONS AND PERSPECTIVES

The probability to exceed the wind load due to gust buffeting at the base of a WTG tower is calculated through the GEF technique. Such a risk is widely underestimated if the variability of the $M_{b.max}$ around its mean value is neglected, whereas the uncertainty of damping and aerodynamic coefficients reduces such an underestimate. Further investigations are needed to assess in which extent the outcome of the present case study applies to towers of different WTG platforms and potentially to tower-type structures in general, with a focus on the parameters controlling the narrowness of the PDF of $M_{b.max}$.

REFERENCES

ASCE, 2005. ASCE 7-05, Minimum design loads for buildings and other structures. American Society of Civil Engineers, Reston, VA, USA.

Davenport, A., 1967. Gust loading factors. Journal of the Structural Division, ASCE 93(3), 11-34.

Pagnini, L., 2010. Reliability analysis of wind-excited structures. Journal of Wind Engineering and Industrial Aerodynamics 98(1), 1-9.

Piccardo, G., Solari, G., 2002. 3-D gust effect factor for slender vertical structures, Probabilistic Engineering Mechanics 17, 143-155.

Effects of flow accelerations typical of thunderstorm outflows on the vortex-shedding from a square cylinder

Stefano Brusco [1], Guido Buresti [2], Yuan-Lung Lo [3], Giuseppe Piccardo [4]

[1] *University of Genoa,Genoa, Italy, stefano.brusco@edu.unige.it*
[2] *University of Genoa, Genoa, Italy, guidoburesti@gmail.com*
[3] *National Taipei University of Technology, Taipei, Taiwan, yllo@mail.ntut.edu.tw*
[4] *University of Genoa, Genoa, Italy, giuseppe.piccardo@unige.it*

SUMMARY
Accelerating flows acting on a sectional model of a sharp-edged square cylinder are reproduced through the action of a multiple-fan wind tunnel. The model is equipped with 94 pressure sensors, while the wind flow around the body is characterized through three Pitot-static tubes. The accelerations generated by the 72 individually controlled fans of the facility are compatible with those typical of thunderstorm outflows. Particular attention is devoted to the acquisition of signals associated with vortex-shedding, for which tailored time-frequency analyses, based on the continuous wavelet and Hilbert transforms, are proposed. Time intervals in which the shedding frequency is constant, separated by discontinuities, are found during the transients. The number and magnitude of such discontinuities seem to be connected with the flow acceleration. The appearance of constant-frequency time cells is not strictly repetitive; moreover, the Strouhal number is seen to decrease for higher levels of acceleration.

Keywords: Transient aerodynamics; vortex-shedding in accelerating flows; constant-frequency time cells

1. INTRODUCTION

The main source of fluctuating cross-wind forces acting on slender structures is the alternate shedding of vortices in their wakes (e.g., Solari, 1985). Research on this phenomenon, which is typical of bluff bodies, has been carried out since the second part of the last century and the description of its main features has been the subject of several reviews (e.g., Buresti 1998). An adequate level of knowledge of bluff-body aerodynamics allowed the definition of sets of pressure and force coefficients which were estimated for a large range of design configurations. These were essential for the design of structures, since they could be treated as constant quantities and combined with the knowledge of the dynamic pressure in order to derive the full-scale aerodynamic loading. This procedure is possible by invoking the strip and quasi-steady theory (Kawai, 1983), whose applicability is well-consolidated when studying effects on structures induced by synoptic winds, which have indeed steady characteristics in both wind speed and direction. On the other hand, its application might be subverted by the transient nature of thunderstorm outflows. These are non-stationary phenomena occurring at the mesoscale, whose duration may be limited and whose flow direction might exhibit remarkable irregularities (e.g., Solari, 2019). A transient condition is expected to affect the vortex-shedding development, as well as the pressure and force coefficients, which depend on the regularity and configuration of the shedding of the vortices (Buresti, 2012). However, the available literature on transient aerodynamics is often not relevant for thunderstorm outflows. Indeed, the pioneering work proposed by Sarpkaya (1963, 1966) was conducted for accelerations which are too high to be considered representative of thunderstorm outflows.

The present work, collocated within the framework of the ERC Project THUNDERR, proposes the results of a wind tunnel test campaign carried out at the multiple-fan wind tunnel of the Tamkang University (TKU-MFWT), in Taipei. A sectional model of a sharp-edged square cylinder has been subjected to the action of accelerating flows, whose magnitude was calibrated to be consistent with full-scale thunderstorm outflows (Brusco et al., 2022). The analyses herein reported focus on the temporal variation of the shedding frequency during the transients, which is studied through tailored time-frequency analyses.

2. WIND TUNNEL TEST CAMPAIGN

The TKU-MFWT is equipped with 72 individually controlled fans, arranged in a 12 x 6 matrix. The test chamber is 1.32 m x 1.32 m in cross section and no roughness elements are used to develop the velocity profile, so that all the internal surfaces are smooth. The contraction rate is 2:1 and is obtained by reducing the vertical dimension only. The total length of the facility is 10.43 m and the contraction beyond the wall of fans covers 4.39 m of this dimension. The maximum speed is about 16 m/s. The average turbulence intensity in the TKU-MFWT has been estimated as approximately 2.5 %, being higher for low levels of wind velocity and lower for higher wind velocities. The sectional wind tunnel model has a side of 6 cm, spans the entire width of the test section, and is equipped with 94 pressure taps. In particular, 46 of them are installed in correspondence of its mid-span section. Two circular end-plates, whose diameter is 40 cm, are installed 60 cm apart, leading the model to a slender ratio equal to 10.

The wind tunnel test campaign has been articulated in two different phases. The first one regarded the simulation of steady flows, employing the multiple-fan wind tunnel as a traditional facility. As far as the simulation of unsteady flows is concerned, a total of 13 different conditions have been simulated, each one characterized by a number of repeats equal or higher than 30. The baseline test UF1 (UF = unsteady flow) has been reproduced for a total of 90 repeats, and the signal of the reference velocity of one of them is presented in Fig. 1 (in black). In the following, preliminary results from a selected repeat of UF1 will be analyzed. The other 12 unsteady conditions have been reproduced by setting different values of the flow parameters, such as the flow acceleration, initial and target wind velocity and the time length between the ramp-up and the ramp-down (see Brusco, 2021 for further details). Amongst these, another case of interest is represented by test UF6 (Fig. 1, in grey), which follows the same path as UF1, but with a lower flow acceleration.

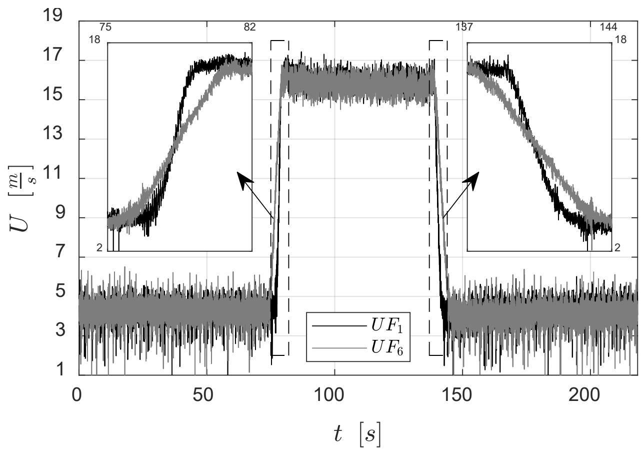

Figure 1. Comparison between the freestream velocity time histories of single repeats of UF_1 and UF_6.

Great attention is devoted to the non-dimensional coefficient linked with vortex-shedding in transient conditions, $c_{\Delta P_L}$, which is connected with the pressure difference between upper and lower model surfaces. Fig. 2 shows one of the relevant ramp-up time-histories.

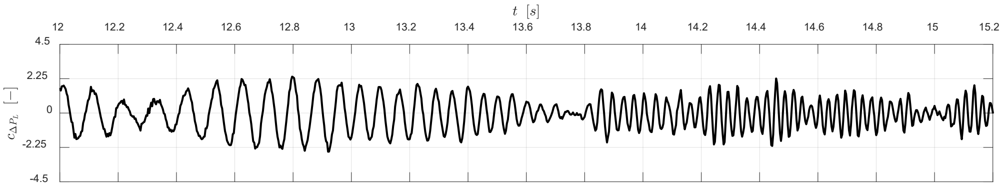

Figure 2. Time-history of $c_{\Delta P_L}$ from one repeat of UF1, focusing on the ramp-up.

From a visual inspection of the signal, the variation of the shedding frequency evidently appears not to be always regular. The passage from one condition to another seems to occur either with a regular pattern or through phases in which the frequency is quite constant, interspersed with abrupt changes. These are characterized by a sudden decrease of the signal amplitude and correspond to a local violation of the Strouhal law, so that the shedding frequency does not vary with the same trend as the incoming velocity. The time-histories acquired in the ramp-down case point out the same outcome. Inspired by these initial remarks, time-frequency analyses based on the continuous wavelet and Hilbert transforms have been carried out, discussing the suitability of the relevant parameters.

3. TIME-FREQUENCY ANALYSES AND PRELIMINARY RESULTS

As for the continuous wavelet transform, the complex Morlet wavelet is employed, since it provides an excellent compromise between time and frequency resolution. The crucial parameter to be set is the central frequency ω_0, whose increase improves the frequency resolution, whereas its reduction produces an enhancement of the temporal one. Therefore, different cases are considered and analyses are carried out by assuming ω_0 equal to 2π, 4π and 6π. The relevant energy maps are treated to extract the corresponding ridges, which are the curves that follow the time-variation of the instantaneous dominating frequency of the signal. Figures 3a and 3b report some results obtained from such time-frequency analyses applied to the time-history of the signal $c_{\Delta P_L}$. In particular, Fig. 3a displays the corresponding wavelet energy map, evaluated by adopting ω_0 equal to 6π, on which the white line represents the ridge. Further, Fig. 3b shows the time-histories of the ridges extracted from the different energy maps evaluated with three values of ω_0. The dash-dotted line provides the theoretical variation of the frequency following the Strouhal frequency-velocity law. Finally, the black dots indicate the estimates of the instantaneous frequency obtained from the temporal spacing between the maxima. The entire set of techniques shows a satisfactory level of similarity with the theoretical curve for low levels of acceleration, whereas time intervals in which the frequency remains constant (denoted as constant-frequency time cells) are observed when the highest level of flow acceleration are achieved. The passage from one cell to another occurs with discontinuities, which become even more evident by studying the time-varying Strouhal number, which points out the violation of the Strouhal law. The conclusion that may be drawn from the analysis of these results is that in presence of an accelerating flow the vortex-shedding frequency does not always follow linearly the variation of the wind speed. Furthermore, from a careful analysis of all the repeats and conditions considered in the present campaign, it is possible to observe that the number of constant-frequency cells, as well as the timing of their occurrence, are not completely regular. Finally, when analyzing the mean behavior of the variation of the shedding frequency, it is possible to observe that the shedding frequency at a certain instantaneous velocity appears to be similar to or definitely lower than its steady counterpart.

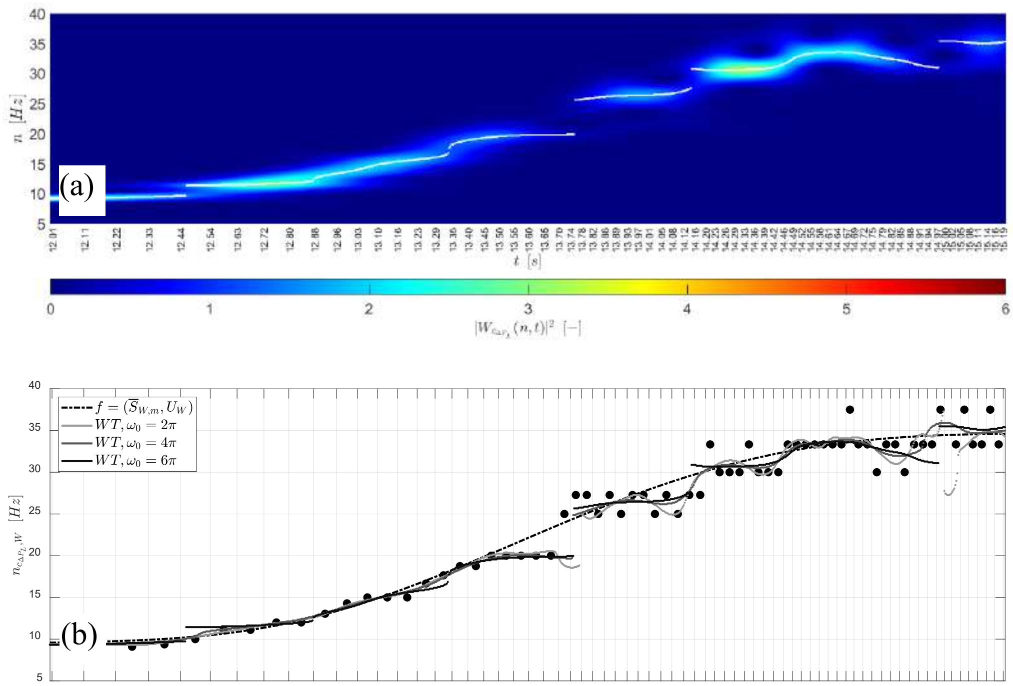

Figure 3. Time-frequency analyses carried out on the signal $c_{\Delta P_L}$ (Fig. 2): (a) $\left|W_{c_{\Delta P_L}}\right|^2$, $\omega_0 = 6\pi$, (b) variation of the shedding frequency in the transient.

ACKNOWLEDGEMENTS
This research has been financially supported by the European Research Council under the European Union's Horizon 2020 research and innovation program (grant agreement No. 741273) for the project THUNDERR. The authors desire to thankfully acknowledge Professor Giovanni Solari, Principal Investigator of the project THUNDERR and promoter of the collaboration between the University of Genoa and Tamkang University. His passion and genuine kindness will always be an example and inspiration for those who had the fortune to meet him.

REFERENCES
Brusco, S., 2021. Transient phenomena induced by thunderstorm outflows on slender structures. PhD Thesis, University of Genoa.
Brusco, S., Buresti, G. and Piccardo, G., 2022. Thunderstorm-induced means wind velocities and accelerations through the continuous wavelet transform. Journal of Wind Engineering and Industrial Aerodynamics, 221, 104886.
Buresti, G., 1998. Vortex shedding from bluff bodies. In: "Wind Effects on Buildings and Structures" (Riera, J. D., Davenport, A. G., Eds.), Balkema, Rotterdam, 61-95.
Buresti, G., 2012. Elements of Fluid Dynamics, Imperial College Press.
Kawai, H., 1983. Pressure fluctuations on square prisms – Applicability of strip and quasi-steady theories. Journal of Wind Engineering and Industrial Aerodynamics, 13, 197-208.
Sarpkaya, T., 1963. Lift, drag, and mass coefficients for a circular cylinder immersed in time dependent flow. Journal of Applied Mechanics, 30, 13-15.
Sarpkaya, T., 1966. Separated flow about lifting bodies and impulsive flow about cylinders. AIAA J4, 414-420.
Solari, G., 1985. Mathematical model to predict 3-D wind loading on buildings. Journal of Engineering Mechanics, 111(2), 254-276.
Solari, G., 2019. Wind Science and Engineering, Springer Nature Switzerland.

The new Laboratory of Environmental Aerodynamics of Cracow University of Technology

Aleksander Pistol [1], Łukasz Flaga [2], Renata Kłaput [2], Michał Polak [2], Agnieszka Kocoń [2], Fabio Rizzo [2], Andrzej Flaga [2]

[1]*Cracow University of Technology, Cracow, Poland, aleksander.pistol@pk.edu.pl*
[2]*Cracow University of Technology, Cracow, Poland*

SUMMARY
Laboratory of Environmental Aerodynamics is the new investment of Cracow University of Technology in Poland. Housing two large wind tunnels with air circulation around a vertical plane, each equipped with two separate working sections for different purposes, it will be one of the largest state-of-the-art wind tunnels in Europe. The laboratory building has two above-ground floors and one underground floor. The first wind tunnel TA.1 is dedicated to aerodynamic tests of buildings, bridges and other engineering structures, with elaborate turbulence generation possibilities, and wind turbines. The second wind tunnel TA.2, has the lower section dedicated for environmental tests, with the possibility of rain simulation and frost and thaw cycles in combination with the wind flow. Its upper section will be dedicated to artificial snow simulations and smoke visualizations. The project was started in 2017. The contract for co-financing was signed in July 2019 and the opening is planned for March 2023.

Keywords: wind tunnel, environmental aerodynamics, model experiments

1. INTRODUCTION

With the wind tunnel of the Wind Engineering Laboratory of Cracow University of Technology (wind tunnel details and schematics in Flaga et al, 2020) not being sufficient for all the experimental work being conducted or planned, both due to size limitations and busy schedule from commercial projects, grants and educational purposes, an idea was conceived to design and build a new, larger and more advanced facility. The project was started in 2017 and the opening is planned for March 2023. The state of the building, actual as of March 2022, can be seen in Fig. 1.

(a) (b)

Figure 1. Laboratory of Environmental Aerodynamics external view – work progress as of March 2022: North-East corner (a) South-West corner (b)

2. WIND TUNNEL TA.1

The TA.1 closed-circuit wind tunnel has two working sections. The lower section dimensions are 9.7 m in width and 2.3 m in height, with an 8 m diameter of a turning table. It is dedicated to aerodynamic tests of buildings, bridges and other engineering structures, with elaborate turbulence generation possibilities. Its upper section dimensions are 9.7 m in width and 3.37 m in height, with an 8 m diameter of a rotational table. It will be mostly used for tests of wind turbines and potential large-scale elements. The wind flow in this tunnel will be generated by 3 fans, each of them 2920 mm in diameter, located on the upper floor. The longitudinal cross-section of TA. 1 and TA.2 are shown in Fig. 2.

3. WIND TUNNEL TA.2

The TA.2 closed-circuit wind tunnel is a climatic/environmental wind tunnel with an infrastructure allowing for temperature adjustment in the range of -10° C to +25° C. It has two working sections. The lower section dimensions are 7.9 m in width and 4.05 m in height. The lower section is dedicated to environmental tests, with the possibility of rain simulation and frost and thaw cycles in combination with the wind flow. The upper section dimensions are 7.9 m in width and 4.15 m in height. This working section will be dedicated to artificial snow simulations and smoke visualizations. The sieve will be located on a special movable grate, enabling the simulation of precipitation and redistribution of artificial snow (Flaga et al, 2019; Flaga and Flaga, 2019). The wind flow in this tunnel will be generated by 6 fans in 2 rows, each of them 2115 mm in diameter, located on the upper floor.

(a) (b)

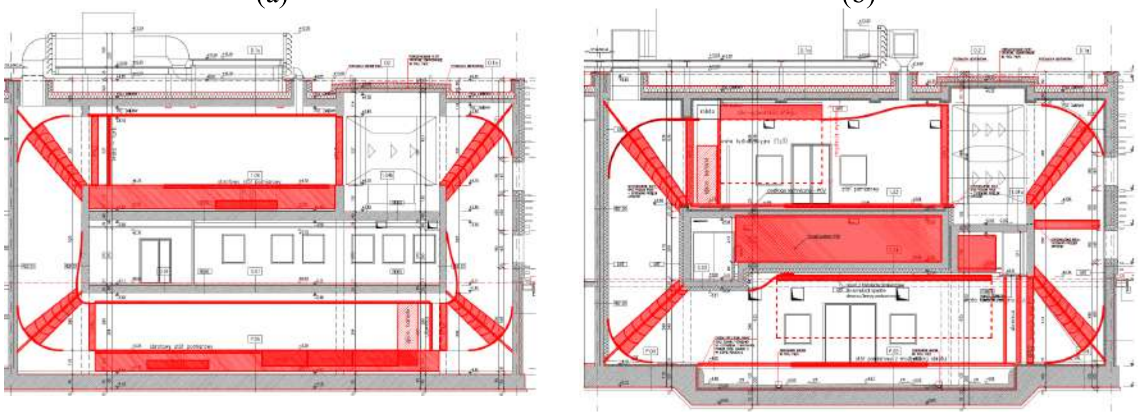

Figure 2. Longitudinal cross-sections with an indication of specialized internal equipment and technical infrastructure of the wind tunnels (a) TA.1, (b) TA.2 Wind tunnel TA.2

ACKNOWLEDGEMENTS

This project was financed from the regional operational program of the Marshal's Office – project number RPMP.01.01.00-12-0141/18; Operational Program of the Małopolska Region for 2014-2020; Priority Axis 1 – Knowledge economy; Action 1.1 – Research infrastructure for the science sector and with Cracow University of Technology financial contribution.

REFERENCES

Flaga A., Pistol A., Krajewski P., Flaga Ł., 2020. Aerodynamic and aeroelastic wind tunnel model tests of overhead power lines in triangular configuration under different icing conditions. Cold Regions Science and Technology 170 (2020): 102919. https://doi.org/10.1016/j.coldregions.2019.102919

Flaga A., Pistol A., Bosak G., Flaga Ł., 2019. Wind tunnel model tests of snow precipitation and redistribution on rooftops, terraces and in the vicinity of high-rise buildings. Archives of Civil and Mechanical Engineering 19 (4/2020), p. 1295-1303. DOI: 10.1016/J.ACME.2019.07.007

Flaga A., Flaga Ł., 2019. Wind tunnel tests and analysis of snow load distribution on three different large size stadium roofs. Cold Regions Science and Technology 160 (2019), p. 163-175. DOI: 10.1016/j.coldregions.2019.02.002

A comparison between two metaheuristic optimization algorithms for downburst simulation

Andi Xhelaj [1], Massimiliano Burlando [1]

[1]University of Genoa, Genoa, Italy, andi.xhelaj@edu.unige.it

SUMMARY
Strong downbursts can produce surface winds that can threaten civil structures. From the wind engineering prospective, modelling and simulating such severe wind is therefore extremely important for structural safety and design wind speed evaluation. This study deals with downburst wind field reconstruction by means of an analytical model, developed previously by the authors, coupled with two metaheuristic algorithms, the Differential Evolution (DE) and the Teaching Learning Based Optimization (TLBO), for the evaluation of downburst kinematic and geometrical parameters. The optimization problem minimizes the relative error between recorded and simulated wind speed and direction time histories. A comparison is made between the performance of the two algorithms for ten thunderstorm downburst events measured in northwestern Italy between October 2011 and October 2015. Both algorithms provide solutions which are coherent with the downburst parameter values presented in literature. TLBO outperforms DE since it has a faster convergence rate toward the optimal solution.

Keywords: Downburst analytical model, metaheuristic algorithms, single-objective optimization, differential evolution, teaching-learning-based optimization, downburst kinematic parameters.

1. INTRODUCTION

The study of intense thunderstorm-related downburst winds and their actions and effects on structures has been a dominant topic of the research in the wind engineering community over the last forty years (Letchford et al., 2002). Thunderstorms are non-stationary phenomena at the mesoscale, which occur in convective conditions with velocity profiles substantially different from those that are typical of the atmospheric boundary layer (ABL). Design wind velocities with mean return periods greater than 10-20 years are often associated with such phenomena (Solari, 2014). The great complexity of downburst outflow winds requires, from the wind engineering perspective, the formulation of analytical and empirical models able to capture the main features of this phenomenon.

The current study investigates the reconstruction/simulation of downburst outflow winds using an analytical model developed by the authors (Xhelaj et al., 2020) which has been coupled in the current work with two global metaheuristic optimization algorithms, namely the Differential Evolution (DE) (Storn and Price, 1997) and the Teaching-Learning-Based Optimization (TLBO) (Rao et al., 2011). The procedure consists in the creation of an optimization problem which minimizes the relative error between anemometric measurements of downburst outflows and simulated time histories of downburst wind speed and direction. The minimizing solution, relative to a specific downburst case, consists in a set of 11 model parameters which are needed to reconstruct the geometrical and kinematical features of the downburst under consideration. The purpose of the minimization is the determination of the most accurate model's parameters. The algorithms are compared through the simulation of ten selected full-scale downburst events that occurred in the port area of La Spezia, Genoa and Livorno between October 2011 and October 2015. These time series were collected during the European Projects "Wind and Ports" (Solari et al., 2012) and "Wind Port and Sea" (Repetto et al., 2017; 2018). Only the 30 s moving average time series of the wind speed and direction are considered for the purpose of this study.

2. SIMULATION RESULTS AND COMPARISON OF DIFFERENTIAL EVOLUTION AND TEACHING LEARNING BASED OPTIMIZATION ALGORITHMS

The application of the DE and TLBO algorithms to the downburst model of Xhelaj et al. (2020) is performed through the definition of an optimization problem which represents a single-objective, nonlinear and bound constrained problem. The lower and the upper bound of the 11 parameters which ultimately identify the search space ($\Omega \subseteq \mathbb{R}^{11}$), are set according to values present in literature. Table 1 reports a brief description of the model parameters and their range of variation.

Table 1. Model parameter description and their variability (lower and upper bound)

Model parameters	Range of variation
Maximum radial velocity $V_{r,max}$ (m/s)	$0\ to\ 40$
Downdraft radius R (m)	$200\ to\ 2000$
Dimensionless radial distance from downburst center at which $V_{r,max}$ occurs: $\rho = \frac{R_{max}}{R}$ $(-)$	$1.6\ to\ 2.6$
Period of linear intensification T_{max} (min)	$2\ to\ 15$
Duration of the downburst event T_{end} (min)	$15\ to\ 45$
x-component touchdown location (at $t = 0$) x_{C0} (m)	$-10000\ to\ 10000$
y-component touchdown location (at $t = 0$) y_{C0} (m)	$-10000\ to\ 10000$
Downburst translational velocity V_t (m/s)	$0\ to\ 40$
Downburst translational direction α_t (deg)	$0\ to\ 359.9$
Low-level ABL wind speed V_b (m/s)	$0\ to\ 40$
Low-level ABL wind direction α_b (deg)	$0\ to\ 359.9$

The comparison between the algorithms is based on the performance of each algorithm in finding a "good" optimal solution, given the incomplete information provided by the objective function. The latter is defined as the relative error between the observed and the simulated 30 s moving average mean wind speed and direction. Since DE and TLBO are stochastic algorithms, they are run independently 256 time in order to achieve a best solution. The number of iterations for both the algorithms is set to $T = 500$. The comparison metrics are based on the best, mean and standard deviation (std) objective function value of the 256 independent runs that both algorithms reach after 500 iterations. The best objective function value represents the lowest value reached by a specific algorithm; the mean and the std objective function value after 500 iterations gives respectively an overall behavior of the performance and of the robustness of each algorithm.

Fig. 1 describes the performance of both algorithms for one of the 10 downburst cases occurred in the port area of Livorno on 4 October 2015. This case highlights some important features of the behavior of the objective function which are also found in the other nine remaining cases (not shown). Fig.1 (a) displays the "performance chart" which describes the convergence of the objective function, for both algorithms, as the number of iterations increases. The chart contains the upper and lower envelope of all the 256 independent runs for both the algorithms. At the end of 500 iterations, the value of the upper envelope coincides with the worst objective function value (worst solution) while the lower envelope coincides with the best objective function value (best solution). In the performance chart is also traced (dashed line) for both the algorithms the mean convergence curve. The analysis of the performance chart shows an important feature, which can be crucial for reducing the computational time for the application of the analytical model. The lower envelope curve associated with TLBO have lower values than the DE counterpart, except when they get closer to the maximum number of iterations. The TLBO lower envelope curve reach almost stable values after 50 iterations, which indicates that TLBO converges at a much faster rate than DE (almost 1 order of magnitude faster). Similar trend for the rate of convergence is achieved by the other 9 downburst events. In general, for the ten downburst cases, the algorithm that has better convergence value both in the best and mean solution is the TLBO. On the other hand, DE has lower std than TLBO for all the 10 cases, which indicates that DE is more robust than TLBO.

Fig. 1 (b) shows, for the case of the Livorno downburst, the time history of the best simulation results (i.e., the one that produce the lowest objective function value), in terms of the moving average mean wind speed (top) and direction (bottom) for both the algorithms, compared to the recorded data. The figure shows in qualitative way the goodness of fit between simulation and full-scale measurements. Both algorithms give very similar best results, as expected according to their corresponding objective function value (see Fig. 1 (a)). This trend is confirmed for the other nine downburst events. The values of the 11 parameters which produces the best solution allows to reconstruct the geometrical and kinematical features of the downburst under consideration.

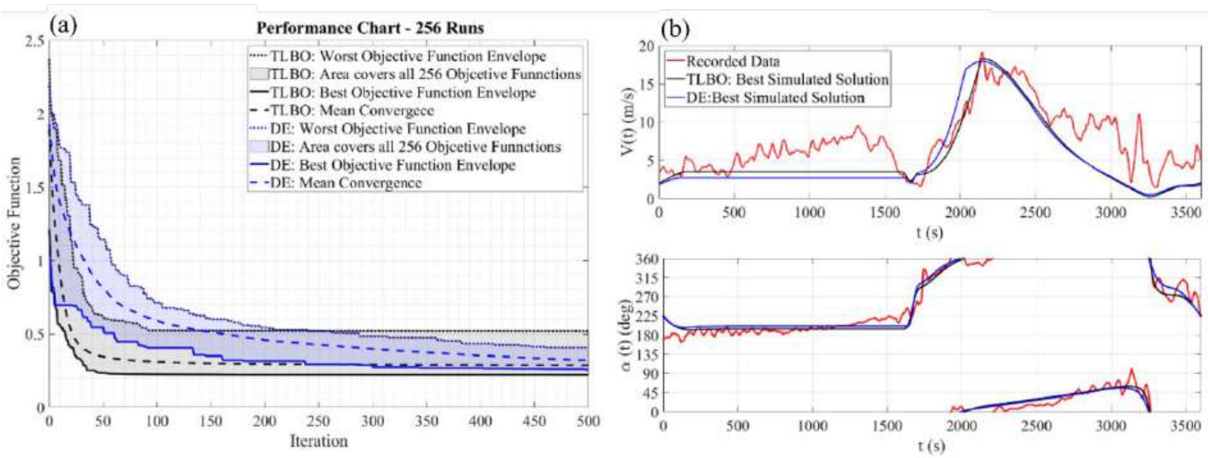

Figure 1. Performance chart (a) and simulations results (b) in terms of the moving average wind speed (top) and direction (bottom) for the downburst event occurred in Livorno on 4 October 2015.

Fig. 2 shows the reconstruction of the downburst wind field according to the best overall solution achieved with TLBO. The downburst outflow wind field is plotted at the height of the station/anemometer which in this case is equal to 20 m above the ground. The figure shows the downburst at its maximum intensity which is achieved 8.8 minutes after touch down. The downburst radius for this case is $R = 1500$ m, and the position at which maximum radial velocity is achieved is $R_{max} = 3550$ m. The downburst translation velocity is $V_t = 4.5$ m/s and the direction of translation is $\alpha_t = 300$ deg from the North (i.e., following the meteorological convention). The downburst reaches its maximum intensity at $T_{max} = 8.8$ minutes (see Fig. 2) and the whole phenomena last $T_{end} = 30$ minutes.

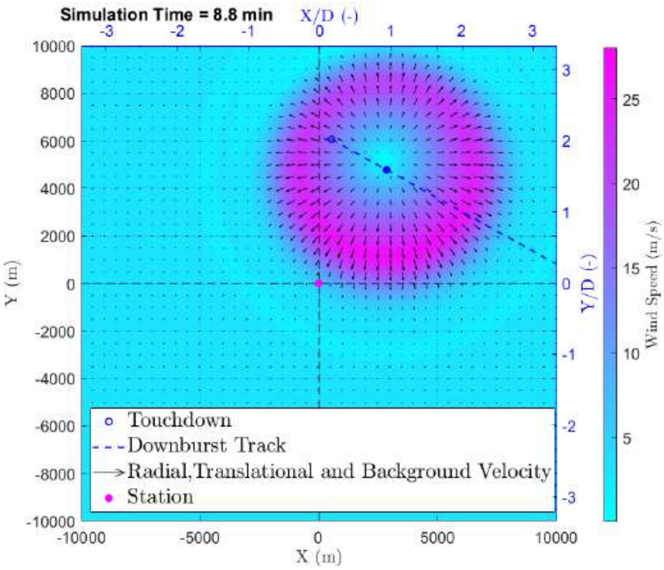

Figure 2 Wind field simulation of the downburst event occurred in Livorno on 4 October 2015. The bidimensional wind field is evaluated at the height of 20 meters above the ground. The simulation time referees at the instant of downburst maximum intensity. The letter D in the auxiliary axis referees to the downdraft diameter.

ACKNOWLEDGEMENTS
This research is funded by the European Research Council (ERC) under the European Union's Horizon 2020 research and innovation program (grant agreement No. 741273) for the project THUNDERR—Detection, simulation, modelling and loading of thunderstorm outflows to design wind-safer and cost-efficient structures—supported by an Advanced Grant 2016. The authors are deeply grateful to Prof. Giovanni Solari for his essential contributions to the conceptualization and supervision of this research.

REFERENCES
Letchford, C.W., Mans, C., Chay, M.T., 2002. Thunderstorms – their importance in wind engineering (a case for the next generation wind tunnel). J. Wind Eng. Ind. Aerodyn., 90, 1415-1433.
Rao, R.V., Savsani, V.J. and Vakharia, D.P., 2011. ''Teaching–learning-based optimization: a novel method for constrained mechanical design optimization problems'', Comput. Aided Des., 43(3), pp. 303–315.
Repetto, M.P., Burlando, M., Solari, G., De Gaetano, P., Pizzo, M., 2017. Integrated tools for improving the resilience of seaports under extreme wind events. Sustain Cities Soc 32: 277-294.
Repetto, M.P., Burlando, M., Solari, G., De Gaetano, P., Pizzo, M., Tizzi, M., 2018. A web-based GIS platform for the safe management and risk assessment of complex structural and infrastructural systems exposed to wind. Adv. Eng. Software, 117, 29-45.
Solari, G., 2014. Emerging issues and new frameworks for wind loading on structures in mixed climates. Wind Struct. 19, 295-320.
Solari, G., Repetto, M.P., Burlando M., De Gaetano P., Pizzo M., Tizzi M., Parodi M. 2012. The wind forecast for safety and management of port areas. J. Wind Eng. Ind. Aerodyn. 104-106, 266-277.
Storn, R., 1996. "On the usage of differential evolution for function optimization". Biennial Conference of the North American Fuzzy Information Processing Society (NAFIPS). pp. 519–523.
Xhelaj, A., Burlando, M., Solari, G., 2020. A general-purpose analytical model for reconstructing the thunderstorm outflows of travelling downburst immersed in ABL flows. J Wind Eng. Ind. Aerodyn. 207 104373.

Effect of surface roughness on large-scale downburst-like outflows

F. Canepa [1,2], M. Burlando [1], D. Romanic [2,3], H. Hangan [2,4]

[1]*Department of Civil, Chemical and Environmental Engineering, Polytechnic School, University of Genoa, Italy, federico.canepa@edu.unige.it – massimiliano.burlando@unige.it*
[2]*Wind Engineering, Energy and Environment (WindEEE) Research Institute, Western University, London, ON, Canada, fcanepa@uwo.ca – dromanic@uwo.ca – hmhangan@uwo.ca*
[3]*Department of Atmospheric and Oceanic Sciences, Faculty of Science, McGill University, Montreal, QC, Canada, djordje.romanic@mcgill.ca*
[4]*Faculty of Engineering and Applied Science, Ontario Tech University, Oshawa, ON, Canada, horia.hangan@ontariotechu.ca*

SUMMARY
Downbursts are negatively buoyant descending winds coming from thunderstorm clouds that spread on the horizontal upon impinging the ground. Surface roughness is known to govern the characteristics of synoptic-scale atmospheric boundary layer (ABL) winds. This study assesses whether the same holds for downburst outflows and to which degree. The downburst winds are experimentally reproduced as a large-scale impinging jet at the WindEEE Dome, at Western University (Canada). Three different surfaces were tested and the equivalent full-scale roughness length is quantified through a best-match approach between experimentally produced ABL winds and ESDU profiles. The highest roughness produces an outflow vertical profile with maximum velocity reduced in magnitude and occurring at higher elevation with respect to the smaller-roughness cases.

Keywords: Downburst, Surface roughness, Wind tunnel.

1. INTRODUCTION

Surface roughness length z_0 plays a key role in the characterization of magnitude and structure of the mean velocity and turbulence profiles in boundary layer winds. There is still little literature assessing the quantitative contribution of surface roughness to the developed downburst outflow that forms upon the downdraft impingement on the surface (Fujita, 1985). Xu and Hangan (2008) and Mason et al. (2009) analyzed the dependency of the maximum slowly-varying mean radial velocity $\bar{V}_{max}$ and its height of occurrence z_{max} with the surface roughness. They concordantly found that an increase of z_0 decreases the magnitude of $\bar{V}_{max}$ and raises its elevation z_{max} above the surface. The offset of the two quantities with respect to the smooth surface tests increases along the radial direction of outflow convection, as turbulence has more time to influence the developing wall jet flow that radially diverges onto the surface. The diverging radial trend of $\bar{V}_{max}$ and z_{max} continues until a balance is reached between inner layer, affected by the wall friction, and the sheared flow in the outer layer. The extent of such variations is strictly dependent to the Reynolds number, Re, as expected in case of rough wall boundary layer. Xu and Hangan (2008) observed that for $Re > 1.0 \times 10^6$ the flow can be considered as "fully turbulent" and be representative of full-scale downburst winds. In this flow regime, the roughness term governs the equation and the detachment of $\bar{V}_{max}$ and z_{max} from the smooth-surface reference case appears much more pronounced with respect to the laminar flow regime at low Re.

The impinging jet (IJ) experiments described in the current study were performed at the WindEEE Dome, which is currently the largest-scale wind simulator capable of reproducing extreme wind events, such as downburst winds, at "fully turbulent" regime.

2. EXPERIMENT SETUP

Figure 1 schematically shows the experimental setup top view. Three different surfaces were tested: (i) WindEEE Dome bare floor; (ii) Carpet; (iii) Artificial grass. Each surface was characterized with an equivalent full-scale roughness length z_0 that was assessed by running different ABL-like profiles inside the testing chamber and varying the length scale. A geometric scale of 1:200 was determined based on a qualitative matching of the mean velocity vertical profiles between physically reproduced and ESDU ABL profiles. The resulting equivalent roughness lengths were respectively z_0 = 0.007, 0.02 and 0.32 m. The downburst-like IJ was released from a nozzle of diameter D = 3.2 m located on the ceiling of the testing chamber. The nozzle-to-surface distance was H = 3.75 m. Two different intensities of IJs were used corresponding to centerline jet velocities W_{jet} at the nozzle outlet of 8.9 and 12.4 m s^{-1}. These are equivalent to $Re = W_{jet} D/\nu = 1.92 \times 10^6$ and 2.68×10^6, which allows to consider the flow in "fully turbulent" regime (Xu and Hangan, 2008).

A stiff mast with eleven Cobra probes was placed at 10 radial positions, r/D, in the range 0.2–2.0 with an increment of 0.2. The cobra probe heights above the WindEEE Dome floor were z = 0.040, 0.070, 0.100, 0.125, 0.150, 0.200, 0.300, 0.400, 0.500, 0.700 and 1.000 m.

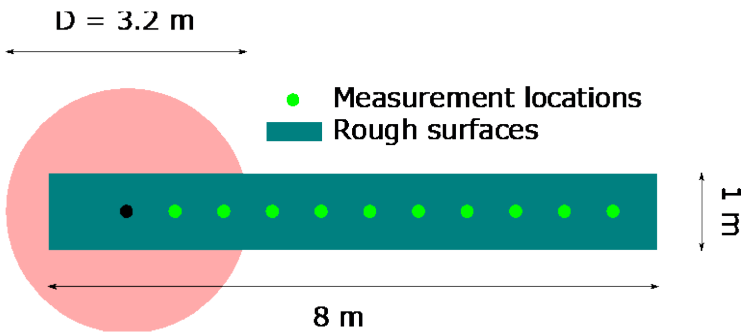

Figure 1. Experimental setup top view.

3. RESULTS

Figure 2 shows the vertical profiles of the slowly-varying mean horizontal velocity at the time of their maximum intensity. The dependency of $\bar{V}_{max}$ and z_{max} with z_0 strongly corroborates the observations above. Also, the increasing offset of the two quantities with the radial position is validated. The surface with the highest roughness length z_0 = 0.32 m produces a much larger shear in the velocity vertical profile. However, no significant variations are observed between the two smaller-roughness cases, i.e., z_0 = 0.007 and 0.02 m.

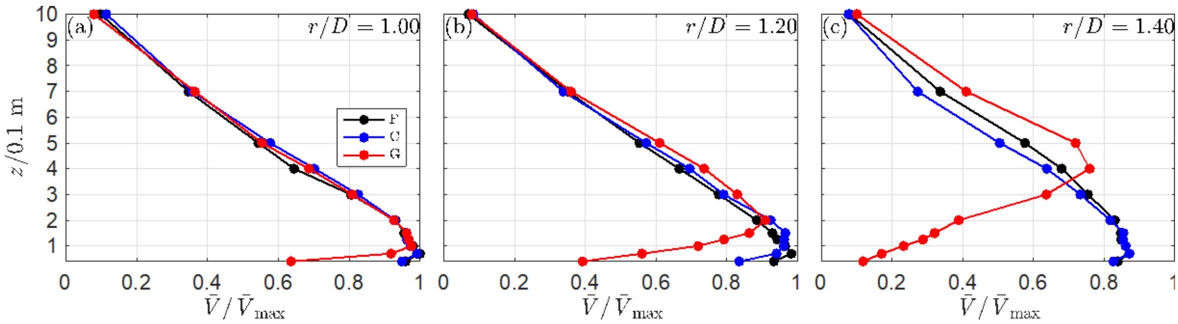

Figure 2. Slowly-varying mean wind speed $\bar{V}$ vertical profiles at the peak for Re = 2.68×10^6 and r/D = 1.0, 1.2, 1.4 (F – WindEEE bare floor, C – Carpet, G – Artificial grass). $\bar{V}$ is normalized by the maximum slowly-varying mean velocity among the three cases and three radial locations investigated.

ACKNOWLEDGEMENTS

The authors are deeply grateful to Prof. Giovanni Solari for his essential contributions to the conceptualization and supervision of this research. F. Canepa and M. Burlando acknowledge the support of the European Research Council (ERC) under the European Union's Horizon 2020 Research and Innovation Program (Grant agreement No. 741273) for the project THUNDERR – Detection, simulation, modelling and loading of thunderstorm outflows to design wind-safer and cost-efficient structures – awarded with an Advanced Grant 2016. F.Canepa, D.Romanic and H. Hangan acknowledge the support of the Canada Foundation for Innovation (CFI) WindEEE Dome Grant (No. X2281B38).

REFERENCES

Fujita, T.T., 1985. The Downburst - Microburst and Macroburst - Report of Projects NIMROD and JAWS.

Mason, M.S., Wood, G.S., Fletcher, D.F., 2009. Influence of tilt and surface roughness on the outflow wind field of an impinging jet. Wind Struct. 12, 179–204.

Xu, Z., Hangan, H., 2008. Scale, boundary and inlet condition effects on impinging jets. J. Wind Eng. Ind. Aerodyn. 96, 2383–2402. https://doi.org/10.1016/j.jweia.2008.04.002

City4CFD: an open-source framework for automatic reconstruction of simulation-ready 3D city models

I. Pađen, C. García-Sánchez, H. Ledoux

3D Geoinformation, Delft University of Technology, Delft, The Netherlands,
i.paden@tudelft.nl, c.garcia-sanchez@tudelft.nl, h.ledoux@tudelft.nl

SUMMARY
Body fitted mesh generators often have specific requirements on geometry quality to aid the mesh generation process: geometries should be watertight, without self-intersections and should not be non-manifold, i.e. not more than two faces should share an edge. The larger and more complex the geometry, the longer the necessary work, meaning this issue is amplified for urban flows where large areas of complex geometries are involved. The problem lies in 3D city models which are not made with urban flows in mind. To address this issue, we propose a framework that aims at automatically creating 3D urban environments tailored for urban flow simulations. The workflow not only reconstructs buildings and terrain surfaces, but also imprints such polygons such as roads, water, and vegetation which are later used to model the atmospheric boundary layer. Furthermore, the software can automatically define the zone of influence and domain dimensions based on best practice guidelines. Our approach reduces the geometry preparation time to the order of hours.

Keywords: 3D city modeling, automatic city reconstruction, geometry preparation, pre-processing, computational fluid dynamics

1. INTRODUCTION

In the Computational Fluid Dynamics (CFD) simulation workflow, the geometry preparation step is often regarded as a tedious, time-consuming task. This is why many practitioners consider it as one of the main bottlenecks in the whole simulation process (Slotnick et al. 2014). Geometry preparation generally consists of geometry creation, cleanup, and modification to meet the requirements of CFD software; these operations are usually done (semi) manually. The issue is that 3D city models are usually not constructed with CFD requirements in mind, since the 3D city modeling and the fluid dynamics fields are disconnected. To address this issue, we developed an open-source framework (which we called City4CFD) that automatizes geometry preparation for urban flow simulations. The workflow uses 2D datasets, such as cadastral data and topographic maps, and point cloud-based elevation data for input. Those datasets are often available in various parts of the world. It can also import existing geometries and combine them with other types of reconstruction. It was implemented in C++, using modern and state-of-the-art libraries. We tested our implementation on a real-world dataset in the Netherlands, and the results of the subsequent simulation will follow.

2. METHODOLOGY

We can define four main feature classes within the framework: buildings, terrain, surface layers, and boundaries. The input data that can be used are:

- 2D datasets such as cadastral data and topographic maps,
- Airborne point cloud-based data such as LiDAR and photogrammetry,
- Existing building geometries stored in Wavefront OBJ, STL, or CityJSON (standard for 3D city models) format.

Schematics of the workflow are shown in Figure 1.

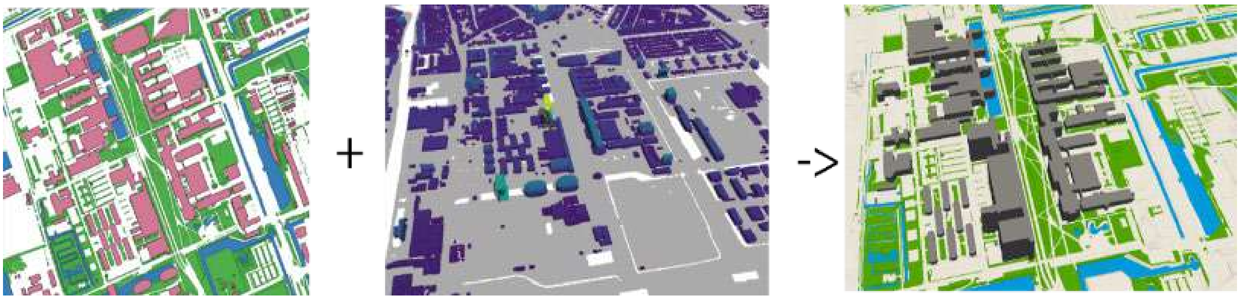

Figure 1 Schematic representation of the input data (2D polygons and a point cloud) and output geometry.

The digital terrain model of the domain is constructed as a triangulated irregular using points from the point cloud. The terrain is then smoothed using the Gaussian filter to avoid sharp edges created by the triangulation. Afterwards, different 2D surface layers, such as water, low vegetation regions, roads are imprinted into the terrain using the constrained Delaunay triangulation (CDT). The natural neighbor interpolation is used to calculate the height of layer points. Those layers have surface roughness attributes attached to them, later used to model the atmospheric boundary layer close to the ground. Parts of an entity, for example, surface layers in the terrain, with attached attributes (e.g. surface roughness) are referred to as semantics in 3D city modeling.

Building footprints are also added to the terrain using the CDT. Buildings within the influence region are extruded to a height depending on LiDAR points detected in the area encompassed by building footprints. Buildings reconstructed from footprint extrusion are defined as level-of-detail (LoD) 1.2 in 3D city modelling (Biljecki, Ledoux, and Stoter 2016). The height can be calculated as a certain percentile of all detected points, usually 50 (i.e. median), 70, or 90.

Decision on which buildings are being reconstructed (the zone of influence) can be made manually, but also automatically using the best practice guidelines (BPG's) (Liu et al. 2018). Finally, the framework constructs domain boundaries in two steps. First, it extrudes the outer rim as a flat surface to avoid perturbations close to inlet and outlet boundaries. Second, it makes side and top boundary faces, creating the closed volume ready for mesh generation. The domain size can also be defined with the BPG's, using the ones mentioned in (Blocken 2015).

The result of the framework is a valid geometry - it is watertight, without self-intersections or non-manifold edges. The output geometry can be exported in OBJ, STL or CityJSON file format.

In its current state, the framework lays groundwork for further developments. They include:

- Implementation of advanced building reconstruction algorithms that enable LoD1.3 (multi-segment height per footprint) and LoD2.2 (LoD1.3 plus roof surfaces) reconstruction,
- Footprint simplification to remove small edges that can cause problems in the meshing process,
- Tree modelling. Trees can be reconstructed at different LoDs and serve as detection zones for porosity modelling.

3. TEST CASE

We verified our implementation on a real-world dataset in Delfshaven area, Rotterdam, the Netherlands. We used freely available datasets to extract building footprints, polygons denoting water and vegetation area, and the airborne LiDAR-based point cloud. The geometry is round, with the total area of 1.25km^2, shown in Figure 2. The whole process that includes extracting the data, configuring reconstruction parameters and reconstructing took about two hours. The reconstruction by the algorithm took 120 seconds. We will verify the model by conducting a mesh sensitivity analysis, using *snappyHexMesh* for mesh generation, and *OpenFOAM* to run the simulation.

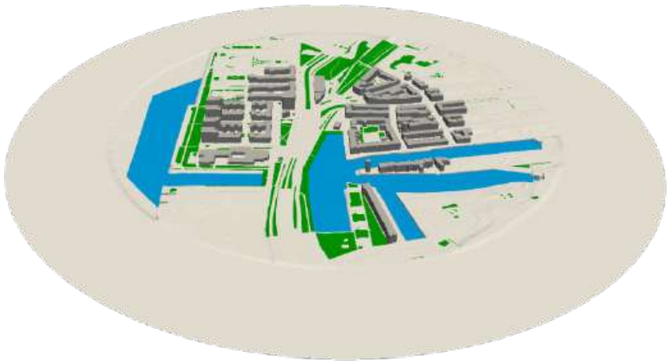

Figure 2 Reconstructed geometry of Delfshaven.

REFERENCES

Biljecki, Filip, Hugo Ledoux, and Jantien Stoter. 2016. "An Improved LOD Specification for 3D Building Models." *Computers , Environment and Urban Systems* 59: 25–37.

Blocken, Bert. 2015. "Computational Fluid Dynamics for Urban Physics: Importance, Scales, Possibilities, Limitations and Ten Tips and Tricks towards Accurate and Reliable Simulations." *Building and Environment*. https://doi.org/10.1016/j.buildenv.2015.02.015.

Liu, Sumei, Wuxuan Pan, Xingwang Zhao, Hao Zhang, Xionglei Cheng, Zhengwei Long, and Qingyan Chen. 2018. "Influence of Surrounding Buildings on Wind Flow around a Building Predicted by CFD Simulations." *Building and Environment* 140: 1–10. https://doi.org/10.1016/j.buildenv.2018.05.011.

Slotnick, J., A. Khodadoust, J. Alonso, and D. Darmofal. 2014. "CFD Vision 2030 Study: A Path to Revolutionary Computational Aerosciences." *NNASA/CR-2014-218178*.

Influence of stochastic load perturbations on the performance of a torsional-flutter wind harvester

Luca Caracoglia[1]

[1]*CEE Department, Northeastern University, Boston, MA 02115, USA, lucac@coe.neu.edu*

SUMMARY
Wind energy technologies are emerging as the need for clean energy resources has considerably increased in the last decade. Apart from horizontal-axis wind turbines, less efficient at the intermediate scales (or meso-scales) and for moderate wind speeds, a competitive alternative is necessary. This alternative is represented by simpler, smaller-size wind-based energy systems, activated by various aeroelastic phenomena. An ongoing investigation on the performance of an aeroelastic harvester, which can efficiently replace meso-scale wind turbines, is discussed. The apparatus exploits the torsional flutter of a streamlined "rigid" blade that rotates about a pre-set axis through a nonlinear torsional spring mechanism that activates post-critical behavior A stochastic model of the apparatus, including output power estimation, has been derived to evaluate relevance of uncertain wind loads, induced by imperfect characterization and simplified load assumptions. Studies are carried out to examine mean square stability.

Keywords: wind energy technology, aeroelastic harvester, torsional flutter, random loads, stochastic differential equations.

1. INTRODUCTION

Wind energy is rapidly emerging field because of the need for clean energy. Current technology advancements mainly focus on large-scale, horizontal-axis wind turbines that are less efficient at intermediate scales, i.e., the meso-scales. An interesting alternative is represented by simpler wind-based systems, triggered by various aeroelastic phenomena such as galloping (Abdelkefi et al., 2012), vortex induced vibration (Bernitsas et al., 2008) and coupled flutter (Pigolotti et al., 2017; Shimizu et al., 2008). Caracoglia (2018) proposed the use of torsional flutter of a blade-airfoil in Fig. 1(a), simpler than coupled flutter and other aeroelastic phenomena, to produce energy.

Building on previous studies, a new stochastic model has been recently derived to investigate effects of random perturbations (i.e., load variability) on the performance of the apparatus. Parametric perturbations are employed to describe aeroelastic load variability as a first attempt to replicate imperfect fluid-structure interaction. Examples are three-dimensional flow effects, neglected in standard aeroelastic theory and nonlinear coupling. Stochastic differential equations are employed to study mean square stability (and output power) of the apparatus, conditional on the value of the wind speed that triggers the instability. This study also preliminarily evaluates output energy and identifies physical properties controlling output power.

2. METHODOLOGY

A seven-state model, based on stochastic differential equations, is employed to study the mean square stability of the apparatus as a function of mean flow speed U. The physical states are the flapping or torsional rotation α and its first time derivative. In the reduced-order state-space model, aeroelastic torque is simulated using unsteady load formulation. The triggering mechanism depends on the following quantities: reduced frequency $k_\alpha = \omega_\alpha b/(U)$, damping ratio ζ_α generalized inertia ε and cubic stiffness κ. The main 1DOF dynamic equation is:

$$\psi_0 \frac{\mathrm{d}^2\alpha}{\mathrm{d}\tau^2} + \left(\frac{1.5\varepsilon\eta_{3D}}{k_\alpha} + 2\zeta_\alpha\right)\frac{\mathrm{d}\alpha}{\mathrm{d}\tau} + (\alpha + \kappa\alpha^3) = -\varepsilon\eta_{3D}k_\alpha^{-2}\begin{bmatrix}\Phi_0\left(\alpha + 1.5k_\alpha \dfrac{\mathrm{d}\alpha}{\mathrm{d}\tau}\right) \\ +1.5\left(\nu_{ae,1} + \nu_{ae,2}\right) + \mu_{ae,1} + \mu_{ae,2}\end{bmatrix} - \Psi\iota \quad (1)$$

with time $\tau = t\omega_\alpha$. The right-hand side of Eq. (1) shows, within square brackets, the indicial function formulation with $\nu_{ae,1}$, $\nu_{ae,2}$, $\mu_{ae,1}$ and $\mu_{ae,2}$ being aeroelastic states; the formulation is corrected for three-dimensional flow effects by quasi-static, simplified correction function η_{3D} that depends on aspect ratio AR= ℓ/b. [blade-airfoil's chord half-length b in Fig. 1(a) *vs.* depth of the apparatus ℓ]. Quantity Φ_0=0.5 denotes the unit-step Wagner function at time τ=0 while ψ_0=(1+9/8$\varepsilon\eta_{3D}$) accounts for non-circulatory flow load effects ("added mass"). On the left-hand side of the equation the nonlinear cubic stiffness term is proportional to $\kappa\alpha^3$, thus ensuring that the apparatus can efficiently work in a post-critical regime.

On the right-hand side of Eq. (1), $\iota(\tau)$ is a normalized output current. Coupling with an eddy-current power circuit is enforced by $\Psi=4b^2(\Phi_{\mathrm{e.m.c.}})^2/(\omega_\alpha I_{0\alpha} R_C)$, dimensionless electro-mechanical coupling coefficient. The quantity λ_{RL} is a generalized impedance of the power circuit with R_C resistance [ohms] and L_C inductance [Henries].

The Itô-type differential equation is derived from Eq. (1) in dimensionless time domain,

$$\mathrm{d}\mathbf{W}_{\mathrm{em}} = \mathbf{q}_{\mathrm{NL},\Delta}(\mathbf{W}_{\mathrm{em}})\mathrm{d}\tau + \sqrt{2\pi}\mathbf{Q}_{\mathrm{L},\Delta}\mathbf{W}_{\mathrm{em}}\,\mathrm{d}B(\tau) \quad (2)$$

where $\mathbf{W}_{\mathrm{em}}$ is the state vector, $\mathbf{q}_{\mathrm{NL},\Delta}$ is a nonlinear drift vector, $\mathbf{Q}_{\mathrm{L},\Delta}$ is a diffusion matrix, $B(\tau)$ is a scalar Wiener noise of dimensionless time. Turbulence is neglected in this formulation. Eq. (2) is solved numerically to get the second Moment Lyapunov Exponent $\Lambda_\Xi(2)$ that is used to study stability. The second-moment Lyapunov exponent (Xie, 2006) examines the propensity of a stochastic dynamic system to become unstable in terms of mean squares (variances and co-variances). This is scalar quantity that measures the rate of change of the "slow time dynamics" and evaluates the state as time tends to infinity; in other words, it can be assimilated to the total damping of the system at steady state after an initial, transitory stage.

A negative value of $\Lambda_\Xi(2)$ is needed for mean-square stability; therefore, $\Lambda_\Xi(2)>0$ yields an apparatus that produces energy. The stability limit varies as a function of wind speed. By varying U, both incipient and post-critical conditions are evaluated. Relevance is attributed to the output current $\iota = w_{\mathrm{em},7}$ that is extracted from the secondary system and, consequently the output power.

The $\Lambda_\Xi(2)$ quantity is found by solving Eq. (2) using a standard numerical integration scheme (Kloeden et al., 1994); $\Lambda_\Xi(2)$ is approximated as:

$$\Lambda_\Xi(2) \approx \log\left(\mathrm{E}\left[\|\Xi(\tau_j)\|^2\right]\right)/\tau_j \quad (3)$$

with $\Xi(\tau)$ being a suitable, dynamic sub-vector of $\mathbf{W}_{\mathrm{em}}$ and τ_j a discrete time, needed by step-by-step integration. The time index j is taken sufficiently large, i.e., tending to infinity.

3. RESULTS

Numerical solution of the stochastic Eq. (2) in a post-critical regime is studied. The main physical properties selected for energy conversion are: damping ratio ζ_α, electro-mechanical coupling coefficient Ψ, generalized impedance λ_{RL} and aspect ratio AR. The following reference quantities are set as deterministic: Ψ=0.01, λ_{RL}=0.75, AR={4,10} and κ=100 in dimensionless units. Three basic configurations are investigated:

- *Type 0* with $\omega_\alpha/2\pi$=0.25 Hz, b=0.25 m, $I_{0\alpha}/\ell$=20 kg-m^2/m;
- *Type 1* with $\omega_\alpha/2\pi$=0.20 Hz, b=0.25 m, $I_{0\alpha}/\ell$=40 kg-m^2/m;
- *Type 2* with $\omega_\alpha/2\pi$=0.10 Hz, b=0.50 m, $I_{0\alpha}/\ell$=300 kg-m^2/m.

Figure 1(b) shows an example of the numerical results for various apparatuses (Ty. 0,1,2) with AR=10; this AR value is used to simulate (negligible three-dimensional flow effects).

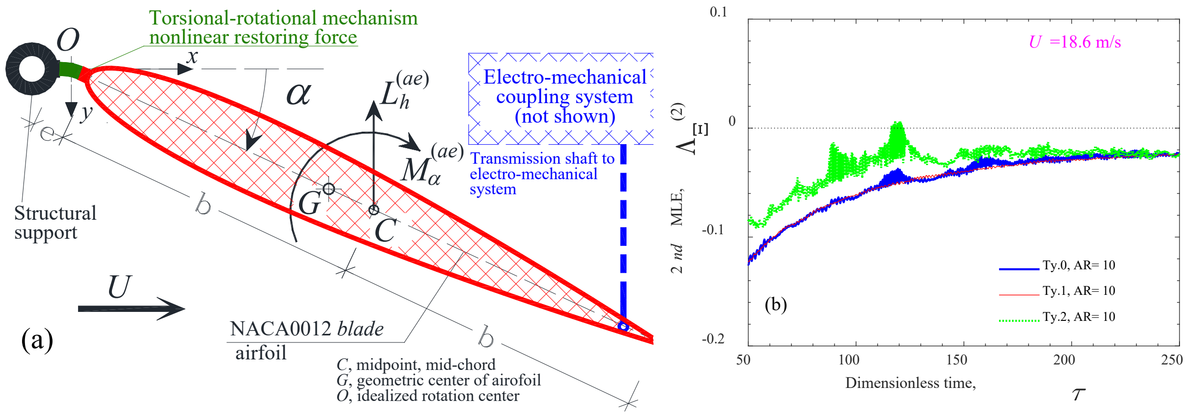

Figure 1. (a) Cross-sectional schematics of the apparatus and its components; (b) example of mean square dynamic stability analysis via 2nd MLE, $\Lambda_\Xi(2)$ at flow speed U for apparatus with aspect ratio AR=10

Figure 1(b) demonstrates that, as an example, at the stated wind speed all three systems are stable and do not trigger energy conversion since $\Lambda_\Xi(2)<0$ asymptotically, despite initial trend of Type 2.

4. CONCLUSIONS AND OUTLOOK

Further studies will confirm that uncertainty in the aeroelastic loads, depending on the standard deviation of the random-parameter Wanger function, may be “detrimental” since it delays the occurrence of flutter and reduces the efficiency of the apparatus. The final goal of the research is the identification and exclusion of low-efficiency operational regimes by rigorous probabilistic analysis. Anticipated results will open new avenues for future wind tunnel verification.

ACKNOWLEDGEMENTS

This material is based in part upon work supported by the National Science Foundation (NSF) of the USA, Award CMMI-2020063. Any opinions or conclusions are those of the author and do not reflect NSF’s views.

REFERENCES

Abdelkefi, A., Nayfeh, A.H., and Hajj, M.R., 2012. Design of piezoaeroelastic energy harvesters, Nonlinear Dynamics 68 (4), 519-530.

Bernitsas, M.M., Raghavan, K., Ben-Simon, Y., and Garcia, E.M.H., 2008. Vivace (vortex induced vibration aquatic clean energy): A new concept in generation of clean and renewable energy from fluid flow, Journal of Offshore Mechanics and Arctic Engineering 130 (4), 041101.

Caracoglia, L., 2018. Modeling the coupled electro-mechanical response of a torsional-flutter-based wind harvester with a focus on energy efficiency examination, Journal of Wind Engineering and Industrial Aerodynamics 174, 437-450.

Kloeden, P.E., Platen, E., and Schurz, H., 1994. Numerical solution of stochastic differential equations through computer experiments. Springer-Verlag, Berlin-Heidelberg, Germany.

Pigolotti, L., Mannini, C., Bartoli, G., and Thiele, K., 2017. Critical and post-critical behaviour of two-degree-of-freedom flutter-based generators, Journal of Sound and Vibration 404, 116-140.

Shimizu, E., Isogai, K., and Obayashi, S., 2008. Multiobjective design study of a flapping wind power generator, Journal of Fluids Engineering, ASME 130 (2), 021104.

Xie, W.-C., 2006. Dynamic stability of structures. Cambridge University Press, New York, NY, USA.

Free-stream turbulence effects on a square cylinder with a forebody screen at a small distance

Andrea Giachetti [1], Gianni Bartoli [1], Claudio Mannini [1]

[1]*CRIACIV/Dept. of Civil and Environmental Engineering, University of Florence, Italy,*
andrea.giachetti@unifi.it, gianni.bartoli@unifi.it, claudio.mannini@unifi.it

SUMMARY

This work shows that the presence of a forebody screen fixed at a relatively small distance from the windward face of a square cylinder can significantly influence the aerodynamic behaviour of the latter, even for a flow perpendicular to the screen and in presence of free-stream turbulence. The present investigation represents an extension of a previous two-dimensional study conducted by the same Authors on rectangular and square cylinders in smooth flow. Experiments in the wind tunnel were carried out by reproducing two different homogeneous isotropic turbulent flows and setting different distances between the screen and the front face of the cylinder. The pressure measurements around the screened section in turbulent flow revealed qualitatively the same behaviour observed in smooth flow, though the effects of the screen are less pronounced. A pressure reduction immediately behind the front corners and a faster pressure recovery moving towards the back corners are the most apparent features.

Keywords: square cylinder, turbulent flow, screened body

1. INTRODUCTION

Permeable building envelopes are often used in modern buildings. The complexity of the problem and the lack of studies stress the need for a research effort on this topic, even starting from basic geometries. However, to the Authors' best knowledge, the literature concerning screened bluff bodies (*e.g.*, Koenig and Roshko, 1985, Cooper, 1988) is mainly focused on the drag reduction of the overall system, and the screen distances considered are of the same order as the body characteristic dimension, instead of those typical of a permeable building envelope. Therefore, a series of two-dimensional exploratory studies were performed by the Authors in the last years (Giachetti, 2018, Giachetti et al., 2019). Experimental tests and numerical simulations were performed on a 2:3 rectangular and a square prism with a forebody screen at small distances (between $D/10$ and $D/40$, where D is the characteristic cross-flow dimension). Tests were carried out for different angles of attack. The screen was solid, so the internal cavity was connected to the exterior through the lateral sides only. That campaign was devoted to the comprehension of possible screen effects in smooth flow (namely, the approaching flow turbulence intensity was lower than 1%). The current work aims at extending the study to approaching turbulent flows.

2. EXPERIMENTAL SET UP

The experimental campaign was carried out in the CRIACIV (Inter-University Research Centre on Building Aerodynamics and Wind Engineering) wind tunnel. The sectional models were mounted horizontally (Figure 1). The model cross-flow section depth (D) was equal to 0.12 m (which corresponds to a blockage ratio of 7.5%) and the section model length was 1.24 m. Circular end plates with a radius of about $3.5D$ were employed to confine the flow. The model was fixed to the wind tunnel through a computer-controlled rotating system able to set the desired angle of attack with high accuracy. The screen was obtained from 1 mm thick stainless-steel foils. Steel and/or plastic spacers were used to create gap widths equal to $D/10$, $D/20$ and $D/40$. Pressure taps were installed around the middle section of the model, and pressure signals at about 500 Hz were simultaneously sampled. Due to the limited screen thickness, it was not possible to install pressure taps around it. The smooth flow in the wind tunnel presented a turbulence intensity lower than 1%, while two different turbulent flow conditions, hereafter referred to as Turb_1 and Turb_2, were obtained through a wooden grid installed at two different upwind positions. These approaching flows were characterized by longitudinal integral length scales (L_{ux}) of about 1.2D and 1.6D, and by longitudinal turbulence intensities (I_u) of about 13% and 10%, respectively for Turb_1 and Turb_2. The turbulent flow was uniform along the model.

3. RESULTS

Firstly, the mean pressure coefficients obtained in smooth and turbulent flow around the square section without screen are compared with some data available in the literature (Fig. 2). No blockage corrections are adopted.

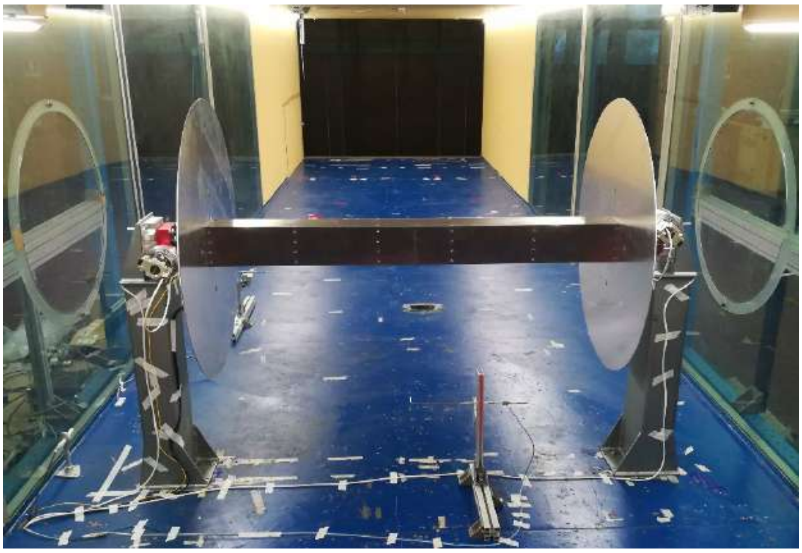

Figure 1. A picture of the section model in the wind tunnel without turbulence generators.

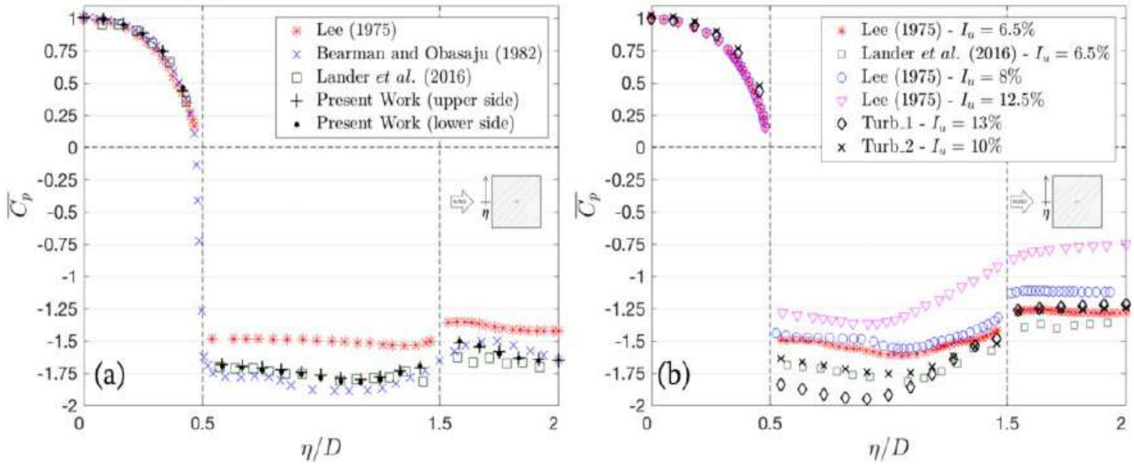

Figure 2. Mean pressure coefficients measured in smooth (a) and turbulent (b) flow around the square cylinder. See Giachetti et al. (2019) for the literature references.

Then, the following features can be noticed in Fig. 3, indicating the aerodynamic interference caused by the screen in smooth flow: (i) a pressure reduction due to the presence of the screen on the lateral sides behind the separation point; (ii) a mean pressure recovery on the lateral sides towards the back edges; (iii) a pressure jump between the first point on the lateral sides behind the front corners and the pressure in the cavity. Fig. 4(a) and (b) show the mean pressure coefficients for the approaching flows Turb_1 and Turb_2, respectively. Generally, the turbulent flow tends to attenuate the screen effects, partly because in this case the pressure recovery on the rear portion of the lateral sides occurs even without the screen. The pressure reduction on the lateral sides behind the separation point also occurs in turbulent flow. In both turbulent flow conditions, the screen effects on the rear portion of the lateral sides of the cylinder are nearly negligible for a gap width of $D/40$, while they become clearer by increasing it. The previously mentioned jump between the pressure measured on the lateral sides, in correspondence of the front corners, and the mean cavity pressure is reduced by the turbulent flow. Furthermore, in smooth flow, when the screen distance is larger than $D/40$, some local effects can be observed the cavity close to the openings, due to the separation of the flow periodically sucked into the cavity (Giachetti et al., 2019). Indeed, in correspondence of the taps located around $0.25 < \eta/D < 0.5$ (see Fig. 4), the mean pressure coefficients are lower than in the rest of the cavity. When the approaching flow is turbulent, for a gap width larger than $D/40$, such local effects are still visible, suggesting a flow mechanism similar to that observed in smooth flow.

4. CONCLUSIONS

The presence of a solid screen at a relatively small distance from the windward face of a square cylinder produces an aerodynamic interaction. The study conducted in smooth flow revealed a complex flow mechanism, driven by the vortex shedding, where internal and external flows mutually interact through the cavity that connects opposite upwind corners. The current investigation shows that these screen effects are still visible when the approaching flow is turbulent, but they are less marked.

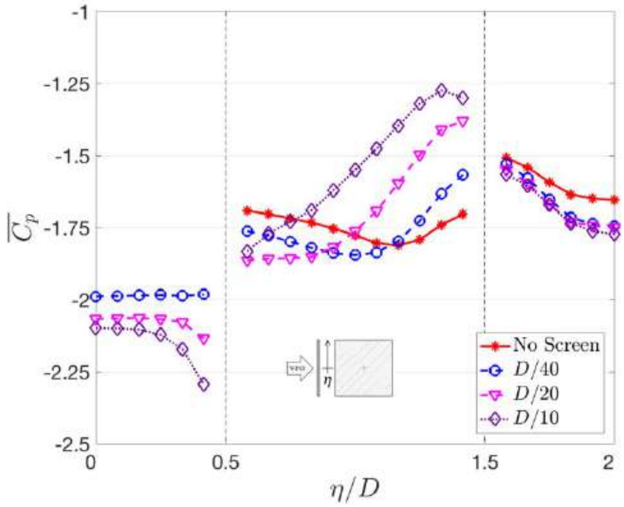

Figure 3. Mean pressure coefficients around the square cylinder for a wind perpendicular to the screen in smooth flow.

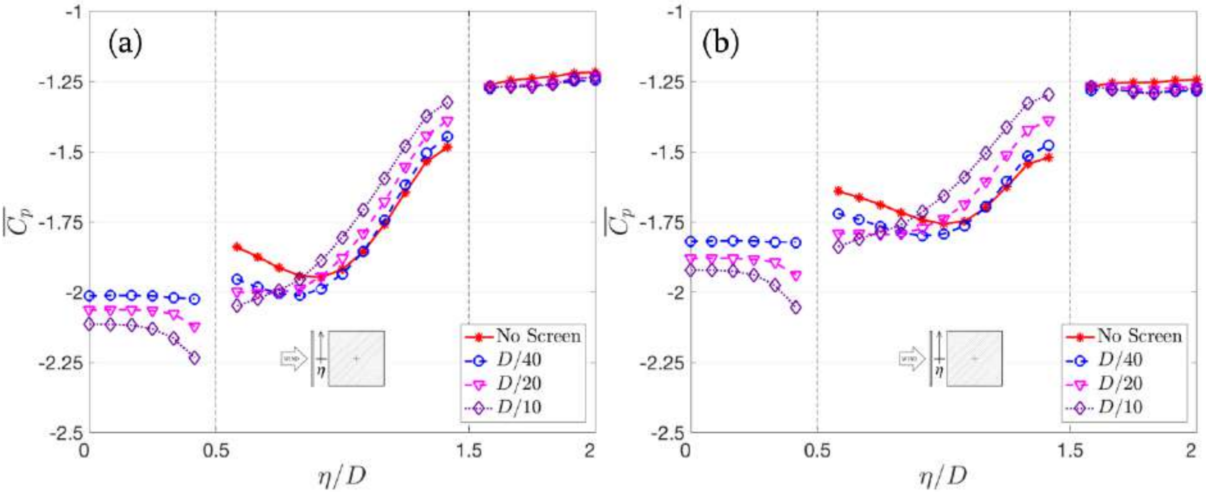

Figure 4. Mean pressure coefficients around the square cylinder for the approaching turbulent flows: Turb_1 turbulent flow (a) and Turb_2 turbulent flow (b). The wind is perpendicular to the screen.

REFERENCES

Cooper, K.R., 1988. The use of a forebody plate to reduce the drag and to improve the aerodynamic stability of a cylinder of square cross-section. Journal of Wind Engineering and Industrial Aerodynamics 28, 271-280.

Giachetti, A., 2018. Wind effects on permeable building envelopes: a two-dimensional exploratory study. PhD Dissertation, University of Florence, Italy – TU Braunschweig, Germany.

Giachetti, A., Bartoli, G. and Mannini C., 2019. Two-dimensional study of a rectangular cylinder with a forebody airtight screen at a small distance. Journal of Wind Engineering and Industrial Aerodynamics 189, 1-11.

Koenig, K. and Roshko, A., 1985. Experimental study of geometrical effects on the drag and flow field of two bluff bodies separated by a gap. Journal of Fluid Mechanics 156, 167-204.

Pressure distribution of a 6:1 rectangular cylinder obtained in TUCLA wind tunnel

J. Quintela [1], M. Roca [1], J. Á. Jurado [1], S. Hernández [1]

[1]*Structural Mechanics Group, School of Civil Engineering, University of A Coruña, Spain, juan.quintela.suarez@udc.es; miguel.roca.rodriguez@udc.es; jose.angel.jurado@udc.es; santiago.hernandez@udc.es*

SUMMARY
An experimental study of a 6:1 rectangular cylinder tested in the wind tunnel TUCLA of the University of A Coruña is presented. Data acquisition connected on 128 pressure taps located in eight cross-sections. Values of mean pressure coefficients and its standard deviation for different Reynolds number are presented. Future works will include the evaluation of aerodynamic coefficients, forces and correlation studies.

Keywords: Rectangular cylinder, pressure distribution, boundary layer wind tunnel

1. INTRODUCTION

The behavior of rectangular cylinder under wind flow has been of relevance in the recent years and research initialed at BARC are an example of such interest. Several computational and experimental studies have been carried out (Álvarez et al., 2019; Nguyen et al., 2018).

In that regard this extended abstract describes a test of a 6:1 rectangular cylinder in a wind tunnel of the University of A Coruña using a data acquisition system with a finite high number of pressure taps. The results presented are the values of the mean pressure coefficient and its standard deviation in eight sections span-wise and sixteen points in each cross-section. The future works include the evaluation of the aerodynamic coefficients and forces and also a correlation span-wise of the experimental results.

2. TEST DESCRIPTION AND DATA ACQUISITION

The Boundary Layer wind tunnel named TUCLA at the University of A Coruña features a 22.0 m long working section with a cross section of 3.0 m by 2.0 m and a turntable of 2.8 m of diameter and a maximum wind speed of 25 m/s. The setup of the sectional model in the wind tunnel and the instrumentation are shown in Fig. 1.

The 6:1 rectangular sectional model has a 2.750 m span with a cross section of 0.600 m width and 0.100 m height and consists of an aluminum main spar with wooden stringers and fiberboard skin.

The reduced model was instrumented with 8 arrays of 3D printed pressure taps as shown in Fig. 2; The distance between the array and the center line of the model is listed in Table 1.

Figure 1. Wind tunnel setup

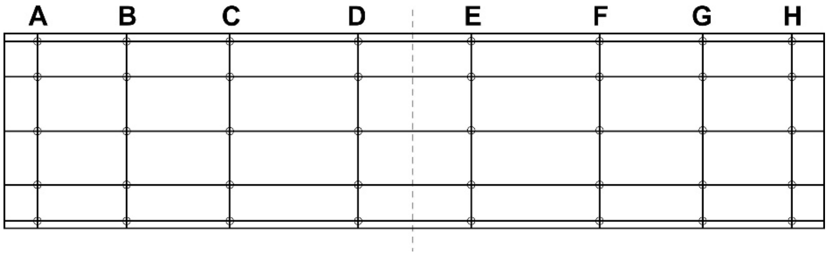

Figure 2. Arrangement of the pressure taps

Each array has a total of 16 pressure points distributed along the section of the model. Five points are located in the top and bottom faces, and three points are in the windward and leeward edges.

Table 1. Distance between the arrays and the center of the model

Array	A	B	C	D	E	F	G	H
Distance (mm)	1314	1013	678	227	227	678	1013	1314

Pressure taps were connected individually to pressure sensors while reference sensors in both modules were connected to the Pitot tube static port. Moreover, an additional pressure input was connected to the Pitot tube stagnation port to obtain a reference value of the free-stream dynamic pressure.

Pressure sensors were sequentially logged at a data acquisition rate of 625 Hz; since a total of 10,000 samples were acquired, the duration of each test was 16 s.

3. RESULTS

The mean pressure coefficient $\bar{C}_p$ and its standard deviation C'_p are calculated as shown in Eq. (1). For each case considered five tests were carried out to average the results for different time histories.

$$\overline{C_p} = \frac{\overline{\Delta_p}}{\frac{1}{2}\rho U_\infty^2}, \qquad C'_p = \frac{\sigma_{\Delta_p}}{\frac{1}{2}\rho U_\infty^2} \tag{1}$$

where ρ is the air density, U_∞ is the free-stream velocity, $\overline{\Delta_p}$ is the time averaged differential pressure and $\sigma_{\Delta p}$ is the standard deviation of the differential pressure.

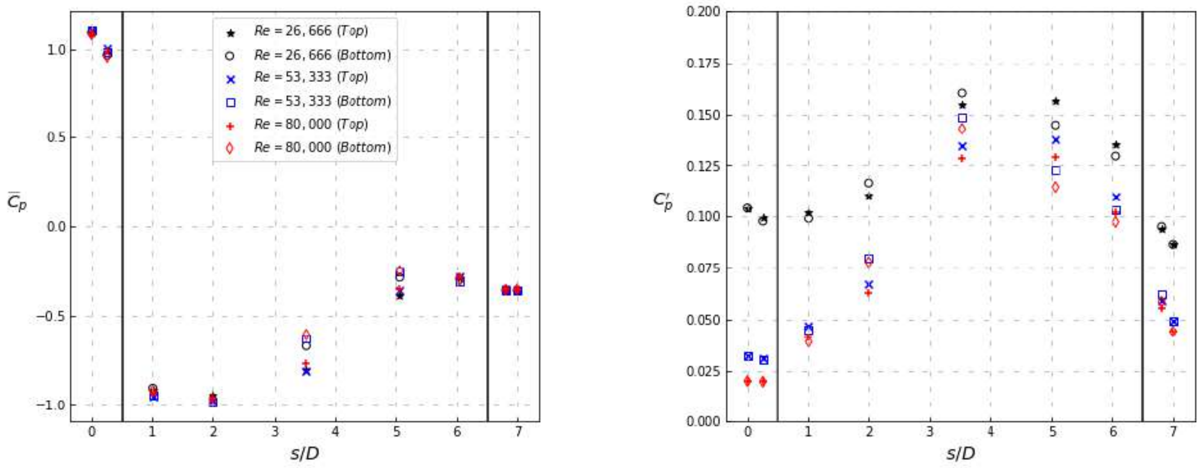

Figure 3. Mean (left) and standard-deviation (right) values of the pressure coefficients in smooth flow for α=0º. s/D=0 and s/D=7 denote respectively the windward and the leeward-face midpoints.

The Reynolds number $Re=U_\infty D/v$ was varied between 26,666 and 80,000. Its effect on the mean pressure coefficient obtained was marginal, as shown in Fig. 3. A small difference can be appreciated in the standard deviation, especially for low Reynolds numbers similarly to previous works (Mannini et al., 2011; Mannini et al., 2017).

Mean values of pressure coefficients for various angles of attack in the range of -8° ≤ α ≤ +8° are shown in Fig. 4.

For each case, the values represented are the mean of the pressure coefficient obtained for the central sections, B, C, D, E, F, and G, in Table 1. The outermost sections (A and H) were dismissed due to the effect of the wind tunnel walls.

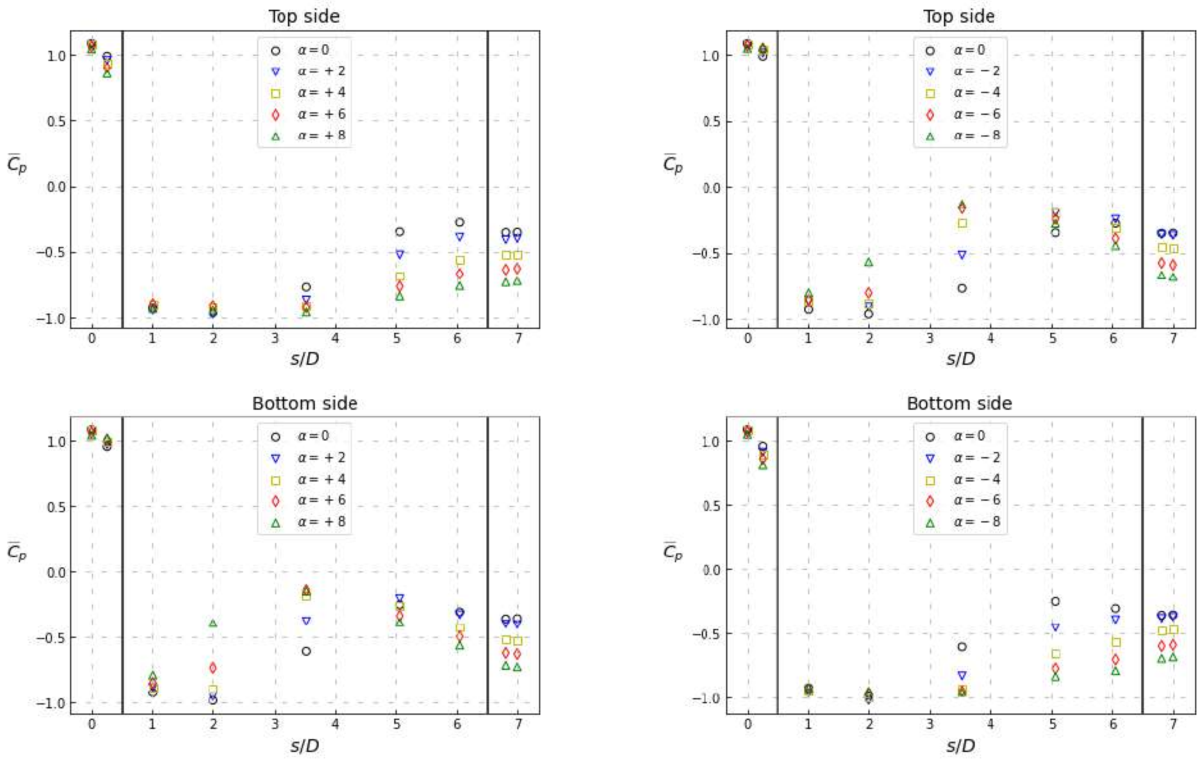

Figure 4. Mean values of pressure coefficients for various angles of attack for the top and bottom side of the model (Re = 80,000).

4. DISCUSION AND FUTURE WORKS

The $\bar{C}_p$ obtained in the stagnation point is slightly over one. In addition to the inherent error of the measurement systems, this is caused because a Pitot tube in the wind tunnel was used as the reference pressure used for the calculation of the pressure coefficients.

The standard deviation is significantly higher for the lower Reynolds number, especially in the windward and leeward-face points. This is due to the flow not being completely developed as well as these areas are the ones which experiment more turbulence.

Lastly, considered future research lines include study of correlation/coherence of pressure and forces, comparison of aerodynamic coefficients to load cell direct measurements and evaluation of endplates influence around tip areas.

REFERENCES

Álvarez, A., Nieto, F., Nguyen, D., Owen, J. and Hernández, S. 3D LES simulations of a static and vertically free-to-oscillate 4:1 rectangular cylinder: Effects of the grid resolution. Journal of Wind Engineering and Industrial Aerodynamics 192, 31–44. (2019).

Mannini, C., Marra, A.M., Pigolotti, L., Bartoli, G. The effects of free-stream turbulence and angle of attack on the aerodynamics of a cylinder with rectangular 5:1 cross section. Journal of Wind Engineering and Industrial Aerodynamics 161, 42-58. (2017).

Mannini, C., Šoda, A., Schewe, G. Numerical investigation on the three-dimensional unsteady flow past a 5:1 rectangular cylinder. Journal of Wind Engineering and Industrial Aerodynamics 99 (4), 469–482. (2011).

Nguyen, D., Hargreaves, D. and Owen, J. Vortex-induced vibration of a 5:1 rectangular cylinder: a comparison of wind tunnel sectional model tests and computational simulations. Journal of Wind Engineering and Industrial Aerodynamics 175: 1–16 (2018).

Aerodynamic loading of tall buildings with porous double-skin façade systems

Petar Škvorc [1], Andrea Giachetti [2], Hrvoje Kozmar [3], Gianni Bartoli[4]

[1]*Faculty of Mechanical Engineering and Naval Architecture, University of Zagreb, Zagreb, Croatia, petar.skvorc@fsb.hr*
[2]*Department of Civil and Environmental Engineering, University of Florence, Florence, Italy, andrea.giachetti@unifi.it*
[3]*Faculty of Mechanical Engineering and Naval Architecture, University of Zagreb, Zagreb, Croatia, hrvoje.kozmar@fsb.hr*
[4]*Department of Civil and Environmental Engineering, University of Florence, Florence, Italy, gianni.bartoli@unifi.it*

SUMMARY
Model experiments were performed in a boundary layer wind tunnel to study the effect of porous double-skin façade (PDSF) systems on wind loading of tall buildings. A high-frequency force balance was used to determine integral aerodynamic loading of a tall building model, and pressure transducers were employed to assess surface pressure distributions on the inner façade of the building model. The results indicate that the PDSF system yields a decrease in the maximum mean across-wind moment by ~13% regardless of the degree of the outer façade porosity, while the PDSF system negligibly affects the mean integral along-wind moment. A significant influence of the PDSF porosity was observed regarding pressure distribution on the inner façade. In particular, a low-porosity outer façade causes a decrease in peak pressures by ~10% to ~20% depending on the flow incidence angle, while an increase in the PDSF porosity does not have a noticeable effect on surface pressures on the inner façade.

Keywords: Tall building, porous façade, wind load, experimental aerodynamics, wind-tunnel experiments

1. INTRODUCTION
A cladding system made of two skins, with uniformly distributed openings on the external layer, can be called a porous double-skin façade (PDSF). The outer surface is porous, i.e. allows the wind to flow through it and into the gap between the inner, solid façade and the outer, porous façade. The goal of the present work was to experimentally determine integral wind loading of a tall building model equipped with PDSF systems of various porosity and pressure distribution on the inner façade of the building model. Experiments were carried out in the CRIACIV (Inter-University Research Centre on Building Aerodynamics and Wind Engineering) boundary layer wind tunnel at the University of Florence, Italy.

2. EXPERIMENTAL SETUP
A model of the atmospheric boundary layer (ABL) was created in accordance with the international standard (EN1991-1-4:2005, 2005) for terrain category III. This is a highly turbulent ABL, which corresponds to urban environments where tall buildings are generally situated. The ABL simulation length scale was 1:400.

A regular prism with a square cross section characterized by 100 mm long edges and 500 mm height was used to assess wind loads and surface pressure distributions. The building model without a PDSF system, thus a standard single-skin building model, was used as a reference case. The outer, porous façade was made of 1 mm thin aluminum sheets with laser-cut, 10 mm diameter circular openings that mimic porosity effects. In total, three porosities were tested, i.e. 25%, 50% and 65%, calculated as the ratio between the total area of the openings and the total area of the façade. The gap between the inner and outer façades was 5 mm. The building model was subjected to the ABL simulation at flow incidence angles from 0° to 45° with an increment of 5°, while additional flow incidence angles of 12.5° and 17.5° were also studied. A high-frequency force balance was used to record integral aerodynamic loads acting on the building model. Time record length was 100 s at the sampling rate of 2000 Hz. Surface pressures were recorded on the inner façade by an array of pressure sensors mounted in a square pattern. In these experiments, the time record length was 100 s at the sampling rate of 500 Hz.

3. RESULTS AND DISCUSSION

The presence of a PDSF system of any porosity yields a decrease in the maximum mean across-wind moment coefficient. This decrease is of the order of ~13% regardless of the outer façade porosity, which was observed at the 12.5° flow incidence angle. The effect of the PDSF system on the mean integral along-wind moment coefficient is negligible. Regarding surface pressures, 25% porosity causes a decrease in the peak pressure coefficient (C_p) by ~10% to ~20% for all building surfaces depending on the flow incidence angle. An increase in the PDSF porosity diminishes the effect of the PDSF system on maximum inner surface pressures, Fig 1.

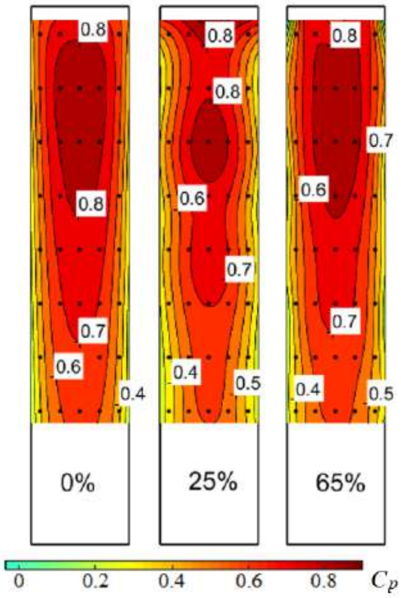

Figure 1. Mean surface pressure coefficient (C_p) on the inner windward façade of the building model equipped with single-skin, 25% and 65% PDSF systems subjected to the ABL simulation at 0^O flow incidence angle

4. CONCLUSIONS

The implementation of porous double-skin façade systems on tall buildings favorably affects aerodynamic characteristics of these complex engineering structures by causing a decrease of their integral across-wind loads and surface pressures on the inner façade.

REFERENCES

EN1991-1-4:2005, 2005, Eurocode 1: Actions on structures – General actions, Part 1-4: Wind actions. CEN.

Can Wind Lidars be used to calibrate mean wind profiles?

V. Sepe [1], A.M. Avossa [2], F. Rizzo [3], F. Ricciardelli [2]

[1]*Università "G. d'Annunzio" di Chieti-Pescara, Pescara, Italy, vincenzo.sepe@unich.it*
[2]*Università della Campania "Luigi Vanvitelli", Aversa, Italy, albertomaria.avossa, friccia@unicampania.it*
[3]*Cracow University of Technology, Crakow, Poland, fabio.rizzo@universityresearch.it*

SUMMARY
This paper explores to which extent Wind Lidars may be used to calibrate mean wind profiles, depending on the extension and accuracy of the available measurements.

Keywords: wind LIDAR, mean wind profile, wind models

1. INTRODUCTION

Measurement of the wind velocity field at a given site can be useful for defining and validating analytical and numerical models for wind actions on structures.

To this aim the use of Doppler Lidar (Light Detection and Ranging) has become popular in the last decades (e.g., Drew et al. 2013; Lane et al. 2013; Wood et al. 2013; Lim et al. 2016; Demartino et al. 2017; Kent et al. 2018), in spite of the inaccuracies associated with space averaging and with non-synchronous measurement of continuous beam LIDARs.

LIDARs, in fact allows a relatively easy acquisition of wind velocities at different heights, in a range of several hundred meters above the ground and with a sampling rate up to 1 Hz or more.

Very often, however, it is difficult or impossible to measure by means of LIDAR the wind speed close to the ground. Depending on the characteristics of this device, in fact, only points can be measured whose distance from LIDAR is larger than a given threshold (around 30 m).

On the other hand, the variation of the mean wind speed is more pronounced near the ground, therefore the parameters that characterize analytical models are deeply influenced by wind speed values at low elevations.

This paper explores to which extent Wind Lidars may be used to calibrate mean wind profiles, depending on the available measurements.

2. METHODOLOGY

It is widely accepted that in the urban environment any analytical law for the wind speed profile has to include, as a starting point for the elevation coordinate, the zero-plane displacement height, i.e. the level below which the flow is nearly blocked by the obstructing buildings.

As a part of a wider research on the effectiveness of the LIDAR methodology for the experimental characterization of wind fields, this paper describes numerical analyses devoted to investigate how the identification of the parameters z_0 (roughness length) and d (zero-plane displacement height) is affected by the extension and accuracy of the available measurements.

To this respect, and with no loss of generality, the logarithmic law has been assumed as representative of the wind speed profile. Assuming a synoptic wind regime and for different values of z_0 and d, a set of profiles of 10-minutes averaged wind speed are simulated for moderately strong winds ($V_{ref} > 12$ m/s, where V_{ref} is the wind speed measured at a reference elevation from ground of 50 meters), affected by a numerical noise varying in a range representative of the typical accuracy of LIDAR measurements.

Pseudo-experimental wind speed profiles are then assumed as input data for a least-square fitting procedure, that allows to identify the parameters z_0 and d of the logarithmic profile.

3. EXPECTED RESULTS

Based on the results of the numerical investigation, the values of z_0 and d used to generate the pseudo-experimental data are compared with the corresponding identified values. Their difference, assumed as the identification error that can be expected from an on-site measurement campaign, is discussed in the paper as a function of several variables: the number of measuring points, their distribution along the vertical, the characteristics of noise added to the simulated data.

In particular, the reliability of the identified values of z_0 and d is discussed as a function of the lowest available measuring point. This allows quantifying the random uncertainty associated with the identified profile, that in turn may significantly affect the evaluation of wind-induced loads on low- to medium-rise buildings.

REFERENCES

Demartino C, Avossa AM, Ricciardelli F, Calidonna CR (2017) Wind profiles identification using wind LIDARS: an application to the area of Lametia Terme. In: Proceedings of “7th European and African Conference on Wind Engineering”, EACWE, 4-7 July 2017, Liège, Belgium.

Drew DR, Barlow JF, Lane SE (2013) Observations of wind speed profiles over Greater London, UK, using a Doppler lidar. Journal of Wind Engineering and Industrial Aerodynamics, 121, 98-105.

Kent CW, Grimmond CSB, Gatey D, Burlow JF (2018) Assessing methods to extrapolate the vertical wind-speed profile from surface observations in a city centre during strong winds. Journal of Wind Engineering and Industrial Aerodynamics, 173, 100-111.

Lane SE, Barlow JF, Wood CR (2013) An assessment of a three-beam doppler lidar wind profiling method for use in urban areas. Journal of Wind Engineering and Industrial Aerodynamics, 119, 53-59.

Lim KEW, Watkins S, Clothier R, Ladani R, Mohamed A, Palmer JL (2016) Full-scale flow measurement on a tall building with a continuous-wave Doppler Lidar anemometer. Journal of Wind Engineering and Industrial Aerodynamics, 154, 69-75.

Wood CR, Pauscher L, Ward H, Kotthaus S, Barlow J, Gouvea M, Lane S, Grimmond CSB (2013) Wind observations above an urban river using a new lidar technique, scintillometry and anemometry. Sci Total Environ 442, 527-533.

Numerical and experimental investigation of a TLP wind turbine under wind and wave loads

M. Vardaroglu [1], Z. Gao [2], A.M. Avossa [1], F. Ricciardelli [1]

[1] *Department of Engineering, University of Campania "Luigi Vanvitelli", Aversa, Italy*
mustafa.vardaroglu@unicampania.it
[2] *Department of Marine Technology, Faculty of Engineering, Norwegian University of Science and Technology, Trondheim, Norway*

SUMMARY
Research on offshore wind technologies has increased in the last two decades following the progress and cost reduction in turbine design and operation, and the increased demand for renewable energy production. Coupled dynamic responses of a floating offshore wind turbine under simultaneous wind and wave loading can be investigated by experimental and computational methods. In the scope of this paper, a numerical study is conducted on a floating offshore wind turbine. A standard baseline wind turbine supported by a Tension Leg Platform is investigated under simultaneous wind and wave loading. For comparison, cases with only wind loading and only wave loading were also simulated to identify the dominating contributions in various responses for this TLP wind turbine. Larger platform surge response is observed due to the resonance triggered by the turbulent wind at platform surge natural frequency. Pitch motions are profound at the wave frequencies and the resonant frequency, mainly due to the first-order wave loads. Aerodynamic damping related to the rotating rotor conditions resulted in decreased platform pitch. Results of this study are the basis of a sensitivity study aiming at improving the MIT/NREL TLP wind turbine design.

Keywords: Floating Offshore Wind Turbines, Tension Leg Platform, Resonant motions, Turbulent Wind, Aerodynamic Damping.

1. INTRODUCTION

Offshore wind energy has been developing rapidly in the last two decades in the way to achieve the net-zero targets in carbon emissions and fight against global warming. Decreasing costs in floating offshore wind energy technology makes it possible to generate energy in deep water areas, where wind speeds are constant and relatively higher. A Tension Leg Platform (TLP) wind turbine achieves stability by using the tension in the mooring lines that connects the floating platform and the wind turbine. TLP wind turbines perform smaller heave and pitch motions compared to the alternative platform types such as spar buoys and semi-submersibles. The dynamic response of floating offshore wind turbines under simultaneous wind and wave loading is a complex phenomenon in offshore wind engineering.

In this study, the coupled response of a TLP wind turbine is discussed under simultaneous wind and wave loading over numerical analyses. Fully coupled motion response analyses are conducted in the time domain by using the open-source Fatigue, Aerodynamics, Structures, and Turbulence code OpenFAST (NREL). The numerical model has been calibrated and validated by Vardaroglu et al. (2022) under regular and irregular waves. Hydrodynamic damping in the numerical model was calibrated by using scaled physical model decay tests. A modified version of the MIT NREL TLP (Matha, 2010) design and its mooring system, supporting the NREL 5 MW standard baseline turbine (Jonkman, 2009), was used for this purpose, which is termed as DHI TLP wind turbine.

In this paper, the effect of wind excitation on the response of the numerical model turbine is investigated by comparing wave loading and operational wind conditions. The importance of aerodynamic damping is highlighted over comparisons between operational and parked turbine cases when the floater is under irregular wave loads. Platform motions, tendon tensions, tower base bending moments, and blade root moments from the numerical analyses are discussed through response spectra and statistics. Scaled physical model response is going to be evaluated in a future study, where wave & wind misalignment will also be considered.

2. NUMERICAL MODEL

2.1. TLP floating wind turbine

The structure consists of a floating cylinder, the tendons, and the wind energy generator. Figure 1 shows the numerical model, the global coordinate system and system degrees of freedom. As shown in Figure 1, the structure is anchored to the seabed (200 m) by four groups of tendons. Horizontal cylinders (pontoons) connect the floating platform to the anchors. The wind turbine tower is fixed to the floating platform at still water level. The basic features of the model are shown in Table 1.

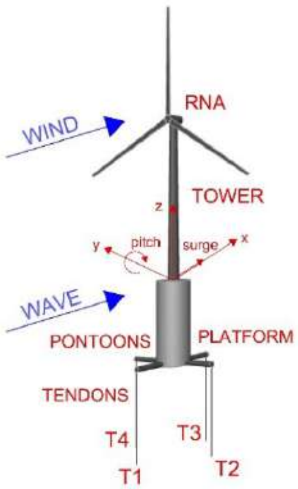

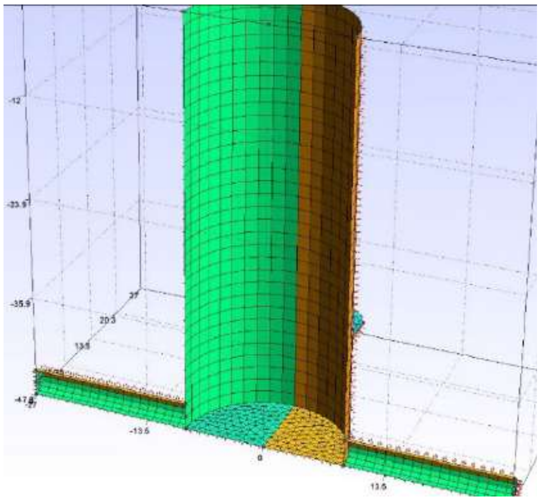

Figure 1.. TLP model (left, Edited from: Vardaroglu et al., 2022) and hydrodynamic analysis model mesh (right, Source: Vardaroglu, 2022).

Table 1. Principal features of the model

Feature	Value	Unit
Platform radius	9.0	m
Platform height	47.89	m
Pontoon length	18.0	m
Nacelle height	90.0	m
Total mass	9806	tons
Water displacement	12696	m3
Unstretched line length	151.58	m

2.2. Numerical Modelling Approach

The numerical model is based on the readily available MIT/NREL TLP standard baseline design (Matha, 2010). Vardaroglu et al (2022) calibrated the hydrodynamic damping in the numerical model according to a scaled physical model, which was tested in the offshore wave basin of the Danish Hydraulic Institute in 2012 (Armenio & D'Alessandro, 2013; Tomasicchio et al., 2014). The hydrodynamic problem is solved with frequency-domain computations by using an open-source Boundary Element Method (BEM) tool, NEMOH (Babarit and Delhommeau, 2015). Mean-drift loads on the platform are also considered in hydrodynamic calculations. In the scope of this paper, rated wind speed (11.4 m/s) is considered only, which is the wind speed when blade pitch control starts to activate. Turbulent wind field time series are calculated according to the Kaimal spectrum using the open-source turbulent wind simulator, TURBSIM (Jonkman and Buhl Jr.). Spatial coherence parameters are selected according to the IEC 61400-1. The aerodynamic problem is solved according to Blade-Element Momentum (BEM) approach within the AeroDyn module. Wind- and wave- induced loads and responses of the turbine, tower, platform, and tendons are calculated by using a combined time-domain approach in OpenFAST.

Dynamic response analyses are conducted on the numerical model for wave loading (LC1), simultaneous wave and turbulent wind (LC2), and simultaneous wave and uniform & constant wind conditions (LC3). Uniform and constant wind conditions are simulated by considering a uniform wind profile along the turbine height, where wind shear is not considered. Uniform and constant wind loading is not realistic but helps to show the effects of turbulent wind conditions clearly. Furthermore, to better understand the effects of wind-induced loads, analyses under solely wind excitation are conducted considering turbulent wind (LC4) and uniform & constant wind conditions (LC5). Besides, due to the match of platform pitch natural frequency (0.200 Hz) and rotor rotation frequency (0.202 Hz), an additional case (LC6) is simulated, considering also the tower shadow.

3. RESULTS & CONCLUSIONS

In this paper, dynamic responses of a TLP wind turbine are evaluated by using numerical computations under simultaneous wind and wave-induced loads. Time histories, power spectra, and statistics of the platform surge, heave, and pitch, windward and leeward tendon tensions (T1 and T3), tower base bending moment in the fore-aft direction (Mbyy), and rotor blade root flap-wise moments (RootMyb1) are evaluated. For this purpose, spectral analyses are conducted by using a MATLAB toolbox, Wave Analysis for Fatigue and Oceanography (WAFO) (Brodtkorb et al., 2000). Figure 2 shows the comparison of platform pitch spectra obtained from the time-domain analyses for six different load conditions. The first group of the peaks are observed at 0.099 Hz. under LC1, LC2, and LC3 (data series in black), which is due to the peak wave frequency and is dominated by wave loading. On the other hand, a higher peak is observed close to the platform pitch natural frequency (0.200 Hz.,) under the wave loading case (LC1), which is the resonance response triggered by the irregular wave loading components. Standard deviations of the responses are listed in **Table 2**. Statistical evaluation of the platform pitch and related responses (T1, T3, Mbyy) resulted in smaller response dynamics under the rotating rotor (operational) conditions (LC2 and LC3) compared to the wave-only case (LC1). The comparison of the responses between turbulent wind loading (LC4) and uniform & constant wind (LC5) conditions reveals the importance of turbulent wind loading on the resonant response of the TLP wind turbine, which should be considered in the design of the structure. Due to the tendon stiffness difference compared to the original design (MIT NREL TLP), the platform pitch natural frequency and rotor rotation frequency match, and the tower fore-aft first bending mode natural frequency and rotor blade passing frequency of the TLP wind turbine also match in this study. These coincidences resulted in increased loads at the blade root and should be avoided. A broader response assessment of the structure (not only at rated wind speed but also cut-off, extreme wind speeds) under turbulent wind conditions is in progress, which aims on enhancing the standard baseline design of the MIT/NREL TLP wind turbine.

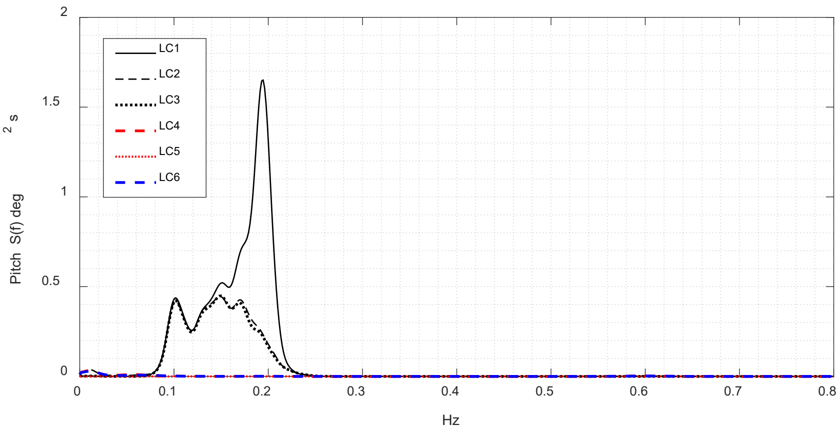

Figure 2. Platform pitch PSD and close-up view.

Table 2. Standard deviation values

Load Case	Surge (m)	Pitch (deg)	T1 (kN)	T3 (kN)	Mbyy (kNm)	RootMyb1 (kNm)
LC1	0.63	0.28	1964	1956	46940	535
LC2	1.32	0.21	1451	1438	25571	1627
LC3	0.61	0.20	1411	1401	22455	779
LC4	1.30	0.04	270	209	10142	1476
LC5	0.03	0.00	8	8	445	240
LC6	1.20	0.04	277	210	11267	1598

ACKNOWLEDGEMENTS

The experimental results used in this research were produced within a project funded under the Integrated Infrastructure Initiative HYDRALAB IV of EU FP7. Release of the data is acknowledged.

REFERENCES

Armenio, E., D'Alessandro, F. Dynamic response of floating offshore wind turbines under random waves and wind action HyIV – DHI - 01 Offshore wave basin, DHI Data Storage Report. Denmark, Copenhagen, January 2013.

Babarit, A. and Delhommeau, G., 2015, September. Theoretical and numerical aspects of the open source BEM solver NEMOH. In 11th European wave and tidal energy conference (EWTEC2015).

Brodtkorb, P.A., Johannesson, P., Lindgren, G., Rychlik, I., Ryden, J., Sjö, E., et al., 2000. Wafo-a matlab toolbox for analysis of random waves and loads, in: The tenth international offshore and polar engineering conference, International Society of Offshore and Polar Engineers.

Jonkman, J., Butterfield, S., Musial, W., Scott, G. Definition of a 5-MW Reference Wind Turbine for Offshore System Development. Tech. rep. NREL/EL-500- 38060. National Renewable Energy Laboratory; February 2009.

Jonkman, B.J. and Buhl Jr, M.L., 2006. TurbSim user's guide (No. NREL/TP-500-39797). National Renewable Energy Lab.(NREL), Golden, CO (United States).

Matha, D., 2010. Model development and loads analysis of an offshore wind turbine on a tension leg platform with a comparison to other floating turbine concepts: April 2009 (No. NREL/SR-500-45891). National Renewable Energy Lab.(NREL), Golden, CO (United States).

NREL: OpenFAST v2.5.0 Documentation. https://openfast.readthedocs.io/en/latest/index.html. – (Accessed: 2021-07-19)

Vardaroglu, M., Gao, Z., Avossa, A.M. and Ricciardelli, F., 2022. Validation of a TLP wind turbine numerical model against model-scale tests under regular and irregular waves. Ocean Engineering, 256, p.111491.

Tomasicchio, G.R., D'Alessandro, F., Musci, E., Fonseca, N. Mavrakos, S.A., Kirkegaard, J., Katsaounis, G.M., Penchev, V., Schüttrumpf, H., Wolbring, J., Armenio, E. Physical Model Experiments on Floating Off-Shore Wind Turbines. Proceedings of the HYDRALAB IV Joint User Meeting, Lisbon, July 2014.

Full-scale validation of a wind-induced response calculation model for a light tower

Andrea Orlando[1], Luisa Pagnini[2], Maria Pia Repetto[3]

[1]*DICCA – Polytechnic School, University of Genoa, Italy, andrea.orlando@edu.unige.it*
[2]*DICCA – Polytechnic School, University of Genoa, Italy, luisa.pagnini@unige.it*
[3]*DICCA – Polytechnic School, University of Genoa, Italy, repetto@dicca.unige.it*

SUMMARY
The paper discusses the outcomes of the structural monitoring of a light tower in the port of La Spezia (Northern Italy) using accelerometers and strain gauges. Full-scale structural response is compared with the predictions coming from an analytical model for the calculation of wind effects on monotubular towers. The dynamic and aerodynamic parameters, which are input quantities for the calculation model, are evaluated from experimental surveys: full-scale dynamic identification of the structure is performed by applying OMA techniques; aerodynamic parameters were evaluated from wind tunnel tests in a previous step of the research. The observed agreement between measured and calculated response quantifies the reliability of the calculation model.

Keywords: structural monitoring, wind-induced vibrations, aerodynamic damping

1. INTRODUCTION

The behavior of slender structures subject to wind action is well established in the scientific literature (Repetto and Solari, 2004). The main calculation models for synoptic wind actions are included in current codes and standards (EN 1991-1-4, 2005; CNR-DT 207, 2018) for the most common structural types. However, the practical application of such methods involves uncertainties that can strongly affect the final calculation. Indeed, the implementation of these models in the design stage requires the knowledge of several parameters characterizing the structure, whose evaluation is very delicate and awkward.

Experimentation is therefore a fundamental tool for the application, the validation and the improvement of calculation models. The use of in-field measurements is a valuable resource for many reasons: from one hand, full-scale data supply direct information on structural response that can be used as input in the calculation methods; from the other, they represent a benchmark against which loading and response models can be compared and calibrated (Tamura and Suganuma, 1996; Li et al., 2008; Kijewski-Correa et al., 2013).

Starting from these premises, the paper presents the results of a monitoring campaign over a light tower in Italy. Due to its structural simplicity, this structure is very attractive for a comparison between measured and predicted behavior. Outcomes of the monitoring activity are used to assess the capability of simplified calculation models available in the literature to predict the actual wind-induced response of vertical slender structures.

2. METHODOLOGY

The light tower under investigation (Fig. 1a) is located in the port of La Spezia, Northern Italy. It is 16.6 m high. The steel shaft has a 16-sides polygonal cross-section with rounded corners. A steel ladder runs along the shaft. At the top, a squared platform houses the lighting devices.

The pole has been equipped with a monitoring system including wind speed and structural response sensors (Fig. 1b). A three-axial ultrasonic anemometer is installed on the top platform, recording wind speed with sampling rate of 10 Hz. The structural response is measured by two biaxial accelerometers (placed at the top and at two-thirds of the height) and eight uniaxial strain gauges (placed at the base of the shaft) recording at 200 and 100 Hz, respectively. All sensors are cable-connected to an acquisition unit inside a watertight box at the foot of the pole.

Data have been recorded continuously since March 2019. Wind velocity records have been analyzed in order to identify and separate stationary and transient events (De Gaetano et al., 2014). The separation algorithm has been enhanced to extract wind events that are stationary both in velocity and in direction.

Measured response of the tower is compared with the predictions coming from an analytical model specifically devoted to the calculation of wind effects on poles and monotubular towers, based on the gust response factor (GRF) technique (Solari and Pagnini, 1999). According to the model, the maximum wind-induced displacement in along wind and crosswind direction, $\alpha=x, y$, in the time interval T=10 minutes is given by:

$$\alpha_{\max}(z) = G_\alpha(z)\bar{\alpha}^x(z), \quad G_x = 1 + 2 g_x I_x \sqrt{Q^2_x + R^2_x}, \quad G_y = g_y I_y \left(\left| \bar{C}_D + \bar{C}'_L \right| / \bar{C}_D \right) \sqrt{Q^2_y + R^2_y} \tag{1}$$

where $\bar{a}^x$ is the static displacement due to the application of the mean aerodynamic force $\bar{F}_x$ in direction α, G_α is the GRF, g_α and I_α are peak coefficient and turbulence intensity, C_D is mean drag coefficient and C'_L is the prime angular derivative of lift coefficient, Q_α and R_α are non-dimensional parameters associated respectively to the quasi-static part and to the resonant part of the response:

$$Q_\alpha = \left(1/\bar{K}_{\alpha x}\right)\left(K'_0 Q_{0\alpha} + \sum_{k=1}^{N} K'_{k\alpha} Q_{k\alpha}\right) \qquad R_\alpha = \left(1/\bar{K}_{\alpha x}\sqrt{\delta_{\alpha 1}}\right)\left(K'_0 D_{0\alpha} + \sum_{k=1}^{N} K'_{k\alpha} D_{k\alpha}\right) \tag{2}$$

where $\delta_{\alpha 1}$ is the logarithmic decrement of the first modal damping in direction α; $Q_{0\alpha}$ and $D_{0\alpha}$ are respectively quasi-static and resonant parameters associated to aerodynamic actions on the shaft; $Q_{k\alpha}$ and $D_{k\alpha}$ are quasi-static and resonant parameters associated to aerodynamic actions on the kth localized mass applied to the shaft, e.g. the platforms or the equipment.

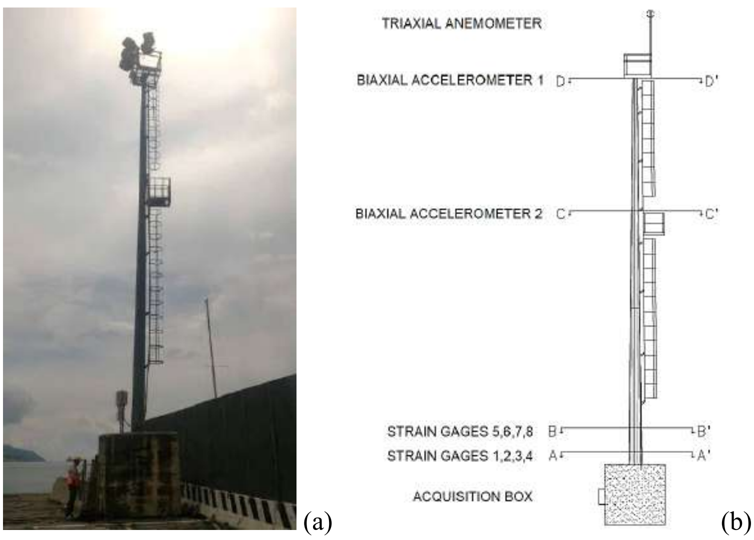

Figure 1. The light tower in the Harbor of La Spezia, Italy (a). Position of sensors (b).

The dynamic and aerodynamic parameters, which are input quantities for the response calculation model, are evaluated from experimental surveys. In a previous step of the research, the aerodynamic coefficients have been evaluated from an extensive wind tunnel test campaign (Orlando, 2021). Full-scale dynamic identification of the structure is performed by applying Operational Modal Analysis (OMA) techniques. Assuming that the estimated parameters have good reliability, the agreement between measured and calculated response quantifies the reliability of the calculation model.

3. RESULTS

Natural frequencies and mode shapes of the light tower have been identified from full-scale measurements, guided by the outcomes of a finite element model. The first bending modes along the principal axes of inertia occur at two separate frequencies (f_{1x}=0.76 Hz, f_{1y}=0.85 Hz) due to the presence of the ladder, which produces a non-symmetric behavior. Fundamental frequencies do not appear sensitive to wind speeds (coherently, e.g., with Pagnini and Piccardo, 2021), contrary to what is reported for tall buildings (Tamura and Suganuma, 1996).

The evaluation of damping has been carried out by OMA techniques applied in both frequency and time domain (Brincker and Ventura, 2015; Pagnini et al, 2018). Damping values turn out to be essentially made by the aerodynamic contribution, as the dissipative capacity is almost evanishing at the low wind velocities. In addition, a non-linear trend of damping with the wind velocity is observed, due to the drag crisis in the critical Reynolds range. To the best of author's knowledge, no scientific research has ever detailed such effect.

The comparison between measured and calculated response shows that, in the alongwind direction, the model is able to predict excellently the mean value (Fig. 2a), while it slightly overestimates the maximum value at high wind velocities (Fig. 2b). In the crosswind direction, a greater discrepancy between calculations and predictions is noted. In this case, however, the prime derivative of the lift coefficient (assumed equal to zero in the calculations) represents a further source of uncertainty, as experimental analyzes in the wind tunnel have highlighted the onset of non-zero values for some directions of the incident wind.

In the overall, the results prove the goodness of the model for the considered structural typology and confirm the validity of the engineering simplifications of the closed-form solution applied (Solari and Pagnini, 1999).

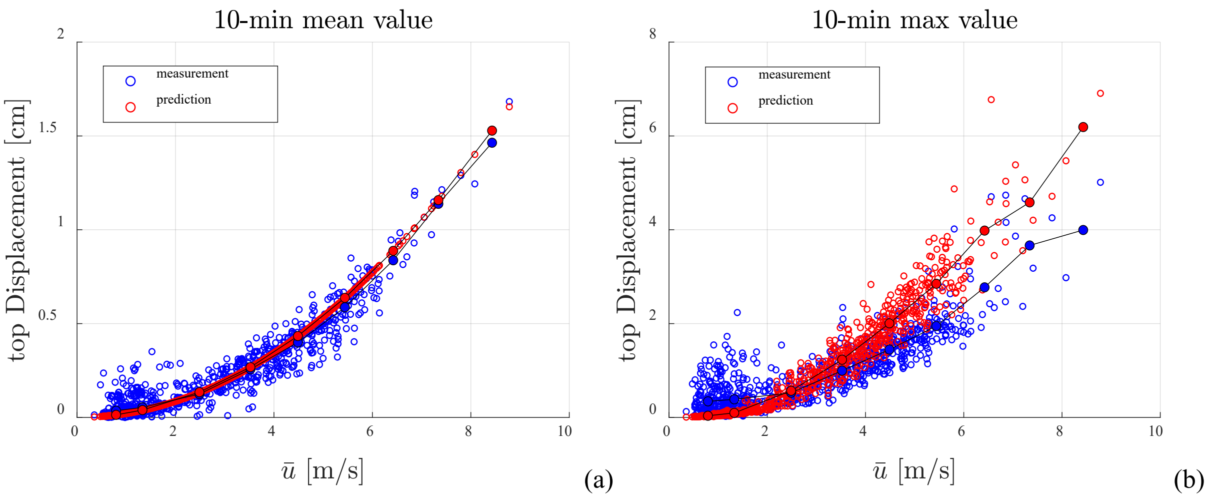

Figure 2. Comparison of alongwind mean (a) and maximum (b) displacements of the tower.

ACKNOWLEDGEMENTS

This research is funded by the European Research Council (ERC) under the European Union's Horizon 2020 research and innovation program (grant agreement No. 741273) for the project THUNDERR – Detection, simulation, modelling and loading of thunderstorm outflows to design wind-safer and cost-efficient structures – supported by an Advanced Grant 2016.

REFERENCES

Brincker R., Ventura C. E., 2015. Introduction to operational modal analysis. John Wiley & Sons, Ltd.

CNR-DT 207 R1/2018, 2018. Guide for the assessment of wind actions and effects on structures. Rome: National Research Council of Italy.

De Gaetano P., Repetto M.P., Repetto T., Solari G., 2014. Separation and classification of extreme wind events from anemometric records. Journal of Wind Engineering and Industrial Aerodynamics 126, 132-143.

EN 1991-1-4, 2005. Eurocode 1: Actions on Structures – Part 1.4: General Actions – Wind Actions. CEN, European Commitee for Standardization. Brussels, Belgium.

Kijewski-Correa T., Kwon D.K., Kareem A., Bentz A., Guo Y., Bobby S., Abdelrazaq A., 2013. SmartSync: An integrated real-time structural health monitoring and structural identification system for tall buildings. Journal of Structural Engineering 139(10), 1675-1687.

Li Q.S., Xiao Y.Q., Wu J.R., Fu J.Y, Li Z.N., 2008. Typhoon effects on super tall buildings. Journal of Sound and Vibration 313, 581–602.

Orlando A., 2021. Full-scale monitoring of the wind-induced response of vertical slender structures, with fixed and rotating masses. Ph.D. Dissertation, University of Genoa, Italy.

Pagnini L., Piccardo G., Repetto, M.P., 2018. Full scale behavior of a small size vertical axis wind turbine. Renewable Energy 127, 41-55.

Pagnini L.C., Piccardo G., 2021. Modal properties of a vertical axis wind turbine in operating and parked conditions. Engineering Structures 242, 112587.

Repetto M.P., Solari G., 2004. Equivalent static wind actions on vertical structures. Journal of Wind Engineering and Industrial Aerodynamics 92, 335-357.

Solari, G., 1982. Alongwind response estimation: closed form solution. Journal of the Structural Division ASCE 108, 225–244.

Solari G., Pagnini L.C., 1999. Gust buffeting and aeroelastic behaviour of poles and monotubolar towers. Journal of Fluids and Structures 13(7-8), 877-905.

Tamura Y., Suganuma S., 1996. Evaluation of amplitude-dependent damping and natural frequency of building during strong winds. Journal of Wind Engineering and Industrial Aerodynamics 59, 115-130.

Improving long-span bridge flutter reliability through gyroscopic stabilizer, considering random aeroelastic loads

Gian Felice Giaccu [1], Luca Caracoglia [2]

[1]*Department of Architecture, Design and Urban Planning, University of Sassari, Alghero, Italy, gf.giaccu@uniss.it*
[2]*Department of Civil and Environmental Engineering, Northeastern University, Boston, MA, USA, lucac@coe.neu.edu*

SUMMARY
Long span suspended bridges are challenging structures generally sensitive to wind effects and to wind-induced instabilities. Torsional rotation of the bridge deck plays an important role for the dynamic stability of the structure. The study proposes to use a gyroscopic device as an active stabilizer of the long span bridge. The proposed apparatus has been modeled as a lumped 3DOF system installed inside a specific section of the bridge deck. To assess effectiveness in increasing the critical wind speed and performance, a numerical study was conducted on a benchmark long-span cable-supported bridge as a function of its gyricity. Deck aeroelastic loads are randomly perturbed to simulate modeling simplifications and measurement errors. Monte Carlo simulations are used to predict flutter probability and efficiency of the stabilizer, within a practical operational range, in the presence of random aeroelastic loads.

Keywords: Long- span cable-supported bridges, Flutter control, Gyroscopic stabilizer

1. INTRODUCTION

The last decades have witnessed significant steps in the evolution of long-span, cable-supported bridges. The need for longer and longer spans necessitates the study of new methodologies to increase the performance of these structures under wind loads. Flutter aeroelastic instability occurs when a bridge is exposed to a wind speed above a certain critical threshold. Above this threshold vertical and torsional deck vibrations couple together (Scanlan and Tomko, 1971).

Gyroscopic devices have routinely been employed in mechanical engineering (Kan et al., 1992) for vibration suppression but more seldom employed in structural engineering. This type of devices is proposed herein to improve bridge reliability against flutter threshold. The main component of the system is a rotating mass with a horizontal angular momentum $\mathbf{\Omega}$ parallel to the section-model of the deck. The mass is connected to the deck by a rotational spring and is schematically depicted in Fig. 1 (Giaccu and Caracoglia, 2021). The system allows relative rotations between the deck cross section model and the rotating mass in the bridge deck plane. The gyroscopic system reacts to the torsional vibrations of the deck coupling torsional vibrations with the other degrees of freedom of the system, transferring the energy from the torsional mode to the other frequencies of the system. A mathematical model of the gyroscopic device has been derived.

The proposed device is effective in suppressing flutter. Robustness against variations of its aeroelastic properties are examined by perturbation of the Scanlan derivatives, simulating modeling simplifications and measurement errors.

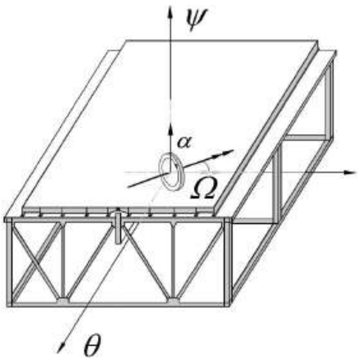

Figure 1. Schematics of 3D bridge model with gyroscopic stabilizer device

2. MODEL DERIVATION

The gyroscopic dynamics is modeled as a system with lumped mass moment of inertia and three rotational DOFs (degrees of freedom) (D'Eleuterio, 1986). Fig. 1 illustrates the rotating mass model geometry. The model assumes a lumped-inertia discretization, where quantities $J_{\Omega,11} = J_{\Omega,22} = J_\alpha$ and $J_{\Omega,33} = J_{\Omega,11} + J_{\Omega,22} = J_{\Omega,\mathrm{p}}$ represent the moment of inertia of the rotating mass with respect to the reference axes 1-1 and 2-2; $J_{\Omega,\mathrm{p}} = M_{\Omega,TOT}\rho_\Omega^2$ is the polar moment of inertia with respect to the rotating axis 3-3, where ρ_Ω is the radius of gyration of the gyroscopic stabilizer and $M_{\Omega,TOT}$ the total mass. The gyricity of the gyroscopic device can be expressed as $\mathbf{\Omega} = J_{\Omega,\mathrm{p}}\boldsymbol{\omega}$ where $\boldsymbol{\omega}$ is the angular velocity vector of the gyroscope. The model equations with DOFs θ, ψ and α are:

$$\begin{aligned} &(J_\theta + J_\alpha)\ddot{\theta} + c_\theta\dot{\theta} + k_\theta\theta = -\Omega(\dot{\psi} + \dot{\alpha}) \\ &(J_\psi + J_\alpha)\ddot{\psi} + c_\psi\dot{\psi} + k_\psi\psi = \Omega\dot{\theta} \\ &J_\alpha(\ddot{\alpha} + \ddot{\psi}) + C_\alpha\dot{\alpha} + k_\alpha\alpha = \Omega\dot{\theta} \end{aligned} \tag{1}$$

The benchmark bridge in Fig. 1 is the Golden Gate Bridge (Jain, 1996). Aeroelastic deck loads are described by Scanlan derivatives. Scanlan derivatives are randomly perturbed about their reference values to account for wind load uncertainties (e.g., modeling simplifications, measurement errors, etc.) The critical flutter speed is evaluated by multimode approach through Monte Carlo sampling, to determine the empirical flutter probability and evaluate the effectiveness of the stabilizer from a reliability perspective

3. PRELIMINARY RESULTS

A numerical investigation has been conducted on the benchmark model of the Golden Gate bridge. The stabilizer is installed in the deck section at ¼ span length. Critical speed has been calculated for a constant gyricity Ω=30000 kg m^2 rad s^{-1}. Structural properties and experimental data of the Scanlan derivatives of the Golden gate are derived from Jain (1996); derivatives are perturbed with independent Gaussian random noises with zero mean and maximum coefficient of variation of 10%. Multimode analysis is employed to study flutter. Preliminary results are shown in Fig. 2 that illustrates the empirical probability distribution of the critical flutter. Results confirm the beneficial effects of the gyroscopic stabilizer in terms of increment of critical flutter speed if compared with the reference solution by Jain (1996), where critical flutter velocity was determined as equal to 22.0 m/s. Nevertheless, the lower tail of the flutter speed distribution is precariously close to uncontrolled bridge value.

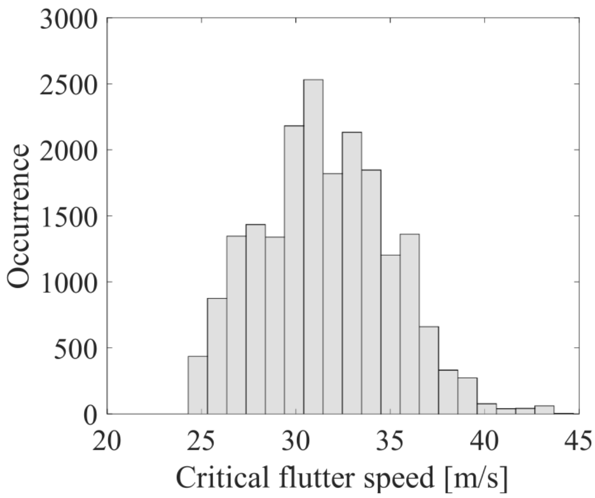

Figure 2. Empirical probability distribution of the critical flutter speed (Golden Gate Bridge case study)

Research is still ongoing. Future studies will further investigate the behavior of the gyroscopic device for structural reliability. Among future research scopes we note the study of the gyroscope as an active stabilizer against buffeting, forcing the bridge deck through active impulsive forces that limit displacement thresholds typical of serviceability limit states.

REFERENCES

D'Eleuterio, G.M.T., 1986. Dynamics of gyroelastic vehicles. Institute for aerospace studies, Toronto. Giaccu, G.F., and Caracoglia, L., 2021. A gyroscopic stabilizer to improve flutter performance of long-
span cable-supported bridges, Engineering Structures 240, 112373.

Jain, A., 1996. Multi-mode aeroelastic and aerodynamic analysis of long-span bridges. PhD Dissertation, Johns Hopkins University, Baltimore, Maryland, USA.

Kan, Y., Psinh, Y., and Lee, A.-C., 1992. Investigation on the steady-state response of a symmetric rotors, Journal of Vibration and acoustics 114.

Scanlan, R.H., and Tomko, J.J., 1971. Airfoil and bridge deck flutter derivatives, Journal of Engineering Mechanics, ASCE 97 (EM6), 1717-1737.

An innovative solution to the direct measurement of fluctuating and peak pressures appropriate to a finite area

Luca Amerio [1], Giulia Pomaranzi [2], Alberto Zasso [3], Andrew Allsop [4]

[1]*Advanced Technology + Research group, ARUP, UK,* luca.amerio@arup.com
[2]*Politecnico di Milano, Via G. La Masa 1, 20156, Milan, Italy,* giulia.pomaranzi@polimi.it
[3]*Politecnico di Milano, Via G. La Masa 1, 20156, Milan, Italy,* alberto.zasso@polimi.it
[4]*Advanced Technology + Research group, ARUP, UK,* andrew.allsop@arup.com

SUMMARY
Wind tunnel testing is one of the available techniques to accurately estimate wind pressure on building facades, especially for high-rise or unusually shaped buildings, where the standards are considered not reliable. During such tests, pressures are usually acquired through single-point measurements and are then made representative of a finite area by using a temporal filter to remove fast transient events. This process is assumed to be equivalent to an area-averaging operation, removing small negligible pressure peaks. Being the equivalence between the time domain filter and the spatial averaging procedure widely questioned in the current literature, in this paper we will propose a novel measurement device that allows to completely overcome the need of a time-space equivalence, allowing direct measurement of the area-averaged pressure field. The accuracy of the novel device is assessed through a comparison with the real area-averaged pressure, calculated using high-resolution pressure measurements.

Keywords: Wind Tunnel Tests, Pressure Measurements, Pressure Peak, Cladding Load

1. INTRODUCTION

During cladding pressure wind tunnel tests, wind pressure is usually measured on few hundreds pressure taps distributed across the surface of the building. The data measured by these are then post-processed and the design wind pressure is extrapolated to derive the design wind pressure acting on each area of the surface. Since the designer is usually interested in a design pressure value representative of the peak spatially-averaged pressure acting on the surface, it is common practice to post-process pressure time histories using a low-pass filter in the time domain (often a moving average filter), removing fast pressure events. The analogy of a time-filtering to an area-averaging was first popularized by T.V. Lawson in (Lawson, 1976) and in (Lawson, 1980) introducing the so-called TVL equation:

$$T = KV/L$$

where the appropriate moving-average window size T was assumed to be proportional to the reference wind speed V, a characteristic length L times a fixed constant K. This approach spread rapidly in the wind tunnels, and it is now considered the best practice.

In (Amerio, 2018) and (Pomaranzi et al., 2022), it was shown how the hypothesis underpinning the TVL equation of a direct linear proportionality between the averaging area characteristic length L and the equivalent moving average span T was flawed and not universal.

A possible approach to solve this is to work around completely the time-averaging post-processing step and measure directly the area averaged pressure value by mean of a modified pressure tap. The idea of a pneumatic average to solve the area-averaging problem was firstly proposed by Surry and Stathopoulos (Surry and Stathopoulos, 1978), that experimentally assessed the performance of a pneumatic averaging device which interconnects tubes connected to different pressure taps distributed over a finite area. Other examples may be found in (Gumley, 1984), (Holmes, 1984) and (Kareem, 1989).

In this paper the authors propose a different solution realized by a thin porous panel placed in front of a small cavity within which the pressure is measured with a usual pressure tap. A photo of the device can be seen in Figure 1a. We will present the results of an experimental campaign aimed at validating the performance of such device and at understanding the effect of design choices (e.g. the porosity of the front surface) on the final measured value.

The basic structure of the paper should be: Introduction, Methods (background and/or materials), Results, Discussion, Conclusions, Acknowledgments, References. Preparation of figures and tables must follow the indications provided on the next pages. All pertinent references should be included.

(a) The device

(b) Devices with different values of porosity

Figure 1. The proposed device to the direct measurement of the area-averaged pressure

2. EXPERIMENTAL SETUP

The proposed devices were realized using a 3D-printing technique for the main body and a thin PMMA laser-cut disc for the front face. The interior of each device was then connected to a PSI ESP-32 HD high-speed pressure scanners connected to a data acquisition system with a sampling frequency equal to 500 Hz.

The front area of the devices was chosen equal to the wanted averaging area, corresponding to about 8 square meters in scale 1-to-50. After fixing this, the geometry of the device is essentially defined by the following parameters:

- depth of the device chamber
- porosity value of the outer plate
- diameter of the pores drilled in the outer plate

To understand the behaviour of the proposed device in different flow conditions, a prismatic model with 24 measuring positions was tested. 22 different combinations - summarized in Table 1 - of the above-mentioned parameters were realized. Each individual device was then tested in each position for each flow configuration.

A 23th reference pressure tap was realized with an aluminum disc with the same frontal area of the averaging devices and equipped with 253 pressure taps. This allowed to measure the pressure field in each position with extreme detail. The measured pressure field could then be area-averaged analytically obtain the reference area-averaged value for each location.

Table 1. Combination of geometrical parameters of the devices used in the test

Porosity [%]	Hole Diameter [mm]	Depth [mm]
15	1	30
40	1	30
20	1	30
10	1	30
30	0.5	30
30	2	30
30	1	40
30	1	15
30	1	10
30	1	20
10	1	40
10	1	20
40	1	20
40	1	40
40	0.5	30
10	0.5	30
10	2	30
40	2	30
30	0.5	40
30	0.5	20
30	2	20
30	2	40

Figure 1a shows an example of two devices characterized by different geometrical parameters, while Figure 2 shows the tested device installed on the model. Each device is instrumented with one pressure tap on the back of the device, as clarified in Figure 1b.

Figure 2. Devices installed on the building model

Figure 3 shows the top view of the building model to clarify the positions where each device has been placed: two of them are on the roof and positions from F101 to F111 are placed at 1m from the ground, while the remaining ones (F112 to F121) are close to the top edge at 2m height.

The model was tested considering three wind exposures, i.e. 0deg, 90deg and -10deg, as depicted in Figure 3.

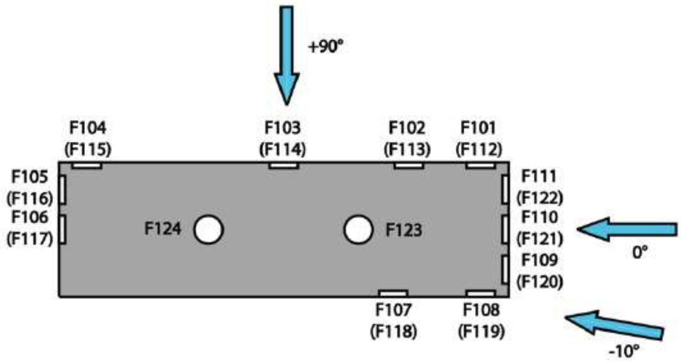

Figure 3. Positions on the building model and wind exposures considered in the tests

3. RESULTS

Results in the full paper will focus on analysing the capability of each device to reproduce the true area-averaged pressure (as measured with the reference pressure tap); and the dependency of this on the geometry of each device. This dependency will then be studied for each angle of attack and position on the building, and the configuration leading to the smallest error for all the positions will be discussed.

REFERENCES

Amerio, L., Experimental high-resolution analysis of the pressure peaks on a building scale model facades. PhD thesis, Italy, 2018.

Gumley, S., A parametric study of extreme pressures for the static design of canopy structures. Journal of Wind Engineering and Industrial Aerodynamics, 16(1):43–56, 1984.

Holmes, J., Effect of frequency response on peak pressure measurements. Journal of wind engineering and industrial aerodynamics, 17(1):1–9, 1984.

Kareem, A., Cheng, C.-M. and Lu, P. C., Pressure and force fluctuations on isolated circular cylinders of finite height in boundary layer flows. Journal of Fluids and Structures, 3(5):481–508, 1989.

Lawson, T.V., The design of cladding. Building and Environment, 11(1):37–38, 1976.

Lawson, T.V., Wind Effects on Buildings: Design Applications, volume 1. Spon Press, 1980.

Pomaranzi, G., Amerio, L., Schito, P., Lamberti, G., Gorlè, C. and Zasso, A., Wind tunnel pressure data analysis for peak cladding load estimation on a high-rise building. Journal of Wind Engineering and Industrial Aerodynamics, 220:104855, 2022.

Surry, D. and Stathopoulos T., An experimental approach to the economical measurement of spatially-averaged wind loads, Journal of Wind Engineering and Industrial Aerodynamics, 2(4):385–397, 1978.

Bridge flutter stability in turbulent flow

Niccolò Barni [1], Massimiliano Gioffrè [2], Claudio Mannini [1]

[1]CRIACIV/Department of Civil and Environmental Engineering, University of Florence, Florence, Italy, niccolo.barni@unifi.it,claudio.mannini@unifi.it
[2]Department of Civil and Environmental Engineering, University of Perugia, Perugia, Italy, massimiliano.gioffre@unipg.it

SUMMARY
Despite the scientific community's effort in studying suspension bridge flutter stability, the influence of turbulence has not been completely understood yet. This work aims to investigate the alteration of the flutter stability threshold due to the effect of large-scale turbulence on self-excited forces. First, Floquet multipliers are used to study the stability of the periodic system obtained by simplifying the slowly-varying angle of attack due to turbulence. Then, the stochastic stability of a 3-Dof system and of a complete suspension bridge is addressed via a Monte Carlo method. The paper emphasizes the significant effect on flutter stability of large-scale turbulence and partial correlation along the bridge girder of wind velocity fluctuations.

Keywords: Nonlinear self-excited forces, flutter stability, time-variant system

1. INTRODUCTION

The coupled flutter stability has thoroughly been investigated in the last decades. However, the question about turbulence effects on stability remains largely unanswered. Generally, bridge flutter is addressed with self-excited forces, usually considered unaffected by atmospheric turbulence. Quite the opposite, the latter introduces different sources of randomness in some of the fundamental parameters of self-excited forces. Along this line, Bucher and Lin (1988) studied the stability of the second statistical moment of the bridge response for a simplified Gaussian random variation of the mean wind velocity. The flutter stability threshold may also be affected by the random angle of attack produced by large-scale turbulence. Indeed, aerodynamic derivatives often strongly depend on the angle of attack (e.g., Argentini et al., 2020; Barni et al., 2021). This dependence translates into a random variation of bridge aerodynamics when large changes in the angle of attack occur. First, the current work addresses this problem in a simplified form, namely assuming a sinusoidal variation of the angle of attack and a three-degree-of-freedom (3-Dof) system. Then, the stability of the same 3-Dof system and a full-bridge structure immersed in a real turbulence wind field is determined through a Monte Carlo approach.

2. MODELLING APPROACH

Time-variant self-excited forces are modelled based on the rational function approximation of the aerodynamic derivatives measured for different mean angles of attack (Barni et al., 2021). Indeed, the model interprets the effect of large-scale turbulence as a slow variation of the angle of attack. The bridge dynamics is described through a state-space differential equation [linear time-variant model (LTV)], where the state matrix depends on time through the slowly-varying angle of attack $\tilde{\alpha}$, as explained in detail in Barni et al. (2022).

First, $\tilde{\alpha}$ was simply assumed as a sinusoidal function with amplitude A and frequency f, simulating a sinusoidal gust. This leads to a periodic dynamic system, whose stability can be studied with the Floquet theory. A simple 3-Dof model of the Hardanger Bridge, Norway, is used as a case study (Barni et al., 2021). Fig. 1(a) shows the evolution of the flutter stability threshold through different curves (one for each mean wind velocity considered), representing the values of A and f for which a Floquet multiplier reaches the value of one. The dynamical system highlights a more stable or unstable behaviour depending on the sinusoidal gust frequency. In particular, typical features of nonlinear dynamic systems are apparent, such as parametric resonances for forcing frequencies that are either multiples of the torsional one or algebraic sums of multiples of the latter and of the lateral or vertical frequencies (Lin 1996). The variability of the stability threshold is mainly due to the aerodynamic coefficient A_2^*, which shows positive values (negative aerodynamic damping in torsion) for $\tilde{\alpha} > 4.5$ deg. This simple analysis helps understand how the slowly-varying angle of attack comes into play in bridge flutter onset.

However, the angle of attack produced by atmospheric turbulence is a broad-band stochastic process. In this case, the flutter stability limit can be assessed by using a Monte Carlo approach. The same 3-Dof dynamic system is analyzed considering the turbulent wind field estimated for the Hardanger Bridge site (Barni et al., 2022). Fig. 1(b) shows that the LTV model predicts a flutter stability threshold 20% lower than the classical linear time-invariant (LTI) model. Similar results were also observed for a full bridge structure (Barni et al., 2022), where a key role is played by the partial correlation of the angle of attack due to turbulence that modulates the self-excited forces.

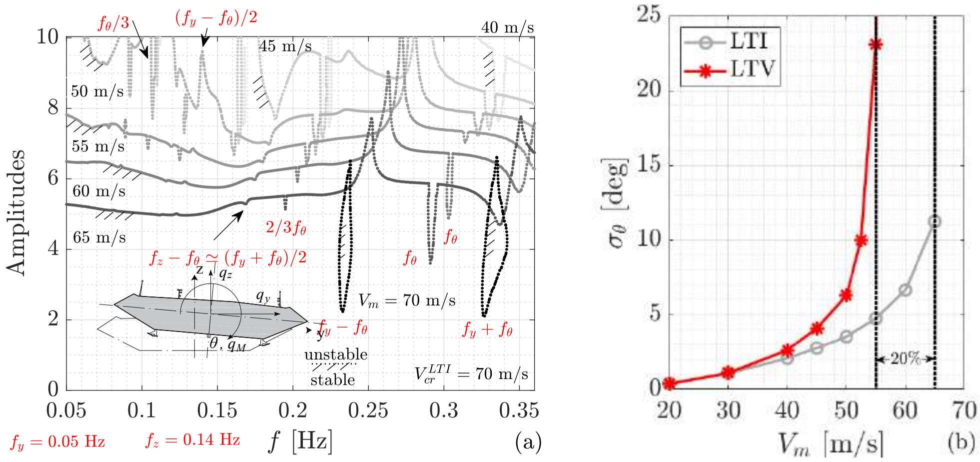

Figure 1. (a) Stability map obtained for different amplitudes and frequencies of the input gust and different mean wind velocities. V_{cr}^{LTI} represents the time-invariant flutter threshold. (b) RMS of the torsional buffeting response for the 3-Dof bridge system.

REFERENCES

Argentini, T., Rocchi, D. and Somaschini, C., 2020. Effect of the low-frequency turbulence on the aeroelastic response of a long-span bridge in wind tunnel. Journal of Wind Engineering and Industrial Aerodynamics, 197, 104072.

Barni, N., Øiseth, O. and Mannini, C., 2021. Time-variant self-excited force model based on 2D rational function approximation. Journal of Wind Engineering and Industrial Aerodynamics, 211, 104523.

Barni, N., Øiseth, O. and Mannini, C., 2022. Buffeting response of a suspension bridge based on the 2D rational function approximation model for self-excited forces. Engineering Structures, 261, 114267.

Bucher, C.G. and Lin, Y.K., 1988. Stochastic stability of bridges considering coupled modes. Journal of Engineering Mechanics, 114(12), 2055-2071.

Lin, Y. K. 1996. Stochastic stability of wind-excited long-span bridges. Probabilistic engineering mechanics, 11(4), 257-261.

Shared infrastructures for wind engineering: the European project ERIES

Maria Pia Repetto [1], Massimiliano Burlando [1], Giuseppe Piccardo [1]

[1]*Department of Civil, Chemical and Environmental Engineering, University of Genoa, Italy,*
repetto@dicca.unige.it – massimiliano.burlando@unige.it – giuseppe.piccardo@unige.it

SUMMARY
In June 2022, Project ERIES "Engineering Research Infrastructures for European Synergies", funded in the framework of the Horizon Europe research and innovation programme 2021-2027, will began. The project will provide research institutes and companies all over Europe with transnational access to experimental testing facilities for earthquakes, wind, and geotechnical engineering for 4 years. The project aims at boosting experimental research through advanced laboratory synergies and capabilities not generally available worldwide, developing new and innovative techniques to improve the response of the structures to multiple hazards to result in more integrated mitigative solutions, and promoting a more harmonized and integrated community of research infrastructures (RIs) across Europe.

Keywords: shared European research infrastructures, boundary-layer wind tunnel, scanning lidar

1. INTRODUCTION

Natural hazards continue to cause immense harm worldwide through their direct and indirect impacts on the built environment, the economy and the overall functionality of society. In particular, direct damage, financial losses and operation interruptions caused by windstorms are critical issues that still need to be fully addressed via innovative research and development. For instance, during the past decades, strong windstorms have induced severe human losses and extensive damage to properties: the great storm of 15th October 1987 caused €5M in damage and killed 34 people in France and the United Kingdom; the Lothar and Martin storms in December 1999 caused €13.5M of damage in Europe and killed 125 people. These impacts of windstorms are continually growing in terms of economic losses along with their occurrence frequency as a result of climate change. The database of the European Severe Storm Laboratory (ESSL, Dotzek et al., 2009) documents almost 60,000 cases of structural damage and collapse due to extreme winds recorded in Europe in the last 3 years. According to Munich Re (GeoRisk Research Group), windstorm-related economic losses are 28% of all natural hazards and 45% in terms of fatalities.

Society is still somewhat behind in addressing important "open" issues in the design and retrofit of structures against natural hazards and more shrewdly oriented research is required to address them. In this context, Project ERIES "Engineering Research Infrastructures for European Synergies" (coordinated by IUSS, Italy) was funded under the Horizon Europe framework programme to offer transnational access to the best European experimental testing facilities for earthquakes, wind, geotechnical engineering and structural interaction with the aim of developing new and innovative techniques to improve the response of structures and infrastructures to multiple hazards.

2. SHARED EXPERIMENTAL FACILITIES FOR WIND ENGINEERING

Regarding wind engineering, the European experimental facilities for civil and environmental tests have a strong tradition related to classical boundary layer wind tunnel (BLWT) tests, capable of reproducing the effects of synoptic extra-tropical cyclonic winds on structures and structural elements, as well as on the built environment. They serve a wide range of public and private companies and furnish great impact on theoretical and industrial research and engineering standard sector. On the other hand, European facilities are lacking in some aspects, such as the absence of BLWT facilities in many countries prone to wind storms, the absence of advanced facilities for simulation of non-synoptic wind phenomena and the lack of integrated laboratory and free field experimental facilities.

ERIES involves four major research organisations in Europe and North America, offering some of the most advanced facilities for wind engineering worldwide, including two BLWTs used to assess wind loads on structures, structural elements and complex environments from small scale experiments; two large-scale BLWTs equipped with climate control capacities; two worldwide unique advanced facilities capable of replicating large scale synoptic and non-synoptic winds as well as their combination and their effects on the built environment; a facility able to simulate full-scale aerodynamic pressures experienced during severe storms on typical building; one advanced Doppler Wind Lidar system for monitoring high resolution continuous free-field wind flow.

2.1. The experimental facilities offered by the University of Genoa

In the context of ERIES project, the Giovanni Solari Wind Engineering and Structural Dynamics (GS-WinDyn, http://www.gs-windyn.org) Research Group of the University of Genoa (Italy) will open to transnational access two facilities:

1. Closed-circuit Atmospheric Boundary Layer Wind Tunnel
2. Doppler Wind Lidar system – Leosphere WindCube 400S

The Atmospheric Boundary Layer (ABL) Wind Tunnel is a closed loop subsonic circuit, with a maximum wind velocity of about 32 m/s. The working section is 8.8 m long, with a cross-section of 1.70 (width) × 1.35 (height) m. The wind tunnel features two different test sections: one test section located immediately after the contraction cone, at the beginning of the working chamber, mainly used for aerodynamic and aeroelastic testing of sectional models; a second test section placed at the end of the working chamber equipped with an automated turning table and mainly used to evaluate the action of wind on structures, the pedestrian comfort, and to analyse the wind fields in topographically complex terrain.

The WindCube 400S is a state-of-the-art heterodyne pulsed Doppler Lidar which can scan the atmosphere using fully configurable PPI (Plan Position Indicator) and/or RHI (Range Height Indicator) mixed patterns or DBS (Doppler Beam Swinging). It is the most powerful scanning Lidar produced by Vaisala-Leosphere (https://www.vaisala.com/en/wind-lidars), one of the leading companies in wind Lidar technology worldwide, with the capability to take measurements up to ranges of 15 km and 50 m physical resolution. The instrument is installed on a quay at 5 m above sea level within the port of Genoa (Burlando et al., 2020).

REFERENCES

Dotzek, N., Groenemeijer, P., Feuerstein, B., and Holzer, A. M., 2009. Overview of ESSL's severe convective storms research using the European Severe Weather Database ESWD. Atmospheric Research 93, 575- 586.

Burlando, M., Romanic, D., Boni, G., Lagasio, M., and Parodi A., 2020. Investigation of the Weather Conditions During the Collapse of the Morandi Bridge in Genoa on 14 August 2018 using Field Observations and WRF Model. Atmosphere 11, 724.

Aerodynamic loads on wind turbine towers arranged in groups with and without helical strakes

Claudio Mannini [1], Tommaso Massai [1], Andrea Giachetti [1], Alessandro Giusti [2]

[1] *CRIACIV/DICEA University of Florence, Florence, Italy*
andrea.giachetti@unifi.it, gianni.bartoli@unifi.it, claudio.mannini@unifi.it
[2] *Siemens Gamesa Renewable Energy A/S, Brande, Denmark*
alessandro.giusti@siemensgamesa.com

SUMMARY
This work investigates the aerodynamic behavior of wind turbine towers when they are temporary placed in groups at small distance at the quayside of harbors. In this phase, many different arrangement geometries are possible, which makes wind tunnel tests a precious tool to pursue the economic design of the tower supporting structures. The effects of helical strakes, often employed to mitigate vortex-induced vibrations, is assessed through models at two different scales. The wind tunnel test results revealed complicated features of the problem and stressed the importance of the correct simulation in the experiments of the high Reynolds number regime. In particular, the strakes were found to reduce the mean base moment in the subcritical regime but to increase it in the developed supercritical regime.

Keywords: tower groups, high Reynolds number, helical strakes

1. INTRODUCTION

Offshore wind turbine towers are usually assembled at the quayside of pre-assembly harbors in groups including up to 10-12 towers at a relatively small distance (say, less than two diameters), prior to being loaded onto special ships for the final offshore installation. Pre-assembly activities usually last 6 to 12 months. An accurate estimate of static and dynamic wind loads (in particular, the resultant base moment) in this temporary condition is crucial for the optimization of the design of the tower supporting structures (e.g., interfaces and foundation).

In the literature, most of the results refer to groups of infinite circular cylinders in smooth flow (e.g., Price and Paidoussis, 1984; Sayers, 1988) rather than finite towers in turbulent shear flow. Moreover, the wind actions on each tower are strongly dependent on the specific geometric configuration of the group (in terms of number of towers, grid arrangement and centre-to-centre spacing), which makes necessary specific wind tunnel tests.

The most challenging issue in the study of the aerodynamics of groups of towers is the very high Reynolds number expected at full scale for the design wind speed, which cannot be matched, and in many cases not even approached, in the wind tunnel. Another peculiar feature of these structures is that they can be equipped with helical strakes to mitigate vortex-induced vibration (Zdravkovich, 1981). The effect of these aerodynamic appendices is well known for isolated circular cylinders and towers, but it has not been sufficiently studied for groups of closely spaced towers.

The present work investigates the aerodynamic behavior of small groups of tapered towers (up to four towers), arranged according to a square mesh, in terms of base force and moment coefficients. Configurations both with and without helical strakes are considered.

2. CASE STUDY AND EXPERIMENTAL SETTING

The considered towers are located in Taichung, Taiwan. They present a cylindrical lower portion ($0.586 \cdot H$, being H the height of the tower) and a linearly tapered upper part ($0.414 \cdot H$). The diameter at the top of the tower is $0.694 \cdot D_b$, where D_b is the bottom diameter. The strakes have a triangular cross section with a height of $0.025 \cdot D_b$. The center-to-center tower distance is $1.333 \cdot D_b$. Besides the free-standing configuration, a row of two towers, a two-row pack of four towers, and an L-shaped configuration of three towers were tested.

The experimental campaign was carried out in the CRIACIV (Inter-University Research Centre on Building Aerodynamics and Wind Engineering) wind tunnel. The models of the towers were reproduced at a scale 1:130 (Fig. 1), though a model at a scale 1:75 was also employed to further investigate in smooth flow the effect of the strakes. The target turbulent wind profile was satisfactorily reproduced both in terms of mean wind speed and turbulence intensity (Fig. 2). Base forces and moments were measured through a high-frequency force balance placed below the wind tunnel floor. Only one tower was connected to the force balance, while the others were dummies fixed to the turning table of the wind tunnel floor

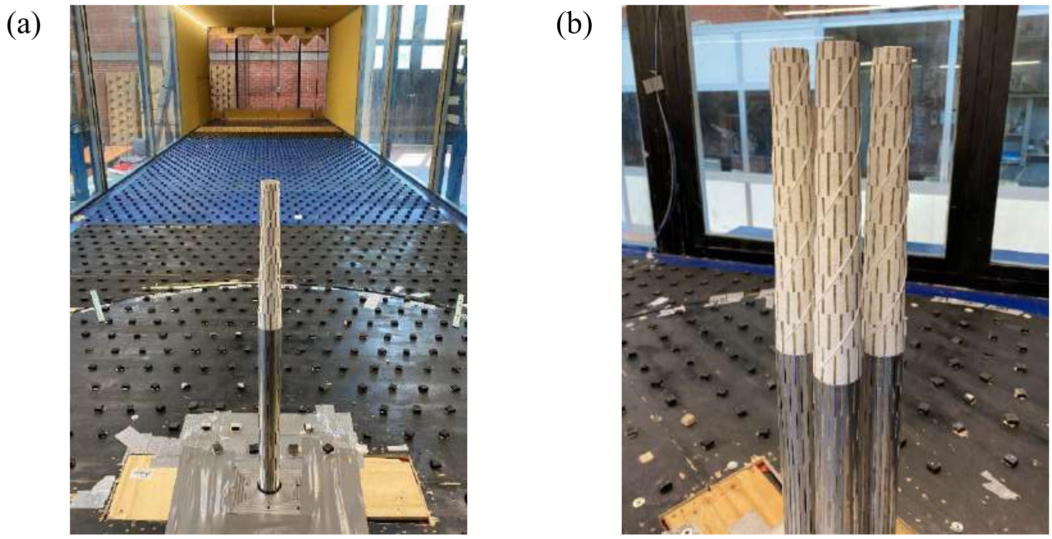

Figure 1. Model of an isolated tower (a) and of a group of four towers mounted in the wind tunnel (b).

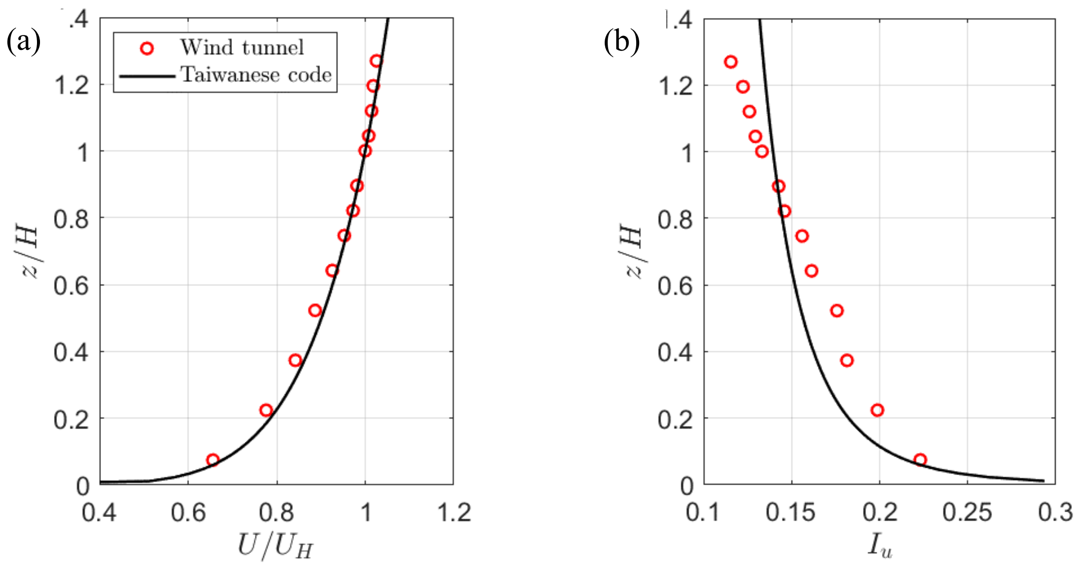

Figure 2. Measured and target mean wind velocity (a) and longitudinal turbulence intensity profiles (b).

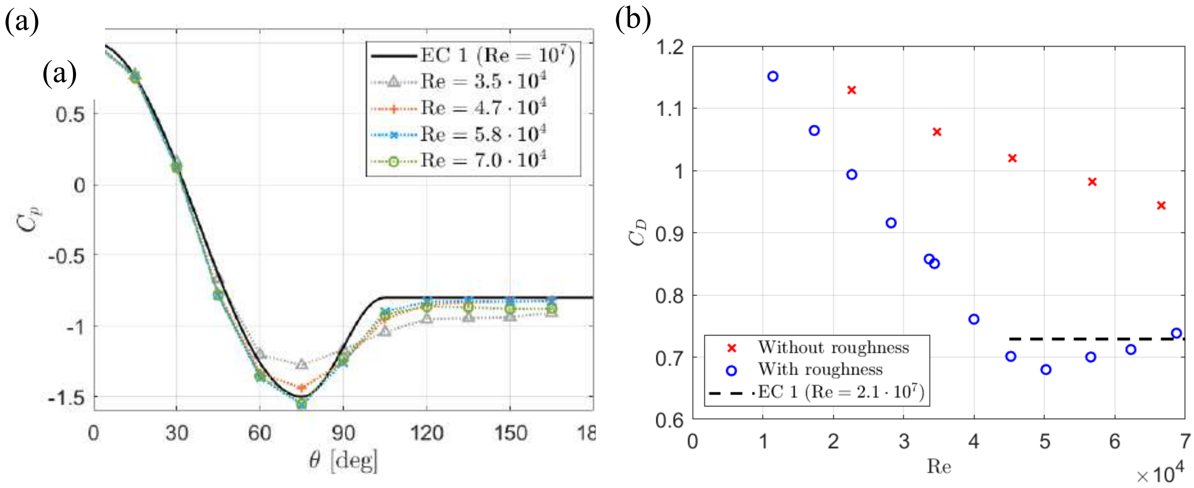

Figure 3. Pressure coefficient distribution (a) and integrated drag coefficient (b) for the confined turbulent flow configuration of a circular cylinder.

3. SIMULATION OF THE SUPERCRITICAL REYNOLDS NUMBER REGIME

The crucial issue in this study was the simulation of the behavior of the towers, either isolated or arranged in groups, at a Reynolds number (Re) of the order of 10^7 (based on an average of the tower diameter and the mean wind speed at the height H), whereas the maximum Re-number attainable in the wind tunnel was lower than 10^5. A developed supercritical Reynolds number regime was then simulated by distributing discontinuous small strips of sandpaper over the surface of the models. The effectiveness of this measure was verified by recording the pressure distribution on a circular cylinder in a confined turbulent flow, for which several data are available for high Reynolds numbers (Mannini et al., 2022). The results are reported in Fig. 3(a) along with the target pressure distribution provided by Eurocode 1 (EN 1991-1-4, 2005). While a subcritical pressure coefficient pattern was found for the smooth cylinder, in the high wind speed range (say, beyond a wind tunnel Reynolds number of about $5 \cdot 10^4$) such a distribution is stable and very close to the target one. This is confirmed by the drag coefficient reported in Fig. 3(b). The same strategy of simulation of the supercritical Re-number regime was then employed also for the three-dimensional towers that are the main object of the current work. The reliability of this approach was also supported by the results obtained for the 1:75 scale model of the isolated tower in smooth flow.

4. RESULTS

Examples of results for a group of two and four towers are reported in Fig. 4 for various wind directions in terms of mean base resultant moment coefficient, defined as follows:

$$C_M = \frac{M}{q_H \int_0^H D(z)\, z\, dz} \tag{1}$$

where M is the base resultant moment, q_H is the mean wind velocity pressure at the height of the top of the tower, and $D(z)$ denotes the diameter of the tower along its height.

For the considered tower spacing, all the group arrangements are associated with an apparent increase of the loads compared to the isolated tower (for the latter, the results are not reported here in the interest of brevity). Moreover, the rise of the base shear force and moment due to the presence of the helical strakes is non-negligible. In contrast, an opposite effect of these devices has been encountered in smooth subcritical flow for the free-standing tower, due to the attenuation of vortex shedding and the attendant drag reduction. This behavior was confirmed by the results in smooth flow obtained for the 1:75 scale model of the tower.

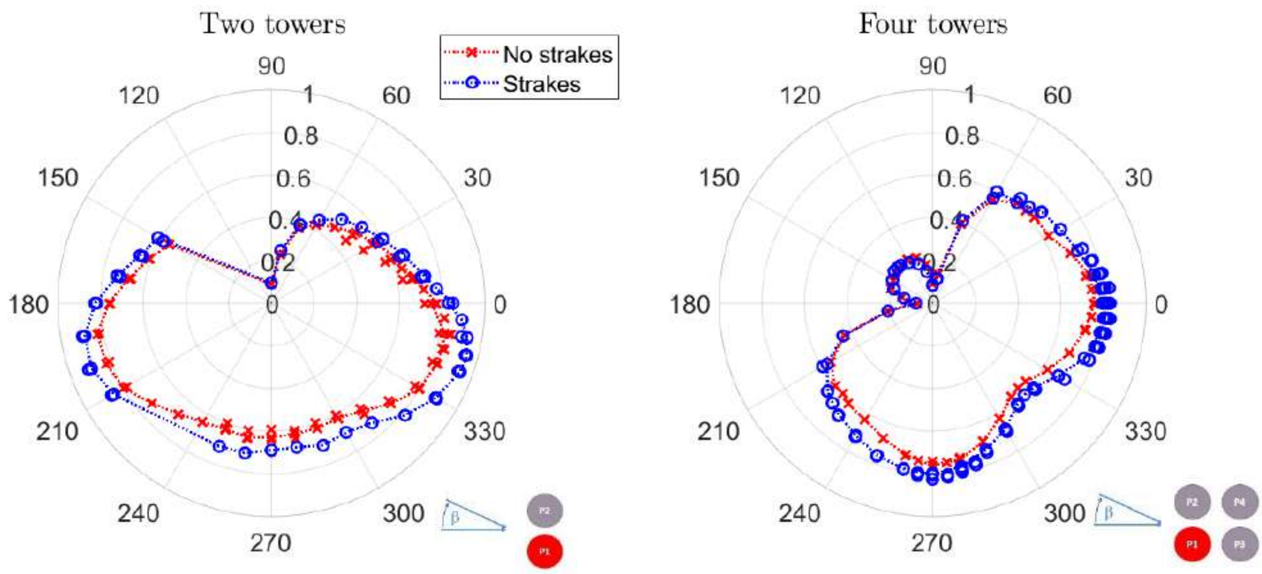

Figure 4. Mean base resultant moment coefficient for the highlighted tower in a group of two and four towers.

5. CONCLUDING REMARKS

This study reveals the complicated aerodynamic behavior of groups of towers at small distance and emphasizes the importance of a correct simulation in the wind tunnel of the high Reynolds number regime expected at full scale.

Despite the limited height of the considered helical stakes, their effect on the aerodynamic loads is clearly detectable, and it is confirmed by the measurements carried out on a larger scale model of the isolated tower. At low Reynolds number, the reduction of vorticity in the wake due to vortex-shedding mitigation is dominant, and the base shear and moment coefficients reduce when the helical strakes are present. In contrast, at high Reynolds number, both in smooth and in turbulent boundary layer flow, a rise of the mean wind loads is observed due to the increased effective diameter of the tower.

The load increment due to the helical strakes is slightly more pronounced for the towers arranged in a group than for the isolated tower, with a growth of the design value of the base moment coefficient of the order of 10%.

REFERENCES

EN 1991-1-4, 2005. Eurocode 1: Actions on structures - Part 1-4: General actions.

Mannini, C., Massai, T., Giachetti, A. and Giusti, A., 2022. Aerodynamic loads on offshore wind turbine towers arranged in groups at the quayside. Proceedings of the 8th European and African Conference on Wind Engineering (EACWE 2022), Bucharest, Romania, in press.

Price, S.J. and Paidoussis, M.P., 1984. The aerodynamic forces acting on groups of two and three circular cylinders when subject to a cross-flow. Journal of Wind Engineering and Industrial Aerodynamics 17 (3), 329-347.

Sayers, A.T., 1988. Flow interference between four equispaced cylinders when subjected to a cross flow. Journal of Wind Engineering and Industrial Aerodynamics 31 (1), 9-28.

Simiu, E. and Yeo, D., 2009. Wind Effects on Structures: Modern Structural Design for Wind. John Wiley and Sons, Oxford, UK.

Zdravkovich, M.M., 1981. Review and classification of various aerodynamic and hydrodynamic means for suppressing vortex shedding. Journal of Wind Engineering and Industrial Aerodynamics 7 (2), 145-189.

Modelling effect of varying fetches of ground roughness – Can we do better?

Andrew Allsop

ARUP, London, United Kingdom, andrew.allsop@arup.com

SUMMARY

The paper will review the theory behind the Harris and Deaves 'strong wind' model as published by the Engineering Sciences Data Unit [ESDU], which is widely used by wind engineers around the world for correction of anemometer data in conditions of variable exposure fetch, for prediction of wind exposure, and in simplified form in various codes of practice.

The package also includes estimations for three-dimensional turbulence properties of intensity, length-scale, coherence and spectral energy. It was issues with these 3D properties in variable fetch conditions that first drew this author's attention to the need for a review.

The paper will further discuss the applicability of local friction velocity, u_z^*, and roughness length parameters, z_{0z}, e.g. following ideas of local equilibrium expressed by Jon Wieringa [e.g Ulden, 1996], to improve and simplify the formulations used.

This work is highly relevant to codification, for which further simplification may be needed.

Keywords: codification, wind profile modelling

1. INTRODUCTION

The ESDU strong wind model [ESDU] has been in use in the industry since the late 1980s and 1990s without major revision. It forms the background for several international codes of practice, including Australian and New Zealand [AS/NZ1170.2], British [BS6399-2] (now superseded), and the UK and Irish National Annexes to the Wind Actions Eurocode [EN1991-1-4], and is referenced as an alternative method by the American Society of Civil Engineers [ASCE7].

The model was mostly developed over a 5-year period between 1982 and 1986 by the Engineering Sciences Data Unit (notably Neil Thompson) guided by a committee led by Tom Lawson, which included Ian Harris, David Deaves, Nick Cook, and a number of 'industrial representatives' including Andrew Allsop. The aim was to provide a usable package of advanced (beyond code) wind engineering capability to build on and sustain the considerable research efforts which had been made in the 1970s and 1980 with funding via the Construction Industry Research and Information Association (CIRIA), the UK Building Research Establishment, and other industry and government research and investment.

At the time state-of-the-art statistical methods and computer programming skills were used to provide a package considered by many that the author has spoken to as a 'black box' calculation, and certainly beyond the skills and experience of this author at that time.

The model was systematically calibrated against high quality wind data where this was available, but perhaps the best testament is that it has subsequently proved very effective for correcting anemometer data from different sites to a common base.

The experience of the author and of others using it (or the underlying Deaves approach)

[Deaves] for correction of anemometer data has been generally very favourable. It has however been observed by the author and others [Irwin] that turbulence length-scales in variable fetch conditions may be outside the limits of the underlying assumptions, indicating some calculation issue that has not been fully resolved.

Through use of independently developed software based on the published ESDU theory, the issues were found to be connected to the modelling of the variation between near surface properties of u^*, z_0 and $\tilde{u}$, and those above the transition height. The height variations of u^*, z_0 and $\tilde{u}$ commence at different heights, resulting unexpected variations of the mean and gust wind profiles and of derived values such as turbulence length-scale.

An alternative simplified procedure was therefore considered by author and compared to the previous version. There are two fixed points of the transition predicted by the Deaves model. At the surface (a height of 2.5 z_0 works well) u^*_0 and other turbulence properties should be in equilibrium with the local mean speed and surface roughness length, z_0, as assessed using the Deaves model. At the top of the transition layer (the matching height) turbulence conditions are assumed unchanged by the change in surface roughness. A new model is based on fitting local u^*_z and z_{0z} parameters between these two points to match the Deaves mean windspeed predictions.

All other turbulence parameters may be plausible derived from these based on a local equilibrium concept e.g. as expressed by J. Wieringa. The paper discusses the considerations of how the local values can be derived and goes on to show that the new model does not substantially change the previous ESDU predictions of mean and gust speeds but reduces unexpected variability.

2. RESULTS AND CONCLUSION

The predicted variation of dynamic wind pressure with effective height from ESDU and from the new model is shown in Figure 1 and Figure. 2 respectively. For the moment, these show hourly-average and 1s gust pressure ratios directly compatible with the original Harris and Deaves work as implemented by ESDU.

The use of pressure factors is intended to emphasise differences between the models. The gust pressure profiles (perhaps q_p equivalent) have been normalised to unit gust pressure at 10m height in open country, z_0 = 0.03m, of infinite fetch. (Note these are full Harris and Deaves wind profiles and the z_0 values do not necessarily match the simplified log-law EN1991-1-4 modelling.)

The fetches used have been chosen to keep the plotted lines largely separated, and in general have been calculated between Sea (ESDU z_0 = 0.003m), Country (z_0 = 0.03m) and Urban (z_0 = 0.3m) in various combinations. Again, to emphasise differences, only the sea to urban fetch transition is included in this abstract. It is intended to include a wider range of cases in a final paper.

Given the emphasis of the differences, the figures in fact show very reasonable agreement of the predicted pressures, but the simplified form and calculation of the curves should allow easier codification. A further advantage is that local values of turbulence intensity, length-scale, and spectra will always be in appropriate equilibrium with the local values of u^*_z, and z_{oz}.

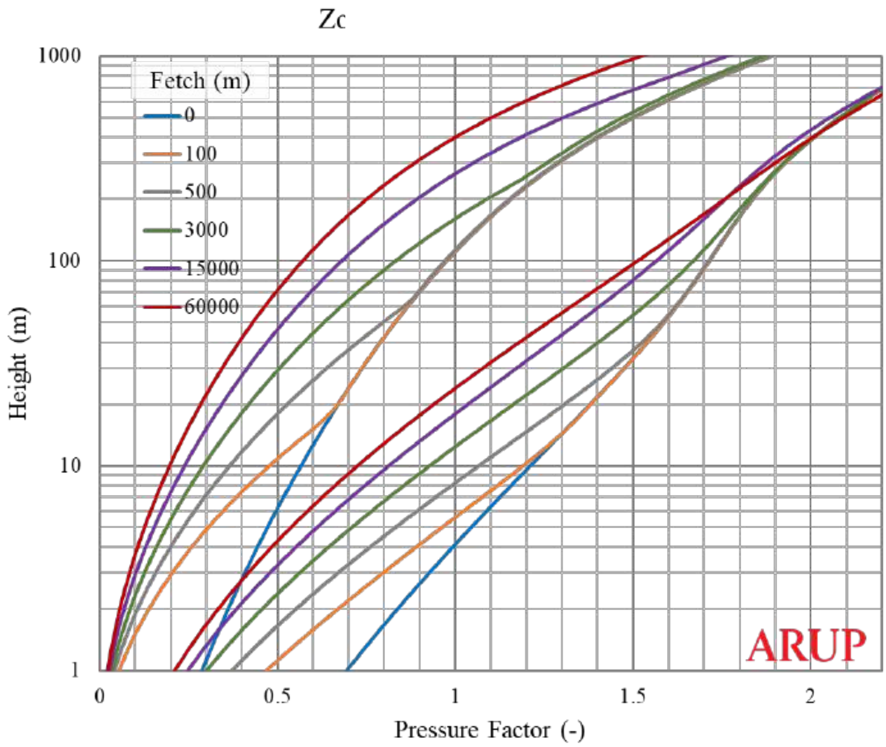

Figure 1. New Harris and Deaves. Sea to urban transition

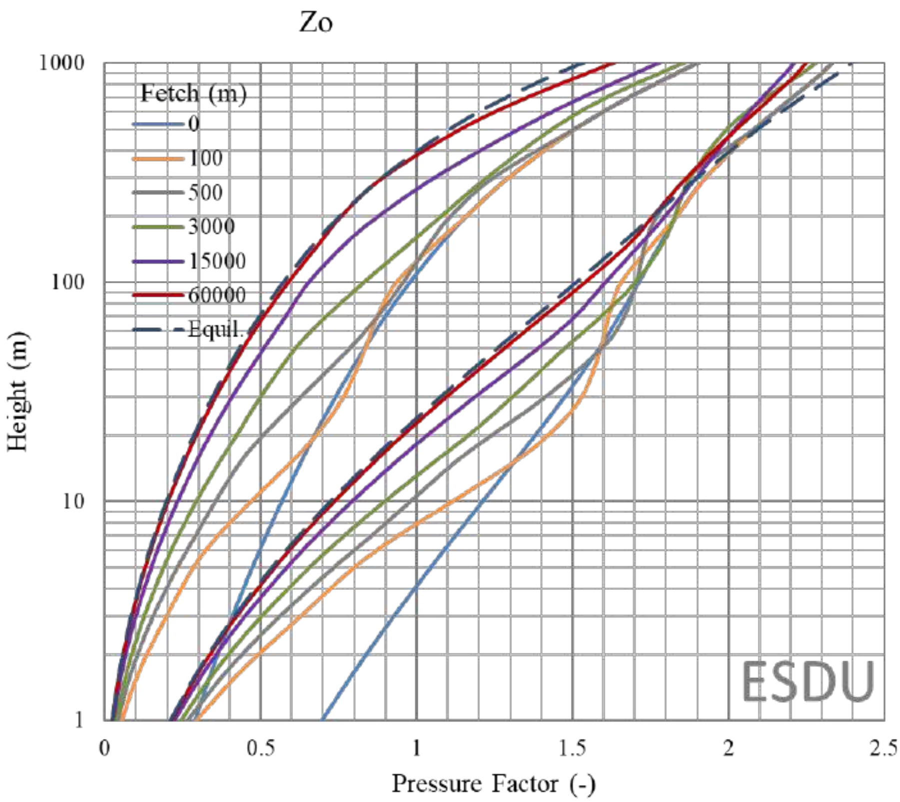

Figure. 2. ESDU 01005. Sea to urban transition

REFERENCES

References subject to amendment may be assumed to be current versions (in 2022) unless otherwise noted.

ASCE7 Minimum Design Loads and Associated Criteria for Buildings and Other Structures, American Society of Civil Engineers, e.g. page 877 of ASCE7-22.

AS/NZ1170.2 Structural Design Actions: Part 2 Wind Actions, Australian/New Zealand Standard

BS6399-2, Loading for buildings – Part 2: Code of practice for wind loads, British Standard, 1997 (2002)

Deaves, D.M., 1981, Computations of wind flow over changes in surface roughness. J. Wind Eng. & Ind. Aero., Vol. 7, pp. 65-94

EN1991-1-4 Eurocode 1: Actions on structures – Part 1-4: General actions – Wind Actions, 2005, incorporating UK or Irish National Annexes

ESDU 82026, 1982, Strong winds in the atmospheric boundary layer. Part 1: Mean-hourly wind speeds. London

ESDU 83045, 1983, Strong winds in the atmospheric boundary layer. Part 2: Discrete gust speeds. London

ESDU 84011, 1984, Wind speed profiles over terrain with roughness changes. London

ESDU 84030, 1984, Longitudinal turbulence intensities over terrain with roughness changes. London

ESDU 85020, 1985, Characteristics of atmospheric turbulence near the ground. Part II: Single point data for strong winds (neutral atmosphere). London

ESDU 86010, 1986, Characteristics of atmospheric turbulence near the ground. Part III: Variations in space and time for strong winds (neutral atmosphere). London

ESDU 86035. 1986, Integral length scales of turbulence over flat terrain with roughness changes. London

Harris, R.I., Deaves, D.M., 1980, The structure of strong winds. Paper 4 of CIRIA Conf. on "Wind Engineering in the Eighties", London

Irwin, P.A., Private communication.

Ulden, A. P. and J. Wieringa, 1996. Atmospheric boundary layer research at Cabauw. Boundary Layer Meteorology, 78, 39-69

Parametric evaluation of the wind induced response in photovoltaic solar trackers using a simplified equivalent wind loads approach

Filippo Calamelli [1], Tommaso Argentini [2], Giorgio Frontini [3], Sara Muggiasca [4]

[1] *Politecnico di Milano, Milan, Italy, filippo.calamelli@polimi.it*
[2] *Politecnico di Milano, Milan, Italy, tommaso.argentini@polimi.it*
[3] *Politecnico di Milano, Milan, Italy, giorgio.frontini@polimi.it*
[4] *Politecnico di Milano, Milan, Italy, sara.muggiasca@polimi.it*

SUMMARY
Nowadays, the improvement of the structural performances of the photovoltaic solar trackers led to the development of lightweight and slender systems, significantly susceptible to turbulent winds. In the current design practice, the wind effects on these kind of structures are typically taken into account with a simplified approach which defines equivalent static wind loads employing the so called Dynamic Amplification Factors (DAFs). Despite its simplicity, the aforementioned procedure is characterized by several drawbacks which restrict its scope of application. In this paper the DAF methodology is compared with a more refined approach varying several parameters to assess its capability to predict the wind induced response, with the main purpose of defining practical design guidelines.

Keywords: Photovoltaic solar trackers, Equivalent wind loads, Dynamic amplification factors, Wind tunnel.

1. INTRODUCTION

In the recent years, the use of Photovoltaic (PV) systems with tracking mechanism significantly increased. These structures are characterized by a longitudinal torque tube to which the solar panel modules are bounded. Furthermore, a series of motor drives allows the panels to align towards the Sun during the day, leading to a greater efficiency with respect to more traditional stationary systems.

Beside the energy efficiency, the structural optimization of the PV trackers led to systems more and more lightweight and slender, significantly sensitive to turbulent wind. Specifically, in the current design procedures, wind effects are taken into account by defining equivalent loads which are statically applied to the structure (Chen and Kareem (2001)). Moreover, it is possible to assess the dynamic response to turbulent wind including in the definition of the equivalent loads the so called Dynamic Amplification Factors (DAFs) (Browne et al. (2020), Taylor and Browne (2020)). This simplified approach requires the knowledge of the spectrum related to the unsteady wind pressures acting on the tracker panels, estimated with wind tunnel tests, and a limited set of structural parameters, i.e. the damping and the frequency of just one modal shape, typically defined employing numerical models.

From a design point of view, the main advantage of the DAF application is the possibility of avoiding more complex and computationally expansive methods which are alternatively required to determine the structural response due to the incoming turbulent wind. Nevertheless, despite its simplicity, the DAF procedure has several drawbacks. First of all it is a method that, to assess the equivalent wind loads, accounts for just one modal frequency, typically the one related to the modal shape more excited by the incoming turbulent wind. In addition, as wind tunnel tests are generally performed on rigid models of the solar trackers, the experimental results can be considered reliable assuming small wind-induced deflection and thus, that the structure is not predisposed to aeroelastic instabilities. Therefore, a comparison with a more refined approach could be useful to investigate the scope of application of the DAF method whose definition, for the aforementioned reasons, is not straightforward.

In this paper, based on a wind tunnel study, the results obtained applying the simplified DAF formulation are compared with those derived by performing numerical simulations which, with a modal approach, directly loads the structure with the experimental time histories of sectional force and torque. Specifically, the comparison is carried out varying a set of parameters, i.e. the structural damping, the inclination angle of the panels with respect to the horizontal (commonly named pitch angle), the exposure of the panels to the incoming wind as well as the spacing between the rows of the PV trackers park. The main purpose of the analysis is to validate the applicability of the DAF approach with the final aim of providing reasonable guidelines for the designers.

2. METHODOLOGY

2.1. DAF approach

In the design practice the wind effects on a structure can be taken into account defining equivalent static wind loads which must take into account both the static action, associated to the mean wind speed, and the dynamic response, mainly due to the resonance effect that occurs when the modal frequencies of the structure approach the range of frequencies of the incoming wind turbulence. The latter can be included in the definition of the equivalent static wind loads adopting the so called DAF methodology. Specifically, integrating the experimental pressures, measured during wind tunnel tests, on a specific surface area of the solar panels, it is possible to assess the time histories of the normal force $F(t)$ and of the torsional moment $M(t)$ applied to the torque tube of the PV trackers. Subsequently, for both of the aforementioned internal forces, the total coefficients related to the equivalent static wind loads are defined as

$$C_{F,\text{total}} = C_{F,\text{static}} \pm C_{F,\text{dynamic}} \tag{1}$$

$$C_{M,\text{total}} = C_{M,\text{static}} \pm C_{M,\text{dynamic}} \tag{2}$$

where $C_{F,\text{static}}$ and $C_{M,\text{static}}$ are derived directly from the time histories and are representative of the mean wind loads and of the background component caused by the pressure fluctuations while, $C_{F,\text{dynamic}}$ and $C_{M,\text{dynamic}}$ take into account the resonant effects and are defined using the DAFs, which are evaluated with the following formulation:

$$DAF = \sqrt{1 + \frac{\pi}{4\zeta}\frac{fS(f)}{\sigma^2}} \tag{3}$$

where ζ is the structural damping, f is the natural frequency of the mode selected, $S(f)$ is the power spectral density associated to the time-varying normal force or torsional moment and σ^2 is the related variance. Afterwards, from the knowledge of these coefficients, it is possible to evaluate the equivalent static wind loads necessary for the design of the PV trackers.

2.2. Numerical simulations

To investigate the applicability of the equivalent static wind loads assessed employing the DAF approach, a modal analysis was performed applying the experimental time histories of the internal forces and of the torsional moments directly to a numerical model of a PV tracker. Specifically, the equations of motion governing the problem can be distinguished in a mean and in a fluctuating component. Gathering the structural parameters from a FE model of a solar tracker, the problem can be easily solved, in modal coordinates, numerically integrating the dynamic equilibrium. As a final results, the total structural response can be defined from the sum of the static and the time-variant dynamic displacements.

2.3. Wind tunnel tests

The experimental data presented in this paper were obtained carrying out tests in the wind tunnel of the Politecnico di Milano. Specifically, the wind pressure distributions acting on the panels surface were evaluated employing rigid models of the structures arranged in a typical configuration of a PV trackers park. Furthermore, the measurements were performed taking into account the variation of different parameters, i.e. the pitch angle of the trackers, the exposure of the panels to the incoming wind and the spacing between the rows of the park. Figure 1 depicts a typical experimental configuration.

Figure 1. Experimental setup of the PV trackers in the wind tunnel of the Politecnico di Milano.

3. RESULTS AND CONCLUSIONS

The main purpose of the current research is to perform a parametric analysis to assess the scope of application of the simplified DAF methodology. Specifically, the aforementioned method is compared with a more refined approach varying a set of significant parameters, i.e. the structural damping, the pitch and the exposure angles of the panels and the spacing between the rows of the array. To illustrate the parametric analysis, a selection of cases of particular interest is presented. Specifically, Figure 2 depicts the comparison between the results coming from the application of the DAF approach (continuous lines) and those of the numerical simulations (dotted lines) in terms of Von Mises stresses along the longitudinal development of the torque tube. Two reference trackers were selected, i.e. the second one of the first row (R1C2) and the second one of the second row (R2C2), and the variation of several parameters is taken into account. First of all, the plots presented are the outcome of an envelope procedure over the all the incoming wind directions. Furthermore, Figure (a) shows the results for a pitch angle equal to 30° and a Ground Cover Ratio (GCR, defined as the ratio of the distance between two rows and the chord of the panels) of 2.65. With respect to Figure (a), the pitch angle is varied to 60° in Figure 2(b) while, in Figure (c), the GCR is increased to 4. At last, two levels of damping ratio are report, i.e. 2% and 10%.

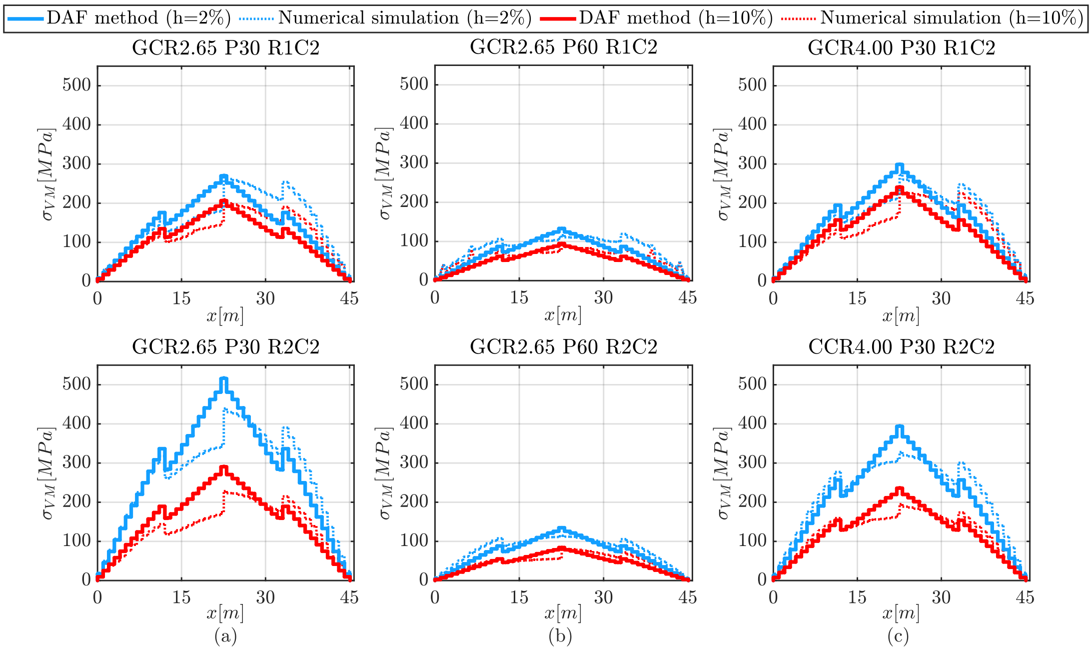

Figure 2. Comparison between the results of the DAF approach and of the numerical simulations, reported in terms of the Von Mises stresses along the torque tube of two solar panels taken as reference case.

As shown in the figures, the DAF approach tends to be conservative, with respect to the numerical simulations, in correspondence of the peak values of the stresses located in the center of the torque tube. Nevertheless, this is not necessarily true for all the sections along the longitudinal development of the structure. As for the pitch angles, the 30° configuration appears to be more critical, mainly in the second row of the array, where the dynamic effects are enhanced by the turbulence generated by the previous row. Indeed, the shielding effect due to the perimetral PV trackers is intensified increasing the value of the pitch angle. Moreover, as confirmed in Figure 2(c), the increase of the GCR seems to have a beneficial effect reducing the stresses in the tracker of the second row. As expected, raising the value of the structural damping, the stresses reduces.

The results reported show that the DAF approach is deemed to be adequate for a rough pre-dimensioning of the structure based on the peak stress values. Nevertheless, to optimize the design of the solar panels, the employment of more accurate approaches would be desirable. However, since alternative methods are often computationally too expansive, a different possibility could be to consider combinations of more localized equivalent wind loads assessed using DAFs coefficients obtained integrating the experimental pressures on different areas, i.e. on the full, half or quarter surface of the solar panels. In the full version of the paper, the set of results will be extended also investigating the effect of different integration surfaces, with the main purpose of defining more detailed and not over-conservative design procedures.

ACKNOWLEDGEMENTS

The results presented in this research were obtained in the development of a project founded by ENEL S.p.A. The authors would like to acknowledge and thank the company for the questions that initiated the development of the presented analysis and the provided technical knowledge.

REFERENCES

Browne M.T.L., Taylor Z.J., Li S., Gamble S. (2020), A wind load design method for ground-mounted multi-row solar arrays based on a compilation of wind tunnel experiments, Journal of Wind Engineering and Industrial Aerodynamics

Chen X., Kareem A. (2001), Equivalent static wind loads for buffeting response of bridges, Journal of Structural Engineering

Taylor Z.J., Browne M.T.L. (2020), Hybrid pressure integration and buffeting analysis for multi-row wind loading in an array of single-axis trackers, Journal of Wind Engineering and Industrial Aerodynamics

Comparison of Wake Oscillator Models to Predict Vortex-Induced Vibration of Tall Chimneys

Saba Rahman[1], Arvind K. Jain[2], S. D. Bharti[3], T. K. Datta[4]

[1]*Research Scholar, Indian Institute of Technology, Delhi, India,* sabarahman807@gmail.com
[2]*Professor, Indian Institute of Technology, Delhi, India,* akjain@civil.iitd.ac.in
[3]*Professor, Malaviya National Institute of Technology, Jaipur, India,* sdbharti@mnit.in
[4]*Adjunct Professor, Malaviya National Institute of Technology, Jaipur, India,* tushar_k_datta@yahoo.com

SUMMARY
A comparative study has been carried out for tapered chimney considering various wake oscillator models available in the literature. These models are Facchinetti, Farshidian and Dolatabadi and Skop and Griffin. Tip displacement of 210m tall, tapered chimney is evaluated. The structure is analyzed using the stated models in first mode oscillation, and their results are compared with Eurocode method-I response. The nonlinear approach is adopted for analyzing wake oscillator models where the solution of the coupled equation is assumed to be non-harmonic, unlike the analytical models, and is solved using the ODE solver of MATLAB. The nonlinear method is then compared with the analytical solution proposed by the mentioned models, confirming that the nonlinear approach should be chosen for analyzing the lightly damped slender structures. It is observed that except for the models proposed by Farshidian and Dolatabadi, other models predict nearly the same responses. The parameters causing the variation among the models are also discussed.

Keywords: Fragility curve, Reliability analysis, Vortex-induced vibration

1. INTRODUCTION

Chimneys are tall and slender structures with circular cross-sections, which are highly prone to wind forces. Wind exerts pressure on the chimneys' walls, producing unwanted forces. Vortex-induced vibration is one of such excitations which can lead to the failure of the chimneys. The vortex-induced force grows due to the shedding of vortices from alternating sides of the structures. It can be modeled as a deterministic or random process depending upon the flow regime. When the fundamental structural frequency comes close to the vortex shedding frequency, self-excited oscillation occurs. The self-excited vibration produces a large amplitude of vibration. Many empirical, semi-empirical and experimental studies have been conducted so far to understand the vortex-induced vibration of the structures. Although conducting experiment studies is tedious, many researchers developed empirical and semi-empirical methods. These methods provide comparable responses as obtained from the experiment and can also be used to find the response of arbitrarily shaped chimneys. With technical and infrastructure advancement, chimneys with arbitrary cross-sections or complex modifications have been developed, which is harder to analyze experimentally.

The present study compares the semi-empirical wake-oscillator models used to predict structures' vortex-induced vibration. These models include those proposed by Facchinetti, Farshidian and Dolatabadi and Skop and Griffin. These models combine a wake oscillator model resembling the Van der Pol oscillator model and a single degree of freedom oscillation model. In order to use these models for estimating the top displacement of chimneys, the first mode vibration of the chimneys is only considered. The modal equation of the chimney constitutes the single degree of freedom model (SDOF). The equations of the wake oscillator model and the SDOF are simultaneously solved using an iterative procedure. The ODE solver of MATLAB is used to carry out the iterative solution. To carry out the comparative study, a tall concrete chimney height of 210m has been chosen with a base diameter of 20m, top diameter of 12m and thickness as 0.3m. The responses of the chimney are also determined using the deterministic model given in Eurocode.

The dynamics of fluid-structure interaction were analytically examined to provide a closed-form solution for vortex-induced vibration and provide responses comparable with the experimental outcomes. Three coupled Van der Pol models, namely, displacement coupled model, velocity coupled model and acceleration coupled model, were used for the wake oscillator equation to predict the fluctuating lift coefficient. It was established by analyzing the coupled models for circular cylinders that the most suitable coupled forcing term was proportional to the acceleration of the structure. Therefore, for this study, only acceleration coupled models have been considered.

The reliability analysis of chimneys due to random vortex shedding

Saba Rahman[1], Arvind K. Jain[2], S. D. Bharti[3], T. K. Datta[4]

[1]*Research Scholar, Indian Institute of Technology, Delhi, India, sabarahman807@gmail.com*
[2]*Professor, Indian Institute of Technology, Delhi, India, akjain@civil.iitd.ac.in*
[3]*Professor, Malaviya National Institute of Technology, Jaipur, India, sdbharti@mnit.in*
[4]*Adjunct Professor, Malaviya National Institute of Technology, Jaipur, India, tushar_k_datta@yahoo.com*

SUMMARY
The literature presents the applicability of reliability principles on wind sensitive structures like tall chimney. Many uncertainties involved in the unreliability of any structure subjected to wind induced vibration which are illustrated in the literature. These uncertainties include randomness of incoming inflow and precision of models used for prediction of wind loadings. A 210m tall, tapered chimney is considered as an illustrative example. The reliability analysis is carried out considering the Vickery and Basu spectral analysis for vortex shedding force. Spectral analysis is carried out in frequency domain considering only fundamental mode. It is concluded from the study that threshold crossing reliability of the concrete chimney is greatly affected by parameter like randomness or turbulent of the incoming low, structural damping and other critical parameters involved in the spectral analysis. Strouhal number appears to be not imparting any influence on the reliability of chimney. The study aims to understand the chimney's behavior in reliability point of view.

Keywords: Fragility curve, Reliability analysis, Vortex-induced vibration

1. INTRODUCTION

Chimneys are generally tall and slender structures with circular cross-sections, which are highly prone to wind forces. Wind exerts pressure on the chimneys' walls, producing unwanted forces. Vortex-induced oscillation is one such excitation that can lead to the failure of the chimneys. Therefore, vortex-induced oscillation of chimneys is of great concern to researchers and practitioners since many failures of chimneys due to vortex shedding have occurred in the past. Consequently, extensive research has taken place on the subject over decades. Many laboratory experiments have been performed to verify the theoretical models proposed to predict vortex-induced forces, including aeroelastic effects. Comparatively, very few prototype measurements have been recorded to verify the proposed theoretical models. Because of this reason, the theoretical models developed with the help of experimental laboratory data are utilized for analyzing the chimneys for vortex-induced forces. This calls for reliability analysis of the predictions of the responses of the chimneys produced due to vortex shedding phenomena. Although several works of literature exist on the vortex-induced oscillation of chimneys, including code provisions, the reliability analysis of chimneys against failure caused due to vortex shedding is scanty.

In the present study, the reliability analysis of chimneys against vortex shedding failure is presented, assuming the uncertainty in vortex shedding phenomena to be more significant than other uncertainties, and hence, the latter is ignored. The vortex shedding is modeled as a stationary random process and is represented by a power spectral density function (PSDF). The PSDF of the tip displacement and vortex force of the chimney is obtained by performing a frequency domain spectral analysis using a matrix approach. For this purpose, both chimney and random wind forces are discretized over several points along with the chimney's height. The method of analysis duly accounts for the aeroelastic effects. The double barrier threshold crossing level, as proposed by Vanmarcke, is used for determining the probability of crossing different threshold levels of the tip displacement of the chimney. The reliability estimate is derived from the fragility curve. A 210m tall concrete chimney with a base diameter of 20m, top diameter of 12m and thickness of 0.3m has been taken as an illustrative example. From the study, it is clear that turbulence intensity highly governs the reliability analysis. Other parameters like structural damping and correlation length can also lead to structural failure. Strouhal number, on the other hand, does not affect the structure's response.

The study's results proved that the assumed structural damping, turbulence intensity, correlation length, and lift coefficient significantly influence the threshold crossing reliability of the peak displacement of the chimney. It can also be observed from the paper that the influence of the Strouhal number is negligible on the fragility curve. The influence of turbulence intensity is also examined for the high-rise chimney. As the turbulence intensity increases, the wake region of the chimney gets destroyed, reducing the structure's transverse motion. Turbulence intensity also decreases the correlation length of the structure. The higher the turbulence intensity, the lower the response of the structure; thus, the probability of failure of the structure is meager.

Similarly, the influence of the correlation length shows that at a high correlation length, the eddies formation in the wake region of the chimney is correlated, leading to a narrow band vortex lift spectrum, thus higher response of the structure. The lift force acting on a section of the structure is not perfectly correlated with the lift force at another section, but for simplification, it is assumed to be perfectly correlated for a limited section along the height of the structure. This is known as correlation length, generally expressed in terms of the diameter of the structure. Vickery & Basu has assumed the correlation of one diameter.

Wind loads on unclad automated rack supported warehouses

A. M. Marra [1], T. Massai [1], B. Nicese [1], G. Bartoli [1]

[1] *CRIACIV/Department of Civil and Environmental Engineering, University of Florence, Firenze, Italia.*
Email: antoninomaria.marra@unifi.it; tommaso.massai@unifi.it; bernardo.nicese@unifi.it; gianni.bartoli@unifi.it

SUMMARY
Wind tunnel tests were carried out for estimating the wind loads of typical configurations of rack frame blocks, displayed during the erection phases of automated rack supported warehouses. Aerodynamic coefficients of rack frame members were also measured and used for the direct estimation of the wind loads on isolated uprights and pallet beams as well as to calibrate the wind tunnel test results of the rack frame blocks tested. Base shear forces and overturing moments at the base of each rack frame were used to develop a design method, which allows for the safety checks of the structure as well as the design of temporary bracings.

Keywords: Automated rack supported warehouses, Erection phases, Wind loads

1. INTRODUCTION

The use of Automated Rack Supported Warehouses (ARSWs) has been becoming more and more common in last years. During the erection phases, ARSWs appear as a “steel forests” directly exposed to the wind. The partial collapses due to wind loads occurred during the construction of these structures highlighted the importance of a proper estimation of the wind loads.

The literature is lacking in this specific field, just a wind tunnel test campaign can be found in the paper of Möll and Thiele (1972). Few experimental works have been developed on open framed structures (*e.g.*, Melling, 1978; Sykes, 1978; Jacobs, 1978; Chow, 1978; Georgiou and Vickery, 1979; Whitbread, 1979), which cannot be directly applied for the estimation of the wind loads on RSWs due to the different geometry. The work on open framed structures have been mainly used for the design of petrochemical structures thanks to the development of some guidelines (Nadeem and Levitan, 1997; ASCE. 2011).

This paper proposes a design method for estimating the wind loads on unclad ARSWs based on the results of a new wind tunnel experimental campaign. The tests were carried out on several configurations of three-dimensional automated multi depth shuttle RSWs during construction phases as well as sectional models of their uprights and pallet beams.

The next section is dedicated to the description of the wind tunnel test campaign in which a selection of the results is also reported. Section 3 refers to the proposed design method. Finally, some concluding remarks are reported.

2. WIND TUNNEL TESTS

The wind tunnel tests were carried out in the CRIACIV atmospheric boundary layer wind tunnel on scaled models of typical configurations of rack frame blocks together with portions of uprights and pallet beams. The former models were built to measure the shear force and the overturning moment at the base of a rack frame, called hereafter "measuring frame", for configurations formed by a progressively increasing number of frame racks in front and behind the measuring one (Figure 1). A total of 113 configurations of accompanying frames around the measuring one were tested. The angles of attack considered ranged from 0° to 40°.

The results obtained through the tested configurations are reported in terms of "shielding" coefficients ($\Psi_{F,n_L}^{n_W}$) according to the following relationship:

$$\Psi_{F,n_L}^{n_W}(\alpha) = \frac{C_{F,n_L}^{n_W}(\alpha)}{C_{F,0}^{0}(\alpha)} \in [0,1] \tag{1}$$

where $C_{F,n_L}^{n_W}(\alpha)$ is the aerodynamic force/moment coefficient (drag/lift/moment) for the configuration with n_w accompanying frames in front of the measuring one and n_L accompanying frames behind it, $C_{F,0}^{0}(\alpha)$ represents the aerodynamic force/moment coefficient (drag/lift/moment) for the isolated rack frame. For the sake of brevity, Figure 2 reports only the shielding coefficients for the drag coefficients obtained in configurations characterized by an angle of attack equal to zero.

Regarding the wind load estimation on the portions of rack elements, static tests were carried out on 15 sectional models by rotating the element installed in the test chamber around its longitudinal axis to simulate different incoming flow directions and, for each of them, to measure aerodynamic forces induced by wind. Aerodynamic forces were measured with the angle of attack α value varying between 0° and 180°, considering that all tested profiles exhibit at least one axis of symmetry. The angle was changed 5° by 5°, with a shorter step close to α = 0°.

Figure 1. Three-dimensional model of the rack: a) single measuring rack frame, b) model in the test chamber.

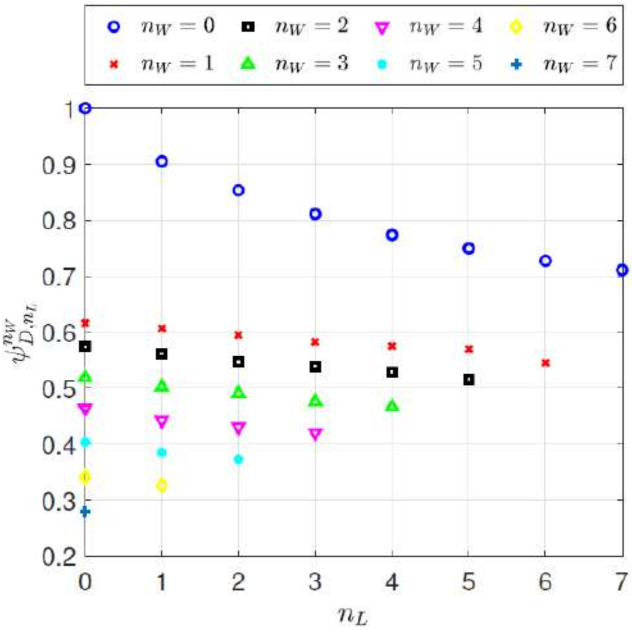

Figure 2. Shielding coefficients of the drag coefficients for configurations with angle of attack equal to zero.

Force measurements were employed to calculate the aerodynamic coefficients. Regarding the definitions of the drag and lift coefficients: $C_D = F_D/0.5\rho V^2 BL$ and $C_L = F_L/0.5\rho V^2 BL$, where F_D and F_L are, respectively, drag and lift force mean values, V is the incoming wind velocity, L = 1.04 m is the length for all the elements and B is the across-flow dimension of the cross-section at α = 0°, while D is the along-wind one. For the sake of brevity, Figure 3 reports just the drag coefficients of the uprights.

As shown in Figure 3, upright results exhibit a large scatter in terms of drag coefficients, probably due to the larger number of differences between their Ω-shaped section geometries and the different distribution of the openings.

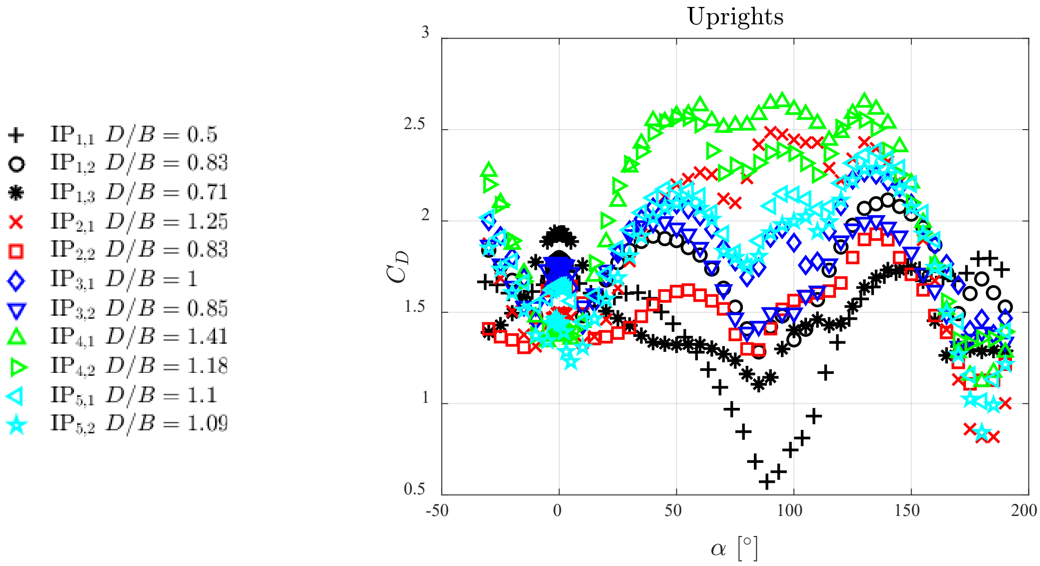

Figure 3. Drag coefficients for uprights. The first subscript in the legend indicates the industrial partner (IP), while the second one indicates the steel profile provided by a certain IP. Side ratio D/B is also specified for each tested element.

3. DESIGN METHOD

To develop the design method the peak values of the shielding coefficients $\hat{\Psi}^{n_W}_{F,n_L}$ were determined starting from the results corresponding to a range of angle of attack of 0° – 40°. Therefore, the design aerodynamic coefficient is obtained through the following relationship:

$$\hat{C}^{n_W}_{Fd,n_L} = C_{F,eq} \cdot \hat{\Psi}^{n_W}_{F,n_L} \tag{2}$$

where $C_{F,eq}$ is the "equivalent aerodynamic coefficients", which requires the results of wind tunnel tests on sectional models with the cross sections of the beams and columns constituting the elements of the rack frames. The shear force and the overturing moment at the base of the n-th rack frame are given by:

$$V_n = q_p(z_{ref} = H) \cdot \hat{C}^{n_W}_{Dd,n_L} \cdot H \cdot L \tag{3}$$

in which $q_p(z_{ref} = H)$ is the peak pressure at the reference height corresponding to the rack frame height (H) and L is the width of the rack frame.

4. CONCLUDING REMARKS

The design method allows estimating the wind loads on the single rack frames displayed during the erection phases. It represents a design tool to check the safety of the structures and to design temporary bracings. Moreover, the new experimental results start to cover the lack of wind tunnel test results on unclad RSWs. Finally, the results reported in the paper together with the procedure developed for estimating the design loads during the erection phase of ARSWs could be implemented in Standards and Codes in which recommendations on this specific structural typology are very poor.

ACKNOWLEDGEMENTS

This work was supported by STEELWAR (Advanced structural solutions for automated STEEL-rack supported WARehouses) Project, a Research Program of the Research Fund for Coal and Steel (RFCS-2016) funded by the European Commission, which is gratefully acknowledged.

REFERENCES

Möll R., Thiele F., 1972. Windkanalversuche am Modell eines Stahlskelett-Hochregals zur Bestimmung des Widerstandsbeiwertes nach DIN 1055 für ein filigranartiges Bauwerk, Der Stahlbau 41: 65-72.

Melling R. J. (1978). Loads on Open Lattice Structures in Nominally Smooth Flow, Proc. of the 3rd Colloquium on Industrial Aerodynamics, Aachen, Pt. 1, pp. 107-127.

Sykes D. M. (1978). Wind loads on lattice structures in turbulent airflow, Proc. 3rd. Colloq. on Industrial Aerodynamics, Aachen, pp. 129-148.

Jacobs B. E. A., 1978. Determination of shielding factors for multiple frame structures. Proc. 3rd. Colloq. on Industrial Aerodynamics, Aachen, pp. 149-164.

Clow D. G. (1978). Loads on Open Lattice Structures - A Comparative Study, Proc. of the 3rd Colloquium on Industrial Aerodynamics, Aachen, Pt. 1, pp. 165-177.

Georgiou P.N., Vickery B.J. (1979). Wind loads on building frames, In J.E. Cermak (Ed.), Proc. 5th Int. Conf. on Wind Engineering, Fort Collins, CO, 1979, Pergamon, Oxford, Vol. 1, pp. 421-433.

Whitbread R. E. (1980). The Influence of Shielding on the Wind Forces Experienced by Arrays of Lattice frames, In J.E. Cermak (Ed.), Proc. 5th Int. Conf. on Wind Engineering, Fort Collins, CO, Pergamon, Oxford, Vol. 1, pp. 405-420.

Nadeem A., Levitan M. (1997). A refined method for calculating wind load combinations on open-framed structures, J. Wind Eng. Ind. Aerodyn., 72:445-453.

ASCE (2011). Wind loads for petrochemical and other industrial facilities. Task Committee on Wind-Induced Forces, American Society of Civil Engineers, Reston, VA.

Performance of a base-moment, passive vibration control device for HAWT towers against variable site wind conditions

N. Caterino [1,2*], E. Sorge[1], C.T. Georgakis[3], C. Demartino[4]

[1]*Department of Engineering, University of Naples "Parthenope", Naples, Italy,*
[2]*Institute of Technologies for Construction, Italian National Research Council (CNR), San G. Milanese, Milan, Italy*
[3]*Department of Civil and Architectural Engineering, Structural Engineering, Aarhus University, Aarhus, Denmark*
[4]*Zhejiang University, Hangzhou, China*
*[*nicola.caterino@uniparthenope.it](mailto:nicola.caterino@uniparthenope.it)*

1. ABSTRACT

This work is focused on the performance evaluation of a control system for wind induced vibrations of horizontal axis wind turbines. Reference is made to a passive system installed at the base of the tower, with the main function of dissipating energy to reduce the demand for bending moment, without increasing the demand for displacement at the top. The system consists of a rotational friction damper (RFD, Mualla and Belev, 2002) intended to be installed at the base of the turbine, connecting the tower to its foundation. Such device, see Fig. 1, is commonly adopted for seismic protection of frame structures. The simplest assembly consists of a central vertical plate a), usually attached to the above girder by means of a hinge h), two external plates g), to whom bracing bars coming from the base of the columns are pin connected, and two circular friction pad discs c) made of high-tech composite materials placed in between the steel plates. All the plates are clamped together by a post-stressed steel bolt composed of different parts (b, d, e, f), see Fig. 1. The energy is dissipated thanks to the relative sliding between friction pads and steel plates, that occurs for cyclic rotation demand into the device caused by the lateral vibration of nacelle. The dissipative capability of such system can be calibrated changing the material (roughness) of friction pads, and/or adding other plates with additional pads in between. The strategy for onshore wind turbines (Di Paolo et al., 2021), is based on the use of a special restraint, that is a hinge, with the addition of a rotational friction devices that dissipates energy thanks to the base rocking, and a system of springs for re-centering, see Fig. 2.

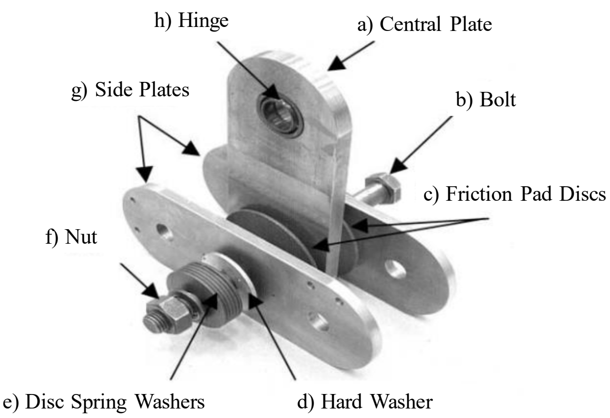

Figure 1. RFD

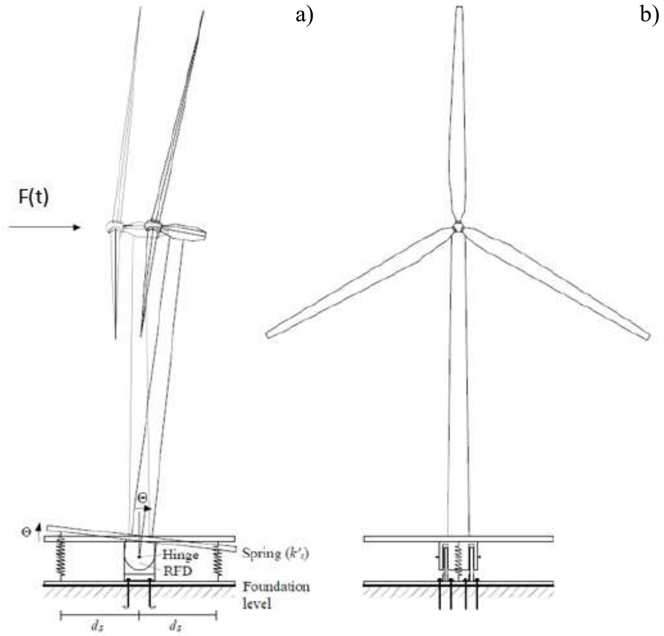

Figure 2. Wind turbine equipped with the RFD. Lateral a) and front b) view.

This system was tested performing several non-linear numerical analyses with reference to a NREL 5 MW (Jonkman et al., 2009) wind turbine, with the aim of evaluating its effectiveness for wind conditions. The system shows that it can have truly remarkable performances, bringing a considerable reduction of bending moment to the base compared to the alternative, conventional "fixed base" configuration, see Fig. 3. It is observed that the performances are different for different wind loads, however always satisfactory because in all cases they lead to a significant mitigation of the structural demand.

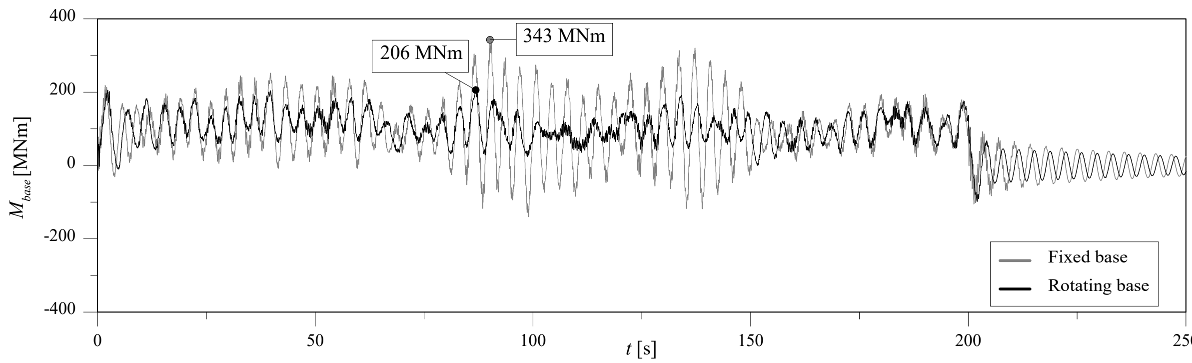

Figure 3. Comparison between base moment for the wind turbine against the same load case for fixed and rotating base configuration, imposing an average wind speed at the hub of 50m/s and in the parked scenario.

REFERENCES

Di Paolo, M., Nuzzo, I., Caterino, N. and Georgakis, C., 2021, A friction-based passive control technique to mitigate wind induced structural demand to wind turbines, Engineering Structures, 232: 111744.

Jonkman, J., Butterfield, S., Musial, W. and Scott, G., 2009, Definition of a 5-MW Reference Wind Turbine for Offshore System Development, Office of Energy Efficiency and Renewable Energy: Washington, DC, USA.

Mualla, H. Belev, B., 2002, Performance of steel frames with a new friction damper device under earthquake excitation, Engineering Structures, 24:3, 365–371.

A bivariate statistical model of large pressure peaks measured in wind tunnel tests

Vincent Denoël [1], Thibaud Bastin [1], Giulia Pomaranzi [2], Alberto Zasso [3]

[1]*Structural & Stochastic Dynamics, University of Liège,* v.denoel@uliege.be
[2]*Politecnico di Milano, Dept of Mechanical Engineering,* giulia.pomaranzi@polimi.it
[3]*Politecnico di Milano, Dept of Mechanical Engineering,* alberto.zasso@polimi.it

SUMMARY
A statistical approach for the treatment of large negative peak pressures is discussed. It is based on spatial correlation so that these large peak values, which are difficult to handle in cladding design, could be smoothed out by invoking the characteristic size associated with these events. The proposed method hinges on a mixture model of bicubic translation processes. Development of the method is summarized and applied to the computation of the area-average pressure on the building façade of a model tested in wind tunnel facilities at Politecnico di Milano.

Keywords: building façades, bicubic translation model, Bayesian regression, mixture model, size effect

1. INTRODUCTION

Several experimental evidences have shown that very high negative pressures could be measured on the facades of a building in the wind tunnel (Lamberti et al., 2020; Pomaranzi et al., 2022). They are being more frequently observed because of the widespread tendency to use higher frequency sampling and number of pressure taps in wind tunnel testing. The management of these major suction peaks remains an important issue today. Indeed, if these were to be treated in complete transparency, experimentalists would not be able to provide reasonable pressure peak values for the dimensioning of the structures. The same experimental evidence also shows that the spatial extent of the peak pressure is relatively limited. This effectively justifies that building façades do not need to be designed accounting these extreme values since integration of pressure over a finite (non-zero) area would result in a smaller average pressure. The data processing techniques traditionally used to limit the impact of these large negative pressure peaks consists of averaging in time rather than in space. The standard approach is to use the well-known TVL method (Lawson, 1976). This approach does not offer a uniformly valid solution in areas with large negative peaks, which is expected given that its origins are based on a stationary (in time) and homogeneous (in space) pressure field.

The origin of large negative peak pressures on the facades of the building corresponds to physical phenomena different from those generally observed in the shear layer. They presumably correspond to small hairpin vortices while a typical shear layer is composed of larger vortices (Simiu and Scanlan, 1996). Therefore, it is possible to model the measured pressure as a mixture of two components, one related to the small-scale phenomenon, and one related to the large scale (Rigo et al., 2020).

The separation of the measured pressure into two components is still an open issue that can be achieved in a statistical sense. This question is addressed in this paper by considering the mixture of different physics in joint distributions of pressure at several neighbouring taps. Ultimately, this will answer the question of the spatial extent of each component and help derive appropriate techniques to determine peak value distribution from wind pressure data, after averaging on finite size (non-zero) areas. The illustration is based on very high-fidelity experimental data, measuring pressure on the facades of a building with a very high density but the proposed methodology is applicable to scarcer tap density.

2. METHODS: THE STATISTICAL MODEL

The proposed statistical model hinges on the cubic translation (Grigoriu M., 1984; Winterstein S.R., 1987) which expresses the pressure p_i at each pressure tap as a cubic transformation of a Gaussian variable u:

$$p_i(u) = h\left(u, \boldsymbol{\pi}_i\right) = \frac{\alpha}{b}\left[\frac{u^3}{3} + au^2 + (b-1)\,u - a\right] + \mu \qquad (1)$$

and where the coefficients $\boldsymbol{\pi}_i = (\mu, \sigma, a, b)$ need to be adjusted to the data. It is possible to express the Probability Density Function (PDF) of the transformed variable $f_i\left(p_i; \boldsymbol{\pi}_i\right)$ as a function of these coefficients (Rigo et al. 2019). So, a suitable way to adjust them is to find the optimal values that minimize the (e.g. least-square) error between the PDF of the experimental data, obtained from a scaled histogram, and the PDF predicted by the model (Rigo et al. 2018).

As introduced earlier, the cubic translation model is not suitable to model the pressure at taps with large negative peaks, where several physics are captured. Instead, a mixture model is used. It is chosen to mix two such cubic translations, such that the PDF at critical pressure taps is modeled as:

$$f_{\mathrm{mix},i}\left(p_i; \boldsymbol{\theta}_i\right) = w_i f_i\left(p_i; \boldsymbol{\pi}_i^{\mathrm{A}}\right) + (1 - w_i)\, f_i\left(p_i; \boldsymbol{\pi}_i^{\mathrm{B}}\right). \qquad (2)$$

where $\boldsymbol{\pi}_i^{\mathrm{A}}$ and $\boldsymbol{\pi}_i^{\mathrm{B}}$ represent two sets of 4 parameters, one for each component of the model, and where w_i represents the mixing ratio. This formulation is sufficiently general and also covers the case where either component is Gaussian, since the cubic translation model is adjustable to Gaussian data, when the transformation is linear. In total, the unilateral PDF at each pressure tap is represented by a set of 9 parameters collected in $\boldsymbol{\theta}_i$, corresponding to twice four parameters plus the mixing ratio.

In this paper, we exploit an extension of the cubic translation model, that had been coined *bicubic translation model* in (Blaise et al., 2017) as it applies to a joint PDF between two different processes which are represented by cubic translation models each. Specifically, the considered joint PDF model $f_{ij}\left(p_i, p_j; \boldsymbol{\Pi}_{ij}\right)$ of the pressures measured at taps i and j is expressed as a function of the 4 parameters of each pressure, plus their correlation coefficient.

Finally, the model is further extended in order to include two components, in the sense of a mixture model. As such, the joint PDF of the pressures recorded at two neighboring pressure taps is represented by:

$$f_{\mathrm{mix},ij}\left(p_i, p_j; \boldsymbol{\Theta}_{ij}\right) = w_{ij} f_{ij}\left(p_i, p_j; \boldsymbol{\Pi}_{ij}^{\mathrm{A}}\right) + (1 - w_i)\, f_{ij}\left(p_i, p_j; \boldsymbol{\Pi}_{ij}^{\mathrm{B}}\right) \qquad (3)$$

where $\boldsymbol{\Theta}_{ij} = \left(\boldsymbol{\Pi}_{ij}^{\mathrm{A}}, \boldsymbol{\Pi}_{ij}^{\mathrm{B}}, w_{ij}\right)$ gathers a set of twice nine, plus one, i.e. the 19 parameters of the bicubic model. In summary, a bicubic translation model is composed of 19 parameters; it generalizes the concept of cubic translation model, while allowing to account for correlation of two non-Gaussian processes, at least to some extent. It falls in the family of parametric models to estimate the statistical properties of experimental data.

3. EXPERIMENTAL SETUP

Figure 1 depicts some details of the test setup that has been used to illustrate the findings of this research. It consists of a regular building with size 2000 x 1000 x 200 mm (H x W x b) at wind tunnel scale, equipped with a set of 254 pressure sensors which are distributed with variable density over the specimen. The smallest distance between two neighboring taps is as small as 3.4 mm. The closeup view in Figure 1-c allow appreciating the high density of the mesh.

The wind pressures have been measured on this building for various wind exposures at a wind tunnel sampling frequency of 500 Hz, and for a total duration of 5 minutes of measurement (N=150,000 sample points per channel). The reference pressure used to determine pressure coefficients is the dynamic pressure at the top of the building. The considered exposure is equal to 10°, which corresponds to a wind attacking the specimen from the back with an incidence of 10° with respect to the large face of the building.

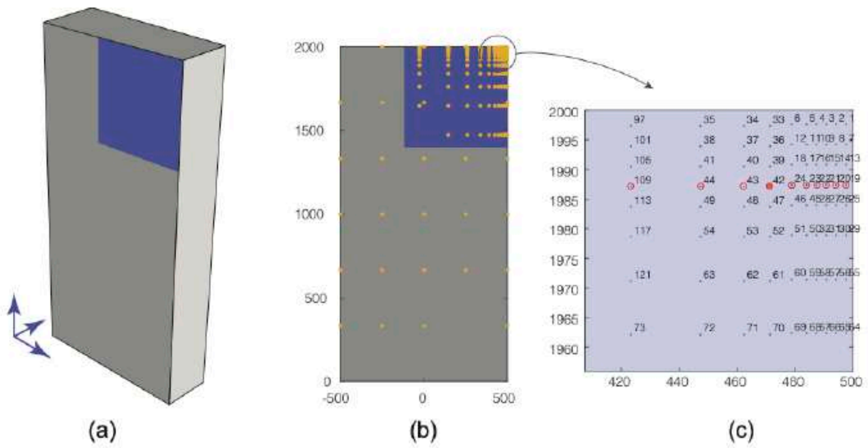

Figure 1. (a) Sketch of the experimental setup, (b) Positions of the pressure taps (units are in mm of the model), (c) Numbering of pressure taps.

4. STATISTICAL ANALYSIS OF LARGE NEGATIVE PRESSURES

A statistical analysis of large negative peak pressures will be presented in the full paper. Wind tunnel pressures will be analyzed by means of joint bicubic distributions with the aims to focus on large extremes, decompose the measured processes in tail and bulk components and quantify the spatial correlation of each of them.

Results to be shown in the full paper include the de-mixing of the pressure coefficient measured by a pressure tap together with the joint PDF between the neighboring pressure taps, where the same decomposition can be applied post the computation of the 19 parameters that are defining this model.

As an example, Figure 2 illustrates the joint PDF between the pressure coefficients at tap 42 and 24. From the univariate analysis, it is known that each of them can be decomposed into two components, A and B. The same development is also possible with the joint PDF: the mixture model is a weighted sum of two bicubic translation processes, and the 19 parameters of this model are adjusted in order to match the PDF of experimental data.

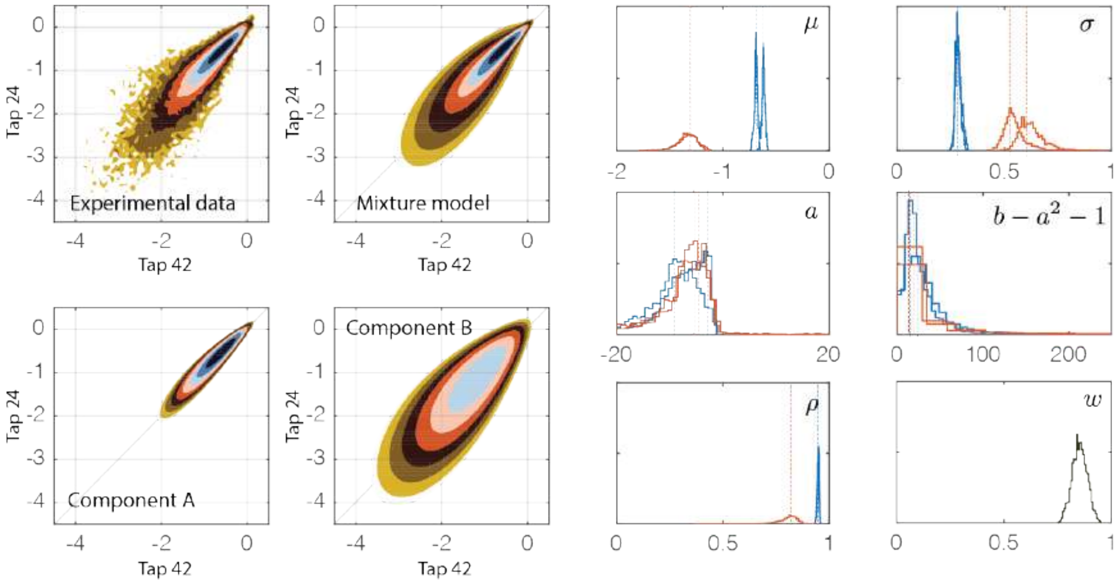

Figure 2. Results of the joint de-mixing of the pressure coefficients measured at pressure tap 42 and 24. (Right) Posterior distributions of the 19 model parameters (Left) Experimental and identified joint PDF.

The 2-by-2 correlation is the necessary and sufficient information to quantify the statistics of the average of the pressure at 2 taps. Providing decisive information about the characteristic scales in the problem, the model can be used to predict area-averaged pressure coefficients that do not require such a dense tap meshing as will be discussed in the full paper. Future works will aim at developing the same analysis to surface-average, possibly apply the same technique to structures with corner vortices (Blaise et al., 2017).

REFERENCES

Blaise N., Andrianne T., and Denoël V.. Assessment of extreme value overestimations with equivalent static wind loads. Journal of Wind Engineering and Industrial Aerodynamics, 168:123–133, 2017.

Grigoriu,M.(1984).Crossingsofnon-Gaussiantranslationprocesses,J.Eng.Mech.,ASCE,110(4),610-620.

Lamberti G., Amerio L., Pomaranzi G., Zasso A., and Gorlé C.. Comparison of high resolution pressure measurements on a high-rise building in a closed and open-section wind tunnel. Journal of wind engineering and industrial aerodynamics, 204:104247, 2020.

Lawson, T. The design of cladding. Build. Environ. 11 (1), 37–38, 1976.

Pomaranzi G., Amerio L., Schito P., Lamberti G., Gorlé C., Zasso A., Wind tunnel pressure data analysis for peak cladding load estimation on a high-rise building, Journal of Wind Engineering and Industrial Aerodynamics, Volume 220, 2022, 104855.

Rigo F., Andrianne T., and Denoël V.. On the use of the cubic translation to model bimodal wind pressures. Mathematical Modelling in Civil Engineering, Vol. 15-No. 2: 20-32-2019 Doi: 10.2478/mmce-2019-0006

Rigo F., Andrianne T., and Denoël V.. Mixture model in high-order statistics for peak factor estimation on low-rise building. In Conference of the Italian Association for Wind Engineering, pages 613–629. Springer, 2018.

Rigo, F., Andrianne, T., & Denoël, V. A de-mixing approach for the management of large negative peaks in wind tunnel data. Journal of Wind Engineering and Industrial Aerodynamics, 206, 104279, 2020.

Simiu, E. and Scanlan, R.H., 1996. Wind effects on structures. John Wiley and Sons, New York, NY, USA.

Winterstein, S.R.(1987) Moment-based Hermite models of random vibration, Lyngby, Report No. 219. Department of Structural Engineering, Technical University of Denmark, Lyngby, Denmark.

17th Conference on Wind Engineering – IN-VENTO 2022
Politecnico di Milano, IT 4 – 7 September 2022

Investigation of wind-induced tonal noise on a permeable double-skin façade

Giulia Pomaranzi [1], Alessandro Aquili [2], Paolo Schito [3], Alberto Zasso [4]

[1]*Politecnico di Milano, Via G. La Masa 1, 20156, Milan, Italy,* giulia.pomaranzi@polimi.it
[2]*Pininfarina S.p.A., Via Ferrero 1, 10095, Grugliasco (TO), Italy,* a.aquili@pininfarina.it
[3]*Politecnico di Milano, Via G. La Masa 1, 20156, Milan, Italy,* paolo.schito@polimi.it
[4]*Politecnico di Milano, Via G. La Masa 1, 20156, Milan, Italy,* alberto.zasso@polimi.it

SUMMARY
The adoption of innovative façade systems poses new challenges from the design point of view. Among them, the permeable double skin façade (PDSF) is a cladding system for building made by a double skin, where the outer layer is constituted by porous panels. When considering the wind interaction with such cladding, some problems related to aeroacoustics may arise and the potential wind-induced tonal noise emission must be considered in the design phase. In this paper, a case study aimed to the investigation of wind-induced tonal noise on a permeable double skin façade is presented. An ad-hoc methodology based on a combined experimental-numerical approach is proposed to identify the building's areas most sensitive to acoustic emissions. As a final step of such methodology, wind tunnel tests in an anechoic facility of full-scale mockups are carried out. Combining the results with a local wind climate analysis allows quantifying the risk of exceeding the threshold velocity associated with the generation of tonal noise, ascribable to the perforated metal.

Keywords: permeable double skin, tonal noise, perforated metals, wind tunnel tests

1. INTRODUCTION

Nowadays building design strategies devote special attention to the energetic and environmental impact of structures, leading to new architectural solutions that contribute to increasing the efficiency of the building. Among them, the Permeable Double Skin Façades (PDSFs) are cladding systems made of two façades, where the outer one is realized by a porous layer. Along with the beneficial effects on energy performance, recent studies (Pomaranzi et al., 2021), (Pomaranzi et al., 2020) have focused on the wind interaction with a PDSF, highlighting the design pressure reduction for the inner skin, ascribable to the shielding effects of the porous outer layer. When wind interacts with a porous screen, a broadband noise may be generated. However, in some special situations, the sound power in a certain frequency band can be enhanced and the level can be more than 5 dB higher than those in other frequency bands. One effect of this sound power enhancement, besides the increase of the total sound power level, is a strong tone-like signal in a windy condition (Feng, 2012). Such situations may arise when the porous façade is made by perforated metal, prone to aero-acoustic issues. If dealing with a PDSF, investigating the risk of tonal noise emission prior to the realization of the building itself is not straightforward, being experimental tests on scaled model not effective. In addition, the acoustic behaviour of isolated perforated panels is expected to differ from the porous double skin, so the investigation of the potential tonal noise emission must encompass the double skin system.

In the present paper a three-step methodology to assess the problem is proposed by referring to the New ENI Head Office case. It is constituted by three main buildings, as shown in Fig. 1, all of them endowed with a permeable double skin façade system: two of them are covered by the so-called *Orange Skin*, made by perforated metal sheets (with circular holes, 6 mm diameter) arranged in such a way they cover the inner glazed skin. The last building is instead characterized by the *Blue Skin*, horizontal louvers made again by circular holes perforated metal sheets.

Figure 1. Render of the New ENI Headquarter in Milan

2. METHODOLOGY

A methodology both based on experimental tests and numerical simulations has been developed allowing a quantitative approach to the risk assessment of tonal noise emission of the permeable façade. It is essentially made by the following steps:

1. Firstly, wind tunnel tests on rigid scaled model have been performed at Polimi Wind Tunnel. The geometric scale is chosen equal to 1:75 guaranteeing a gap between the two skins large enough to let the gap flow develop. In this phase, the scaling procedure has to be applied to the permeable skin too, since a simple geometric scaling is not effective for the porous elements: to ensure the kinematic similitude, e.g. the same flow conditions between real and model scale, the pressure loss coefficient *k* must be maintained (Allori at al., 2013). The buildings in the test section are shown in Fig.2. The model has been equipped with 400 pressure taps, distributed on the inner façade and on the porous layer such that they are able to measure the differential pressure. Pressure measurements are performed using the high-speed scanning pressure equipment Initium and the miniature pressure scanners ESP.

Figure 2. Wind tunnel tests on 1:75 scaled model of the New ENI Headquarter buildings

2. In parallel, Computational Fluid Dynamic simulations have been performed to estimate the velocity flow field and the flow rate across the permeable layer: in this phase, a porous media approach is applied, allowing to not explicitly reproduce the geometry of the porous façade. The porous model used is the Darcy-Forchheimer one for homogeneous porous medium: a sink term S_m is added in the momentum balance of the Navier-Stokes equations (Cheng et al, 2016), (Pomaranzi et al., 2021). The numerical solver used for the analysis is the open-source software OpenFOAM: the flow is calculated by means of a finite volume approach, solving the steady-state incompressible Reynolds-Averaged Navier-Stokes (RANS) equations, using adapted turbulence modelling to achieve closure and suitable boundary conditions. Fig. 3 shows a color map of the velocity speedup, calculated as the crossing speed divided by the reference velocity for a specific wind exposure angle. The simulations results have allowed to identify the more critical portions of the building in terms of highest flow rate across the porous layer.

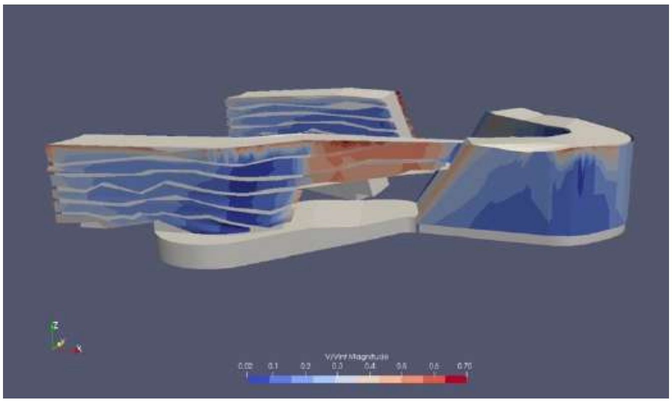

Figure 3. Flow rate across the permeable façade of the New ENI Headquarter buildings, normalized with respect to the refence wind speed

3. Lastly, the characterization of tonal acoustic emission and the investigation of the vortex shedding excitation have been carried out at Low-Noise Pininfarina Wind Tunnel on four different full-scale portions of the building double façade, representing both the *Orange* and the *Blue* skins. Such portions have been previously identified, being the ones interested by the highest flow rate. The models have been realized by using the same materials with respect the full-scale building, such that the same structural characteristics (geometries, masses, and stiffness) of the double skin façade are maintained. Fig. 4 shows one of the mockups during the experimental campaign.

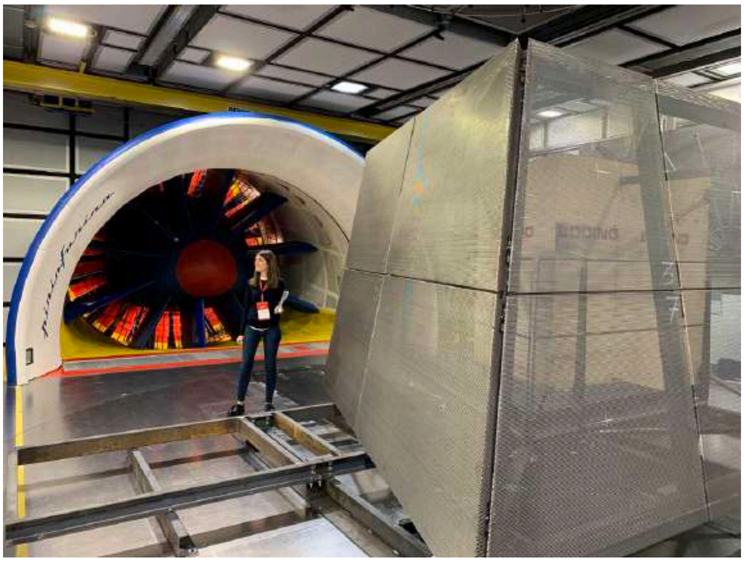

Figure 4. A portion of the cladding system of one of the New ENI Head Office buildings during tests in at Low-Noise Pininfarina Wind Tunnel

3. RESULTS

Results to be shown in the full paper will present first the preliminary analysis carried out to identify which are the buildings' areas interested by the highest flow rates through the permeable façade. Then, the velocity and pressure measurements carried out in the anechoic facility will be shown along with the outputs from the beam forming analysis to locate the sources of tonal noise in the tested mock-ups. Finally, the through velocities responsible for the tonal noise emission will be referred to the undisturbed wind velocity to estimate the probability of exceedance through a wind climate analysis of the buildings' area.

REFERENCES

Allori, D., Bartoli, G. and Mannini, C., 2013. Wind tunnel tests on macro-porous structural elements: A scaling procedure. Journal of Wind Engineering and Industrial Aerodynamics, 123, pp.291-299.

Chen, H. and Christensen, E.D., 2016. Investigations on the porous resistance coefficients for fishing net structures. Journal of Fluids and Structures, 65, pp.76-107.

Feng, L., 2012. Tone-like signal in the wind-induced noise of perforated plates. Acta Acustica united with Acustica, 98(1), pp.188-194.

Pomaranzi, G., Bistoni, O., Schito, P., Rosa, L. and Zasso, A., 2021. Wind Effects on a Permeable Double Skin Façade, the ENI Head Office Case Study. Fluids, 6(11), p.415.

Pomaranzi, G., Bistoni, O., Schito, P. and Zasso, A., 2021. Numerical modelling of three-dimensional screens, treated as porous media. Wind and Structures, 33(5), pp.409-422.

Pomaranzi, G., Daniotti, N., Schito, P., Rosa, L. and Zasso, A., 2020. Experimental assessment of the effects of a porous double skin façade system on cladding loads. Journal of Wind Engineering and Industrial Aerodynamics, 196, p.104019.

Forecasting of wind speed return period based on LSTM classification: a preliminary application to the Copenhagen area

P. Modé [1], C. Demartino [2], C. T. Georgakis [3], N. D. Lagaros [4]

[1]*National Technical University of Athens, Athens, Greece, pmode@mail.ntua.gr*
[2]*Zhejiang University, Haining, China, cristoforodemartino@intl.zju.edu.cn*
[3]*Aarhus University, Aarhus, Denmark, cg@cae.au.dk*
[4]*National Technical University of Athens, Athens, Greece, nlagaros@central.ntua.gr*

SUMMARY
Accurate short-term forecasts of wind speed based on local climate data can be particularly useful in the developing generation of civil cyberinfrastructure systems. In this context, this study proposes a novel approach for forecasting wind speeds corresponding to certain return periods in a short-term horizon (i.e., less than 3 hours). The extreme wind speeds are denoted by classes that are defined in terms of a certain exceedance of return period (or exceedance frequency) based on a model of the extremes calibrated using the Peak Over Threshold (POT) method. The regression problem is tackled using the Long Short-Term Memory (LSTM) time-series modelling performing a classification instead of classical logistic regression. A discussion on the optimization of the framework is given for the problem of imbalanced classification. Preliminary results are provided.

Keywords: Forecasting, extreme wind, return period, LSTM

1. EXTENDED SUMMARY

The present study proposes an approach for forecasting extreme wind speeds in the short term (less than 3 hours). First, using historical data, extreme value analysis is performed based on the Peak Over Threshold (POT) method obtaining a hazard curve of the site of interest (Section 1.1). Then, the hyperparameter fitting of a Long Short-Term Memory (LSTM) time-series model is performed (Section 1.2).

1.1. Wind hazard

The Extreme Value Theory (EVT) provides asymptotic models to describe the distribution of a rare event and is a useful technique to analyse the annual frequency of exceedance (Coles et al., 2001). The POT method allows for the analysis of all values exceeding a specified threshold. An asymptotic distribution, the Generalized Pareto Distribution (GPD), is used to model events above the specified threshold. Assuming a null shape parameter of the GPD distribution, the hazard curve can be expressed as:

$$U(T) = \xi + \alpha ln(\lambda T) \tag{1}$$

where U is the mean wind speed, T is the return period, ξ is the selected threshold and λ is the Poisson frequency rate. The threshold adopted is 12m/s and the time distance of the events is 48h. The METAR wind data from Copenhagen's Kastrup Airport for the period 1976-2020 (i.e., 45yrs) are shown in Fig. 1 left together with 809 extreme wind events (red dots). The previous data are used to estimate the parameters of Eq. (1): ξ = 2.187m/s, α = 12m/s, λ = 809/45yrs = 17.98yrs-1.

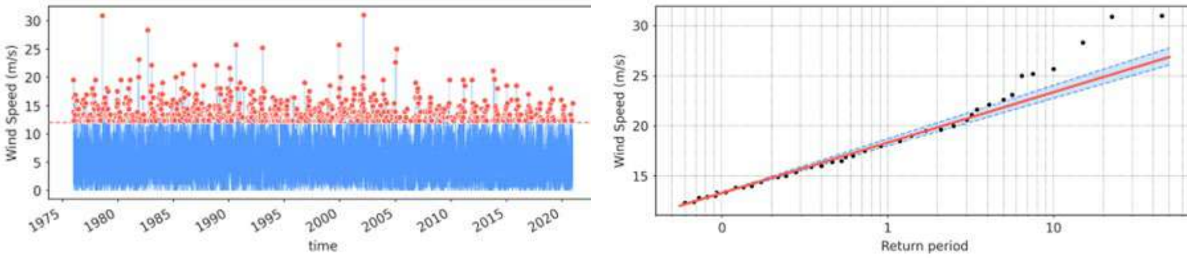

Figure. 1. POT extreme wind events (left), and wind hazard curve, Eq. (1), with 95% confidence interval (right).

1.2. LSTM classification forecasting

The problem is formulated as a binary classification. The two classes are defined in terms of exceedance of wind speed corresponding to T = 1/12yrs (1 month), namely 12.88m/s according to Eq. (1). The positive class is defined as $U \geq 12.88$m/s while the negative as $U < 12.88$m/s. T is chosen as a trade-off between the need of having an extreme wind without extreme imbalanced classes. In particular, this value leads to an imbalanced binary classification problem with an imbalance of around 1:100 in the train set (1976-2011) and 1:180 in the test set (2012-2020) (see Figure 1, left). The classification is considered highly imbalanced and a cost-sensitive method was adopted to deal with it (Brownlee, 2020). The LSTM network is trained using the hourly METAR climatic data of Copenhagen's Kastrup Airport for a 36yrs period. The input consists of 48h data segments of 6 climatic variables (temperature, dew point, wind speed and direction, atmospheric pressure, relative humidity) that are used for 1 step prediction of the class. A precision-recall curve is presented in Figure 2 left. The orange line is representing the precision-recall curve for each threshold (0 to 1) for a binary classification model. The so-obtained models were evaluated based on F-measures (Sokolova et al., 2006) representing the balance between precision and recall. The F-measure is 1 for a perfect model. For a threshold equal to 0.5, the F-values on the train set were F1 = 0.391 and F2 = 0.602. After maximization of F1, the best model (black dot in Figure 2 left) was found to correspond to a threshold of 0.95. The so-optimized LSTM-based model tested for a 9yrs period (test dataset) achieves around 60% precision (Figure 2, right).

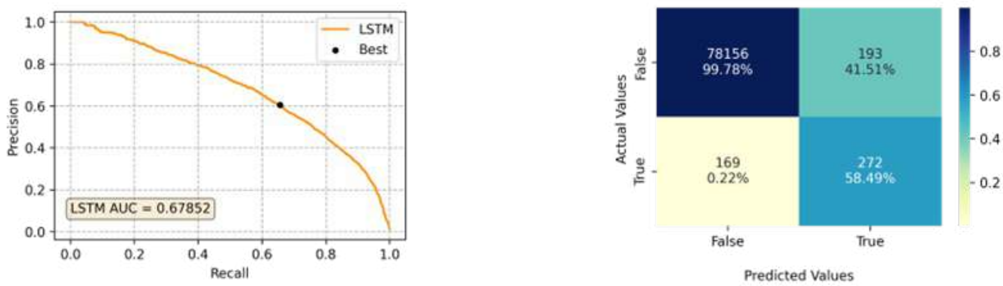

Figure. 2. Precision-recall plot of the train set (left) and confusion plot of the test set (right).

REFERENCES

Brownlee, J. 2020. Imbalanced classification with python: Better metrics, balance skewed classes, cost-sensitive learning (Cost-Sensitive Deep Learning in Keras). Machine Learning Mastery.

Coles, S., Bawa, J., Trenner, L., & Dorazio, P. 2001. An introduction to statistical modeling of extreme values (Vol. 208, 208). London: Springer.

Sokolova, M., Japkowicz, N., & Szpakowicz, S. 2006. Beyond Accuracy, F-Score and ROC: A Family of Discriminant Measures for Performance Evaluation. AI 2006: Advances in Artificial Intelligence, Berlin, Heidelberg, 10151021

Comparison of the results between a rigid and an aeroelastic model of a tall building in wind tunnel

Ivan Marenda [1], Franco Cavenaghi [2], Tommaso Argentini [3], Daniele Rocchi [4], Lorenzo Rosa [5]

[1] Politecnico di Milano, Milan, Italy, ivan.marenda@polimi.it
[2] Politecnico di Milano, Milan, Italy, franco.cavenaghi@polimi.it
[3] Politecnico di Milano, Milan, Italy, tommaso.argentini@polimi.it
[4] Politecnico di Milano, Milan, Italy, daniele.rocchi@polimi.it
[5] Politecnico di Milano, Milan, Italy, lorenzo.rosa@polimi.it

SUMMARY
The present work analyses the results of tests performed at the Wind Tunnel of the Politecnico di Milano on a scaled model of a tall building. The model can be converted either into a rigid or an aeroelastic model, to compare these two standard approaches in the analysis of the effects of the incoming turbulent wind. Since the model wants to be a most general case of a tall building, it features complex structural dynamics (mass eccentricity) and complex aerodynamics (buffeting and vortex shedding). A Synchronous Multi-Pressure System (SMPS) was used to measure the pressure in several points of the model in both configurations. The tests were performed for different angles of attack of the wind and different wind velocities. Finally, the comparison of the results in terms of pressure and dynamic response of the models is shown. The modal numerical procedure differs from the direct measurement of the dynamic response of the structure because it does not consider the vortex-induced vibrations and the non-linear behaviour of the mechanical properties of the building.

Keywords: Rigid model, Aeroelastic model, modal approach, Wind tunnel.

1. INTRODUCTION

In recent years, the civil engineering field has been witnessing new challenges related to the use of new materials and technologies which allow building lightweight and flexible structures. Therefore, if up to now seismic events have dominated the design of structures, the wind load has now become important to address structural solutions. Not only repeated and continuous loading by wind can cause fatigue damage, but it can also induce vibrations in tall buildings affecting the comfort of people. Since international standards do not cover fully issues due to wind induced vibrations, tests performed in wind tunnels have got a foothold ever more. These experiments can be carried out in rigid models without any information in their mechanical behavior or in more detailed aeroelastic models which try to mirror their mechanical impedance.

This work compares the results obtained from tests conducted on a rigid and aeroelastic model of a tall building tested at the GVPM (Wind Tunnel of the Politecnico di Milano), to show the main differences and investigate the response of the structure. The well-known rigid model was already presented to the International Association for Wind Engineering in 2007 and the analysis of the results was performed by John D. Holmes and Tim K. T. Tse. The model represents a rectangular building, 30 m wide, 45 m long and 180 m high with a linear mass of 20000 kg/m. As for the dynamic properties, it is characterized by two flexural modes and a torsional one with frequencies between 0.1 Hz and 0.4 Hz.

2. METHODOLOGY

2.1. Models

The aeroelastic model is designed with an aluminum frame with the possibility of switching to the rigid model trough an additional internal constraint. The model is characterized by a length scale (λ_L) of 1:100, resulting in a model of 0.30 m wide, 0.45 m length and 1.80 m height. Secondly, for the aeroelastic model the velocity scale (λ_U) is set of 1:8. The list of similarities and scaling laws used is listed in Table 1.

Table 1. Similarities and scaling laws for aeroelastic tests

Description	Parameter	Value
Length	λ_L	0.01
Speed	λ_U	0.125
Frequency	λ_f	12.5
Mass	λ_M	10^{-6}
Acceleration	λ_a	1.56

The model is equipped by well distributed pressure taps (Synchronous Multi-Pressure System, density ranging from 0.4 taps/100m^2 near the floor and 3 taps/100m^2 near the top) and a set of accelerometers, placed at different locations, to directly measure the dynamic response.

2.2. Wind Tunnel tests

The tests were performed with different wind speeds (U_R) and different angles of attack (α) in order to investigate the dynamic behavior of the building in different conditions. An image of the model during the wind tunnel tests is shown in Figure 1. Furthermore, the signals were filtered through the equivalent moving average filter.

Figure 1. Model in the Wind Tunnel of the Politecnico di Milano

The study was approached with a dual strategy. On the one hand, tests were performed in the rigid model with high wind velocity U_M of 11.5 m/s for more effective response, and different angles of attack ($0° \leq \alpha \leq 90°$), while the structural response was numerically simulated. The calculation was based on the model approach of the first three modes of vibration [3].

On the other hand, tests were carried out in the aeroelastic model with different wind velocities U_M (2.6 m/s, 3.9 m/s, 5.2 m/s and 6.4 m/s) and different angles of attack ($0° \leq \alpha \leq 90°$). The model was equipped with six accelerometers to directly measure the dynamic response of the structure. Furthermore, the smooth flow decay and vortex shedding phenomenon were analyzed.

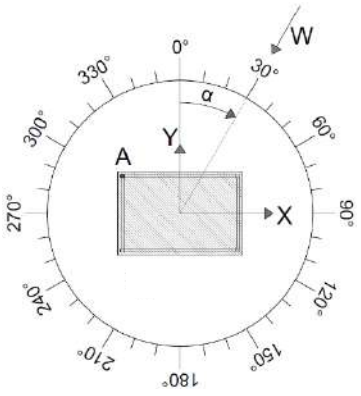

Figure 2. Modal orientation in the Wind Tunnel test section

3. RESULTS AND CONCLUSIONS

The aim of the present research is to investigate the differences in the results between the directly measurement obtained from an aeroelastic model and the modal simulation using results of tests on a rigid and aeroelastic model. The results are expressed in terms of pressure coefficients, base load coefficients and accelerations.

As regarding the pressure coefficients in terms of mean value and standard deviation, the differences between the two models are observed for low wind velocities, while as the test speed increases the response becomes more effective and these coefficients become similar. Figure 3 shows the values of the mean pressure coefficients and the standard deviations at 1.55 m and with a wind angle of attack of 85°.

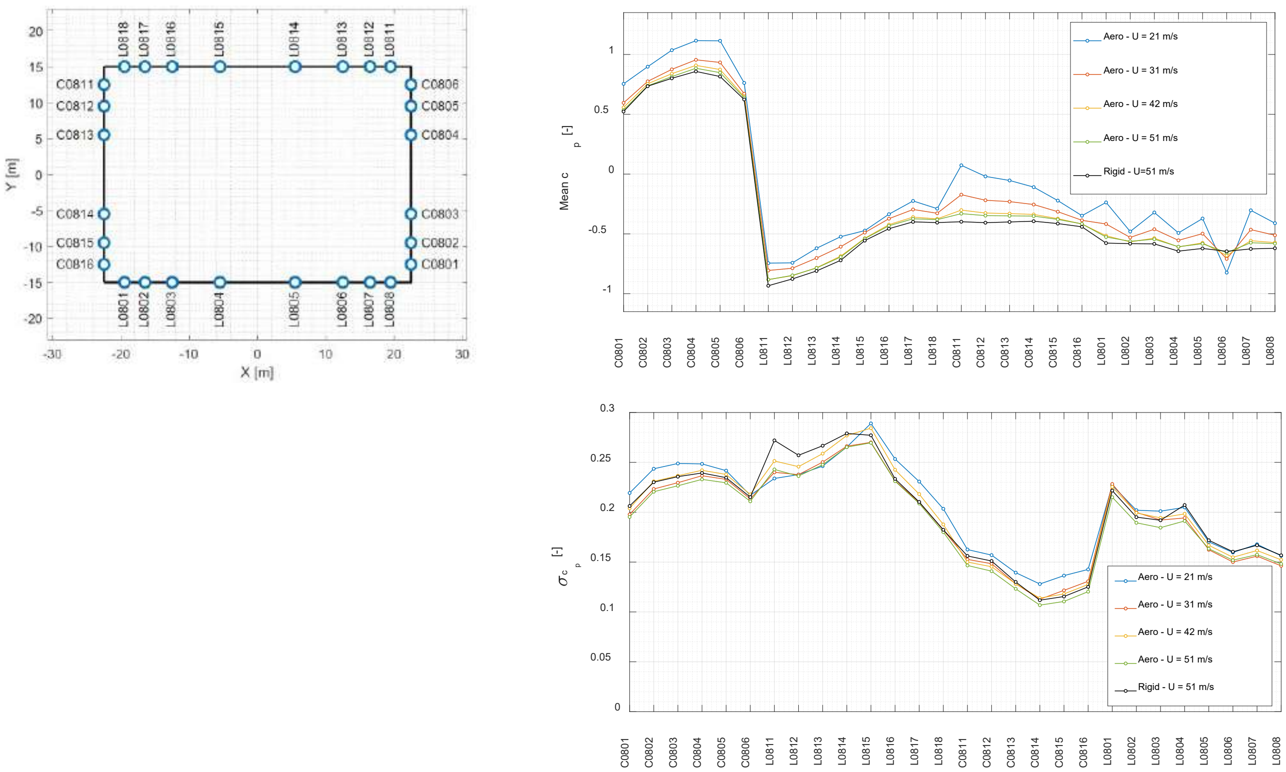

Figure 3. Comparison between rigid and aeroelastic model in terms of mean pressure coefficients and Standard deviations at 1.55 m and α=85°

Regarding the dynamic response of the structure, some differences can be observed in the two models due to the different approach. In the rigid model, the structural dynamic response is performed by a modal simulation with the assumption of constant damping ratio regardless of the amplitude of the vibrations. While the accelerations in the aeroelastic model are obtained by direct measurement with accelerometers. Furthermore, the numerical simulation does not take into account the vortex-induced vibrations which, in the y direction, occurs for wind speed in the test range. Figure 4 shows the differences between the direct measurements of the accelerations and the modal approach using the pressures coming from both models. The line charts show some differences in the standard deviation of the accelerations for angles of attack close to 90 ° and medium-high wind velocities corresponding to the vortex-induced vibrations.

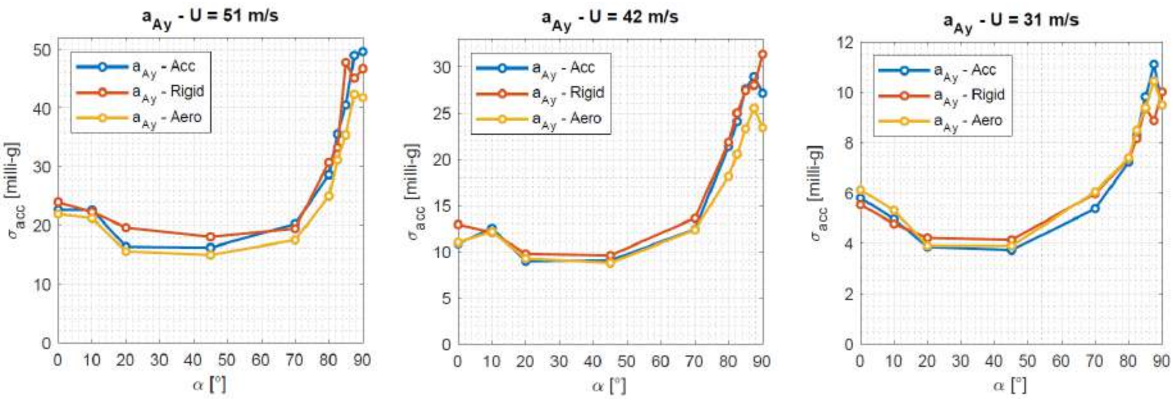

Figure 4. Standard deviation of the accelerations in the corner of the second quadrant at 1.50 m: direct measure of accelerations (Acc), numerical simulation based on rigid model (Rigid), numerical simulation based on aeroelastic model (Aero)

The results reported show that, in terms of mean and standard deviations of the pressure coefficient, the two models give similar results while some differences can be found in terms of dynamic response. These differences will be analysed considering more sophisticated models in order to take into account the non-linear effects of the mechanical properties and the vortex-induced vibrations.

REFERENCES

John D. Holmes, Tim K. T. Tse, International high-frequency base balance benchmark study, Wind and Structures Volume 18 Number 4 (2014) 457-471.

John. D. Holmes, Equivalent time averaging in wind engineering, Journal of Wind Engineering and Industrial Aerodynamics 72 (1997) 411-419.

Lorenzo Rosa, Gisella Tomasini, Alberto Zasso, A.M. Aly, Wind-induced dynamics and loads in a prismatic slender building: a modal approach based on unsteady pressure measurements, Journal of Wind Engineering and Industrial Aerodynamics 107-108 (2012) 118-130.

Wind tunnel experiments on air pollutant exposure time around a generic building

Erfan Keshavarzian [1], Kenny Kwok [2], Kejun Dong [3], Kapil Chauhan [4], Yu Zhang [5]

[1]*ARUP, Sydney, Australia, Erfan.Keshavarzian@arup.com*
[2]*The University of Sydney, Sydney, Australia, Kenny.kwok@sydney.edu.au*
[3]*Western Sydney University, Penrith, Australia, Kejun.Dong@westernsydney.edu.au*
[4]*The University of Sydney, Sydney, Australia, Kapil.chauhan@sydney.edu.au*
[5]*Tsinghua University, Beijing, China, yuzhang2014@tsinghua.edu.cn*

SUMMARY
This paper presents a wind tunnel model study of air pollutant exposure time in haze-fog (HF) phenomenon around an isolated generic building. A novel test setup has been designed to simulate the dispersion of stagnant pre-mixed tracer gas modelled as HF. Air pollutant exposure time at the windward and leeward regions near the building model shows that the exposure time is dominated by wind-structure interaction and is consistent with wind characteristics around the building model. The air pollutant exposure time for the full-scale model is estimated based on the scaled model tested in the wind tunnel. The results provide new insights into the air pollutant exposure time and can be used to validate similar CFD simulations.

Keywords: haze-fog, air pollutant exposure time, wind tunnel, wind tunnel, generic building

1. INTRODUCTION

Densely populated urban areas are more challenging to design for enhanced natural ventilation. Stagnant or slow airflow due to closely packed buildings reduces the effectiveness of natural ventilation. Air pollutants, including suspended particulates, linger in urban areas to form haze-fog (HF) (Zhang et al., 2015), which poses a health hazard to the public. This health risk depends on the air pollutant concentration and exposure time (Blocken et al., 2020). The transient nature of wind-assisted dispersion and air pollutant residual time of HF in an urban environment with an initial concentration C0 has been simulated in CFD studies (Zhang et al., 2021; Zhang et al., 2015). Wind tunnel tests using a tracer gas technique have been widely used to measure mean and fluctuating concentrations associated with a continuous discharge (Tominaga and Stathopoulos, 2013). However, no known wind tunnel test has been conducted to measure dispersing pollutant concentration in a setup of the pre-mixed stagnant volume of simulated HF.

2. OUTLINE OF WIND TUNNEL EXPERIMENT

2.1. Test section and controlled wind flow

Wind tunnel model tests to study HF dispersion around an isolated generic building were conducted in the boundary layer wind tunnel at The University of Sydney in a secondary test section measuring 4.2 m long, 0.8 m high, and 0.8 m wide, as shown in Figure 1(a). A trap compartment 1 m in length is separated by two trap doors in the test section to trap the tracer gas inside. The trap doors were designed to be lifted simultaneously with a pulley and rope lifting design, as shown in Figure 1(b). A set of auxiliary doors were installed at the test section entrance to regulate the approaching wind flow before the trap doors were lifted. These doors were fitted on a sliding frame and opened sideways simultaneously using springs and rollers, as shown in Figure 1(b). This mechanism directs the approaching wind flow into the test section with the least vertical disturbance. The test setup includes the following steps:

- Run wind tunnel fan to reach a desirable test wind speed.
- Fill trap compartment with tracer gas and dilute to a pre-set initial concentration.
- Commence tracer gas concentration measurements.
- Lift trap doors and open auxiliary doors in sequence.

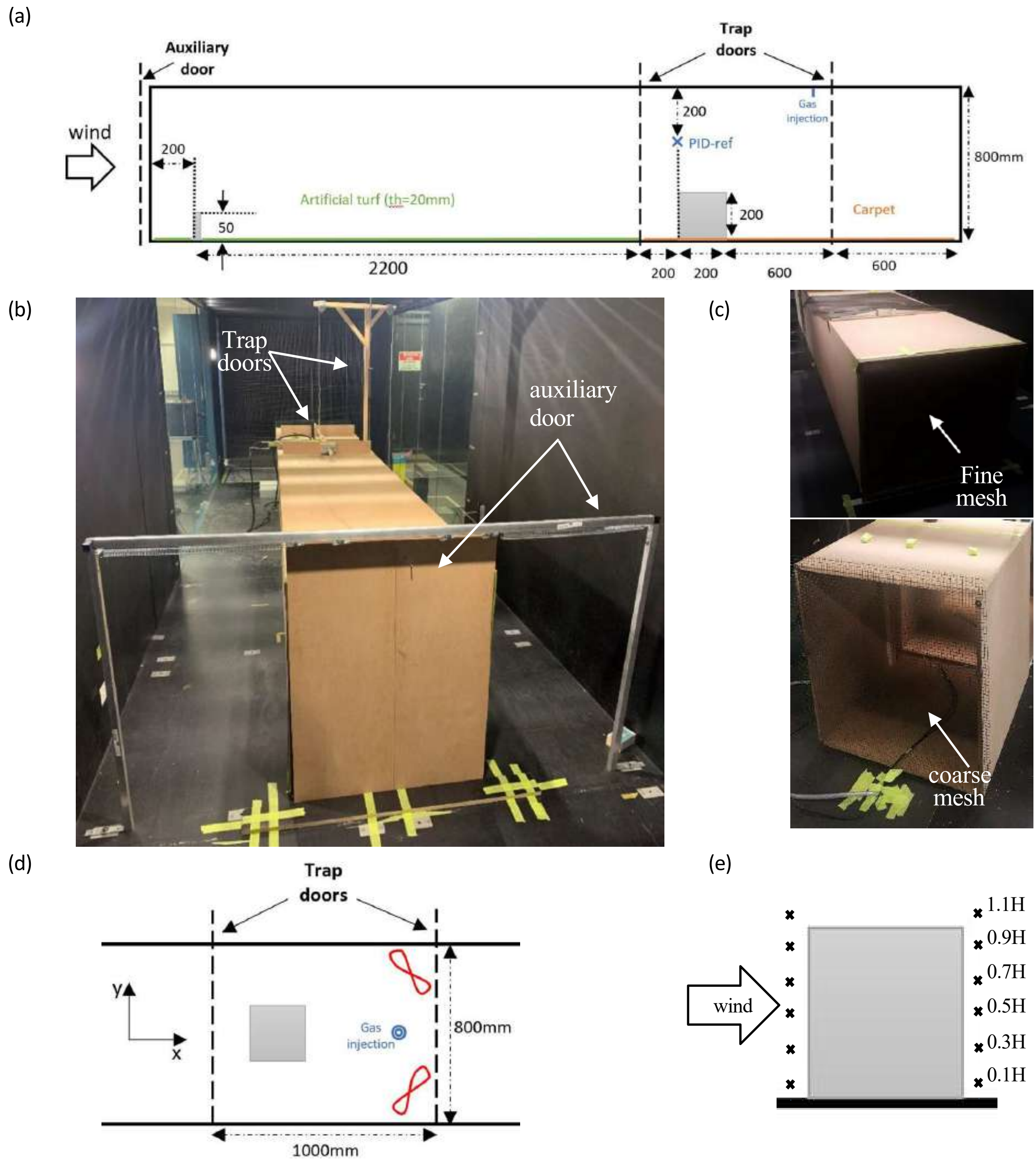

Figure 1. Experimental setup in wind tunnel: (a) Schematic side view, (b) trap doors and auxiliary doors, (c) meshed used for controlling wind speed, (d) schematic top view of trap compartment with the miniature fans, and (e) measurement points

2.2. Experimental settings

A set of fine and coarse meshes were installed at the inlet and outlet, respectively, as shown in Figure 1(c). A combination of artificial turf, carpet and barrier was deployed in the fetch length to generate an approach wind profile representative of Terrain Category 2 (open terrain) in accordance with the Australian/New Zealand wind standard. A 1:150 scale cubical building with a height of H=200 mm was adopted as the test building. The test mean wind speed and turbulent intensity at the building height were 1.3 m/s and 11 %, respectively.

2.3. Concentration measurements

Photo Ionization Detectors (PID) with a 100 parts per billion (ppb) detection limit and a 400 Hz frequency response were used to measure tracer gas concentration. Two miniature PIDs fitted with a 300 mm sampling line were used in the test setup. A mobile PID positioned to minimize flow disturbances, measured gas concentration around the building model. A reference PID was used to measure gas concentration at 400 mm above the building model aligned with the windward face via the 300 mm sampling line connected to the sensor head located outside the test section. Although this extended sampling line reduced the PID frequency response, it was a necessary trade-off between blockage effects and sensor sensitivity (Talluru et al., 2017).

A gas mixture containing 15000 ppm isobutylene was fed into the trap compartment via a discharge port at the centre of the test section ceiling, as shown in Figure 1(a). Two miniature fans were installed to disperse the tracer gas uniformly within the trap compartment, as shown in Figure 1(d). The tracer gas was further diluted with air inside the trap compartment to around 500 ppm isobutylene, the limiting measuring range of the PID. Immediately after the wind entered the trap compartment, the two PIDs captured the decay of tracer gas concentration from the initial concentration of 500 ppm. Figure 1(e) shows the measurement positions along two lines in the vertical centre plane H/10 from the windward and leeward faces of the building model.

3. AIR POLLUTANT EXPOSURE TIME

Figure 2(a) shows concentration-time histories of the mobile PID (PID-1) and reference PID (PID-2). The measured concentrations were normalized by initial concentration for each PID ($C^*=C/C_0$) to determine the air pollutant exposure time t_e as a combined delay and decay time between 98% and 2% concentration, as shown in Figure 2(b). Figure 3 shows the air pollutant exposure time t_e along the building's windward and leeward faces. Evidently, compared to the lee of the building, HF dispersed much faster in the windward region, particularly at heights above the stagnation point. Below the stagnation point, HF migrated downward due to downwash and longer exposure times were registered. In contrast, recirculation and intense turbulent mixing at the lee of the building kept the diluting HF entrapped within the recirculation zone for an extended period, thus resulting in a significantly longer exposure time.

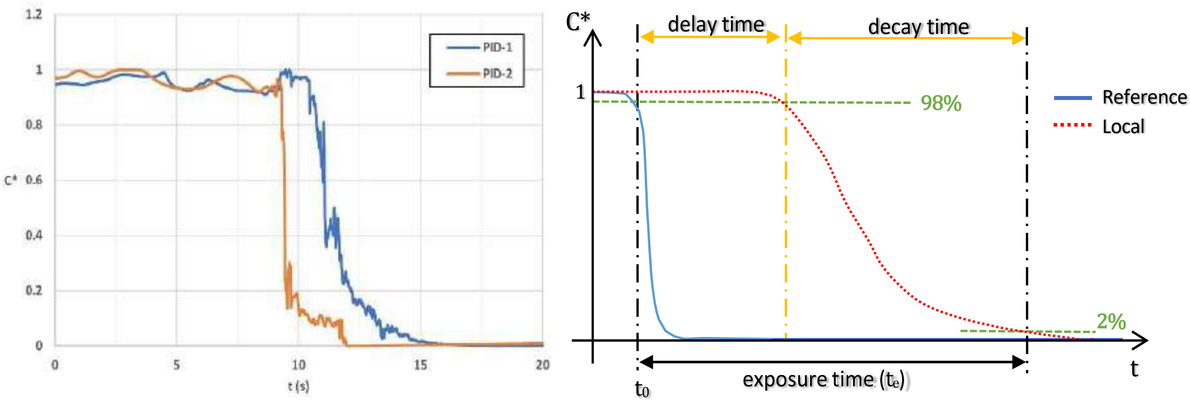

(a) (b)

Figure 2. Concentration time histories of mobile PID (PID-1) and reference PID (PID-2)

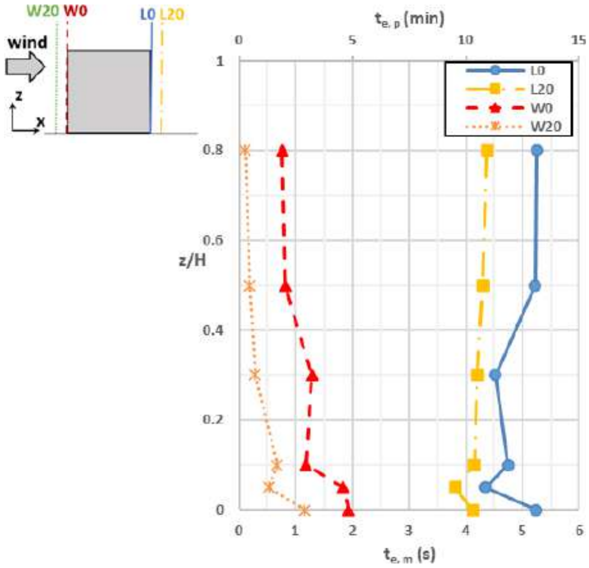

Figure 3. Vertical profiles of air pollutant exposure time in the windward and leeward regions

The model air pollution exposure time measured in this study can be converted into equivalent prototype air pollution exposure time through model scaling parameters for length, velocity and time adopted for the wind tunnel model tests. Based on a length scale of 1:150 and assuming a velocity scale of 1:1, the equivalent prototype air pollutant exposure times shown in Figure 3 suggest exposure of up to 13 minutes in the lee of the building. Such exposure may represent a significant exposure dosage depending on the pollutant type and its toxicity.

4. CONCLUSION

This paper presents a wind tunnel model study of the dispersion and air pollutant exposure time of haze-fog around a generic isolated building. Air pollutant exposure time near the windward and leeward regions of the building was found to be significantly different, with the exposure time in the lee of the building up to 4-5 times longer than in the windward region. This suggests that wind-structure interaction dominates the dispersion processes and air pollutant exposure time, resulting in the initially stagnant haze-fog being entrapped within the recirculation zone in the lee of the building for an extended period. This study offers an experimental platform to validate the CFD dispersion study of complex building configurations in an urban environment.

REFERENCES

Blocken, B., Van Druenen, T., Van Hooff, T., Verstappen, P.A., Marchal, T. and Marr, L.C., 2020. Can indoor sports centers be allowed to re-open during the COVID-19 pandemic based on a certificate of equivalence? Building and Environment, 180, 107022.

Talluru, K., Hernandez-Silva, C., Philip, J. and Chauhan, K., 2017. Measurements of scalar released from point sources in a turbulent boundary layer. Measurement Science and Technology, 28, 055801.

Tominaga, Y. and Stathopoulos, T., 2013. CFD simulation of near-field pollutant dispersion in the urban environment: A review of current modeling techniques. Atmospheric Environment, 79, 716-730.

Zhang, Y., Kwok, K.C.S., Liu, X.P. and Niu, J.L., 2015. Characteristics of air pollutant dispersion around a high-rise building. Environmental Pollution, 204, 280-288.

Zhang, Y., Yu, Y., Kwok, K.C.S. and Yan, F., 2021. CFD-based analysis of urban haze-fog dispersion-A preliminary study. Building Simulation,14, 365–375

A safe baseline approach to evaluate wind shear stress imposed on green vertical wall accounting drag coefficient.

G. Barbotti [1], C. A. Castiglioni [1]

[1] *DABC, Architecture, Built Environment and Construction Engineering, Politecnico di Milano, Via Giuseppe Ponzio 31, Milano, 20133, Lombardy, Italy*
giovanni.barbotti@polimi.it
carlo.castiglioni@polimi.it

SUMMARY
Green walls are emerging as new solution despite the curtain wall for the design of envelope both in existing and new projects. This building product has analogies as well as differences with the glazed envelope. The research opens with a reflection that raises questions and looks forward: if vegetation will assume a fundamental role as response of urban space threats, it will be necessary to manage all aspects of it, including its design and consequently structural verification to comply with. However, currently no guideline supporting designers addressing the structural response under wind actions is available. A better and more accurate estimation of tangential stress affecting the vertical walls is essential at least as baseline guide for designers since those building products are nowadays largely implemented to reduce and mitigate the Urban Heat Islands phenomena. Purpose of the paper is to investigate the effects induced on the subsystem of the façade, revealing the influence given by the plants.

Keywords: shear stress, risk assessment, tangential action, green wall, wind motion

1. INTRODUCTION

Designing envelope of buildings is currently accounted by façade engineering field. The requirements to comply with are linked also to the safety and durability of the system, although façade and curtain wall more generally are not defined as a structural component according with UNI EN 13830:2015 "Curtain Wall. Guidelines product" since they are expected to transfer loads to the main structure (considering the EN1991-1-1:2002. Eurocode 1: Actions on structures – General actions) even if extreme loading configurations, like natural hazard events, are not properly accounted. Recently (2014) in Italy great attention has been grabbed by the challenges posed by the trees and shrubs on the hanged balconies in Milano (Bosco Verticale) verified for the mechanical resistance and safety in wind gallery (respectively first analysis in Milano Politecnico and then in Miami). The issue which lies is embedded in the question "How tall buildings can tame strong winds?" Two main concerns are the core of the discussion:

- Which is the effect of wind motion on vegetation both isolated plant or canopy (Kerzenmacher and Gardiner, 1998; Shaw et al., 1982; Finnigan and Belcher, 2004)
- Considering the weight and size of some plants, how they transfer forces to the ground layer and to verify those effects providing a safe structural assessment.

2. METHODOLOGY

2.1. Literature review

Even if the authors highlight a gap of research in the subject previously introduced, a mention goes to the work performed by several authors (Fischenich, and Dudley, 1999; Schindler, 2008; Tadrist et al., 2018) and based on the contribution coming from previous research (Cionco, 1965; H. Lettau, 1969; Mayer, 1987): an interesting aspect highlighted by the papers is the role played by geometry of the plants in terms of branches, leaf ad trunk, together with the

Reynold's number (Re) accounting different drag (density, shape) even comparing different plants species (Cao et al., 2012; Gillies et al., 2002).

It appears essential to isolate the terms of drag coefficient (C_d) which has not to be confused with the "dynamic coefficient" as referred in the CNR-DT207-2008. It is mathematically a dimensionless number which ranks the resistance of an object into a fluid environment, such as water or air (atmospheric air can be considered as uncompressible gas). A frequent findable form is:

$$\mathrm{Cd} = \frac{2\mathrm{F_d}}{\rho \mathrm{u}^2 \mathrm{A}} \tag{1}$$

$2\mathrm{F_d}$ = drag force
ρ = mass density of the fluid
u = flow [1] speed of the object relative to the fluid
A= is the ref. area

2.1.1. Tangential action in the Standard

Accordingly with the Italian guideline, the tangential action (w_f) can be calculated as prescribed by the CNR standard so:

$$w_f(z) = q_p(z) \cdot c_f \qquad \left[\frac{\mathrm{N}}{\mathrm{m}^2}\right] \tag{2}$$

$q_p(z)$ is the wind kinetic peak pressure [2] and defined positive if aligned with the wind flow direction.
c_f is the drag coefficient, function of the surface roughness.
z is the reference height associated with the definition of c_f.
Some values are listed in Table 2, specifically:

Table 3 Taken by CNR-DT207-2008 and modified by the authors, pag. 137, paragraph G.12

Surface	c_f or c_d
Steel, smooth concrete	0.01
Rough concrete, tar surfaces	0.02
Waved surfaces	0.04
Green walls (porous surfaces)	Not listed or available for designers

3. RESULTS

It is noticed a wide range distribution: almost three orders of magnitude. Furthermore, it is evident that in between a shrubby species and a stiffer one (a tree with large trunk) the drag studied varies consistently. The results presented consider ranks from a clustering analysis (J.N. Tzortzi et al., 2022) then implemented to the Eq. (2).

3.1.1. Estimation for the wind shear stress

The input values in Table 3 are the ones provided and extendedly explained in the guidelines

[1] Consider that the mean wind velocity could be for high urban density area, not a significant value. However, the kinetic peak pressure, prescribed by the standard CNR-DT 207 R1/2018 ROMA – CNR 06 Febbraio 2019 can lead to a very different scenario: for a few ranks' interval measured in seconds, we could experience a severe scenario.

2 See paragraph 3.2.7, pag.52, CNR-DT 207 R1/2018 ROMA – CNR 06 febbraio 2019 "Istruzioni per la valutazione delle azioni e degli effetti del vento sulle costruzioni".

to estimate and calculate the wind actions: here for the sake of simplicity it has been calculated a standard situation.

Table 4 Edited by the author, the ratio in between the greenery accounting the drag values and a standard glazed curtain wall.

		Unit of measurements
$w_f(z)$ vegetated wall	66	N/m^2
	232	
	465	
	631	
$w_f(z)$	1.00	
q_p	664	
Cd greenery	0.1	[-]
	0.35	
	0.7	
	0.95	
Cd glazed curtain wall	0.0015	
$c_{e\,(z)}$ exposure coeff.	1.7	m/s
ρ density of the fluid/gas	1.25	[kg/m^3]
c_r return coeff.	1.00	[-]
v_b base wind velocity	25	m/s
k_r soil coefficient	0.20	[-]
k_a ref. parameter to compute c_a	0.40	[-]
a_0 ref. altitude to calculate ca	1000	[m]
z_0 roughness length	0.10	[m]
z_{min} min. height	5.00	[m]

The case which leads to 66 times more in terms of w_f is equal to 0.1, so two orders of magnitude more than the value of C_D assumed for the glazed façade as 0.0015. If this result is already mathematically significant, more severe becomes the C_D equal to 0.35 and in fact it displays a result of 232 times more. Increasing with 0.7 so closer to the threshold which has been assumed as reliable from the clustering classification, it is observed respectively a w_f very severe if it verified in reality: 465 times more means that our subsystem is facing a stressful case, which is increased considerably if the drag is 0.95, leading to a ratio which is far distant from the theoretical of the curtain wall.

Table 5 Ratio of the w_f greenery and curtain wall compared to the 4 different values of C_D.

Ratio w_f	(C_D = 0.1)	66	[-]
	(C_D = 0.35)	232	
	(C_D = 0.7)	465	
	(C_D = 0.95)	631	

4. CONCLUSIONS

The findings show the effect induced by the wind motion: it is clear to have a complete and deep understanding of the phenomenon especially supporting future analysis, especially if an effect such as the loss and damage of the vegetation caused by high turbulence conditions could expose the users and the other building components to risk for safety of users and building itself or adjacence, for instance flying debris (Gardiner et al., 2016).

Furthermore, it has been understood that the botanicals variety led to wide outcome in terms of values (Vogel S., 2000). As noticed the plants presence can generate different cases of C_D with more than one order of magnitude of difference. So, due to the gap of knowledge, a reasonable path to be paved seems to be the one to assume certain safe and reliable threshold values, such as “ultimate” value.

The proposal from the authors is, therefore, an evaluation of the shear stress with real green panel carrying out wind tunnel tests. Finally, even FEM software analysis to quantify the actual stress imposed on the sub-system might be an interesting application, also developing according with CNR-DT 207 R1/2018 ROMA a computational wind engineering (CWE) model, to validate the numerical considerations so far achieved.

ACKNOWLEDGEMENTS
The extended abstract is the result of the research carried out so far in collaboration and under the aegis of prof. Eng. Carlo Andrea Castiglioni. This activity received no additional external funding, furthermore the authors declare no conflict of interest.

REFERENCES
Cao J, Tamura Y, Yoshida A., 2012. Wind tunnel study on aerodynamic characteristics of shrubby specimens of three tree species. Urban Forestry Urban Greening 11, 465–476. doi:10.1016/j.ufug.2012.05.003.
Cionco, Ronald M. 1965. A Mathematical Model for Air Flow in a Vegetative Canopy. Journal of Applied Meteorology (1962-1982): 517-22. Accessed September 8, 2021. http://www.jstor.org/stable/26172935.
Etnier S, Vogel S., 2000. Reorientation of daffodil (Narcissus: Amaryllidaceae) flowers in wind: drag reduction and torsional flexibility. Am. J. Bot. 87:29–32.
Finnigan J. J; Belcher S. E., 2004. Flow over a hill covered with a plant canopy. Quarterly Journal of the Royal Meteorological Society, 130, 1–29. https://doi.org/10.1256/qj.02.177
Fischenich, C., and Dudley, S.,1999. "Determining drag coefficients and area for vegetation," EMRRP Technical Notes Collection (ERDC TN-EMRRP-SR-08), U.S. Army Engineer Research and Development Center, Vicksburg, MS. www.wes.army.mil/el/emrrp
Gardiner B., Berry P., Moulia B., 2016. Wind impacts on plant growth, mechanics, and damage. Plant Sci. 245, 94–118. doi:10.1016/j.plantsci. 2016.01.006.
Gillies, J. A., W. G. Nickling, and J. King, 2002. Drag coefficient and plant form response to wind speed in three plant species: Burning Bush (Euonymus alatus), Colorado Blue Spruce (Picea pungens glauca), and Fountain Grass (Pennisetum setaceum), J. Geophys. Res., 107(D24), 4760, doi:10.1029/2001JD001259.
Kerzenmacher T., Gardiner B., 1998. A mathematical model to describe the dynamic response of a spruce tree to the wind. Trees 12, 385–394. doi:10.1007/s004680050165.
Lettau H., 1969. Journal of applied meteorology, Volume 8- Note on an Aerodinamic Roughness-Parameter Estimation on the basis of roughness-element description Dept. of Meteorology, University of Wisconsin, Madison 2 April 1969 and 16 June 1969.
Mayer, H., 1987.Wind-induced tree sways. Trees 1, 195–206. https://doi.org/10.1007/BF01816816.
Roger H Shaw, A.R Pereira, 1982. Aerodynamic roughness of a plant canopy: A numerical experiment, Agricultural Meteorology, Volume 26, Issue 1,1982, Pages 51-65, ISSN 0002-1571, https://doi.org/10.1016/0002-1571(82)90057-7.
Tadrist L., Saudreau M, He´mon P, Amandolese X., Marquier A., Leclercq T., de Langre E., 2018. Foliage motion under wind, from leaf flutter to branch buffeting. J. R. Soc. Interface 15: 20180010. http://dx.doi.org/10.1098/rsif.2018.0010
Tzortzi, N., Barbotti, G., Castiglioni C.A., Voza, A. 2022. Changing Cities for Resilience against Climate Changes: Architectural, Engineering and Human Health Implications The H2020 Project HARMONIA. In Book of Abstracts of the International Conference on CHANGING CITIES V Spatial, Design, Landscape, Heritage & Socio-economic Dimensions - ISBN: 978-618-84403-7-1

Observation of flow downstream of a bridge deck model using Cobra probe and lidars

Mohammad Nafisifard [1], Shahbaz Pathan [2], Jasna B. Jakobsen [1], Mikael Sjöholm [2], Alberto Zasso [3], Stefano Giappino [3], Jonas Snæbjörnsson [1,4], Jakob Mann [2]

[1] *University of Stavanger, Stavanger, Norway,*
mohammad.nafisifard@uis.no, jasna.b.jakobsen@uis.no
[2] *Technical University of Denmark, Roskilde, Denmark,*
shpa@dtu.dk, misj@dtu.dk, jmsq@dtu.dk
[3] *Politecnico di Milano, Milano, Italy,*
alberto.zasso@polimi.it, stefano.giappino@polimi.it,
[4] *Reykjavik University, Reykjavik, Iceland,*
jonasthor@ru.is

SUMMARY
The application of lidars in civil engineering is evolving in many areas, for instance in planning and estimating design loads for long-span bridges. This paper presents a measurement campaign initiated to test and validate the performance of two continuous-wave lidars in a wind tunnel study of bridge aerodynamics, by reference Cobra probe measurements. Flow conditions downstream of the bridge deck model, within and outside of the wake region, were monitored in a boundary layer flow at the wind tunnel facility of Politecnico di Milano. The objective is to demonstrate and explore the potential of lidar remote sensing technology for wind tunnel studies relevant to bridge design.

Keywords: wind tunnel tests, bridge deck section, continuous-wave lidar, Cobra probes

1. INTRODUCTION

Wind tunnel studies of long-span bridges are essential for a comprehensive insight into bridge behavior in atmospheric flow. Time-averaged force coefficients are commonly measured with static bridge deck models, using various types of force transducers. Occasionally, surface pressure measurements are performed to increase the understanding of the interaction of the airflow with a bridge deck, both with a fixed and a moving model. Similarly, an investigation of the flow conditions around the bridge deck model, as performed in the present study, increases the understanding of the nature of the wind forces acting on the bridge girder. The present work introduces an application of lidars in a wind tunnel investigation of a bridge deck. The case study concerns a suspension bridge across the Lysefjord in Norway, instrumented by an array of sonic anemometers for long-term wind monitoring (Snæbjörnsson et al., 2017). Several lidar measurement campaigns have also been performed at the bridge site, including (Cheynet et al., 2017a; Cheynet et al., 2016), motivating the present study.

Remote sensing of a wind field by continuous-wave lidars inside a wind tunnel is a fairly unique subject. Previous investigations include validation of mean wind speed measurements by Pedersen et al. (2012), a study of the effect of droplets in an icy wind tunnel on high-frequency velocity data by Sjöholm et al. (2017), and measurements downstream of wind turbine models by Dooren et al. (2017), and Sjöholm et al. (2017).

2. WIND TUNNEL TESTS

The tests were performed in the 13.84 m wide, 3.84 m high, and 35 m long boundary layer test section (Fig. 1a) of the closed-circuit wind tunnel at the Politecnico di Milano, where mean wind speeds up to 16 m/s can be generated. Spires and floor roughness elements were used to create a boundary layer flow, relevant for a prototype bridge, with a horizontal turbulence intensity of about 10%. A 4 m long section model of the bridge deck, 12.3 m wide and 2.76 m tall in full-scale, was fabricated in a 1:15 scale (Fig. 1b) and tested at a zero-pitch angle. A Pitot tube at deck height was used to monitor the reference wind speed in the tunnel.

The lidar measurement equipment was provided by the Technical University of Denmark (DTU) in the form of two 2-inch-wide optical telescopes (lidics) that were connected to a single continuous-wave laser (Fig. 1c) (Sjöholm et al., 2017). Special clamps were designed and 3D-printed at DTU, to attach the telescopes to a supporting aluminum beam. The telescopes could slide along the beam as well as rotate about a fixed axis. The beam was attached to a specially designed frame, providing support for different measurement configurations. An aerosol generator was used to generate droplets of sufficient concentration for the lidar measurements (Fig. 1a).

3. TEST METHOD

In the main part of the measurement campaign, wake profiles (mean wind speeds and turbulence) at several distances from the model were monitored. Measurements of the lateral coherence, in both disturbed and undisturbed flow, were also undertaken. The tests were performed using Cobra probes and lidars in separate runs, so that the lidar measurements were free of any interference in the proximity of the target volume.

The setup adopted for wake profile measurements, in which the two telescopes were orientated at an angle of ±31° from the horizontal is illustrated in Fig. 2b. The two line-of-sight velocities, providing the information on the turbulent flow in the vertical plane, were sampled at a frequency of approximately 600 Hz.

For the study of lateral coherence, a side-by-side arrangement of the telescopes as illustrated in Fig. 1c was used. Simultaneous measurements by two lidars were carried out at three different inclination angles (-30°, 0°, and 30°), to enable the estimation of the lateral coherence of the u- and w-turbulence components.

Simultaneous measurements by lidars and a Cobra probe were carried out, to enable a direct comparison of the turbulence acquired by the two types of sensors. In Fig. 2, the lidars are focusing on a point 303 mm below the deck, 800 mm (~1B) downstream of the model. A reference Cobra probe was deployed, 100 mm from the focus point of the lidars (see Fig. 2c).

(a) Seeding system. (b) Deck section model. (c) Lidars.

Figure 1. The wind tunnel setup.

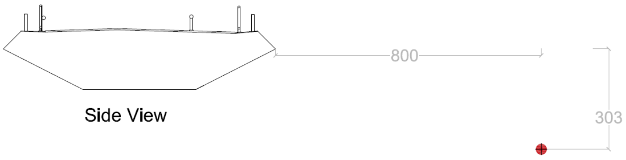

(a) Schematic of tailored scanning.

(b) Side view of the lidar telescopes.

(c) Close front view of instrumentations.

Figure 2. The measurement setup. For clarity, the laser beams are illustrated by red solid lines. Target points of lidars and Cobra probe are marked by red and green circles, respectively.

4. DATA ANALYSIS

An illustration of the preliminary results is given in Fig. 3 and Fig. 4, showing the along wind and vertical velocity profiles of the wake flow as observed by a Cobra probe 800 mm (~1B) downstream from the trailing edge. The mean wind velocity deficit in the wake behind the model embedded in the boundary layer flow is clearly demonstrated. The mean vertical wind speeds imply that the average streamlines deviate from the horizontal direction towards the "wake center". Both the horizontal and the vertical turbulence intensities, displayed in Fig. 4, exceed 30% at the trailing edge level, a triple and a fivefold increase compared to the undisturbed flow for the two components, respectively.

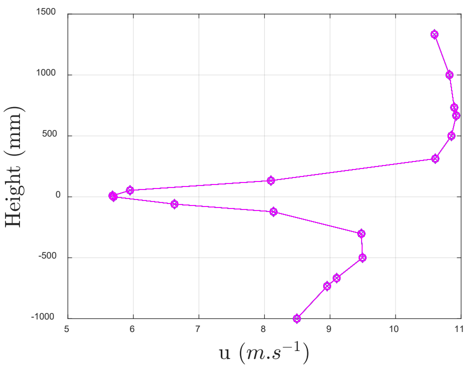

(a) mean along-wind velocity

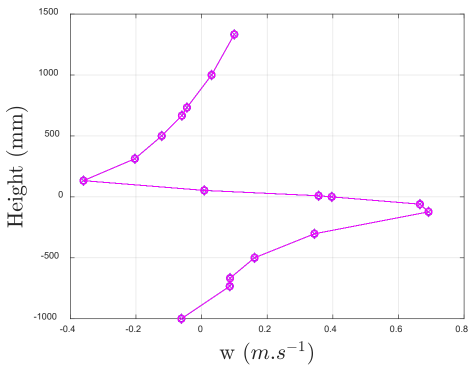

(b) mean vertical velocity

Figure 3. Mean wind velocity in the wake.

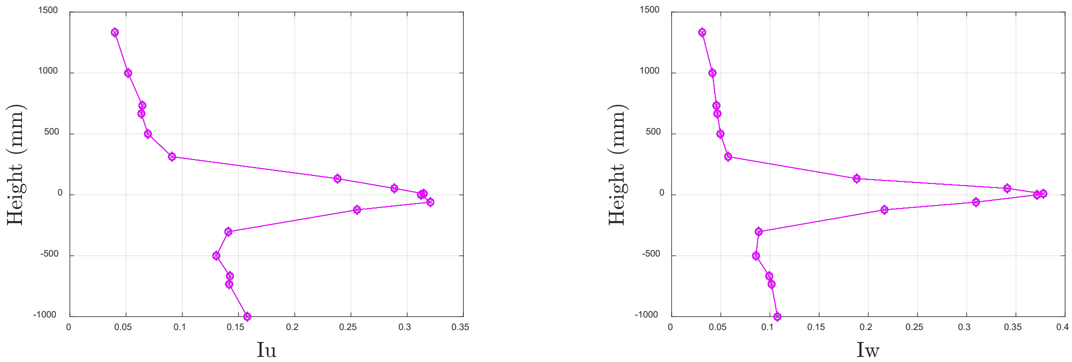

(a) Along-wind turbulence intensity. (b) Vertical turbulence intensity.

Figure 4. Turbulence intensity in the wake.

The full-length paper presents an extended analysis of the wake flow measurement data. This includes a comparison of a mean wind profile and turbulence statistics derived from the lidar and the Cobra probe data.

ACKNOWLEDGEMENTS

This work has received funding from the European Union Horizon 2020 through the Innovation Training Network Marie Skłodowska-Curie Actions: Lidar Knowledge Europe (LIKE (grant no. 858358)). We would like to thank Luca Ronchi and Umberto Spinelli for their assistance in the wind tunnel measurements and Lorenzo Rosa for taking photos of the experiments.

REFERENCES

Cheynet, E., Jakobsen, J. B., Snæbjörnsson, J. T., Angelou, N., Mikkelsen, T., Sjöholm, M., Mann, J. and Svardal, B., 2017a. Full-scale observation of the flow downstream of a suspension bridge deck. Journal of wind engineering and industrial aerodynamics 171, 261-272.

Cheynet, E., Jakobsen, J. B., Snæbjörnsson, J. T., Mikkelsen, T., Sjöholm, M., Mann, J., Hansen, P., Angelou, N. and Svardal, B., 2016. Application of short-range dual-Doppler lidars to evaluate the coherence of turbulence. Experimental fluids 57.

Engineering and Industrial Aerodynamics 161, 17-26.

Pedersen, A. T., Montes, B. F., Pedersen, J. E., Harris, M. and Mikkelsen, T., 2012. Demonstration of short-range wind lidar in a high-performance wind tunnel. Proceedings of European Wind Energy Conference and Exhibition, Copenhagen, Denmark.

Sjöholm, M., Vignarolia, A., Angelou, N., Nielsen, M., Mann, J., Mikkelsen, T., Bolstad, H., Merz, K., Sætran, L., Mühle, F., Tiihonen, M., and Lehtomäki, V., 2017. Lidars for Wind Tunnels - an IRPWind Joint Experiment Project. Energy Procedia.

Snæbjörnsson, J. T., Jakobsen, J. B., Cheynet, E. and Wang, J., 2017. Full-scale monitoring of wind and suspension bridge response. Proceedings of 1st Conference of Computational Methods in Offshore Technology (COTech), Stavanger, Norway.

van Dooren, M. F., Campagnolo, F., Sjöholm, M., Angelou, N., Mikkelsen, T. and Kühn, M., 2017. Demonstration and uncertainty analysis of synchronised scanning lidar measurements of 2-D velocity fields in a boundary-layer wind tunnel. Wind Energy Science, 329-341.

17th Conference on Wind Engineering – IN-VENTO 2022
Politecnico di Milano, IT
4 – 7 September 2022

An affordable Performance-Based Wind Engineering procedure

Mattia Francioli [1], Francesco Petrini [2], Franco Bontempi[3]

[1]*Sapienza University of Rome, Rome, mattia.francioli@uniroma1.it*
[2]*Sapienza University of Rome, Rome, francesco.petrini@uniroma1.it*
[3]*Sapienza University of Rome, Rome, franco.bontempi@uniroma1.it*

SUMMARY:
This paper proposes a procedure for the Performance-Based Wind Engineering of high-rise buildings by extending the well-established SAC-FEMA approach originally implemented in earthquakes for the simplified evaluation mean annual frequency (MAF) of appropriate structural Limit States (LSs) in frame buildings. The development of what we will call the "SAC-FEMA WIND" approach implies the consideration of specific wind engineering peculiarities, like the classification of the across-wind response in two distinct regimes due to buffeting and vortex shedding phenomena, with the consequent adaption of the procedures defined for seismic analysis to these two regimes.

Keywords: SAC-FEMA, Performance Based Engineering, Risk, occupants' comfort

1. INTRODUCTION

Starting from its first formalization by a general procedure (Ciampoli et al 2011, Spence and Kareem 2014), Performance-Based Wind Engineering (PBWE) has been deeply developed and improved during years regarding both the evaluation of Serviceability and Ultimate limit states (SLSs and ULSs). Existing applications of PBWE are based on integral formulations for probabilistic characterization of the occurrence for the considered LSs, meaning that the explicit evaluation of the LSs failure probability implies the solution of an integral making the procedure not suitable for being implemented in Standards for explicit probabilistic PBWE.

The aim of this work is to contribute to the identification of a method that can be used in practical implementation in PBWE in Standards for explicit evaluation of the mean annual frequency (MAF) for pertinent LSs. Therefore, the structural performances of a 3D steel high-rise building under wind loads is assessed using by implementing the SAC-FEMA probabilistic approach already used in earthquake engineering (Cornell et al 2002) for the simplified evaluation MAF in frame buildings, and by specializing it for wind engineering purposes, something leading to the so called "SAC-FEMA WIND" method.

2. THE SAC FEMA WIND APPROACH

As already said in the introduction of the paper, the expression of the structural performances under wind in the same format/framework (called SAC-FEMA WIND in what follows) used for earthquake is crucial for practical implementation of PBWE.

Obviously, the SAC-FEMA WIND approach must be specialized to consider specific peculiarities of structural wind engineering problems. In this view, one of the most relevant specific aspects to take into account in wind engineering response of tall buildings is the pronounced dependence of the involved aerodynamics and the resulting structural D from the incident wind direction θ relatively to the structure. For example, in a square floor plan prismatic building, wind incident angles corresponding to orthogonal directions with respect to building faces (e.g. θ=0°; 90°; 180°; 270° in Fig. 1) are related to square-shape bluff-body aerodynamics, then implying the vortex shedding (*VS*), with potential lock-in phenomenon leading to large floor displacements and accelerations in the across-wind direction. On the contrary, edge-incident winds (e.g. θ=45°; 135°; 225°; 315° in Fig. 1) are related to rhomboidal-shape aerodynamics, usually not associated to relevant *VS* effects or to relevant across-wind structural responses.

For this reason, it appears appropriate to treat the wind-induced demand in the across-wind direction as generated mainly by two distinct response regimes depending on the wind incident angles: i) those potentially characterized by the *VS* and; ii) those induced by the intrinsic atmospheric turbulence (buffering regime *BU*) without any significant *VS* effect.

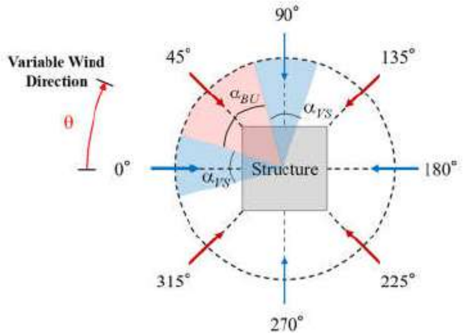

Figure 1. Wind angles of incidence related to different aerodynamic regimes

With these premises, the SAC-FEMA WIND, when used for evaluating the MAF for buildings occupants to feel vibration-induced discomfort, assumes the following general formulation

$$\lambda_i^j = \sqrt{\phi} k_{0-i}{}^{1-\phi_i^j} \left[H_i\left(im^{\hat{C}j}\right)\right]^{\phi_i^j} \cdot exp\left[\frac{1}{2} q_i k_{1-i}^2 \left(\beta_C^{j^2} + \phi_i^j \beta_{D-i}^2\right)\right] \tag{1}$$

With *i*=*VS* or *BU*; *j*=*APT* or *OFF*. In previous equation, k_0, k_1 and k_2 and *a*, *b* are interpolation coefficients for the hazard and the mean wind demand respectively, $q_i = \frac{1}{1+2k_{2-i}\beta_{D-i}^2/b_i{}^2}$ and, $\phi_i^j = \frac{1}{1+2k_{2-i}\left(\beta_{D-i}^2+\beta_C^{j^2}\right)/b_i{}^2}$, $\widehat{D}, \hat{C}$, β_D and β_C, are the median and dispersion values of the demand and the capacity respectively, $im^{\hat{C}}$ is the wind intensity value for which $\widehat{D}$=$\hat{C}$.

The SAC-FEMA WIND is applied to a 74-storey steel high-rise building to evaluate the Mean Annual Frequency (MAF) of the occupants' comfort limit state, resulting MAF has been compared with the failure probability for the same limit state as obtained by a Monte Carlo simulation, showing good accordance and conservative estimation.

REFERENCES

Ciampoli, M., Petrini, F. and Augusti, G., 2011. Performance-Based Wind Engineering: towards a general procedure. Struct Safety 33(6), 367-378.

Cornell, A.C., Jalayer, F., Hamburger, R.O. and Foutch D.A., 2002. Probabilistic basis for 2000 SAC Federal Emergency Management Agency steel moment frame guidelines. Journal of Structural Engineering, ASCE 128(4), 526-533

Spence, S.M.J. and Kareem, A., 2014. Performance-based design and optimization of uncertain wind-excited dynamic building systems. Engineering Structure 78, 133-144.

Vamvatsikos, D., 2014. Accurate Application and Second-Order Improvement of SAC/FEMA Probabilistic Formats for Seismic Performance Assessment. Journal of Structural Engineering, ASCE 140(2), 04013058.

Field measurements of wind microclimate at vehicle level on bridge deck over mountainous (canyon) terrain

Fengying Wu [1], Lin zhao [2]*, Claudio Borri [3]

[1]*State Key Lab of Disaster Reduction in Civil Engineering, Tongji University, Shanghai 200092, China* 1810209@tongji.edu.cn

[2]*State Key Lab of Disaster Reduction in Civil Engineering, Tongji University, Shanghai 200092, China* zhaolin@tongji.edu.cn

[3]*Dip.to di Ing. Civile e Ambientale, Università di Firenze, Via di S. Marta 3, 50139 Firenze, Italy.* claudio.borri@unifi.it

SUMMARY

Field measurements on a bridge deck were conducted to investigate the microclimate wind environment at the vehicle levels. The measurement points were arranged in the mid-span and tower regions along the bridge. The characteristics of microclimate wind at mid-span and tower regions were analyzed, including the wind speed and fluctuation characteristic. Results show that wind profiles at mid-span confirm the power exponential distribution. However, the wind profiles show non-power-exponential distribution at tower regions. The wind speed profiles at mid-span and tower regions were statistically fitted. The wind speed distribution at tower regions show obviously shielding or acceleration effects and a typical wind curve across though tower region was proposed. Furthermore, the measurement results proved that microclimate wind is inconsistent with the variation characteristics of the -5/3 inertial subregion spectrum, and a 3rd double logarithm polynomial was recommended. Extreme wind speeds were also discussed and showing that which are more reasonable.

Keywords: field measurement; microclimate wind; wind profile

1. INTRODUCTION

Several long-span bridges have been newly built in the southwest of China, such as the first Beipan river bridge in Guizhou. Long-span bridges built in mountainous terrains are often suffering from the strong wind attacks by the wind channel effect and high turbulence. Therefore, the wind microclimates at the vehicle level around the bridge decks under complex terrains were significantly differ from those of bridges in flat terrain, which not only affects the bridge aerodynamic characteristics but also had adverse effects on vehicle driving safety on long-span bridges. At present, wind tunnel tests, CFD and field measurements were commonly used to analyse the wind field of long-span bridges in mountain valleys. Compared to the CFD and wind tunnel test, field measurement is a direct and effective method that has been adopted in the wind field characteristics analysis. There have been fruitful research achievements around wind field characteristics at bridge sites under terrains effects (Belu et. al, 2013; Fenerci et. al, 2018). However, few investigations discussed the effects of complex terrains on wind microclimate on bridge decks. It is urgent to implement wind microclimate on-the spot observations to ensure the vehicle driving safety on long-span bridges. In this study, the Honghe Bridge in Yunnan, China, a suspension bridge was considered as the engineering application and the wind microclimate was measured. Results indicate that the wind microclimate on the bridge deck in a typical canyon terrain is crucial for vehicle driving safety and comfort.

2. FIELD MEASUREMENT

The Honghe Bridge with a main span of 700m was considered as the engineering application which located in a typical southwest mountain canyon terrain with large undulations. An 3D ultrasonic anemometer was installed at leading edge of bridge with a height of 2.0 m and a lateral extension of 2.5 m over the girder windward edges as the reference wind measurement to avoid interference effects of bridge and additional structural elements. The cross section and lanes were displayed in Figure 1. The lanes along the lateral direction were defined as lanes A, B, C and D, and subscript w and l represented as windward and leeward, respectively. Four measuring spots for each tower region along the tower were marked as 1, 2, 3 and 4 measuring points, respectively, and one measuring spot was set at the mid-span location. The measurement points arrangement was shown in Figure 2. An 3D ultrasonic anemometer was set up at a height of 5.5 m during measurement, 2 propeller type mechanical anemometers were installed at heights of 4.0 m and 3.0 m, 2 two tail rotor type mechanical anemometers were installed at heights of 1.8m and 0.8 m, respectively. The sampling frequency of all anemometers was 10 Hz.

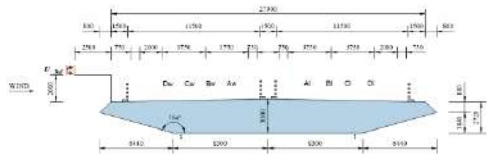

Figure 1 The basic parameters of the Honghe Bridge (unit: mm)

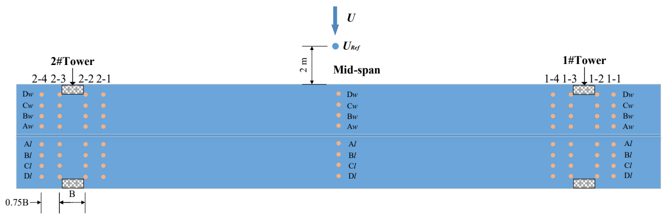

Figure 2 Measurement point arrangement above bridge deck

3. MEAN WIND SPEED CHARACTERISTICS

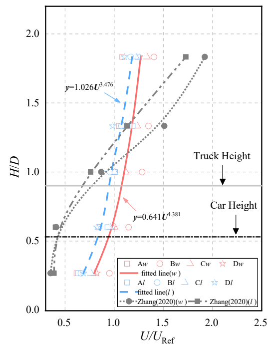

Figure 3 Wind profiles at mid-span

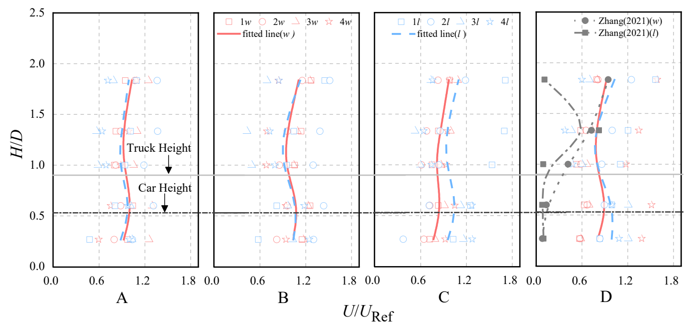

Figure 4 Wind speed profiles at bridge tower regions (2# Tower)

The windward and leeward wind speed profiles in different lanes at mid-span and tower regions (2# tower) were shown in Figure 3 and Figure 4. Wind speeds decreased with decreasing elevation owing to the shielding effects of balustrades. The shielding effect on the wind speed near the bridge deck decayed as the distance from the windward edge, and the wind speed in the leeward lanes became lower than that in the windward lanes, indicating that additional elements were beneficial to the wind microclimate. The measured wind profile in mid-span regions were fitted as shown in Figure 3. The wind speeds at the tower regions exhibited significant wind speed acceleration effects which caused by the tower. Therefore, the mean wind speeds at windward and leeward behaved higher wind speed in the elevation range of 0-2.0 m and 4.0 m-5.5m, lower wind speed in the elevation range of 2.0 m to 4.0 m. The wind profile of the tower regions can be fitted by the Fourier function, as shown in Eq. (1). Compared to Zhang et. al. (2021) results, driving safety and comfort were underestimated based on the wind tunnel tests.

The characteristics of the wind speed along bridge tower regions were depicted in Figure 5. Wind speeds on windward side along the driving direction exhibited a trend of dramatic reduction while entering the tower region, which was followed by a slight increase after leaving the windward bridge tower region. Indicating that strong shielding effects of the bridge tower on the incoming oblique wind flow, and the wind speeds were drastically reduced while entering the windward tower region. However, the windward wind speed increased again after leaving the bridge tower regions which exhibited a significant acceleration effect on wind speed while leaving tower region, which is vital to the vehicle driving safety when a vehicle crosses the tower region. The variation trend of the wind speed across tower region was different from the crosswind variation mode approved by recently researchers (Wang and Xu, 2015) for analysis driving safety when a vehicle crosses tower region and wind curve suggested by Chinese Specification.

(a) Windward (b) Leeward

Figure 5 Wind speed variation through tower regions

4. FLUCTUATING WIND SPEED CHARACTERISTICS

The power spectrum of the windward turbulence wind in the mid-span and bridge tower regions (2# Tower, D lane) were shown in Figure 6. Evidently, the von Kármán spectra were lower than those of the measured results in the higher frequency domain, either in mid-span or tower regions and slightly higher than those ones of the measured results in the lower frequency domain, indicating that spectral energy distribution was inconsistent with spectral variation characteristics of -5/3 in the inertial subregion; finally, the power spectrum of microclimate turbulence components in canyon regions was significantly different from those of flat terrains. Thus, a 3rd double logarithm polynomial was adopted to depict the energy distribution of the turbulence wind in the frequency domain and further study the turbulence characteristics of the microclimate wind environment in a mountain canyon, as shown in Figure 6.

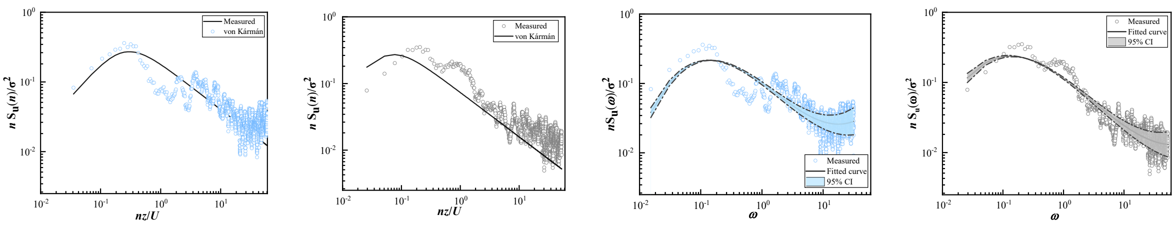

(a) Measured and von Kármán turbulence spectra (Mid-span, u) (b) Measured and von Kármán turbulence spectra (2# Tower, u) (c) Measured and fitted turbulence spectra (Mid-span, u) (d) Measured and fitted turbulence spectra (2# Tower, u)

Figure 6 Characteristics of wind spectra

The extreme wind distributions in tower regions were shown in Figure 7. The extreme wind in tower regions exhibited a decreasing trend as the distance increases from the windward edge owing to the shielding effects of the tower and additional facilities. Towers have significantly shielded effects on crosswinds, leading to much lower extreme wind appearing in the leeward bridge towers regions, and the effects of topography due to different mountain terrains on both sides of the tower. The extreme wind profiles at mid-span and tower regions (2# Tower, 1# measuring spot) are displayed in Figure 8. Extreme wind profiles showed different variations along the elevation direction compared to the mean wind. The extreme wind profiles in the mid-span shows a dramatic increment above a height of 4.0 m. Windward extreme wind result larger than those of leeward in the mid-span region because of the shielding effects of additional facilities. The crosswind distribution in the tower region may be significantly accelerated by the tower according to extreme wind profiles, which is unfavorable for vehicle driving safety when vehicles pass through tower regions.

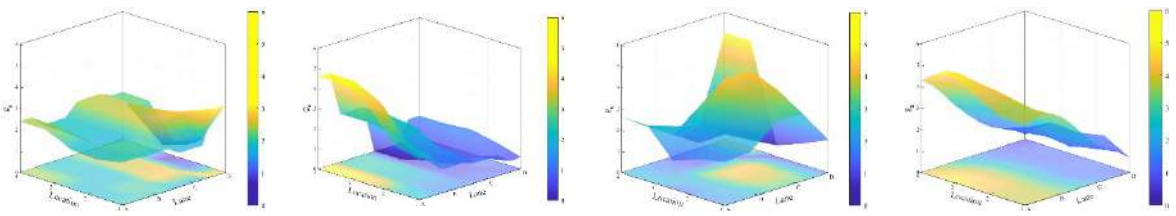

(a) Windward (1#Tower) (b) Leeward (1#Tower) (c) Windward (2#Tower) (d) Leeward (2#Tower)

Figure 7 Extreme wind distribution at bridge tower region

(a) Mid-span (b) Tower region (2# Tower, 1# measuring spot)

Figure 8 Extreme wind profiles variation

5. CONCLUSIONS

The mean wind speed at mid-span shows a trend of reduction as the elevation decreases and additional facilities were beneficial to the wind microclimate of vehicle driving. The wind speed at the tower regions was larger than that one of mid-span exhibiting significant wind speed acceleration effects caused by the tower. Fitted wind speed profiles were suggested. Variations in wind speed at tower regions show a strong shielding effect of the tower on the incoming wind. The von Kármán spectrum cannot accurately describe the characteristics of turbulence in microclimate wind under complex terrain effects, so that a 3rd double logarithm polynomial was proposed to depict the energy distribution of the turbulence. In addition, the extreme wind speeds are more crucial for evaluating the vehicle driving safety and comfort on long-span bridges, especially in bridge tower regions.

ACKNOWLEDGEMENTS

The authors gratefully acknowledge the support of National Natural Science Foundation of China (52078383, 52008314)

REFERENCE

Belu R., Koracin D. 2013. Statistical and spectral analysis of wind characteristics relevant to wind energy assessment using tower measurements in complex terrain. Journal of Wind Energy 2:1049-1051.

Fenerci A., Øiseth O. 2018. Strong wind characteristics and dynamic response of a long-span suspension bridge during a storm. Journal of Wind Engineering and Industrial Aerodynamics 172: 116-138.

Zhang M. J., Zhang J. X., Li Y. L., et al. 2020. Wind characteristics in the high-altitude difference at bridge site by wind tunnel tests. Wind and Structures 30(6): 548-557.

Receiver Sand Mitigation Measures along railways: CWE-based conceptual design and preliminary performance assessment

Marko Horvat[1], Luca Bruno[1,3], Sami Khris[2,3]

[1]*Department of Architecture and Design, Politecnico di Torino, IT*
[2]*Optiflow Company, 160, Chemin de la Madrague-Ville, F-13015, Marseille, France*
[3]*Windblown Sand Modelling and Mitigation joint research group, IT-FR*

Key words: *Windblownsand,Sanderosion,Railway,Design,ReceiverSandMitigationMeasure,Computational Wind Engineering*

Desert railways locally disturb windblown sand drift and induce sand sedimentation and erosion around them. Because of accumulated sand, railways can attain Sand Serviceability Limit States (SSLS) and/or Sand Ultimate Limit States (SULS), as defined first in Bruno et al. (2018). Sand Mitigation Measures (SMM) are essential in countering such adverse effects.
To avoid them, Sand Mitigation Measures (SMMs) are employed. Receiver SMMs are directly located on the infrastructure, e.g. the railroad or its shoulders. In particular, aerodynamic-based Receiver SMMs are intended to promote wind-induced sand erosion from the railway and sand transport far from it. This SMM type is at its infancy: the few solutions proposed up to now are reviewed in Bruno et al. (2018). This is mainly because the Receiver SMM aerodynamics strongly interacts with the railway substructure or the track components (e.g. rail, sleeper or slab, ballast) and depends on the railway functional requirements (e.g. rail gauge, safety distance from the track). The present study is focused on a single track system, called Humped Sleepers (Reissberger et al 2014, Reissberger 2015, Fig. 1).

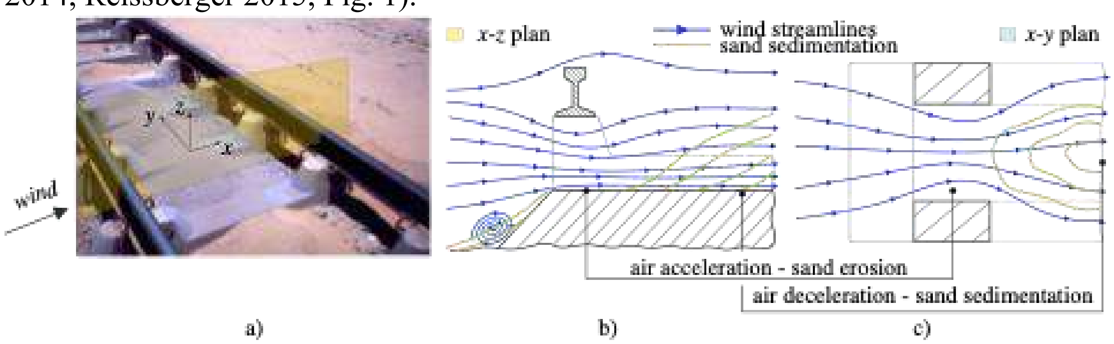

Figure 1. Humped sleepers (Reissberger 2015, a). Qualitative streamlines and sand accumulation levels (b,c)

The qualitative reading of the air flow and sand sedimentation around HS is given in Bruno et al. (2018), and graphically summarized in Figure 2. The gap locally accelerates the airflow thanks to the well-known Venturi effect, locally in duces high wall shear stresses, promotes sand erosion, and allows sand transport. The recent extensive computational campaign in Horvat et al. (2021) quantitatively pointed out the airflow deceleration along the gauge for every incoming wind speed. It involves extensive sedimentation conditions at relatively low incoming wind speeds on most of the upper ballast surface.

The present computational study aims at developing an innovative aerodynamic-based Receiver SMM called *Sand Blower*. It is intended to complement the HS track system and further improve its performances. The proposed Receiver SMM is designed in the form of an S-shaped guide vane (Fig. 2). Its Venturi-based working principle is expected to catch the high-momentum flow from the upper part of the bl; deflect the flow downwards; direct the flow parallel to the upper ballast surface and towards the upwind gap. The momentum across the upwind and downwind gap increases in turn (Fig. 2a, c), as well as the jet flow along the whole gauge (Fig. 2b), so to guarantee erosion conditions along it.

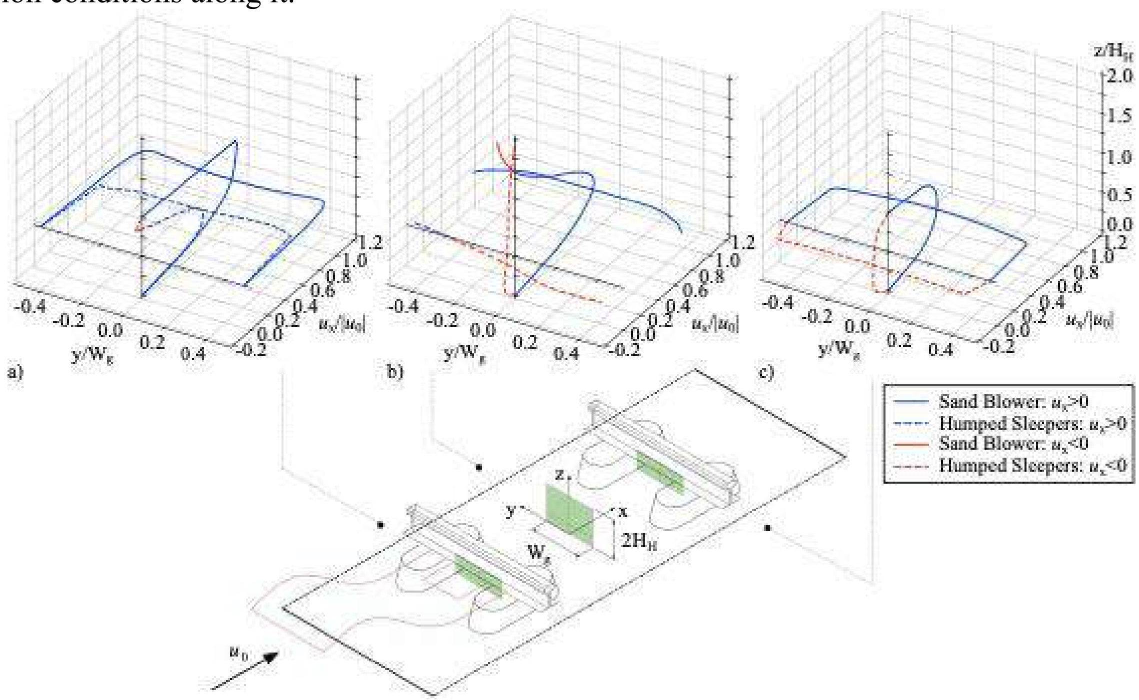

Figure 2. Aerodynamics, sand erosion, and deposition zones

The oral presentation will summarize the adopted computational model, detail the considered setups, critically discuss the conceptual and preliminary design, and the performance assessment of the *Sand Blower* in terms of both controlled wind flow and induced sand erosion.

References

Bruno, L., Horvat, M., Raffaele, L. (2018) Windblown Sand along Railway Infrastructures: A review of Challenges and Mitigation Measures, *J. of Wind Engineering & Industrial Aerodynamics*, 177, 340-365.

Riessberger, K., Guggenberger, E., Ossberger, H., 2014. Sleepers having elevated rail fastening as protection against sand coverage. Patent WO/2014/165871.

Riessberger, K., 2015. Heavy haul in sand environment, in: IHHA 2015 Conference, Perth, Australia. URL: https://docplayer.net/144777747- Heavy- haul- in- sand- environment.html.

Horvat, M., Bruno, L., Khris, S., 2021. CWE study of wind flow around railways: Effects of embankment and track system on sand sedimentation. *J. of Wind Engineering & Industrial Aerodynamics*, 208, 104476.

Piezoelectric Energy Harvesting in tall buildings under wind

Juliano F. Martins [1], Mattia Francioli [2], Francesco Petrini [3]

[1]*Sapienza University of Rome, Rome, juliano.martins@uniroma1.it*
[2]*Sapienza University of Rome, Rome, mattia.francioli@uniroma1.it*
[3]*Sapienza University of Rome, Rome, francesco.petrini@uniroma1.it*

SUMMARY:

Energy harvesting from vibration has received emphasis on areas related to the development of efficient and reliable devices that can be able to convert mechanical into electrical energy. In this context, piezoelectric materials has an special attention due to its natural capacity of converting mechanical into electrical energy. With that, the work explores this material by employing it into new devices named as PiDs – piezo dampers. PiDs are similar to rubber bridge bearings but are provided with a piezoelectric core which provides efficient vibration energy harvesting in tall building subject to wind.

Keywords: Piezoelectricity; Energy Harvesting; Steel Buildings

1. INTRODUCTION

Energy harvesting (EH) is the process of extracting the energy from the environment or a system and converting it into electrical energy. Often the area of application is related to autonomous wireless sensors. An EH equipment typically divides in 3 parts: the energy source (as vibrations), the harvesting mechanism and the load (consumes or stores the electrical output energy).
From the general point of view piezoelectric parts receives attention as harvesting mechanism in the chain, due to their flexibility on obtaining an amount of electrical energy when subject to vibrations. From recent decades such material started to be applied in civil engineering structures by innovative devices for EH and for powering monitoring sensors.

The topic of smart building is of such interest, which englobes areas of application on Structural Health Monitoring (SHM), where piezoelectric EH (pzEH) present a point of interest to avoid cables and, with that the possibility of charging batteries on remote location, not forgetting others effects as maintenance and sustainability (Covaci 2020).

The main issue to solve in pzEH applications in buildings is that piezoelectric materials present generated electrical energy dependent of the frequency of vibration from the input source. Hence, vibration on tall buildings are usually on a low range what makes that this devices does not present an efficiency. Due to this, some frequency-up methods are proposed such as impact interaction, contact and magnetic plugging.

Building automation with EH performance can be observed on a work by Petrini and Gkoumas (2018) where it is presented a concept with analytical and experimental evaluation for piezoelectric energy harvesting from flow induced vibrations placed inside Heating Ventilation and Air Conditioning (HVAC) ducts. The application is focused on powering humidity and temperature sensors and also on transmitting data via wireless. The produced power is ranged between 200 - 400 μW.

Yurcheko (2022) explores an optimization algorithm on piezoelectric multi-beam gravity based device for energy harvesting in wind applications for powering wireless sensors and data transmission . The power output passes from 68 μW to 150 μW on their analsys. Wang (2022) investigates the energy harvesting system's nonlinear dynamic characteristics for micro-actuator's energy storage by introducing nonlinear differential terms to describe the hysteresis phenomena and the results are later compared between numerical and experimental results. The topic of energy harvesting is even aborded on fluid-pressure based vibrations with a piezoelectric harvester film. (Mati 2022).

From this perspective the present work focus on conceiving and modelling a device named PIDs (piezoelectric dampers) which are embed on the structural parts of a building such as a diagonal bracer. The energy source of the device are the displacement of the structural member mainly studied by application of wind loads.

2. PIDs conceptual design

PiDs are composite structural members comprising piezoelectric parts (in form of bars or "core"), which resist loads by axial mode embedded in them.

The pzEH technology is well-established at the micro- and meso- scale applications relevant to communication, space, and medical sectors where it is widely used for vibration or temperature gradient EH to power sensors and/or small actuators. However, no attempts were pursued to extend pzEH usage in macro-scale civil engineering applications such as in structural components in buildings. Such macro-scale applications of pzEH are hindered by the following two limitations:

i) the excessive magnitude of the involved forces. Piezo materials on their own would not be able to sustain loads that are typical of Civil structural/buildings; and

ii) amount of harvestable energy. pzEH from vibrations is proportional to the frequency of the dynamic loads and to the activated mass. In common (meso-, micro-scale) pzEH applications loading frequency is in the range of 0.1-10kHz allowing for significant EH from small vibrating masses, while vibration frequencies in buildings are orders of magnitude lower (within 1-25 Hz) which reduces dramatically EH despite the larger masses involved.

Scaling-up the pzEH by the the PiD device is the aim of this work. by addressing the two above-mentioned limitations via the innovatively designed PiDs (Fig.1):

i) the piezoelectric core in PiDs will be embedded within (connected in parallel with) other structural blocks made of appropriate materials (e.g., steel or rubber) carrying the main part of the whole load acting on the device;

ii) the piezo components inside the PiDs will be designed to operate in two different kinds of nonlinear regimes: near-buckling conditions and impact dynamics. The former involves designing the piezo-bar inside the PiDs to buckle under the operating conditions, then increasing both piezo strains and vibration frequencies with respect to the pre-buckling (linear) dynamic conditions . The second regime allows impact of the vibrating piezo component, in order to convert the low-frequency response to high frequency. In PiDs these two regimes will be enabled by the appropriate calibration of a "clearance gap" between the piezo fin and the other blocks being part of the PiDs for allowing buckling and lateral impact of the piezo core. This will allow the PiDs to harvest significant energy even at the typical low-frequency range of vibration in buildings. Below PiDs are schematically presented in Figure 1.

From Fig. 1 it is possible to note the location of the proposed device in the bracing-column connection of steel buildings. In synthesis, the PiD was planned from a lead rubber bearing (LRB) equipment where the lead core is substituted by a piezoelectric material core. The outer structure is composed by rubber and steel layers which are responsible to the structural integrity of the device.

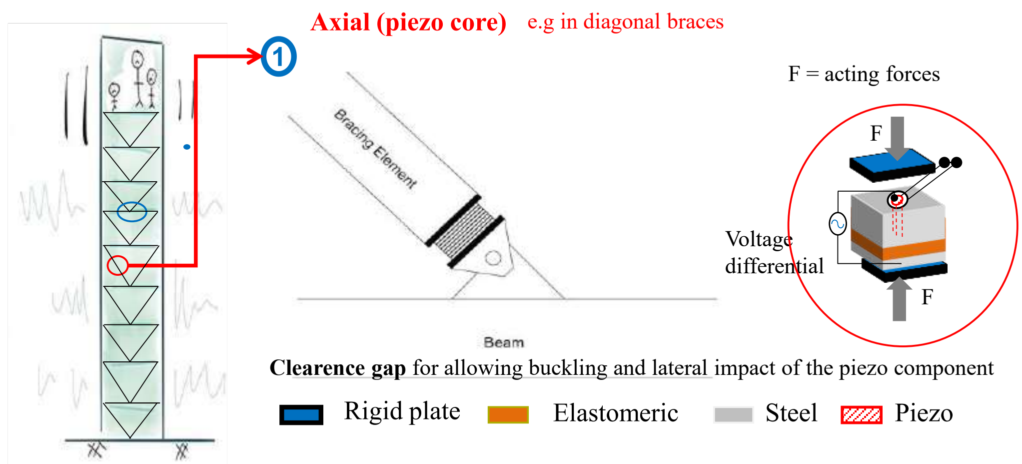

Figure 1. PiD schematic view

3. Analysis methodology

The analysis procedures carried out for exploring the PiDs potential in generating usable energy for powering SHM sensors are synthetically represented in Figure 2.

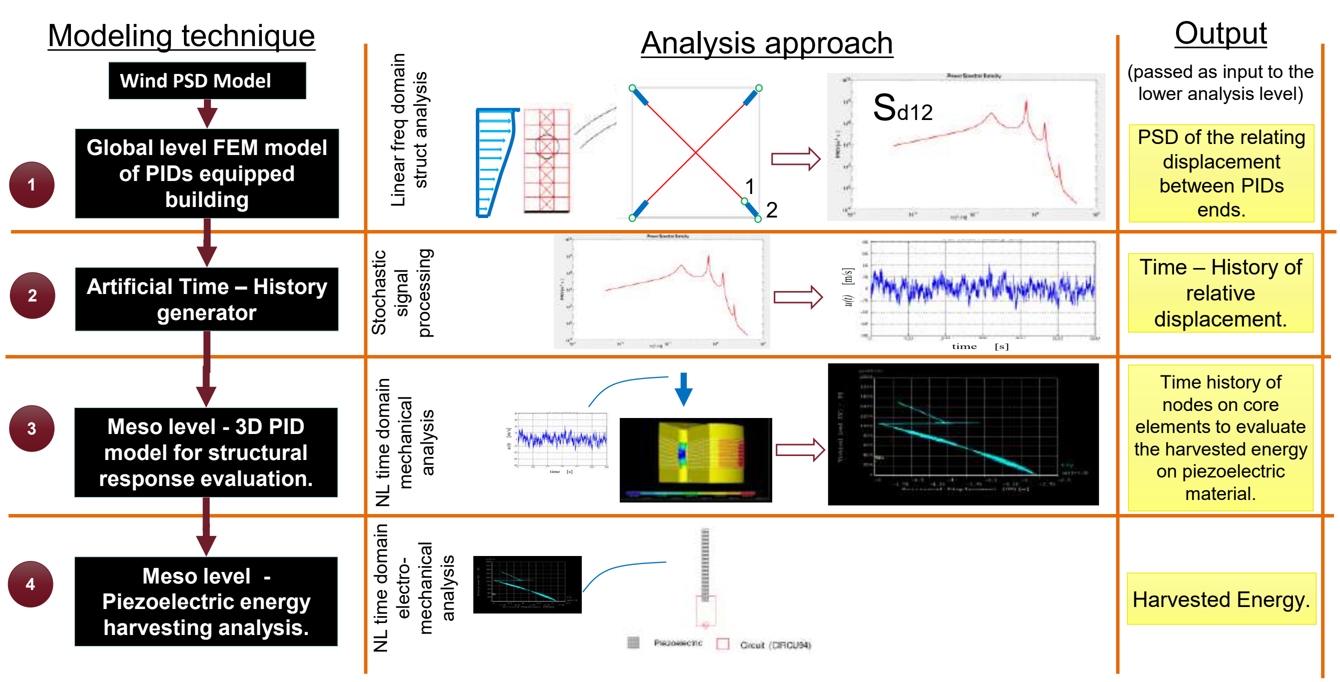

Figure 2. Schematic overview of the analysis of a PiDs' equipped building

The analysis framework is based on a multilevel numerical modeling: 1) the response of an equipped high-rise steel building under turbulent wind is obtained by the avail of a FE model developed in Ansys®, and analyzed by a power spectral density (PSD) approach in frequency domain, the main output of this analysis is the PSD matrix of the relative axial displacements between the two PiD ends (upper and lower plate of the PiD) in a certain location inside the building. The PiDs are modeled here as a two nodes beam with appropriate stiffness and damping carachteristics; 2) this PSD matrix is used as input in a Matlab® code for the artificial time history (TH) generation of the relative displ between the upper and lower plates of the device; 3) this TH is used as input in a non-linear detailed FE mechanical model of the PiD, from which the PiD's core displacements time history is obtained to be used as input in a 4) non-linear multiphysic (mechanical+electrical) model of the piezo core for the evaluation of the harvested energy.
Steps 2) and 3) above imply the correct evaluation of the buckling and impact dynamic.

The final outputs of the procedure are:
- The response of the PiDs' equipped building under wind;
- The mechanical response of the single PiD;
- The RMS of the power of the harvested energy

REFERENCES

Liang, S., Liu, S., Li, Q. S., Zhang, L., & Gu, M. (2002). Mathematical model of acrosswind dynamic loads on rectangular tall buildings. *Journal of Wind Engineering and Industrial Aerodynamics*, *90*(12–15), 1757–1770. https://doi.org/10.1016/S0167-6105(02)00285-4

Colwell, S., & Basu, B. (2009). Tuned liquid column dampers in offshore wind turbines for structural control. *Engineering Structures*, *31*(2), 358–368. https://doi.org/10.1016/j.engstruct.2008.09.001

Erturk, A., & Inman, D. J. (2011). Piezoelectric Energy Harvesting. In *Piezoelectric Energy Harvesting*. https://doi.org/10.1002/9781119991151

Petrini, F., & Gkoumas, K. (2018). Piezoelectric energy harvesting from vortex shedding and galloping induced vibrations inside HVAC ducts. *Energy and Buildings*, *158*, 371–383. https://doi.org/10.1016/j.enbuild.2017.09.099

Zhao, Q., Liu, Y., Wang, L., Yang, H., & Cao, D. (2018). Design method for piezoelectric cantilever beam structure under low frequency condition. *International Journal of Pavement Research and Technology*, *11*(2), 153–159. https://doi.org/10.1016/j.ijprt.2017.08.001

Basshofi Habieb, A., Tavio, T., Milani, G., & Wijaya, U. (2019). 3D-Finite element modeling of lead rubber bearing using high damping material. *MATEC Web of Conferences*, *276*, 01013. https://doi.org/10.1051/matecconf/201927601013

Covaci, C., & Gontean, A. (2020). Piezoelectric Energy Harvesting Solutions: A Review. *Sensors*, *20*(12), 3512. https://doi.org/10.3390/s20123512

Yurchenko, D., Machado, L. Q., Wang, J., Bowen, C., Sharkh, S., Moshrefi-Torbati, M., & Val, D. V. (2022). Global optimisation approach for designing high-efficiency piezoelectric beam-based energy harvesting devices. *Nano Energy*, *93*(December 2021). https://doi.org/10.1016/j.nanoen.2021.106684

Wang, T., & Zhu, Z. W. (2022). A new type of piezoelectric self-excited vibration energy harvester for micro-actuator's energy storage. *Journal of Energy Storage*, *46*(June 2021), 103519. https://doi.org/10.1016/j.est.2021.103519

Ashraf Virk, M. ur R., Mysorewala, M. F., Cheded, L., & Aliyu, A. R. (2022). Review of energy harvesting techniques in wireless sensor-based pipeline monitoring networks. *Renewable and Sustainable Energy Reviews*, *157*(June 2021), 112046. https://doi.org/10.1016/j.rser.2021.112046

High-order scale-resolving simulations of extreme wind loads on a model high-rise building

Giorgio Giangaspero [1], Luca Amerio [2], Steven Downie [3], Alberto Zasso [4], Peter Vincent [5]

[1]*Imperial College London, London, UK, g.giangaspero@imperial.ac.uk*
[2]*ARUP, London, United Kingdom, luca.amerio@arup.com*
[3]*ARUP, London, United Kingdom, steven.downie@arup.com*
[4]*Politecnico di Milano, Milano, Italia, alberto.zasso@polimi.it*
[5]*Imperial College London, London, UK, p.vincent@imperial.ac.uk*

SUMMARY:
Wind pressure is one of the main design forces for medium- and high-rise building façades. To assess these, it is common to use data measured in wind tunnel cladding pressure tests. Previous studies highlighted the presence of highly localized events that could bias the predicted design value toward extremely high loads. This phenomenon could have significant implications for the cost and the total carbon intensity of the cladding system.
In this paper, an open-source CFD code PyFR was used to perform a high-order Implicit Large Eddy Simulation (ILES) to study these phenomena more in detail. The simulations capture, for the first time, the observed space-time localised peaks of extreme low pressure, replicating the experimental findings. The corresponding fluid structures are shown in detail. They are found to be relatively thin and long vortices spinning with an angular velocity approximately normal to the building wall.
This and future works could help to improve the understanding of the statistical characteristics of these events, improving the techniques used to assess the design value for cladding panels from wind tunnel tests data. Also, these simulations could represent a validation case for coarser and more commercially viable CFD simulations aimed at predicting the design wind load on façade panels.

Keywords: Pressure Measurements, Pressure Peak, Cladding Load, Computational Fluid Dynamics, CFD, Implicit Large Eddy Simulation, ILES, High-order

1. INTRODUCTION

Cladding panels might account for a significant portion of the total construction cost for most high-rise building. Part of the cost is driven by the need to withstand wind induced forces acting on the panel. In current practice, wind tunnel test are performed to assess aerodynamic forces acting on the building envelope by measuring the pressure on the surface of a scale model by mean of "pressure taps". Pressure data acquired this way are then post-processed to remove unwanted effects. These include high-frequency components of the signal that are supposedly related to spatially small events that do not contribute to the overall load acting on the façade elements. The choice of the filter cut-off frequency is often based on the so-called TVL equation [Lawson 1976, Lawson 1980] which linearly relates the duration of the pressure acting over a surface to a size parameter and a reference wind speed.
Another approach to study wind-induced loads on buildings is to carry out Computational Fluid Dynamics (CFD) simulations. These offer a series of advatages over wind tunnel tests such as a greater resolution in both time and space with respect to experiments, a better measurability of

the flow phenomena around the building and the possibility to be used in early stage design to drive initial design decision. However, while experiments are assumed to capture all physics up to the spatial/temporal resolution of the instrumentation, traditional CFD solvers may give inaccurate results due to excessive numerical dissipation and/or turbulence modelling errors.
Despite the associated technological challenges, CFD simulations have been used successfully in many wind engineering applications. In particular, LES of high-rise buildings have provided predictive values of pressure fluctuations that are comparable to wind tunnel experimental data, see [Thordal 2019, Giangaspero 2021, Tominaga 2008, Vermeire 2017, Loppi 2018], albeit without extreme negative pressure peaks.
Recent wind tunnel tests [Amerio 2017, Pomaranzi 2022, Zasso 2009, Lamberti 2020] of a model high-rise building have shown local temporally-varying areas of extremely low pressure (Cp ≈ -6 to -10) on the leeward face of the model building for certain wind directions. To the authors' knowledge, the extreme low-pressure events of the experiments [Amerio2017, Lamberti 2020] have not been previously captured by CFD simulations. The phenomenon is unexpected, very localised and time dependent; its flow physics are not fully understood. Designing for pressures in this extreme range has significant implications for the cost and carbon intensity of cladding systems. It is therefore critical to understand the associated spatial characteristics to limit the potential for over-conservative designs.
In this research we carry out unsteady high-order Implicit LES (ILES) to study the turbulent flow over the model high-rise building, focusing on the wind direction of 10 degrees. We employ high-order schemes, which are considerably less dissipative than traditional low-order schemes [Zasso 2009]. Furthermore, the ILES approach is taken to reduce the turbulence modelling error typically associated with RANS models. In particular, ILES allow for explicit simulation of vortex structures which govern design pressure loads and are only implicitly represented using RANS methods. We also employ a recent development of the Synthetic Eddy Method (SEM) [Huynh 2007] to inject synthetic turbulence and reproduce the incoming turbulent boundary layer that was present in the experiments. In this work, for the first time, we show several extreme low-pressure events and we look at the corresponding turbulent structures in detail.

2. RESULTS AND DISCUSSION

Pressure fluctuations at the wall were monitored at the pressure probes, as was the entire surface distribution. Both of these time histories were used to identify when extreme events occurred.
Several severe extreme low-pressure peaks have been observed. The signal recorded by the probes and the minimum have similar behaviour indicating that the physical resolution of the experimental probes is sufficient to detect the occurrence of an extreme event.
However, the actual value of recorded with the two approaches is significantly different as the minimum on the surface (fig. 1-b) is always considerably lower than the measured by the probes (fig. 1-a). For instance, for the first event, occurring at $/ \approx 33$, the probes measured a of ≈ -5 while the minimum on the building surface was ≈ -16. Similarly, for the event at $/ \approx 44.5$, the most extreme one, the Cp measured by the probes was ≈ -6.5 while the minimum on the wall was ≈ -30. This demonstrates how the spatial scale of the minima is smaller than the spacing between the experimental probes.
We now focus our attention on the turbulent structures that generate the extreme fluctuations. In particular, we look at the events A, B and C occurring at $/ \approx 33$, $/ \approx 45$. The corresponding turbulent structures are shown in figs. 2 and 3, respectively. It is clear how the vortical structures that generate such pressure peaks are long and thin vortices spinning around an axis almost normal to the leeward building façade. This is especially clear for the most extreme event (fig. 3).

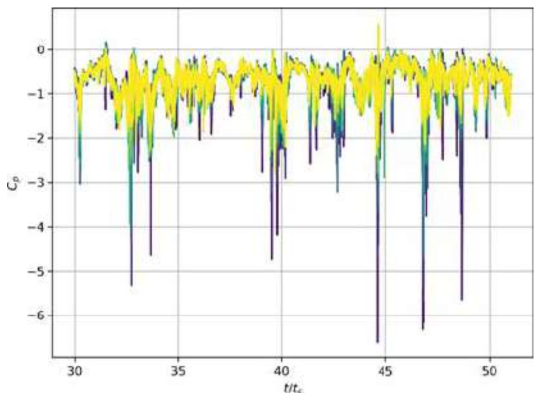

(a) history measured at pressure taps location

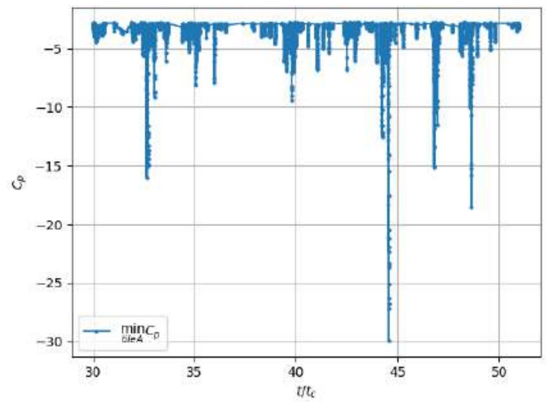

(b) Minimum measured on the surface area covered by tile A

Figure 1. Comparison of histories measured at taps location versus minimum over the tile A area

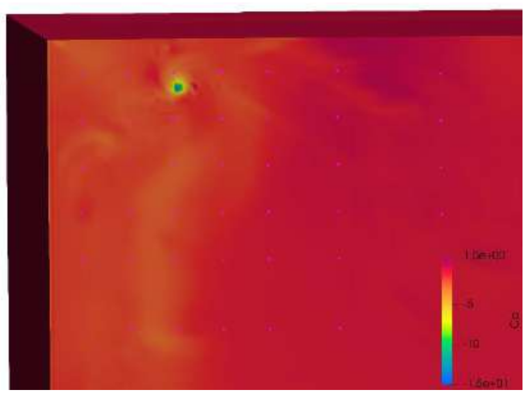

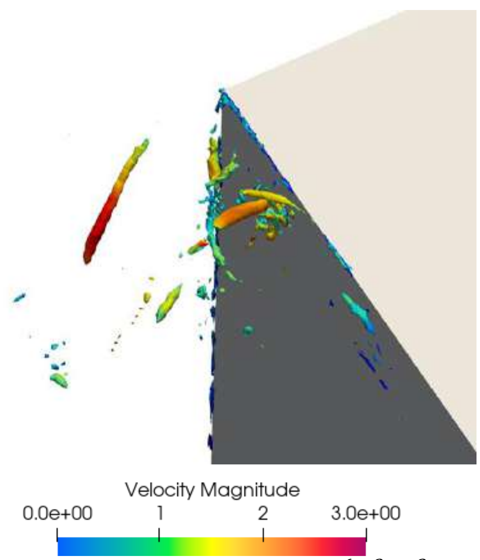

(a) Cp, side view. Black dots indicate the location of the experimental pressure probes. Mean wind direction is right to left.

(b) Q-criterion isosurfaces ($= 3.25 \times 10^6$ $^2_\infty/$ ^{2}) coloured with velocity magnitude. Mean wind direction is from bottom-right

Figure 2. Event at $/$ ≈ 33. Minimum ≈ -16

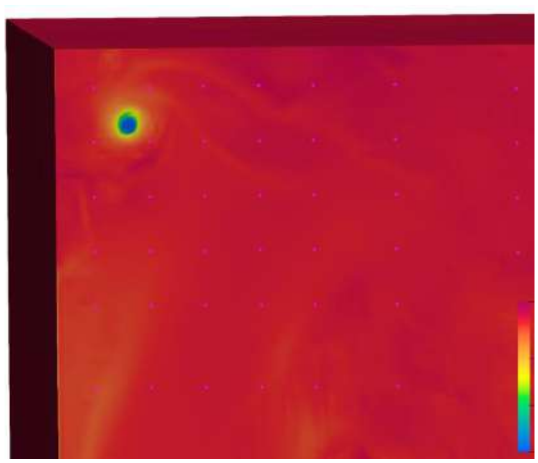

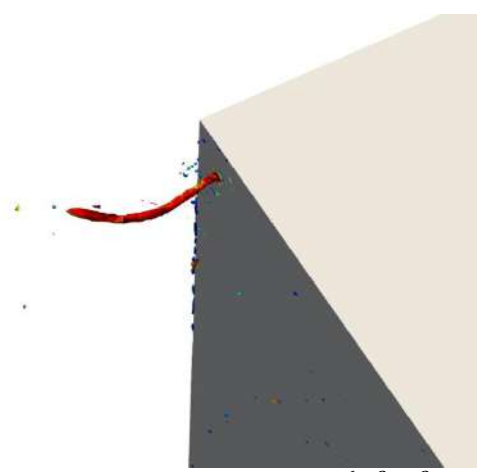

(a) Cp, side view. Black dots indicate the location of the experimental pressure probes. Mean wind direction is right to left.

(b) Q-criterion isosurfaces ($= 7.5 \times 10^6$ $^2_\infty/$ ^{2}) coloured with velocity magnitude. Mean wind direction is from bottom-right.

Figure 3. Event at $/ \approx 45$. Minimum ≈ -30.

3. CONCLUSIONS

The turbulent flow over a model high-rise building has been analysed using high-order scale-resolving ILES. Wind tunnel experiments of the same model have shown space-time localised peaks of extremely low pressure (< -8) on the building façade for certain wind directions. Such strong fluctuations constitute an unexpected phenomenon that no previous CFD simulations have captured. Yet they are of interest to the wind engineering community for their potential impact on the design of building facades. To replicate the experimental findings, we have carried out CFD simulations of the model high-rise building using the open-source software PyFR, which combines high-order discretization schemes (FR) with the high-fidelity scale-resolving approach of ILES.
Point-wise pressure signals were collected at the same location of the experimental pressure taps.
For the first time, several extreme low-pressure peak events (< -10) have been captured and the corresponding three-dimensional fluid structures have been shown in detail. The most extreme one caused a minimum of ≈ -30. These structures are relatively thin and long vortices spinning with an angular velocity approximately normal to the building wall. The spatial extent of these vortices can be smaller than the spatial resolution of the experimental probes. The location where these structures formed is consistent with the experimental findings, i.e. they appeared close the downstream leeward (suction-side) corner of the building, in particular closer to the top edge rather than to the side one. While the experimental campaigns clearly highlighted the occurrence of extreme low-pressure events, their spatial characteristics was unclear due to the limited spatial resolution of the probes. The numerical simulations carried out in this work give important insights into the physics of these phenomena and in particular they allow the designer to estimate more accurately the spatial extent and duration of the low-pressure structures and thus the expected load on the cladding systems. This in turn limits the potential for over-conservative designs which would have been likely if based only on the experimental results.
In future work, extended duration simulations will be undertaken in order to allow quantitative analysis of the frequency at which extreme events are observed. In this context, future work will also investigate whether relatively short-duration simulations, that provide spatially continuous data on the entire building surface, can recover comparable statistics to relatively much longer-duration experiments that only provide data at a finite number of point probe locations. Finally, future work will investigate the genesis of the fluid structures that cause the extreme suction pressures.

REFERENCES

Amerio, L., 2017. Experimental high resolution analysis of the pressure peaks on a building scale model facades. PhD thesis, Politecnico di Milano, Italy

Giangaspero, G., Witherden, F., Vincent, P., Synthetic turbulence generation for high-order scale-resolving simulations on unstructured grids. AIAA Journal, 0(0):1-20, 2021

Huynh, H. T.. A flux reconstruction approach to high-order schemes including discontinuous Galerkin methods. 18th AIAA Computational Fluid Dynamics Conference, 2007.

Lamberti, G., Gorlé, C.. Sensitivity of LES predictions of wind loading on a high-rise building to the inflow boundary condition. Journal of Wind Engineering and Industrial Aerodynamics, 206:104370, 2020.

Lawson, T.V., 1976. The design of cladding. Building and Environment, 11(1): 37–38

Lawson, T.V., Wind Effects on Buildings: Design Applications, volume 1. Spon Press, 1980.

Loppi, N.A., Witherden, F.D., Jameson, A., Vincent,P.E., A high-order cross-platform incompressible navier-stokes solver via artificial compressibility with application to a turbulent jet. Computer Physics Communications,233:193 205, 2018.

Pomaranzi, G., Amerio, L., Schito, P., Lamberti, G., Gorlè, C. and Zasso, A., Wind tunnel pressure data analysis for peak cladding load estimation on a high-rise building. Journal of Wind Engineering and Industrial Aerodynamics, 220:104855, 2022.

Thordal, M.S., Bennetsen, J.C., Holger, H., Koss, H., Review for practical application of cfd for the determination of wind load on high-rise buildings. Journal of Wind Engineering and Industrial Aerodynamics,186:155-168, 2019.

Tominaga, Y., Mochida, A., Murakami, S., Sawaki, S., Comparison of various revised k-ϵ models and LES applied to flow around a high-rise building model with 1:1:2 shape placed within the surface boundary layer. Journal of Wind Engineering and Industrial Aerodynamics, 96(4):389-411, 2008

Vermeire, B.C., Witherden, F.D., Vincent, P.E., On the utility of gpu accelerated high-order methods for unsteady flow simulations: A comparison with industry-standard tools. Journal of Computational Physics, 334:497-521, 2017.

Zasso A., Rocchi D., Schito P., Experimental and numerical study of the flow around a low rise building, EACWE5, Firenze – Italia, July 2009

A new method for synthesising wind loads using the results of two independent wind tunnel tests

Zhenhua Jiang [1], Yin Fai Li [2], Quincy Ma [3], Richard G.J. Flay [4]

[1]*Department of Mechanical and Mechatronics Engineering, The University of Auckland, Auckland, New Zealand, zjia709@aucklanduni.ac.nz*
[2]*Department of Mechanical and Mechatronics Engineering, The University of Auckland, Auckland, New Zealand, fai.li@auckland.ac.nz*
[3]*Department of Civil and Environmental Engineering, The University of Auckland, Auckland, New Zealand, q.ma@auckland.ac.nz*
[4]*Department of Mechanical and Mechatronics Engineering, The University of Auckland, Auckland, New Zealand, fai.li@auckland.ac.nz*

SUMMARY:
A circular cylinder based on the HFPI method has been built and used to study the segmented model test method. The authors verify that the coherence of the wind load between different measuring levels would be markedly diminished if these wind loads are obtained from the independent wind tests. The author proposes a new method to synthetical the time series of the signal such that the synthetical signal embodies the characters of the signal sampled simultaneously. The establishment of this method is of great importance for the development of a sound system for segmental-rigid model wind tunnel testing methods in the near future.

Keywords: Synthetic wind load, Sectional model test method, Wind tunnel test method

1. GENERAL INSTRUCTIONS

Population urbanisation (United Nations, 2015) and the scarcity of land in cities have promoted the construction of super-tall buildings to meet the growing demand. This has contributed to the rapid development of super-slender buildings in developed city centres over the past two decades. Super-slender buildings are significantly taller (z direction) than they are in the other two directions (x and y directions), greater than 12:1 ratio. They maximise the land use and can accommodate more occupants on a small footprint. The desire by developers to break current records is also a strong driving factor for this building trend. The Dubai Creek Tower, which is under construction, will be around 1300 m high and this is set to become the tallest supported tower in the world (Alabbar and Safarik, 2018). Super-slender buildings and super-tall structures with large aspect ratio are difficult to test in wind tunnels due to the size limitations of most wind tunnels. Limited research has been conducted in overcoming this issue by combining wind tunnel test results of multiple building sections from separate tests. One such study was carried out by Zhou, et al. (Zhou, Huang, Gu, Zhu, and Pan, 2010) who tested separate segmented models of the Guangzhou TV tower using the High-Frequency Force Balance (HFFB) method. Since the segmented models were tested separately, the wind force spectral matrix was incomplete. To get the complete wind force spectral matrix, Zhou, et al. (Zhou et al., 2010) modified a coherence function proposed by Davenport (Simiu and Yeo, 2019) for turbulence fluctuations at two different points in space and used the modified coherence function to obtain the cross-spectrum of the wind loads between different sectional models. Their segmented-rigid model tests were successfully adopted in the design process, and the Guangzhou TV Tower opened in August 2009 (Chen et al., 2011). The present study outlines an alternative approach for using the sectional model test results to derive a set of wind load time histories for the entire structure.

2. METHOD

In this study, the surface pressure of a 2.5 m high circular cylinder with a diameter of 0.16 m has been tested simultaneously sampled in the boundary layer wind tunnel of the Mechanical Engineering Department, the University of Auckland, as shown in Fig. 1(a). The circular cylinder's surface is fitted with two tripping wires, which are symmetrically placed on either side and parallel to the front stagnation line, as shown in Fig. 1(b). The effect of the tripping wires is to delay the separation of the boundary layer on the circular cylinder, and hence simulate the flow regime of a higher Reynolds number. The incoming wind speed u_0 of the test is ~5 ms^{-1} with 1% turbulence intensity. The each data acquisition in the wind tunnel is repeated successively under the same flow conditions. The sampling frequency and sampling time of the test are 400 Hz and 2 minutes, respectively. The drag force coefficient and the lift force coefficient are determined as $C_d = \frac{F_x}{0.5 \cdot \rho \cdot u_0^2}$ and $C_l = \frac{F_y}{0.5 \cdot \rho \cdot u_0^2}$, where F_x and F_y are the forces in the along wind direction and the cross wind direction, respectively. Air density ρ is taken as a value of 1.2 kgm^{-3}.

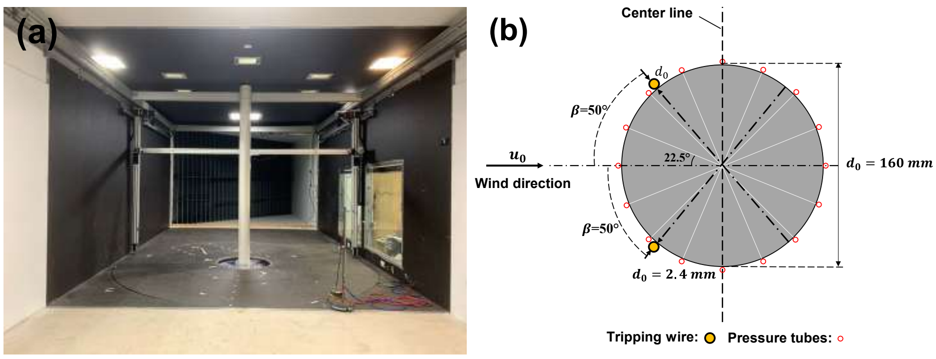

Figure 1. Experiment setup: (a). Circular cylinder physical model; (b). Cross-sectional view

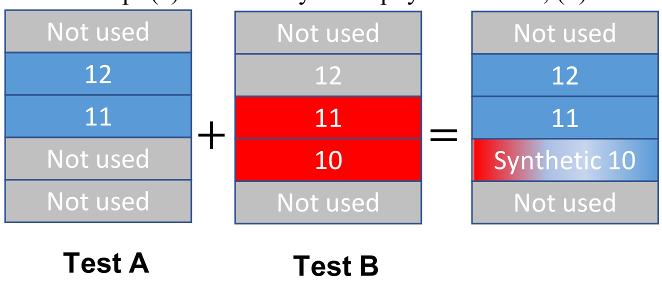

Figure 2. The schematic figure for the new method concept

3. RESULTS AND DISCUSSION

The data measured from two successive tests, namely to A and B. The 10, 11 and 12 correspond to the test results obtained from pressure taps at instrumented level 10, level 11 and level 12, respectively, as shown in Figure 2. Figure 3. shows the sectional lift force coefficient time histories. It is found that the mean coefficient and normalised spectra of the lift forces between the two independent tests are very similar, as shown in Figure 4. Besides, the coherence between different instrumented level is also markedly diminished, as shown in Figure 5. The diminished of the coherence between C10T1 and C11T2 indicates the cross-spectrum of the lift force coefficient between C10T1 and C11T2 is also significantly reduced compared with the cross-spectrum of the lift force coefficient between C10T2 and C11T2 measured simultaneously.

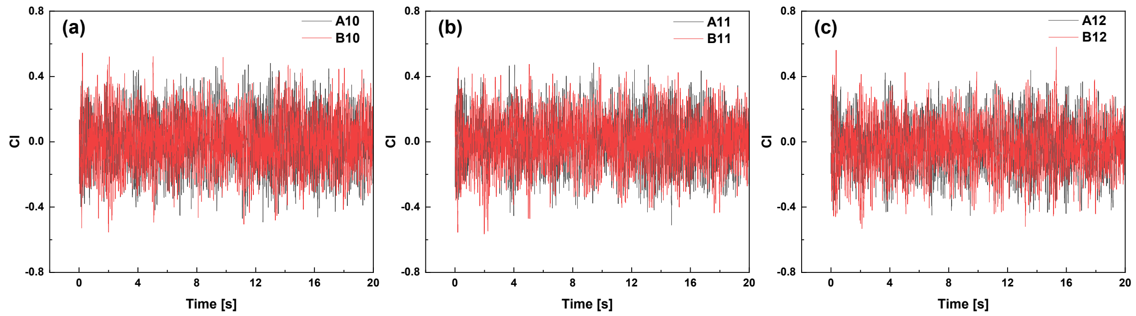

Figure 3. The time history of the lift force coefficient between test 1 and test 2: (a). Measuring level 10; (b) Measuring level 11; (c). Measuring level 12

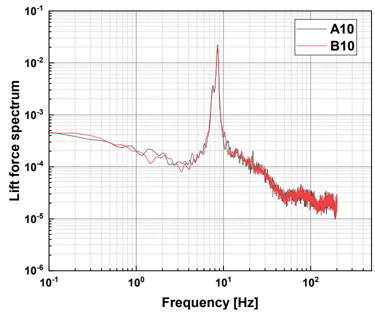

Figure 4. Lift force spectra from two independent tests

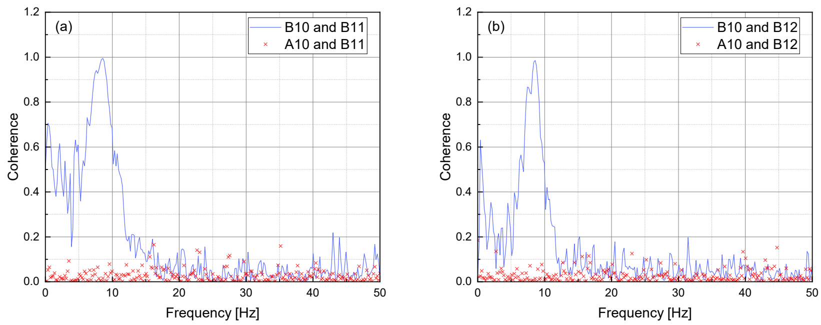

Figure 5. (a). Coherence obtained from B10 and B11 compared with coherence obtained from A10 and B11; (b). Coherence obtained from B10 and B12 compared with coherence obtained from A10 and B12

The authors developed a new method for synthetical a new signal based on the theory concept as described in Figure 2, which enables to embody the characteristics of the signal sampled simultaneously. The co-spectrum $S_{A10_{syn},\ B11}$ between $A10_{syn}$ and $B11$ is close to the co-spectrum $S_{B10,\ B11}$ between $B10$ and $B11$. The co-spectrum $S_{A10_{syn},\ B12}$ between $A10_{syn}$and $B12$ is close to the co-spectrum $S_{B10,\ B12}$ between $B10$ and $B12$ as shown in Figure 6. (a) and (b). The quadrature spectrum is very small which is negligible for the application of atmospheric boundary layer (Simiu and Yeo, 2019). Besides, the coherence between $A10_{syn}$, B11 and B12 is very close to the coherence between B10, B11 and B12, as shown in Figure 6. (c) and (d).

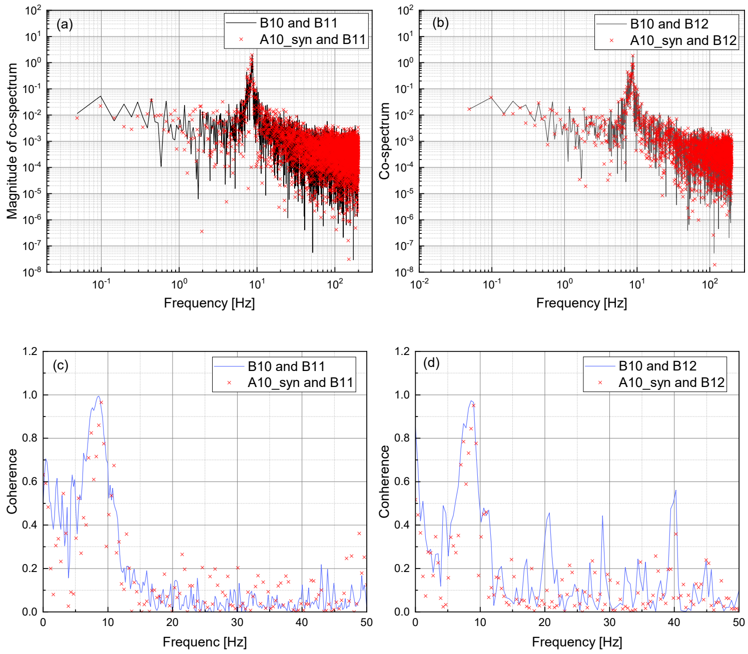

Figure 6. (a). Co-spectrum obtained from B10 and B11 compared with co-spectrum obtained from A10_syn and B11; (b). Co-spectrum obtained from B10 and B12 compared with co-spectrum obtained from A10_syn and B12; (c). Coherence obtained from B10 and B11 compared with coherence obtained from A10_syn and B11; (d). Coherence obtained from B10 and B12 compared with coherence obtained from A10_syn and B12

4. CONCLUSION

This paper verifies that the coherence of the sectional lift force coefficient will be underestimated if they are obtained from several segmented models tested independently. The authors propose a new method to merge the results of two independent wind tunnel tests on a segmented model. The coherence between the synthetical and measured sectional lift forces is similar to the sectional lift forces that are measured simultaneously. A detailed derivation of this method will be presented in the full paper.

ACKNOWLEDGEMENTS

The authors would like to thank the China Scholarship Council (NO.201906370045) for providing financial support for this research.

REFERENCES

Alabbar, M. A., and Safarik, D. (2018). Talking Tall: His Excellency Mohamed Ali Alabbar. CTBUH Journal(4), 54-57.

Chen, W. H., Lu, Z. R., Lin, W., Chen, S. H., Ni, Y. Q., Xia, Y., and Liao, W. Y. (2011). Theoretical and experimental modal analysis of the Guangzhou New TV Tower. Engineering Structures, 33(12), 3628-3646. https://doi.org/10.1016/j.engstruct.2011.07.028

Simiu, E., and Yeo, D. (2019). Wind effects on structures: Modern structural design for wind: John Wiley and Sons.

United Nations, the Department of Economics and Social Affairs. (2015). World urbanization prospects: The 2014 revision. United Nations Department of Economics and Social Affairs, Population Division: New York, NY, USA, 41

Zhou, X., Huang, P., Gu, M., Zhu, L., and Pan, H. (2010). Wind Loads and Wind-Induced Responses of Guangzhou New TV Tower. Advances in Structural Engineering, 13(4), 707-726. 10.1260/1369-4332.13.4.707

Wind Field Simulation and Wind Damage Assessment of Typhoon Rai in the Philippines

J. C. Agar [1], T. S. Acosta [2], A. A. Barros [3] J. Y. Hernandez Jr. [4]

[1]University of the Philippines, Quezon City, Philippines, jcagar@up.edu.ph
[2]University of the Philippines, Quezon City, Philippines, tsacosta @up.edu.ph
[3]University of the Philippines, Quezon City, Philippines, aabarros@up.edu.ph
[4]University of the Philippines, Quezon City, Philippines, jyhernandez@up.edu.ph

SUMMARY:

Typhoon Rai (Local Name: Odette) was regarded as the strongest typhoon to have struck the Southern Philippines in the last 31 years. It is also the first violent typhoon classified by the new classifications by the Japan Meteorological Agency. A forensic meteorological analysis was performed to identify the peak intensity of Typhoon Rai at its initial landfall and to simulate and determine the winds experienced by the affected areas using the gradient wind equation. Assuming that the gradient winds are 10-minute sustained winds and considering the effects of the wind exposure to wind spectra and gustiness results in surface winds close to the actual measurements. A subsequent wind damage assessment is performed in the affected areas to identify the severe wind building vulnerability.

Keywords: Typhoon modelling, Typhoon Rai, severe wind building vulnerability

1. INTRODUCTION

Lying on the pathway of Pacific typhoons, the Philippines monitors about 20 typhoons a year (Cinco et al., 2010) within the Philippine Area of Responsibility, where the Philippine Atmospheric, Geophysical, and Astronomical Services (PAGASA) assigns local name to the typhoons within, apart from the international designation by the Japan Meteorological Agency (JMA). One of the hazards that typhoons bring are severe winds, which are considered in the design of buildings in the Philippines.

The National Structural Code of the Philippines (NSCP) has the wind design provisions implemented across engineered structures in the Philippines. The design provisions were then put into the test when Typhoon Rai (Local Name: Odette) caused massive devastation across Southern Philippines in December 2021, where 10-minute sustained winds were estimated to be 185 kph at landfall. The areas affected by Typhoon Rai were previously affected by Typhoon Mike in 1990. The 31-year gap may have explained the social factors that resulted in lack of wind resistance of non-engineered structures. But that doesn't explain some engineered buildings that suffered catastrophic failure, most notably with the recently built Siargao Sports Complex. The Association of Structural Engineers of the Philippines (ASEP), when making the latest design provisions in the NSCP, imposed a design wind speed of 310 kph.

Figure 1. Siargao Sports Complex (Courtesy of: ASEP)

The building failure could indicate two things: first is that the winds brought by Typhoon Rai exceeded the design wind speed or second is that the building is not adequately designed and built in the first place to meet the required wind resistance imposed by the wind design codes. This study aims to simulate the typhoon wind field and validate it using ground surface data in order to determine the winds experienced by the buildings that are assessed in the wind damage assessment.

2. METHODS

This study first simulates the wind field of Typhoon Rai using the gradient wind equation (Holmes, 2001) where the Coriolis force and the Centrifugal force are balanced with the pressure gradient caused by the typhoon's convection:

$$\frac{U^2}{r} + f|U| + \frac{1}{\rho_{air}}\frac{\partial p}{\partial r} = 0 \tag{1}$$

Where U is the velocity field, r is the radius of curvature or the radial distance given that the pressure field is composed of concentric and circular pressure isobars, f is the Coriolis parameter which is dependent on the latitude, ρ_{air} is the density of air, and $\frac{\partial p}{\partial r}$ is the pressure gradient. The pressure gradient is then modeled using the barometric pressures of the automated weather stations by Advanced Sciences and Technology Institute (ASTI)

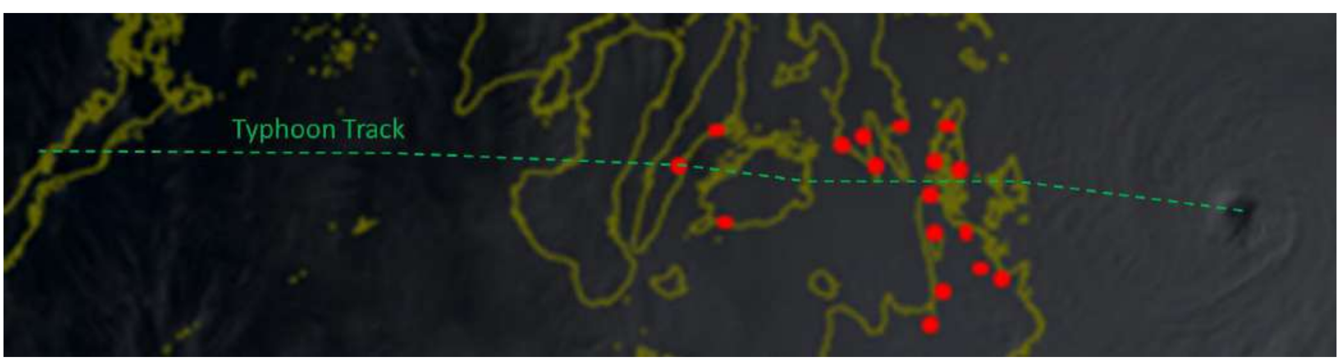

Figure 2. Location of the ASTI Automated Weather Stations

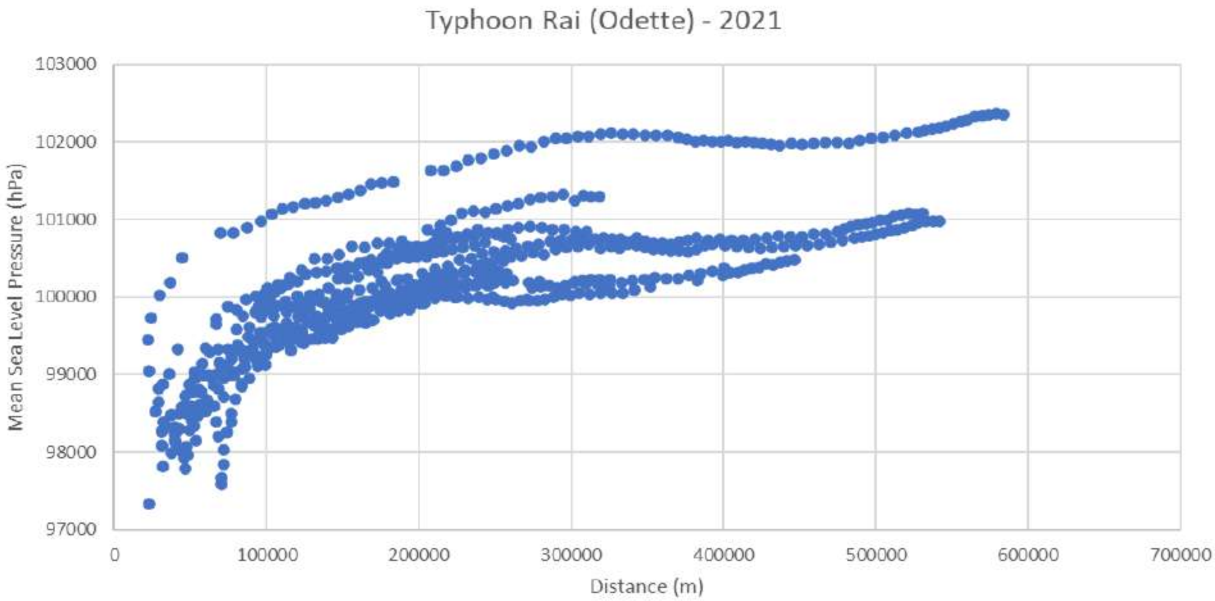

Figure 3. Pressure

The study then relates the pressure readings with the actual position of the Typhoon Rai with respect to time in order to determine the distance. With the barometric pressure points related to distance, shown in Figure 3, a rectangular hyperbolic profile (Schloemer, 1954) is used to model the pressure field which is then used:

$$p(r) = p_0 + (p_n - p_0)e^{-\frac{A}{r^B}} \tag{2}$$

Where p_0 is the minimum central pressure, p_n is the ambient pressure assumed to be equal to 1013 hPa, A is the shape parameter that determines the radius of maximum winds (Holland, 1980), and B is the shape parameter that relates the pressure gradient to the magnitude of the maximum winds. Substituting Eq. (2) to Eq. (1) leads to the gradient wind profile:

$$U(r) = -\frac{fr}{2} + \sqrt{\left(\frac{fr}{2}\right)^2 + \frac{AB}{\rho_{air} r^B} e^{-\frac{A}{r^B}}} \tag{3}$$

The landfall intensity of Typhoon Rai is determined through a Monte Carlo simulation giving an ensemble of values for A and B that satisfies two conditions: (1) goodness of fit to the pressure field in Figure 3 and (2) the wind profile having the 6-km radius pinhole eye exhibited by Typhoon Rai before landfall. The nature on how the intensity of Typhoon Rai changed as it passed over Southern Philippines was then patterned after the forecast data of Japan Meteorological Agency. The study also considers that the gradient wind obtained using Eq. (3) is relative to the center of Typhoon Rai which also has a translation velocity. Obtaining the vector sum of the two results into a magnitude of the winds that is assumed to be the 10-minute sustained winds.

$$\overrightarrow{U_{10-min}(r)} = \overrightarrow{U(r)} + U_{translation} \tag{4}$$

The wind field determined in Eq. (4) must be then multiplied by a gust factor, which mainly depends on the wind exposure (Harper et al., 2010). The gust factors are obtained by comparing to the wind speed data obtained from PAGASA’s synoptic stations. The wind field generated then became the basis of the series of field surveys conducted by the Philippine Institute of Civil Engineers (PICE) and ASEP across the affected areas to document the severe wind damages. Apart from Siargao Sports Complex, the authors mainly focused on Cebu Province where they conducted a building assessment survey before Typhoon Rai made landfall.

ACKNOWLEDGEMENTS

The authors would like to acknowledge the Association of Structural Engineers of the Philippines and the Philippine Institute of Civil Engineers for initiating and funding the severe wind damage assessment across the affected areas. Also, the authors acknowledge Engr. Jihan S. Pacer, Engr. Liezl Tan, and Engr. Dean Ashton Plamenco and Dr. Oscar Victor Antonio of UPD Institute of Civil Engineering who joined the authors in the field survey conducted in Cebu Province.

REFERENCES

Cinco, T., Hilario, F., Tibig, L., Malano, V. III, De Guzman, R., Uson, M., Barba, R., Barlolata, R., and Frial, R., 2010. Updating tropical cyclone climatology in the Philippines. Proceedings on Earthquake and Severe wnid Exposure and Vulnerability Workshops. PHIVOLCS, PAGASA, and Geoscience Australia

Association of Structural Engineers of the Philippines, 2015. National Structural Code of the Philippines

Schloemer, R, 1954. Analysis and synthesis of hurricane wind patterns over Lake Okechobee, FL. Hydromet Rep. 31, pp.49.

Holland, G., 1980. An Analytic Model of the Wind and Pressure Profiles. Monthly Weather Review. Vol. 108. No. 9. Pp. 1212-1218

Gumaro, J., Acosta, T., Tan, L., Agar, J., Tingatinga, J., Musico, J., Plamenco, D., Ereño, M., Pacer, J., Villalba, I., and Hernandez, J., 2021. Identification of key components for developing building types for risk assessment against wind loadings: The case of Cebu Province, Philippines. International Journal of Disaster Risk Reduction. https://doi.org/10.1016/j.ijdrr.2021.102686

Holmes, J., 2001. Wind Loadings on Structures

Harper, B., Kepert, J., and Ginger, J., 2010. Guidelines for converting between various wind averaging periods in tropical cyclone conditions. World Meteorological Or

Gust Factors, Turbulence Intensities, Roughness Lengths, and Wind Direction Factors of Typhoon Winds in the Philippines

J. C. Agar [1], J. Y. Hernandez Jr. [2]

[1]*University of the Philippines, Quezon City, Philippines, jcagar@up.edu.ph*
[2]*University of the Philippines, Quezon City, Philippines, jyhernandez@up.edu.ph*

SUMMARY:

The exposure of a location against winds in the wind design provisions from the National Structural Code of the Philippines is mainly dependent on the topography and the degree of vegetation and urbanization. The wind exposure includes the vertical wind profile, the gust factors, and angles of approach. The current code provisions on the parameters for the wind exposure are mainly dependent on the surface roughness, which has been derived from steady wind conditions. However, winds from typhon, the extreme winds being designed against, are in fact unsteady winds. To evaluate the exposure parameters at these conditions two typhoon events are simulated using an unsteady-state CFD analysis. Wind exposure for typhoon winds reveals higher local gusts factors which are related to the direction of the local wind and change in elevation. The upper limit of the surface roughness is determined by the building density and average roof height of the buildings, while its variation is dependent on the wind flow channeling, separation, and reattachment.

Keywords: Wind exposure, Typhoons

1. INTRODUCTION

Severe wind is one of the multiple destructive hazards that the Philippines is exposed to. In its 2015 edition, the National Structural Code of the Philippines (NSCIP), updated its basic wind speed maps to consider the newer data that were compiled in the Generalized Extreme Value analysis (De Leoz et al., 2014). Being patterned after the provisions of ASCE-07, the NSCP 2015 basic wind speed maps have supposedly return periods of 1700 years (3% probability in 50 years), shown in Figure 1.

However, upon checking the GEV functions from the peak gusts data of synoptic stations from PAGASA, inconsistencies between the extreme values and the basic wind speeds were observed, as stations in Mindanao returned less extreme wind speed values compared to that of the NSCP 2015 wind maps, while the Eastern seaboards of Luzon and Visayas returned higher wind speed values compared to that of the NSCP 2015, shown in Table 1.

One overlooked aspect in the inception of the current wind speed maps was the nature of the extreme winds at each of the weather stations. Evaluating the history of the recorded winds across the weather stations uncovered that the severe winds experienced by some weather stations, like Davao City, Cagayan de Oro City, and Butuan City are not cyclonic in nature and not caused by typhoons.

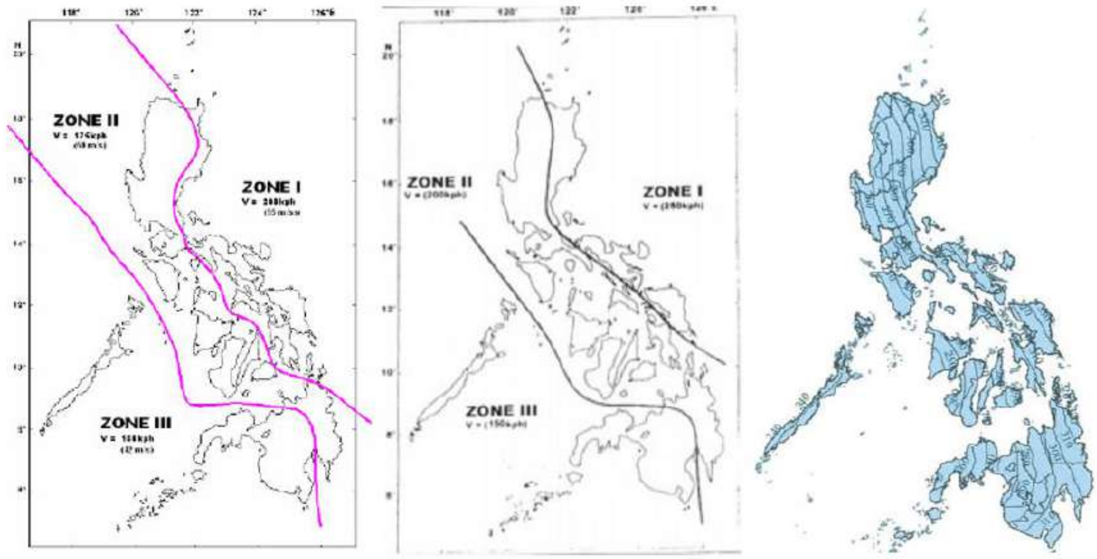

Figure 1. Basic Wind Speed Maps of NSCP

Table 1. Comparison of GEV values to the Basic Wind Speed Map Values

Station	Extreme Winds (kph)	NSCP 2015 (kph)	Difference (kph)	Cyclonic/Non-Cyclonic
Virac Synoptic	402	330	-72	Cyclonic
Guiuan	394	320	-64	Cyclonic
Itbayat	369	340	-29	Cyclonic
Casiguran	366	315	-51	Cyclonic
Manila	259	265	+5	Cyclonic
Mactan	170	285	+115	Cyclonic
Davao City	117	305	+188	Non-yclonic
Cagayan de Oro	97	280	+183	Non-cyclonic
Butuan City	128	300	+172	Non-cyclonic
Tacloban City	212	310	+98	Cyclonic

Another aspect overlooked, particularly in the extrapolation of the extreme values from the synoptic stations, was the factor brought by wind exposure. The weather stations experienced their respective peak winds which was also a result of their distinct wind exposure, which was a factor of topography, vegetation, direction of wind, and other possible local effects.

This study aims to provide feature-based parameters for gust factors, roughness lengths, wind direction factors, and turbulence intensities during typhoon events, considering the urban effects and nonstationary effects. In defining the wind exposure parameters of typhoon winds, a wind field over a complex and urban terrain was simulated using Computational Fluid Dynamics. To capture the nonstationary effects, Large Eddy Simulation is used to model the eddies that carry the turbulent effects.

This study covered two cases: (1) winds brought by Typhoon Haiyan (Local Name: Yolanda) in Bantayan, Cebu at 8:30 am in November 8, 2013, and (2) winds brought by Typhoon Nock-ten (Local Name: Nina) in Virac, Catanduanes at 10:30 am in December 25, 2016.

2. METHODS

2.1. Typhoon Wind Field

The evaluation of the typhoon wind field marked the start of the hybrid procedure that will simulate the wind field over the subject areas. Focusing on the gradient wind balance of typhoons, the pressure gradient force, centrifugal force, and the Coriolis force would be considered, along with the radius of curvature of the pressure isobars.

$$\frac{U^2}{r_{curv}} + f|U| + \frac{1}{\rho_{air}}|\frac{\partial p}{\partial r}| = 0 \quad (1)$$

Where U is the gradient wind, assumed as both the friction-free surface wind and 10-minute sustained winds, ρ_{air} is air density, r_{curv} is the radius of curvature of the pressure isobar, f is the Coriolis parameter, ${}^{\partial p}/_{\partial r}$ is the pressure gradient fitted using a rectangular hyperbolic profile (Schloemer, 1957) (Holland, 1980) from the barometer pressures from synoptic weather stations by PAGASA along the path of the typhoons subjected to this study.

2.2. Complex-Terrain Wind Simulation

The friction-free surface wind that was computed using Equation 1 were then carried over as inlet velocities for the micro-scale analysis where the unsteady dissipation of the wind over the complex terrain - which were the subject areas - were simulated.

To reduce the computational load for feasibility purposes, two measures were made. First, as the building edges indicated higher characteristic changes in the flow leading to higher resolution and higher computational load, the need to reduce the edges led into modeling the buildings as rectangular blocks whilst retaining the key dimensions such as height, width, and length.

Second, the computational model was scaled down by 1:10 in both the length scale and velocity scale. Even though this scaling followed the similitude laws involving the Reynolds Number, the dynamic similarity involving the Navier-Stokes Equations would not be conserved as the viscosity of the air remained unchanged in the setup. The non-conservation of the dynamic similarities in the energy cascade results into the smaller eddies not being modeled. However, it was also assumed that these smaller eddies contributed little to gustiness, hence their effects can be neglected.

The simulation is done using Computational Fluid Dynamics (CFD). Finite volume method was used (Demirdzic, 1983) as the numerical method in solving for the Navier-Stokes Equations in a manner of balancing the pressure field first in an algorithm called Pressure-Implicit with Splitting of Operators or PISO algorithm (Issa, 1986):

$$\frac{\partial p}{\partial x_i} = -\frac{\partial u_i}{\partial t} - u_j\frac{\partial u_i}{\partial x_j} + (\nu + \nu_t)\left(\frac{\partial^2 u_i}{\partial x_j \partial x_j}\right) \quad (2)$$

Where p is the pressure, ui is the velocity field, ν is the kinematic viscosity of air, and νt is the eddy viscosity derived from modelling the eddies using the Filtered Turbulence Kinetic Energy Transport Large Eddy Simulation Model(You and Moin, 2007).

2.3. Extraction of Gust Factors, Turbulence Intensities, Roughness Lengths, and Wind Direction Factors

After the simulation, a filtering procedure was done using three main criteria: (1) The goodness of fit of the logarithmic profile was greater than 0.95 to ensure that a boundary layer profile was observed, (2) the vertical profile contained more than 10 points to ensure robustness and to eliminate the chance of overestimation of the reference velocity which was set at 10 meters from the ground, and (3) the ground elevation computed in the curve fitting was consistent with the modelled profile which was expressed in a power law equation shown below:

$$U(z) = U_{10m} \left(\frac{z}{10}\right)^{\frac{1}{\ln\left(\frac{10}{z_0}\right)}} \tag{3}$$

Where U(z) is the velocity function with respect to a height z, U10m is the reference velocity at 10 meters high, and z0 is the roughness length being extracted. Consequently, U10m was reflected on the computed gradient wind in Equation (1a) to obtain the gust factors.

$$I_{u,prescribed}\,(z) = \frac{1}{\ln\left(\frac{z}{z_0}\right)} \tag{4}$$

Once the roughness lengths were obtained, the turbulence intensities were computed using the equation (1d) from Lumley and Panofsky (1964) and were compared with measured turbulence intensities in the simulation using the equation below:

$$I_{u,\tau} = \frac{\sigma_{u,\tau}}{U_{T0,\tau}} \tag{5}$$

Where $\sigma_{u,\tau}$ is the standard deviation of the fluctuating wind and U_{T0}, τ is the average value of the fluctuating wind.

Wind direction factors are then obtained locally by determining the angle between the local wind from the general direction of the simulated wind.

REFERENCES

Association of Structural Engineers of the Philippines, 2015. National Structural Code of the Philippines.

Charnock, H.,1955. Wind stress on a water surface. Qtly. J. Royal Met. Soc., Vol. 81.

De Leoz, T.A., Kaw, E.R., Qudilla, A., Valbuena, J.G. and Garciano, L.R., 2014. Updating the Wind Zone and Developing Contour Maps For the Philippines: Adaptation Strategies for Extreme Winds. Undergraduate Research. De La Salle University – Manila.

Demirdzic, I. A., 1983. A Finite Volume Method For Computation Of Fluid Flow in Complex Geometries. Dissertation. Imperial College, University of London.

Harper, B., Kepert, J. and Ginger, J., 2010. Guidelines for converting between various wind averaging periods in tropical cyclone conditions. World Meteorological Organization

Holland, G., 1980. An Analytic Model of the Wind and Pressure Profiles. Monthly Weather Review 108(8). Pp. 1212-1218

Issa, R., 1986. Solution of the implicitly discretized fluid flow equations by operator-splitting. Journal of Computational Physics, Vol. 62

Lumley, J. and Panofsky, H., 1964. The Structure of atmospheric turbulence. Wiley Interscience New York.

Powell, M., Houston, S., and Reinhold, T., 1996. Hurricane Andrew's landfall in South Florida. Part I; Standardizing measurements for documentation of surface wind fields. Weather and Forecasting, Vol 11, pp. 304-328.

Richardson, L.F., 1922. Weather prediction by numerical process. Cambridge University Press

Schloemer, R. W., 1954. Analysis and synthesis of hurricane wind patterns over Lake Okechobee, FL. Hydromet Rep. 31, pp.49

Van der Hoven, I., 1957. Power spectrum of horizontal wind speed in the frequency range from 0.0007 to 900 cycles per hour. J. Meteorology, Vol. 14, pp.160-164

Wieringa, J., Davenport, A., Grimmond, C., and Oke, T., 2001. New revision of Davenport roughness classification. Proceedings of the 3rd European and African Conference on Wind Engineering, Eindhoven, The Netherlands, 2-6 July, 2001, 285-292

You, D. and Moin. P., 2007. A dynamic global-coefficient subgrid-scale eddy viscosity model for large-eddy simulation in complex geometries. Center for Turbulence Research. Annual Research Briefs 2006. P.41-53